Interrogating CXCR4 signal integration in human antibody secreting cells using an in vitro model of differentiation

Kieran Anthony Walker

Submitted in accordance with the requirements for the degree of
Doctor of Philosophy

The University of Leeds Faculty of Medicine and Health

Section of Experimental Haematology

May 2022

Acknowledgments

Abstract

The generation of antibody-secreting plasma cells (PCs) is a tightly regulated process that begins with activation of B-cells and rapid proliferation, followed by the transition to a plasmablast (PB) state, eventually developing into mature PCs. The development of antibody secreting cells (ASCs) requires the fine tuning of environmental cues, the collaboration of specific surface receptors and migration of cells to survival niches.

CXCR4 is a key B-cell and PC marker known for its role in driving chemotaxis of B-cells within the germinal centre and of PB as they a directed towards long term survival niches, such as the bone marrow (BM). The role of CXCR4 signalling has been described in B-cells, however it is less clear how these CXCR4 signal transduction events are changed in ASCs. To assess how CXCR4 signal integration in ASCs is affected, key signalling pathways were characterised for PB and PC populations. PCs demonstrated an enhanced AKT and ERK signalling pattern in response to CXCL12, suggesting a re-wiring of CXCR4 signalling response between the two populations.

Furthermore, B-cells and PCs may modulate their signalling capabilities through receptor coordination. CD19 is a key B-cell surface protein that has been implicated in the enhancement of B-cell receptor (BCR) signalling and, more recently, has been described as a signalling hub for a variety of B-cell surface receptors, including CXCR4. Stimulation of CD19 in concert with CXCR4 revealed a reduced ERK signalling pattern compared to CXCL12 stimulation alone in PCs compared to PBs, suggesting a negative regulatory role in PCs. Dual stimulation generated comparable AKT signalling strength compared to CXCL12 stimulation, but again revealed an enhanced response in PCs compared to PBs. Loss of CD19 has been shown to cripple B-cell function. Here we show that a deficiency of CD19 diminishes CXCL12 mediated ERK and AKT signalling in ASCs, suggesting a key role in CXCR4 signal generation at the later stages of B-cell differentiation.

In addition to this, the effect of uncontrolled CXCR4 activation, as seen in Waldenström macroglobulinemia (WM), on MAPK and PI3K signal transduction was assessed with or without CD19 stimulation. Previous studies have shown that Waldenström B-cells which harbour a CXCR4[WHIM] mutation show greater PI3K/MAPK signalling. Here, signalling in PBs and PCs expressing the WHIM mutation reveal a prolonged phosphorylation pattern suggesting a continuation of dysregulated signalling as seen in WM B-cells.

This data provides evidence of CXCR4 signal rewiring in PBs and PCs, which is further modulated by CD19 and the presence of the CXCR4[WHIM] mutation. Together this work builds on the understanding of the biology of ASCs and their malignant counterparts.

Table of Contents

List of figures

List of Tables

List of Abbreviations

7AAD - 7-Aminoactinomycin D

A1- BCL2 related protein A1

AA - Amino acid

Abs – Antibodies

ACKR4 - atypical chemokine receptor 4

AID - Activation induced cytidine deaminase

AIOLOS - Ikaros family zinc finger protein 3

AKT - Protein kinase B

ALL - acute lymphoblastic leukemia

AMP – ampicillin

AP-1 - Activator protein 1

APRIL - A proliferation-inducing ligand

ARRB1 – Arrestin, beta 1

ARRB2 - Arrestin, beta 2

ASC - Antibody secreting cell

ATCC - American Type Culture Collection

BACH2 – BTB Domain and CNC Homolog 2

BAD - BCL2 associated agonist of cell death

BAFF- B-cell activating factor

BC – Blood cone

B-cell – B lymphocyte

BCL6 – B-cell lymphoma 6

BCL-XL - B-cell lymphoma-extra large

BCMA - B-cell maturation antigen

BCR – B-cell Receptor

BLIMP1 – B lymphocyte-induced maturation protein-1

BM – Bone marrow

BMSCs - Bone marrow stromal cells

Bp – base pairs

BSA – bovine serum albumin

BTK - Bruton's tyrosine kinase

C3d – complement component 3d

cAMP – Cyclic adenosine monophosphate

CCL19/21 - C-X-C motif chemokine 19/21

CCR1/2/3/5/7 - C-C chemokine receptor type 1/2/3/5/7

CD138 - Cluster of differentiation 138 - Syndecan 1

CD19 - Cluster of differentiation 19 - B-lymphocyte antigen CD19

CD2 - Cluster of differentiation 2

CD20 - Cluster of differentiation 20 - B-lymphocyte antigen CD20

CD27 - Cluster of differentiation 27

CD38 - Cluster of differentiation 38 - cyclic ADP ribose hydrolase

CD40 – Cluster of differentiation 40

CD44 – Cluster of differentiation 44

C-Fos - Protein c-Fos

CIP – calf intestinal phosphatase

CLEC - Ceiling lymphatic endothelial cells

CSR – Class switch recombination

C-terminal - carboxyl-terminal tail

CXCL12/13 - C-X-C motif chemokine 12/13

CXCR2/4/5 – C-X-C chemokine receptor type 2/4/5

DAG – diacylglycerol

DC – Dendritic cell

DMEM - Dulbecco's Modified Eagle Medium

DNA - Deoxyribonucleic acid

DRC – cyclophosphamide

DZ – Dark Zone

ECM - Extracellular matrix

EDTA - Ethylenediaminetetraacetic acid

ELISA – enzyme-linked Immunosorbent assay

ER – Endoplasmic reticulum

ERK - Extracellular signal-regulated kinases

EtBr – Ethidium Bromide

FACs - Fluorescence-activated cell sorting

FOXO - Forkhead box protein

FRC - fibroblastic reticular cell

FSC-A – Forwards scatter area

FSC-H – forward scatter height

GAB1 - GRB2-associated-binding protein 1

GC – Germinal centre

GDP - guanosine diphosphate

GFP – green fluorescent protein

GLB – Gel loading buffer

GPCR - G protein-coupled receptor

GRB2 - Growth factor receptor-bound protein 2

GRK - G protein-coupled receptor kinase

GTP - guanosine triphosphate

Gα - G alpha subunit

Gβ – G beta subunit

Gγ – G gamma subunit

HA - Human influenza hemagglutinin

HEK - Human embryonic kidney

HEV - high endothelial venules

HIFBS – heat inactivated fetal bovine serum

HRP – Horseradish peroxidase

HSC - Haemopoetic stem cell

IEG – Immediate early gene

IFNγ - Interferon gamma

IgA – Immunoglobulin A

IgD – Immunoglobulin D

IgE – Immunoglobulin E

IgG – Immunoglobulin G

IgM – Immunoglobulin M

Igα – Immunoglobulin α

Igβ – Immunoglobulin β

IKAROS - DNA-binding protein Ikaros

IKK - IκB kinase complex

IL-4 - Interleukin 4

IL-6 – Interleukin 6

IMDM - Iscove Modified Dulbecco Media

IP3 - inositol triphosphate

IRAK - IL-1-receptor associated kinase

IRES – Internal ribosome entry site

IRF4 - Interferon regulatory factor 4

IRF8 - Interferon regulatory factor 8

ISRE - IFN-stimulated response elements

Kd – Kilodalton

LB - Lysogeny broth

LD – labelled depletion

LLPC – Long-lived plasma cell

Lyn - Tyrosine-protein kinase Lyn

LZ – Light Zone

MACs - Magnetic-activated cell sorting

MAPK - mitogen-activated protein kinase

MCL-1 - Induced myeloid leukaemia cell differentiation protein

MCS – multiple cloning site

MEK - Mitogen-activated protein kinase kinase

MEM – Minimum essential medium

MFI – mean fluorescent index

MGUS - Monoclonal gammopathy of undetermined significance

MHCII - major histocompatibility complex II molecule

MiR-148a - microRNA 148a

MITF - Microphthalmia-associated transcription factor

MM - Multiple myeloma

MSC - Mesenchymal stem cell

MSCV - Murine stem cell virus

mTORC - Mammalian target of rapamycin complex

MYC - MYC proto-oncogene, BHLH Transcription Factor

MyD88 - Myeloid differentiation primary response 88

MZ - Marginal zone

NF- κB - Nuclear factor kappa B

NK – Natural Killer cell

N-terminal - amino-terminal tail

ON – overnight

p15Ink4b - Cyclin-dependent kinase 4 inhibitor B

p16Ink4a - cyclin-dependent kinase inhibitor 2A

p53 - Tumour protein P53

PAMP - Pathogen-associated molecular pattern

PAX5 - Paired Box 5

PB - Plasmablast

PBMC - Peripheral blood mononuclear cell

PBS - Phosphate buffered saline

PCs – Plasma cells

PDK1 - Pyruvate dehydrogenase lipoamide kinase isozyme 1

PI3K - Phosphoinositide 3-kinase

PIK3C2G - Phosphatidylinositol-4-Phosphate 3-Kinase Catalytic Subunit Type 2 Gamma

PIK3CB - Phosphatidylinositol-4,5-Bisphosphate 3-Kinase Catalytic Subunit Beta

PIK3R2 - Phosphatidylinositol 3-kinase regulatory subunit beta

PIP2 - Phosphatidylinositol 4,5-bisphosphate

PIP3 - phosphatidylinositol-3, 4, 5-triphosphate

PKCβ - Protein Kinase Cβ

PLC - phospholipase C

PLCγ2 - phospholipase Cγ2

PTEN - Phosphatase and tensin homolog

RIPA - Radio-Immunoprecipitation Assay

RNA - Ribonucleic acid

RPM – Rotation per minute

S473 – serine 473

SCS - subcapsular sinus

SDF-1 - stromal cell-derived factor 1

SDS - Sodium dodecyl sulfate

SH2 - Src Homology 2

SHM – Somatic Hypermutation

SOC – Super optimal culture

SRC - Proto-oncogene tyrosine-protein kinase Src

SSC-A – side scatter area

STAT3 - Signal transducer and activator of transcription 3

STR - short tandem repeat

SYK - Tyrosine-protein kinase SYK

T308 – Threonine 308

TACI - Transmembrane activator and CAML interactor

TBE - Tris/Borate/EDTA buffer

T-cell – T lymphocyte

TD - Thymus-dependent

TF – Transcription factor

TFH - T follicular helper

Th1 - Type 2 helper T cell

Th2 - Type 2 helper T cell

TI - Thymus-independent

TLR – Toll like receptor

TMB - 3,3',5,5'-Tetramethylbenzidine

TNF – Tumour necrosis factor

TRAF6 - TNF Receptor Associated Factor 6

UPR - unfolded protein response

VAV - Guanine nucleotide exchange factor VAV

VDJ - hyper-variable region

WHIM - warts, hypogammaglobulinemia, infection and myelokathexis

WM - Waldenström's Macroglobulemia

WT – Wildtype

XBP1 - X-box binding protein 1

1.0   Introduction

1.1 Generation of the humoral adaptive immune response

1.1.1   B-cell differentiation into antibody secreting cells

The production of antibodies, or immunoglobulins, is a key facet of the adaptive immune response responsible for both short-term and long-term immunity. B-cells are a type of white blood cell that express a unique immunoglobulin on the cell surface, enabling detection of foreign antigens expressed by pathogens. Upon recognition of antigen, B-cells undergo a process of differentiation, a crucial mechanism that transforms B-cells into plasma cells (PCs), which are capable of secreting immunoglobulin.

Naïve B-cells develop from haematopoietic stem cells in the bone marrow, and from there they migrate to secondary lymphoid tissues to begin the maturation process. To become activated, a B-cell receives a signal through its antigen receptor. This activation can be T-cell dependant (figure 1.2), whereby a follicular B-cell internalises, processes, and presents an antigen peptide on a major histocompatibility complex II molecule (MHCII). A T-cell then recognises this antigen through the T-cell receptor and becomes activated. The activated T-cell then expresses CD40L on its surface and produces cytokines such as IL-21. B-cells expressing CD40 and appropriate cytokine receptors are stimulated by the combination of signals. Following this, the B-cells rapidly proliferate and differentiate into short-lived plasmablasts, which can provide a rapid but weak immune response. Alongside this, activated B-cells can re-enter the B-cell follicle and, under the influence of specialized T follicular helper (T_{FH}) cells, proliferate vigorously to form a germinal centre (GC) (Ise and Kurosaki 2019).

Within the GC, the B-cells migrate between the dark zone (DZ) and the light zone (LZ). In the dark zone, GC B-cells undergo extensive proliferation and somatic hypermutation (SHM), a process that induces mutations in the hyper-variable region (VDJ) of the B-cell's immunoglobulin gene, altering affinity for the antigen. The GC B-cell then moves to the LZ, where immunoglobulin class switch recombination (CSR) occurs to generate different isotypes of antibodies that have a range of effector functions. (LeBien and Tedder 2008)**.** Additionally in the LZ, the selection of B-cells is determined by interaction

with follicular helper T-cells, which enable B-cells whose antibody affinity confers an advantage, saving them from apoptosis through activation of contact-dependant survival signals. Cells are selected based on the affinity of competing clones and cells may re-enter the GC to undergo further rounds of affinity selection before they are either selected for maturation or apoptosis (Victora *et al.* 2010). Within the GC, the fate of the activated B-cell has been determined and the result of this process is the generation of highly specific long-lived PCs and memory B-cells which enable long-term immunity (figure 1.1) (Shinnakasu and Kurosaki 2017).
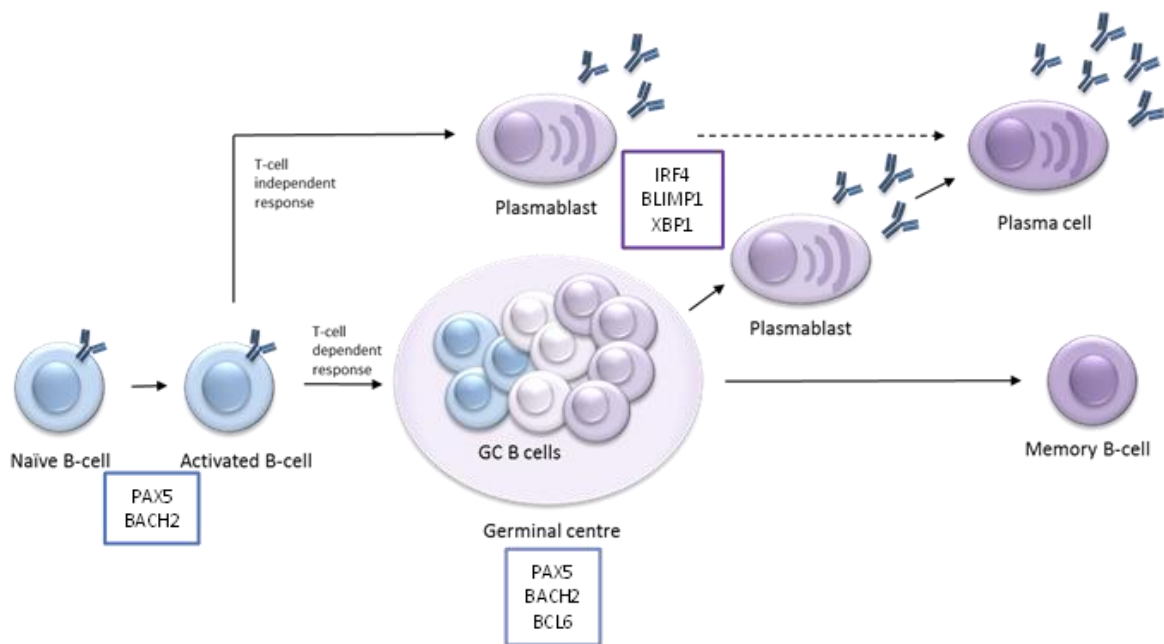
Figure 1.1. - Differentiation of naïve B-cells to PCs and memory B-cells in showing both T-cell dependant and T-cell independent activation. Antigen binding to naïve B-cells initiates activation. Following this, depending on the antigenic stimulation, B-cells either enter germinal centres where they mature to become PCs or memory B-cells, providing long term immunity, or they become short lived plasmablasts, via the T-cell independent pathway, and may mature further into PCs, providing some rapid but short-lived immunity. Key transcription factors that orchestrate the changes in cell state are indicated in boxes.

Alternatively, B-cells (usually marginal zone or B1 B-cells) can also be activated in a T-cell independent mechanism (figure 1.2). Here B-cells are activated in response to bacterial components which bind to Toll-like receptors (TLRs) or by antigen binding that induces extensive BCR cross-linking. This process rapidly generates short-lived plasmablasts that can secrete antibodies with a weaker affinity for the targeted epitope than those generated through the T-cell dependant activation process. Long-lived PCs may also be generated through this mechanism (Allman, Wilmore and Gaudette 2019), (Martin, Oliver and Kearney 2001).
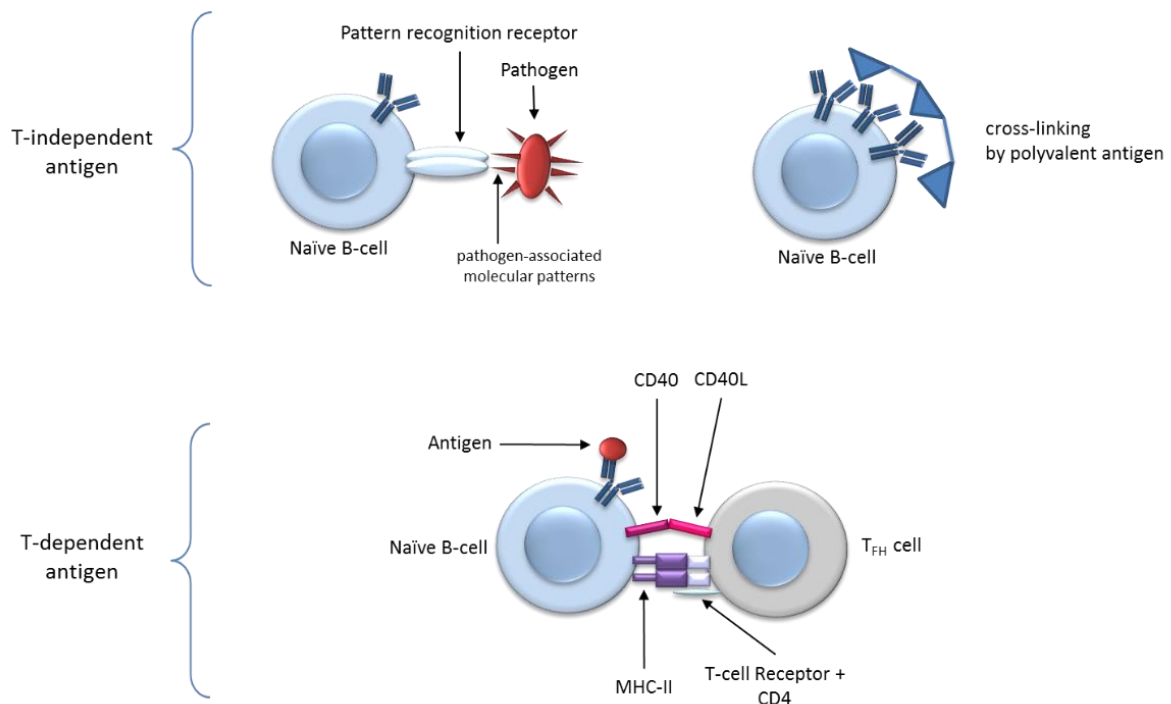
Figure 1.2. – Signals that drive B-cell differentiation. B-cells can become activated through a T-independent mechanism, whereby either pattern recognition receptors (e.g. TLRs) present on the B-cell surface detect pathogen-associated molecular patterns (PAMPs) such as LPS, or repetitive surface antigens from bacteria cause cross-linking of the BCR. Both mechanisms induce the rapid production of polyclonal antibodies. Alternatively, B-cells, once bound to antigen, can become activated by T follicular helper cells (Tfh cells). These cells express a T-cell receptor, which along with its co-receptor CD4, binds recognise the antigen bound to the major histocompatibility complex class II receptor on the naïve B-cells. The Tfh cells also present CD40L and cytokines to the B-cells. This cause the B-cells to begin rapid proliferation and differentiation into PBs. From here the activated B-cells may form a GC and therefore develop into PCs or memory cells for long-term immunity.

1.1.2   Transcriptional regulation of B-cell differentiation

There is a complex gene regulatory network that governs the differentiation of B-cells (figure 1.3), regardless of the initial input of signals. These transcription factors function in a stepwise fashion to transition the cells to the PC state. PAX5 is the master regulator of the B-cell programme (Nera *et al.* 2006) and regulates expression of other TFs including *IRF4* and *BACH2* (Muto *et al.* 2010) , *BCL6* (Chevrier *et al.* 2017), (Duy *et al.* 2010), (Nutt *et al.* 2011) and *PRDM1/BLIMP1* (Basso and Dalla-Favera 2012). PAX5 commits B-cell progenitors to the B-cell identity, whilst suppressing drivers of the PC identity, such as BLIMP1 (B lymphocyte-induced maturation protein 1). BCL6 is a transcriptional repressor identified as the critical regulator of GCs (Dent et al., 1997, Ye et al., 1997). Alongside this, BCL6 has been shown to repress regulators of the PC programme, specifically *BLIMP1*, allowing maintenance of the cell cycle regulator c-MYC, thereby upholding the proliferative traits of B-cells (Dent *et al.* 1997), (Ye *et al.* 1997), (Shaffer *et al.* 2000). BACH2 is a transcriptional repressor that

regulates GC and B-cell fate. It is widely expressed in the B lymphoid lineage, excluding PCs. Deletion of BACH2 induces loss of GC development, CSR and SHM, and therefore cells fail to produce high affinity Abs through a T-cell dependant mechanism (Huang *et al.* 2014). A major role of BACH2 is to prevent PC generation by interacting with a region upstream of the promoter and repressing *BLIMP1*, the main driver of PC differentiation. The outcome of this repression is to halt the PC programme and promote CSR (Ochiai *et al.* 2006), (Muto *et al.* 2010). However, more recent data has uncovered additional roles for BACH2, namely as a major regulator for the generation of a memory B-cell pool from B-cells in response to antigen. Within the LZ of the GC, B-cells with a high affinity for antigen or that are receiving strong help from T cells show a downregulation of BACH2, both at the transcript level and via post translational mechanisms.

AKT mediated phosphorylation of BACH2 sequesters it into the cytoplasm. This prevents BACH2 entry into the nucleus enabling AP-1 family members to access binding sites, allowing expression of genes encoding for effector molecules e.g. CD44, TNF, IFNγ, and BLIMP1. This prevents memory cell formation and therefore these cells are preferentially targeted for plasma cell differentiation instead. In cells that have received weak stimulation (T-cell independent) or possess a BCR with a low affinity, BACH2 outcompetes AP-1 family members and blocks antigen-receptor mediated transcriptional programmes, allowing memory cell differentiation to progress (Sidwell and Kallies 2016), (Shinnakasu *et al.* 2016).

MITF is another transcriptional repressor of *BLIMP1*, and *IRF4*. MITF prevents premature differentiation of GC B-cells. It is expressed highly in naïve B-cells. Once B-cells become activated, MITF must be downregulated to promote differentiation. MiR-148a is a microRNA abundant in PCs and is upregulated in activated B-cells. It is a component of the regulatory network that helps drive the PC programme through targeting of MITF and BACH2 (Lin, Gerth and Peng 2004), (Porstner *et al.* 2015).

Deletion of STAT3 has catastrophic effects on GC maintenance and function and therefore PC development. Specifically, STAT3 signalling has been shown to help with initiation of the GC reaction and also maintenance of GCs for prolonged periods of time. Additionally, STAT3 signalling is an important regulator of anti-apoptotic proteins such as MCL-1 and BCL-XL, suggesting a survival signalling role of PC within the GC. Furthermore, as STAT3 signalling is necessary for GC B-cell maintenance, this modulates the frequency of Tfh cells and their interactions, allowing the development of PCs. In addition to the role of STAT3 within the GC, STAT3 depletion can affect survival of pre- and pro- transitional B-cell development and survival. Finally, STAT3 can mediate up-regulation of *BLIMP1*, helping to drive the PC programme, though it functions mainly as an initiator and requires

downregulation of repressors such as BCL6 to complete the transition (Diehl *et al.* 2008), (Ding *et al.* 2016), (Chou, Levy and Lee 2006), (Diehl *et al.* 2008).

There is also transcriptional regulation of the early B-cell programme before their activation and entry into the germinal centre. AIOLOS and IKAROS are zinc finger transcription factors that are involved in the regulation of B-cell and T-cell maturation. Their importance in these processes has been highlighted through inactivation studies leading to complete loss of B and T lymphopoiesis. AIOLOS forms heterodimers with the largest IKAROS isoform in T/B-cells to help mediate commitment to the B/T-cell lineages. AIOLOS is lowly expressed in lymphoid progenitors whereas IKAROS is expressed in all haemopoietic progenitors, but AIOLOS becomes more highly expressed once progenitor cells are dedicated to the B- or T-cell pathway in pre-B-cells and in double positive thymocyte precursors, respectively. Depletion of IKAROS causes blockages in B-cell development at the pro-B-cell stage. AIOLOS expression peaks in mature B-cells and the greatest IKAROS expression has been detected in in fully mature B-cells (Kirstetter *et al.* 2002), (Wang *et al.* 1998).

The main function provided by AIOLOS is to set the threshold for receptor signalling that regulates B-cell activation and commitment to become a GC B-cell, and therefore the maturation processes with the GC, such as CSR and SHM. Loss of AIOLOS leads to a backlog in B-cell development and therefore a build-up of B-cell precursors. IKAROS is also necessary for the activation threshold of B-cells and IKAROS low expression can negatively affect GC formation (Wang *et al.* 1998), (Kirstetter *et al.* 2002), (Schmitt *et al.* 2002).

During the transition to the PC stage, the B-cell gene expression programme is extinguished with loss of the B-cell phenotype, including the expression of surface immunoglobulin and other cell surface receptors. As the cells progress, they adopt a specialised PC programme geared towards the production of high levels of secreted immunoglobulin and characterised by the activation of IRF4 (Ochiai *et al.* 2013), BLIMP1 (Shaffer *et al.* 2002) and XBP1 (Reimold *et al.* 2001), (Hu *et al.* 2009). BLIMP1 is the master regulator of the PC programme and is necessary for the formation of functional Ig secreting PCs (Shapiro-Shelef *et al.* 2003). Through its repressor activity, it regulates various genes involved in the maintenance of the B-cell identity, such as *PAX5* (Lin *et al.* 2002), (Lin, Lin and Calame 2000).

IRF4 plays a role in both the B-cell and PC programmes and has mutually antagonistic effects dependant on its relative concentration. Specifically, at low concentrations, IRF4 binds to EICE/AICE DNA motifs, thereby inducing the expression of transcription factors including AID and BCL6 which are required for GC processes such as CSR (Sciammas *et al.* 2006), (Ochiai *et al.* 2013). Additionally, higher expression of IRF4 after the GC stage shifts the binding of IRF4 to ISRE DNA motifs, which induces the

expression of *BLIMP1* and downregulates the expression of *BCL6*, therefore driving the PC programme. (Sciammas et al., 2006), (Ochiai et al., 2013), (Willis *et al.* 2014; Saito *et al.* 2007)

To drive the activation of the PC programme, a combination of BLIMP1 and suppression of PAX5 enable the expression of XBP1, a TF highly expressed in PCs (Lin et al., 2002). XBP1 is not required for the formation of PCs (Todd et al., 2009), however XBP1 is necessary for the function of antibody secreting PCs, due to its regulation of the unfolded protein response (UPR), which is initiated due to heightened ER stress caused by the increased load and processing of immunoglobulin protein within the ER. Therefore, XBP1 is crucial for the expansion the ER and driving of secretory pathways needed to process the increased load of unfolded protein (Shaffer et al., 2004), (Lin *et al.* 2002; Todd *et al.* 2009; Shaffer *et al.* 2004).

NF-κB is crucial for the development of PCs and memory B-cells. Constitutive expression mainly drives pro-survival signalling in non-activated pre-B-cells. Additionally, CD40 signals can promote B-cell survival through NF-κB through recruitment of anti-apoptotic molecules BCL-XL and A1 within the follicle. (Jimi *et al.* 2005; Lee *et al.* 1999). NF-κB is involved in CSR. NF-κB transcription factors downstream of both the classical and alternative activation pathways help initiate and promote CSR through several mechanisms. For example, IL-4 cytokine induces transcription of germline C epsilon genes in activated B-cells, allowing these cells to undergo CSR to IgE. NF-kB has been described as a transcription factor necessary for binding to DNA that enables induction of this transcription event (Delphin and Stavnezer 1995).
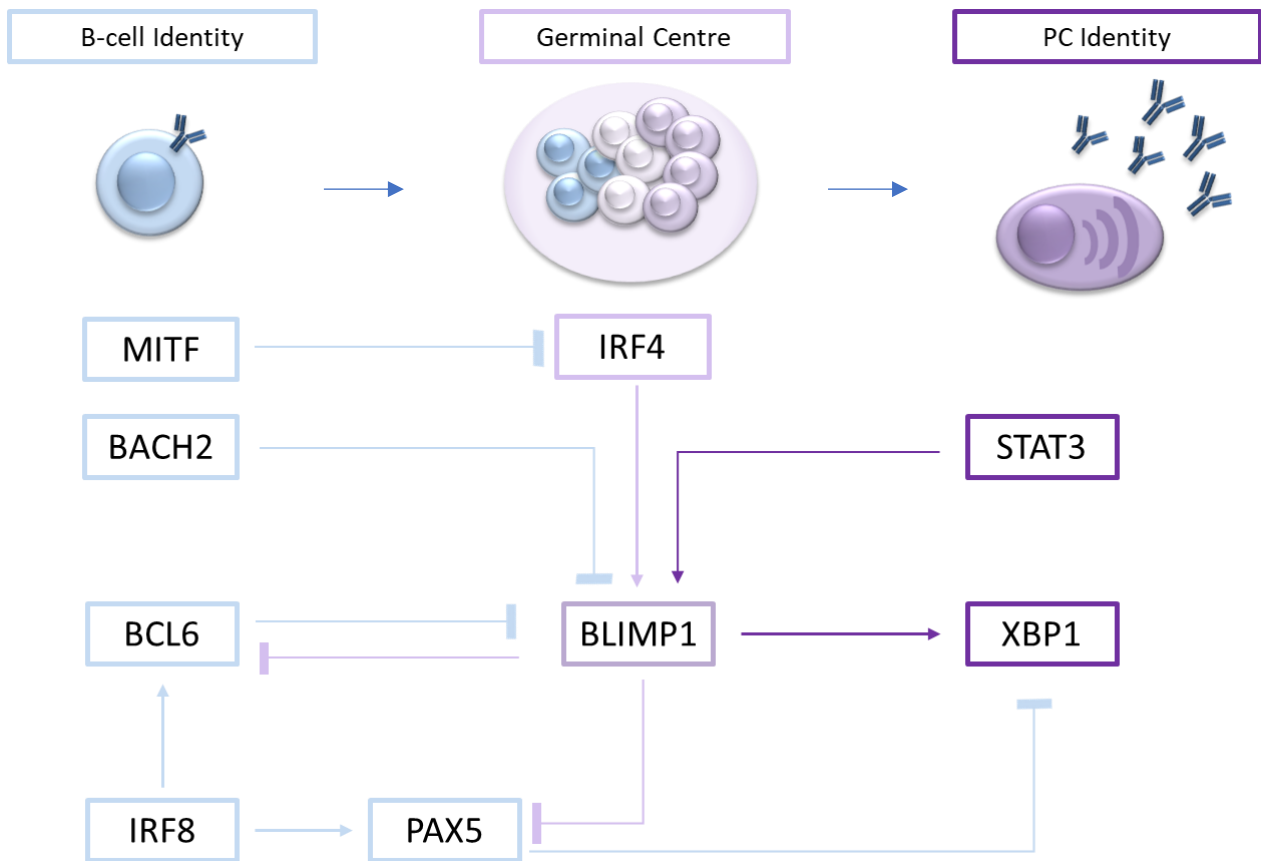
Figure 1.3 – **Transcriptional regulation map depicting the major players in maintaining the B-cell programme and subsequent transition to the plasma cell programme.**

1.1.3 Long-term immunity

Following maturation, a population of PBs migrate to a bone marrow (BM) survival niche where they become long-lived PCs. To get there, PBs are equipped with chemokine receptors that enable response to their cognate ligands. PCs display a sensitivity to CXCR4 ligand CXCL12 (SDF-1), which drives PC migration to survival niches, such as splenic red pulp, medulla of lymph nodes and the BM (figure 1.4) (Hargreaves *et al.* 2001).
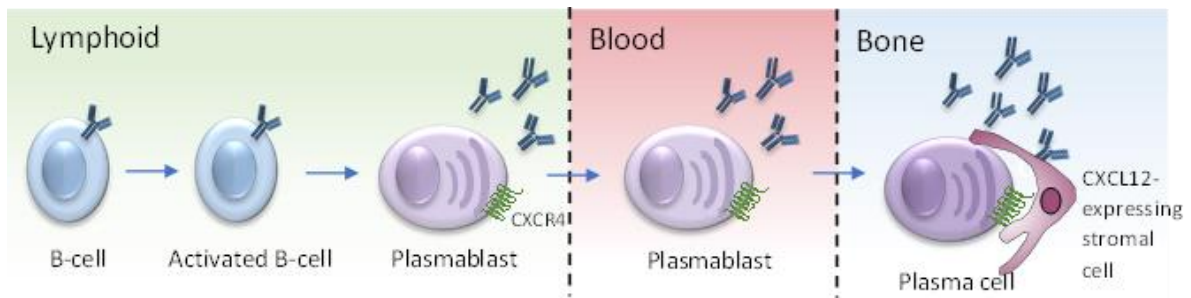
Figure 1.4 – Guided movement of antibody secreting cells. B-cells once activated mature to a plasmablast (PB) phenotype within the lymphoid organs. From here, PBs migrate along a CXCL12 axis through the blood towards survival niches, most notably the bone marrow (BM). CXCL12 is secreted from stromal cells within the BM and attract migrating PB through interaction with CXCR4. Within the BM niche, PBs mature to the plasma cell stage (PC) and will secrete antibody to provide immunity.

Due to the importance of PCs for long-term immunity, the BM provides a specialised niche to maintain their longevity (figure 1.5). Specifically, the cells require factors and signals produced from the stromal cells residing within the bone microenvironment. APRIL and BAFF, cytokines from the TNF superfamily, can bind to BCMA and TACI to promote survival (Benson *et al.* 2008). Alongside this, The BM stroma may secrete other factors such as IL-6 and TNF-α that also aid survival (Minges Wols *et al.* 2002). Furthermore, continued access to CXCL12 expressing reticular stromal cells is also required to retain a viable PC population within the BM (Tokoyoda *et al.* 2004). Additionally, murine studies indicate that eosinophils may promote PC retention and survival in the BM niche, as they are a source of PC survival factors (Chu *et al.* 2011). However more recent data downplays their requirement (Haberland *et al.* 2018). Lastly, PCs survival is enhanced through expression of CD138 and CD44 which increases surface heparin sulphate levels, enabling improved binding to survival cytokines such as IL-6 and APRIL (McCarron, Park and Fooksman 2017), (Van Driel *et al.* 2002).

The maintenance of PCs within the BM is supported by the secretion of various soluble factors and through cell-cell and cell-ECM interaction. APRIL is a particularly crucial cytokine necessary for long-lived survival of PCs, It is crucial for the establishment of the adult BM reservoir of IgG secreting LLPCs. APRIL binds to B-cell maturation antigen (BCMA) and to a lesser degree, transmembrane activator and CAML interactor (TACI) BCMA expression is restricted to PBs and PCs (Vincent *et al.* 2013). APRIL drives expression of Bcl-xL which blocks anti-apoptotic protein release, such as cytochrome C from the the mitochondria, therefore preventing caspase activation and therefore apoptosis (O'Connor *et al.* 2004). Signalling through APRIL-BCMA has also been shown to upregulate expression of another anti-apoptotic protein, myeloid cell leukaemia 1 (MCL1), which is essential for ASC survival (Peperzak *et al.* 2013)

The signal transduction pathways used by BCMA and TACI has been partially characterised. Following APRIL binding, BCMA binds TNF receptor-associated factors (TRAF) 1, 2 and 3, trimeric intracellular intermediates involved in the signal transduction pathways of various YNF receptor family members. TRAF 1, 2 and 3 appear to mediate NF-κB, p38, mitogen activating protein kinase (MAPK) and c-Jun NH2-terminal kinase (JNK) activation. NF-kB signalling drives the upregulation of the ant-apoptotic proteins Bcl-Xl and Bcl-2. Additionally, APRIL binding to both BCMA and TACI has shown association with TRAF 6 and activation of the canonical Nf-κB signalling pathway. TRAFs activate the IKK γαβ complex, leading to phosphorylation and subsequent ubiquitination and degradation of NF-κB inhibitor I-κB, leading to release of NF-κB (Fu *et al.* 2006).

Within their survival niche (figure 1.5), long lived PCs provide immunity through sustained generation of immunoglobulin for decades and even the lifespan of the host. These antigen-specific antibodies are secreted constantly to maintain front line immunity against resurgent pathogens (Lightman, Utley and Lee 2019).

Soluble survival factors
- Il-6
- TNF-α
- BAFF
- APRIL
- CXCL12

Adhesion
- CD138
- CD44
- CXCR4/CXCL12

Intrinsic survival regulation
- Bcl-2
- Blimp1
- XBP1
- IRF4

Cellular associated
- Stromal cells
- Eosinophils

Plasma Cell

BM Stromal cells
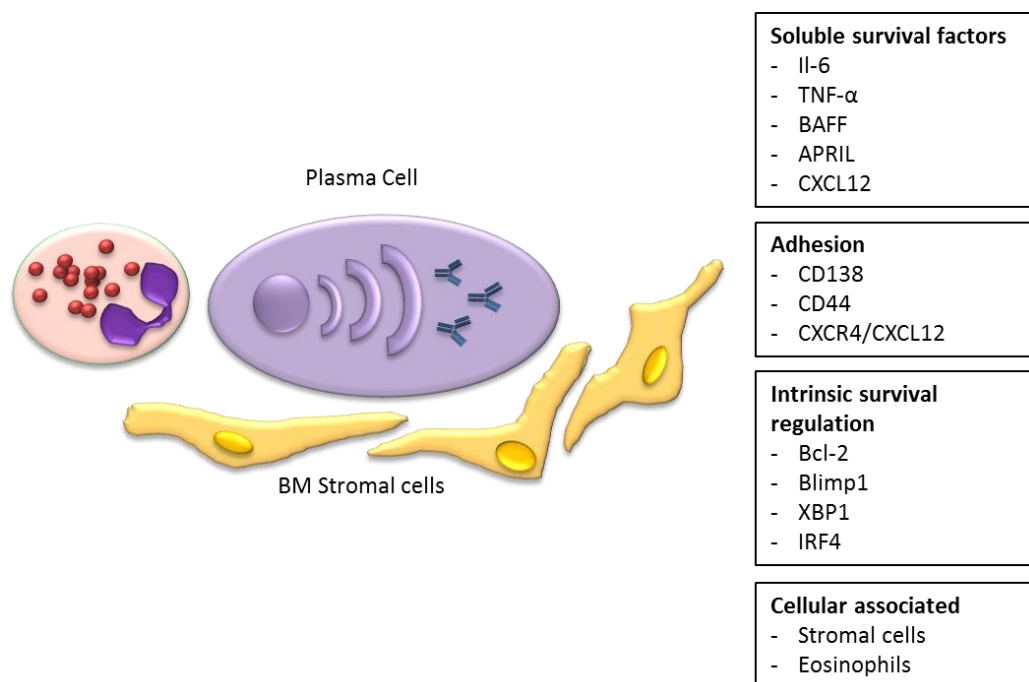
Figure 1.5 – Plasmablasts migrate to survival niches such as the BM via the CXCR4/CXCL12 axis. Once there, they differentiate into mature PCs. The BM survival niche enables long-term survival of PCs through the activity of soluble, intrinsic, adhesion and cellular survival factors, thereby enabling long-term immunity (Adapted from (Tarlinton *et al.* 2008)

In addition to PCs, memory B-cells are also a key contributor to maintaining long-term immunity. They are capable of surviving for extended periods of time, often decades, enabling them to respond to repeated exposures to the same antigen. Memory B-cells are strategically located at peripheral lymphoid organs, at sites such as the tonsillar epithelium (Liu *et al.* 1995) and splenic marginal zone

where there is greater antigen drainage (Tangye *et al.* 1998). When resurgent pathogens are detected, they mount a secondary immune response against their specific antigen by differentiating into PCs at a far greater rate than that of naïve B-cells. This results in the mounting of a rapid and more specific defence against a familiar antigen, thereby potentially preventing severe disease. Alternatively, memory B-cells may re-enter the germinal centre to undergo further rounds of affinity maturation allowing for even greater tailoring of the response to a subsequent re-infection (Tangye and Tarlinton 2009).

1.2 Chemokines and Chemokine receptors

Chemokines are cytokines that act as a chemoattractant to cells (Ozga, Chow and Luster 2021). Chemokines play a large role in both the innate and adaptive immune systems. As part of the innate immune response, they are involved in recruitment of leukocytes, monocytes, and neutrophils to sites of infection and wounds where they often work in conjunction with inflammatory cytokines. As part of the adaptive immune responses, they play crucial roles in the development and migration of B- and T- cells to lymphoid organs, germinal centres, and the bone marrow (Griffith, Sokol and Luster 2014).

Chemokines are categorised based on their structure, specifically the arrangement of two N-terminal cysteine residues (figure 1.6). The first class of chemokine is defined by presence of a single consensus cysteine, these are named C chemokines. The positioning of two consensus cysteines directly adjacent to each other or separated by a non-conserved amino acid is the basis for the next two categories of chemokine: CC chemokines and CXC chemokines, respectively. The final group, CX_3C chemokines possesses two cysteines separated by 3 amino acids, of which there is only one discovered member, CX3CL1 (Rot and von Andrian 2004).
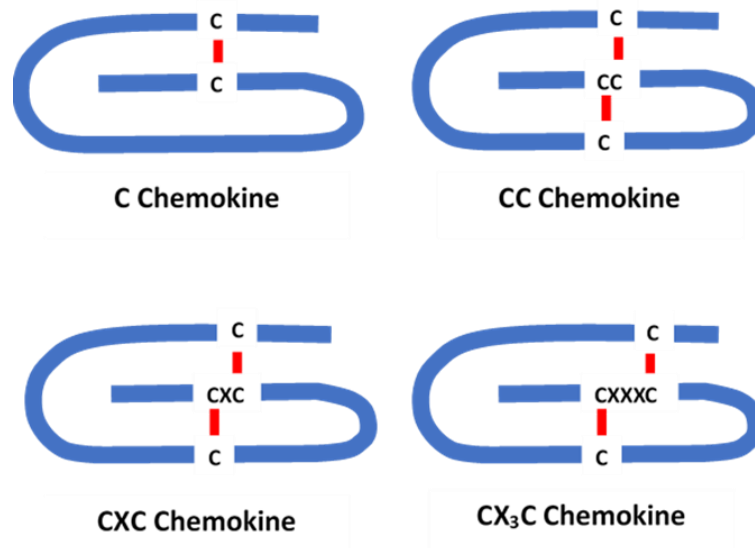
Figure 1.6 - **Basic representation of the different chemokine structures**. The simplest chemokines contain a single consensus cysteine (C chemokines). CC chemokines contains to adjacent cysteines. The number of amino acids separating cysteines determines whether a chemokine is categories as a CXC (one amino acid) or CX_3C chemokine (3 amino acids).

Cells follow the chemokine signals by moving along the chemokine concentration gradient to the source of the chemokine. Cells are able to recognise and respond to chemokines due to the presence of specific cell-surface seven transmembrane G protein-coupled receptors (GPCRs). Some GPCRs can interact with multiple chemokines, however some will only interact with one, e.g., CXCR4 (CXCL12), CXCR5 (CXCL13), CXCR6 (CXCL16), CCR9 (CCL25), CX3CR1 (CX3CL1), etc. Additionally, the downstream effect of these promiscuous GPCRs can vary, as some ligands may induce either an inhibitory or stimulatory effect (Kufareva, Salanga and Handel 2015).

Chemokine binding to a GPCR induces a conformational change in its structure, leading to interaction of the intracellular portion to heterotrimeric G-proteins. These G-proteins become activated and exchange guanosine diphosphate (GDP) for guanosine triphosphate (GTP). This allows for G protein disassociation into its constituent subunits; α and βγ. Both these moieties may now interact with downstream effectors to activate signalling responses (Gustavsson 2020).

1.2.1 Targeting chemokine receptors

Chemokine receptor antagonists have been approved for antiviral therapeutics as entry inhibitors, most notably for HIV, in conjunction with other antiviral therapeutics. CCR5 and CXCR4 act as co-receptors to allow the T cell-tropic (X4) and macrophage-tropic (R5) HIV-1 strains entry into target T-cells and macrophages respectively. Chemokine Inhibitors prevent the binding of the HIV envelope to CCR5 or CXCR4 receptor (Grande *et al.* 2019). Maraviroc and Enfuvirtide are CCR5 antagonists. Maraviroc blocks the HIV protein gp120 from associating with CCR5, preventing viral protein gp41 from initiating viral membrane fusion to host membrane (Tamamis and Floudas 2014). Enfuvirtide

binds to the gp41 subunit of the viral envelope glycoprotein, preventing conformational changes required for the fusion of host and viral membranes (Matthews *et al.* 2004). Treatment targeting CCR5 can cause a shift in tropism, allowing the HIV strain to target CXCR4. Additionally there are strains that can target both chemokines for entry. Therefore, dual antagonism of both receptors can overcome this. AMD3100 (Plerixafor) is a selective CXCR4 antagonist (Schols *et al.* 1997). It blocks interaction of gp120 with CXCR4 similarly to Maraviroc, however due to dosage issues and side effect issues; it is not used in a clinical setting (Liu *et al.* 2015)

Development of therapeutics targeting chemokine receptors in an autoimmune disease setting have been particularly unsuccessful for a number of reasons. Firstly, the efficacy of compounds to decrease receptor activity can be diminished due to a failure to have sufficient levels of compound within the plasma to neutralise the receptor. Whilst some compounds have been shown to block up to 90% of a receptor activity, this may not be sufficient, as activation of only a small population of target cells could be sufficient to drive disease progression (Horuk 2009). Next, Drug development for GPCRs can also be impeded by the development of off target effects. A compound developed against one target may display off target effects through interaction with other members of that receptor family, despite a lower binding affinity (Hesselgesser *et al.* 1998).

Additionally, several receptors can be involved in progressing the pathophysiology of a disease. This redundancy of the target receptor has been evidenced in trails for drug targets for CCR2, ligands for which (CCL2 and CCl5) are highly expressed in the joints of patients with RA, leading to recruitment of monocytes. Whilst highly tolerable, compound MK-0812 failed to show any clinical improvements over the placebo (Braddock 2007). Furthermore, *in vivo* studies of bleomycin lung models for CXCR3 inhibitor AMG-487 showed uptp 7-% reduction in lung inflammation. The remaining inflammation could have been driven by receptors other than CXCR3 (Horuk 2009). These are both indicative of additional players in the pathophysiology of this disease. A potential solution to this problem would be the use mulptiple GPCR targeting compounds, however thorough testing would be necessary.

Further complicating drug development in this area is the problem of species specificity. Compounds that are effective in humans may have limited or zero efficacy in other species used *in vivo*. For example, the CCR1 agonist CP-481,715 is selective for human CCR1 but does not block the effects of CCL3 on mouse, rat, guinea-pig, dog, rabbit or monkey CCR1 (Gladue *et al.* 2003).

1.2.2 Innate immune response

Pathogens can stimulate chemokine production in nearby macrophages and dendritic cells as well as from non-immune cells, e.g. stromal cells resident in the affected tissue. Cells utilise pattern

recognition receptors such as TLRs to identify invading pathogen associated molecular patterns present on pathogens. Cells that have detected pathogens release chemokines, namely the ligands of the more promiscuous chemokines receptors, such as CCR1, CCR2, CCR3, CCR5, CXCR2, and CXCR3 and various cytokines such as TNF-α, IFNγ, interleukins and interferons (Luster 1998) which can amplify the release of cytokines through a paracrine effect. The release of chemokines summons more front-line immune cells such as NK cells (Bernardini *et al.* 2008) neutrophils (De Filippo *et al.* 2013), dendritic cells (Biragyn *et al.* 2002) and additional macrophages (Garcia-Zepeda *et al.* 1996). The chemokines usually involved in these processes are known as 'inflammatory chemokines' and often bind to multiple chemokines receptors and vice versa (Turner *et al.* 2014; Møller *et al.* 2005).

Migration of leukocytes stimulated by a chemoattractant undergo a process of polarisation, generating filamentous actin at the front of the cell, creating pseudopods at their leading edge and a uropod at their trailing end. This actin reorganisation in the pseudopods allows the cell to extend and retract at the uropod, enabling locomotion towards the chemoattractant. Chemokine receptors accumulate at the leading edge and act a sensor to direct migration along the chemokine gradient (Nieto *et al.* 1997; Wilkinson 1986).

1.2.3 Adaptive immune response

Chemokines that are more often involved in migration of cells of the adaptive immune response are called homeostatic chemokines. These cells are usually more monogamous than their inflammatory cousins, often forming a unique pairing with a specific GPCR. (Rot and von Andrian 2004)

During an adaptive immune response, first dendritic cells acquire antigen. From the BM, DCs migrate towards peripheral tissues and secondary lymphoid organs where they obtain and process lymph-borne, intestinal, or blood-borne antigens, depending on the tissue in which they reside (MartIn-Fontecha *et al.* 2003).

Circulating naïve CD4+ T-cells express CCR7 and CXCR4 and respond to CCL21 secreted from lymph vessels and migrate towards the CCL19/21 high T-cell zone. After this, they downregulate CCR7 and upregulate CXCR5, which follows the CXCL13 gradient towards to interfollicular region of the lymphoid organ (figure 1.7) (Förster *et al.* 1999).

Alongside this, the DCs must migrate to the T-cell zone of the lymphoid organ, where they mature and begin educating the resident T-cells about the captured antigen. CCR7 is upregulated to enable interaction with the T-cells via CCL21 and CCL19 (figure 1.7) B-cells also utilise these chemokines via CCR7 and CXCR5 to migrate to the T: B interface, where T-cells may activate the B-cells. Following this both CD4+ T-cells and B-cells downregulate CCR7 but maintain CXCR5 enabling escape from the T-cell

zone and then migration towards the follicle. Here CD4+ Tfh cells mature to Tfh cells and initiate the CD40-CD40L interaction allowing GC B-cells to begin rapid proliferation (figure 1.7). Within the GC, B-cells must migrate between the DZ and LZ to undergo rounds of affinity maturation. Centrocytes move to the LZ along the CXCR5/CXCL13 gradient. Once selection has been completed, cells return to the dark zone, which contains CXCL12-producing reticular cells that attract the cells back via CXCR4. The cells then undergo further proliferation and maturation (figure 1.8) (Gunn *et al.* 1998; Ferretti *et al.* 2016; Lian and Luster 2015; Grant *et al.* 2020; Bromley, Mempel and Luster 2008; Hickman *et al.* 2011; Groom *et al.* 2012; Sung *et al.* 2012; Ansel *et al.* 1999; Castellino *et al.* 2006; Stebegg *et al.* 2018; Klein and Dalla-Favera 2008).
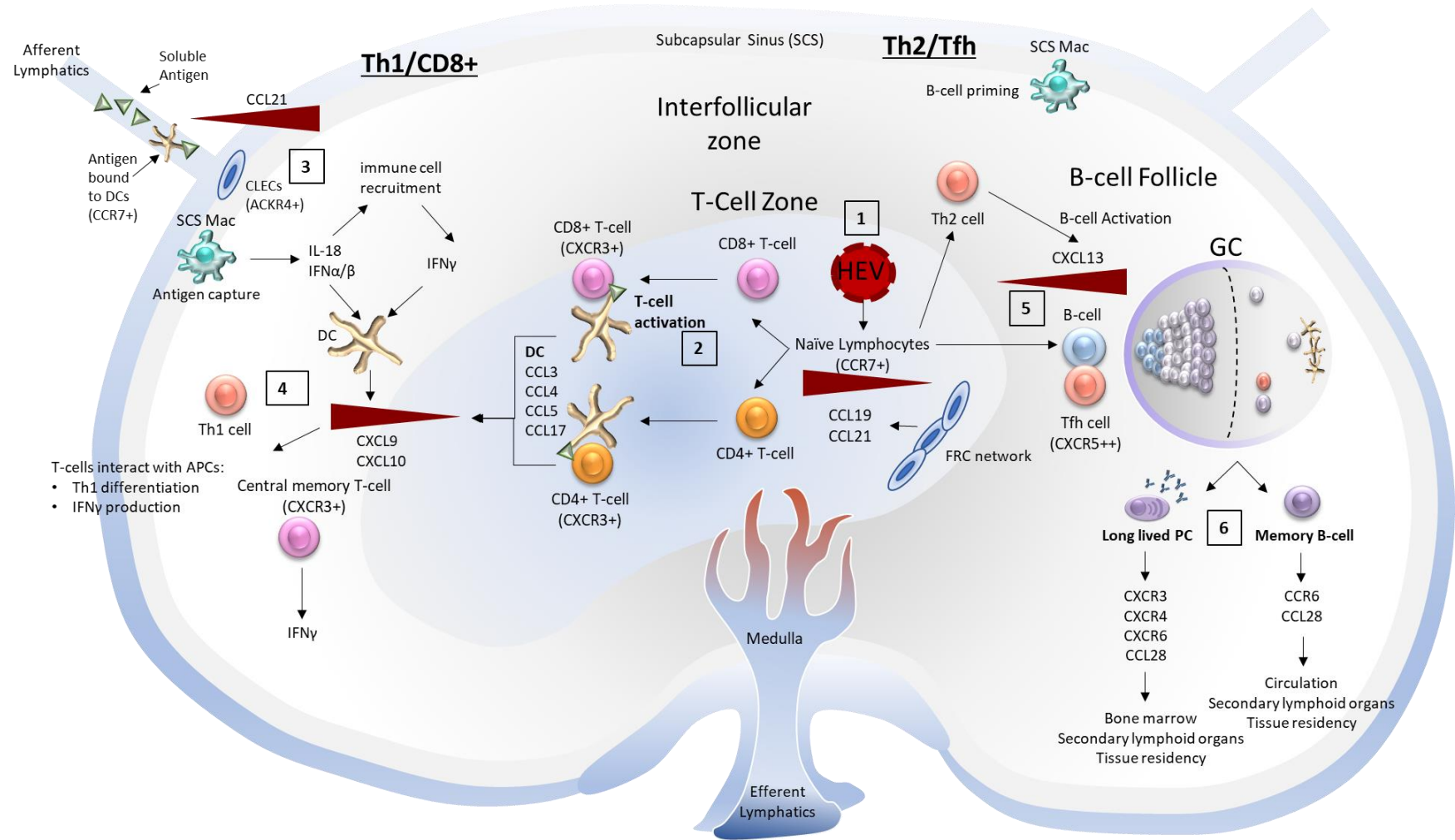
Figure 1.7. - Chemokine interactions within the lymph node drive maturation of B-cells and T-cells, culminating in the development of mature plasma cells, memory B-cells, helper T-cells, and memory T-cells. (1) Naïve lymphocytes expressing high levels of CCR7 are directed towards the lymph node by CCL19 and CCL20 produced from the fibroblastic reticular cell (FRC) network. These naïve lymphocytes enter the lymph node from the blood via high endothelial venules (HEV). (2) T-cells also enter the lymph node through HEVs and migrate through the T-cell area. DCs produce CCL3, CCL4, CCL5 and CCL17 to attract CD8+ T-cells through interaction with CCR5 and CCR4. DCs become licensed by CD4+ T-cells, allowing them to activate naïve CD8+ T-cells which upregulates CXCR3 on the CD8+ T-cell. (3) Antigen-bound DCs also express CCR7 and migrate and enter the lymph node through the afferent lymphatics. Ceiling lymphatic endothelial cells (CLEC) within the subcapsular sinus (SCS) express atypical chemokine receptor 4 (ACKR4) that regulates CCL21 abundance, creating a gradient that allows for DC entry into the lymph node. Specialised macrophages (SCS MAC) scavenge antigen and release IL-18 and IFNα/β. (4) IFNα/β release induces stromal cells and DCs to secrete CXCL9 and CXCL10 which helps activate and prime CD4+ T-cells. CD4+ T-cells travel along the CXCL9 and CXCL10 axis (via CXCR3) to the interfollicular zone, here they mature to become Th1 cells. Additionally, CD8+ T-cells move to the edge of the T-cell zone via CXCL10 and eventually become CD8+ central memory T-cells capable of providing an enhanced secondary immunity against viruses, bacteria and cancer cells. (5) Naïve T-cells activated by a Th2-type inducing stimulus (e.g., IL-4 produced by macrophages) exit the T-cell zone via a CXL13/CXCR5 gradient and move towards the B-cell follicle where they interact with DCs. Here they assist in B-cell activation as Th2 cells. Tfh cells downregulate CCR7 and upregulate CXCR5 to move towards the T-B border of the follicle aiding in activation of the GC reaction. B-cells also follow the CXCL13 gradient to the B-cell follicle. Following activation, they form GCs. Within the GC, B-cells cycle through the DZ and LZ via CXCL12 and CXCL13 and undergo affinity maturation. (6) Following affinity maturation, B-cells mature into either plasmablasts or memory B-cells. PBs migrate via chemokine gradients to secondary lymphoid organs, BM or other tissues where they become established PCs. Memory B-cells similarly migrate along chemokine gradients towards lymphoid organs and other tissues. They may also remain in the circulation. Figure adapted from Lian and Luster (2015).
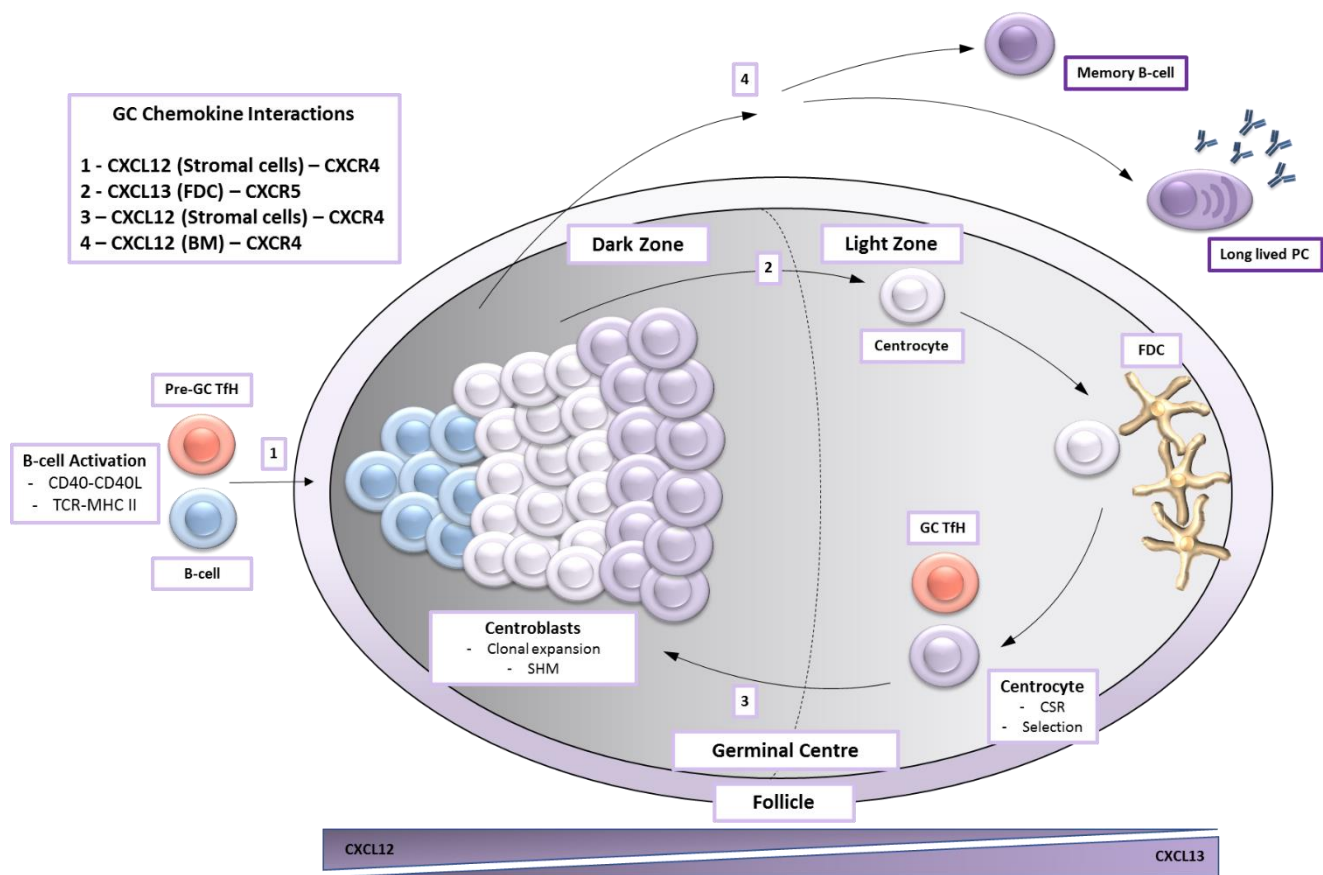
Figure 1.8. - Diagram depicting the generation of memory B-cell and long-lived plasma cells via the germinal centre reaction. In the follicle of a secondary lymphoid organ naïve B-cells become activated and move to the GC and between the dark and zones following specific chemokine gradients. Activated B-cells enter the GC following the CXCL12 gradient and take up residence in the DZ. Here the cells undergo clonal expansion and SHM. B-cells then follow CXCL13, released from follicular dendritic cells (FDCs) to enter the LZ where they are able to undergo CSR and affinity-based selection. B-cells will move between both zones numerous times until affinity maturation is completed. After this process, generated plasma cells will follow the CXCR4 gradient to migrate to their survival niches within the BM. Figure adapted from (Klein and Dalla-Favera, 2008) and (Stebegg *et al*, 2018).

1.3 Waldenström macroglobulinemia

1.3.1 Overview

Waldenström macroglobulinemia (WM) is a B-cell neoplasia that is characterised by malignant B-lymphocytes that retain the capability to differentiate into PCs. Similar to the normal long-lived PC, WM cells are recruited through CXCL12-CXCR4 interactions and localise to areas adjacent to the bony trabeculum (Ngo *et al.* 2008). At these sites, WM cells encounter other BM resident cells that provide survival factors. The resulting WM PCs secrete high levels of immunoglobulin M (IgM) paraprotein (Hunter *et al.* 2017).

WM is a rare disease and incidence is more frequent in elderly populations. WM patients may often present with one of two asymptomatic forms that precede symptomatic WM. In the first of the precursor phases, patients may present with what is known as IgM monoclonal gammopathy of undetermined significance (MGUS), which is characterised by a serum IgM level below 3 gm/dl and a BM infiltration rate of less than 10%. Following this, patients may then go on to develop smouldering WM, where serum IgM increases above 3 gm/dl and BM infiltration increases beyond 10% (Mailankody and Landgren 2016). Patients present with no signs of disease but are at an increased risk of developing symptomatic WM. About 25% of patients with IgM MGUS will go on to develop a symptomatic lymphoproliferative disorder within 15 years (Kyle *et al.* 2005). For smouldering WM patients, 55% of patients will have progression to symptomatic disease in 5 years (Kyle *et al.* 2009), (Ansell *et al.* 2010).

Clinical manifestations of WM are the result of increased BM infiltration and increased IgM secretion from malignant PCs. High serum IgM leads to symptoms of hyper-viscosity syndrome, which presents as headache, retinopathy, stroke, seizures, and coma. Other signs include deficiency of blood cells and organ enlargement (Ansell *et al.* 2010). For asymptomatic patients with IgM MGUS, life-long careful observation is the recommended course of action. However, for those patients that have progressed to symptomatic disease, the main aims of current therapeutics are to limit symptoms, as there is no cure for WM (Castillo and Treon 2017).

1.3.2 WM aetiology

1.2.2.1 MYD88^{L265P} mutation

Whole genome sequencing of bone marrow cells from WM patients has uncovered a major somatic variant leading to a single nucleotide change in myeloid differentiation primary response gene 88 (*MYD88*). This induces an amino acid change at position 265 (Treon *et al.* 2012). This mutation (L265P), is now thought to be the most significant somatic mutation in WM, occurring in greater than 90% of patients (Xu *et al.* 2013). MYD88 is an adaptor protein than transduces signals for the interleukin-1 (IL-1), and TLR signalling pathways by forming IL-1 receptor-associated kinase (IRAK) signalling complex. This mediates the activation of signalling pathways and transcription factors, most notably STAT3 and NF-κB (Poulain *et al.* 2013).

NF-κB pro-survival signalling can also be induced through BTK as a result of BCR, TLR signalling and chemokine receptor signalling (figure 1.9) (Pal Singh, Dammeijer and Hendriks 2018; López-Oreja *et al.* 2021). BTK is a non-receptor tyrosine kinase that plays an important role in B-cell maturation. Upon stimulation of the BCR, BTK is recruited to the membrane through interaction with phosphatidylinositol-3, 4, 5-triphosphate (PIP3), where it is phosphorylated by SYK or SRC family kinases. This phosphorylation activates BTK which then phosphorylates phospholipase Cγ2 (PLCγ2). Activated PLCγ2 hydrolyses PIP2 into diacylglycerol (DAG) and inositol triphosphate (IP3). DAG activation can lead to downstream activation of ERK and NF-κB (Woyach, Johnson and Byrd 2012). MYD88 is also a target of activated BTK, thereby promoting the formation of the myddosome signalling complex with serine/threonine kinase IRAK4 that further enhances NF-κB signalling and drives proliferation and B-cell survival, thereby linking BCR activation with MYD88 stimulation. MYD88^{L265P} can therefore promote constitutive NF-κB signalling that drives cancer cell survival.
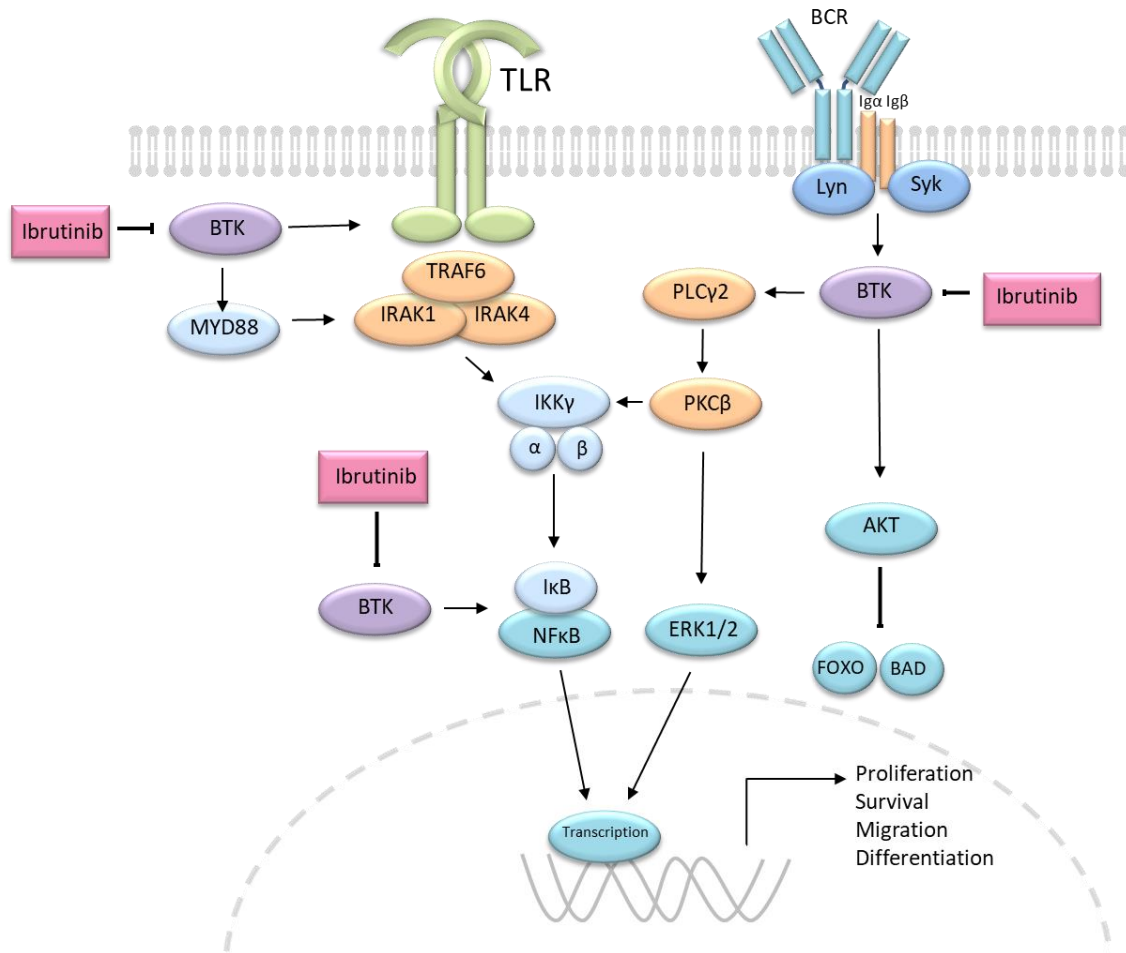
Figure 1.9 – The BCR and TLR receptors can both signal through BTK. TLR signalling forms the Myddosome with IRAK4 through activation of MYD88. The Myddosome signalling complex then induces downstream NF-κB. Upon BCRs stimulation, BTK is recruited to the membrane through interaction with phosphatidylinositol-3, 4, 5-triphosphate (PIP3). Here it is phosphorylated by SYK or SRC family kinases. This phosphorylation activates BTK which then phosphorylates phospholipase Cγ2 (PLCγ2). Activated PLCγ2 hydrolyses PIP2 into diacylglycerol (DAG) and inositol triphosphate (IP3). DAG activation can lead to downstream activation of ERK and NF-κB. Ibrutinib is a BTK inhibitor and can block both BCR and TLR signalling by inhibition of BTK tyrosine phosphorylation activity, thereby blocking survival signals upstream of ERK and NF-κB. Figure adapted from Singh, Dammeijer and Hendricks, 2018 and López-Oreja *et al*, 2021).

1.2.2.2 CXCR4^{WHIM} mutation

About 30% of WM patients may also acquire a CXCR4 mutation (figure 1.10), most frequently on serine 338 (Hunter *et al.* 2014). CXCR4 is a G protein coupled heterotrimeric chemokine receptor. The main ligand to bind to CXCR4 is CXCL12, a chemokine important for chemotaxis and B-cell homing to the bone marrow as described above. CXCL12/CXCR4 signalling is involved with MEK and PI3K signalling pathways, which are important for cell survival and proliferation.
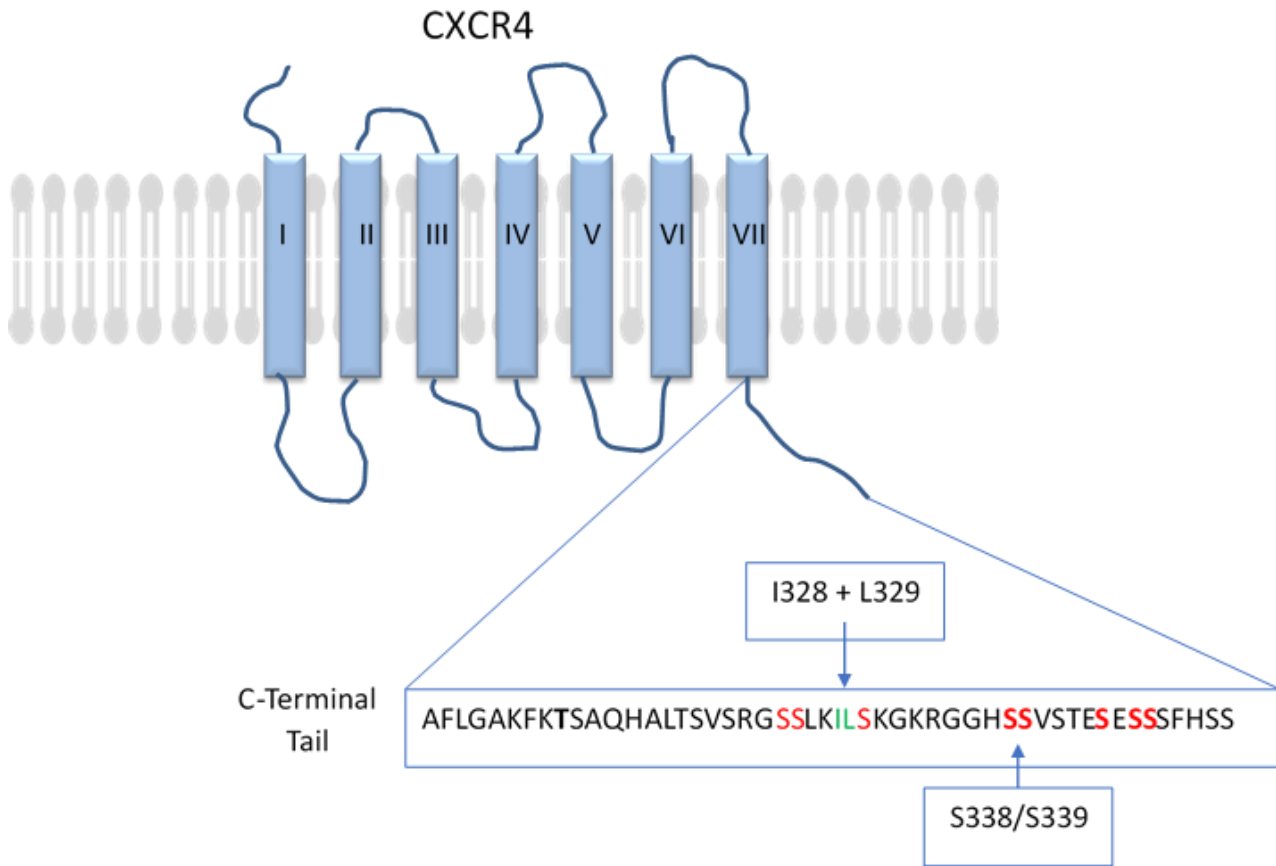
Figure 1.10 – CXCR4 structure and location of common mutations. CXCR4 is a 7 transmembrane G protein coupled receptor present on the surface of many cell types. It is equipped with a N-terminal extracellular tail that is involved in interaction with CXCL12. On the intracellular side, the C-terminal tail contains numerous residues that are involved in mechanisms relating to arrestin recruitment and receptor internalisation and packaging. This figure details the residue components of the CXCR4 C-terminal tail, and the key residues involved in the desensitisation and internalisation process.

CXCR4 interacts with CXCL12 through its N-terminal extracellular tail. The extracellular domain contains 17 residues that are involved in this binding, the first 6 of these play the most dominant role in this process (Gozansky *et al.* 2005). CXCR4 expression is regulated by a tightly controlled desensitisation, internalisation, and degradation/recycling process (figure 1.11) (Busillo and Benovic 2007). Once CXCL12 binds to CXCR4, G protein-coupled receptor kinase (GRK) localises to the C-terminus of CXCR4, and it phosphorylates the C-terminal tail. This recruits β-arrestins which bind to and uncouples the receptor from further G protein activation. Following desensitisation, CXCR4 is then internalised at which point it may be degraded by the lysosome or shuttled back to the membrane.

Table 1.1 - Key residues within the intracellular C-terminal tail of CXCR4 involved in receptor desensitisation

C-terminal tail residue	Function	Reference
S324	Lysosome packaging	Signoret *et al* (1998) Luo *et al* (2017)
S325	Lysosome packaging	Signoret *et al* (1998) Luo *et al* (2017)
I328	Endocytosis	Signoret *et al* (1998)
L329	Endocytosis	Signoret *et al* (1998)
S330	Lysosome packaging	Signoret *et al* (1998) Luo *et al* (2017)
S338	Receptor internalisation	Orsini *et al* (1999)
S339	Receptor internalisation	Orsini *et al* (1999)
S346	Arrestin recruitment	Jiansong *et al* (2017)
S347	Arrestin recruitment	Jiansong *et al* (2017)

The C-terminal tail of CXCR4 is the region necessary for the desensitisation process following CXCL12 stimulation. Notable phosphorylation sites along the C-tail include a region of key serine residues, namely S321, S324, S325, S330, S338 and S339 (Busillo *et al.* 2010). S338 and S339 are critical for receptor internalisation (Orsini *et al.* 1999). Additionally, the isoleucine (I328)/leucine (L329) motifs may play a role in endocytosis of this receptor (Signoret *et al.* 1998). S324, S325 and S330 have been implicated in regulation of internalised CXCR4 into lysosomes for degradation (Signoret *et al.* 1998) S346 and S347 are necessary for arrestin recruitment and initiation of CXCR4 receptor desensitisation (Luo *et al.* 2017) (figure 1.10 and table 1.1) (Teicher and Fricker 2010).

CXCR4 WT Receptor   CXCR4 WHIM (S338 Mutation) Receptor

CXCL12   CXCL12
CXCR4   CXCR4

Receptor Recycling

Gα Gγ Gβ   GRK   Gα Gγ Gβ   GRK

No desensitisation

MEK   PI3K   β-Arrestin   MEK   PI3K

                  Clathrin

                            CXCR4 signalling
                            reduced

Endosome

Receptor   Ubiquitination and
internalisation   lysosomal
(desensitisation)   degradation

                                      Survival
                                      Proliferation
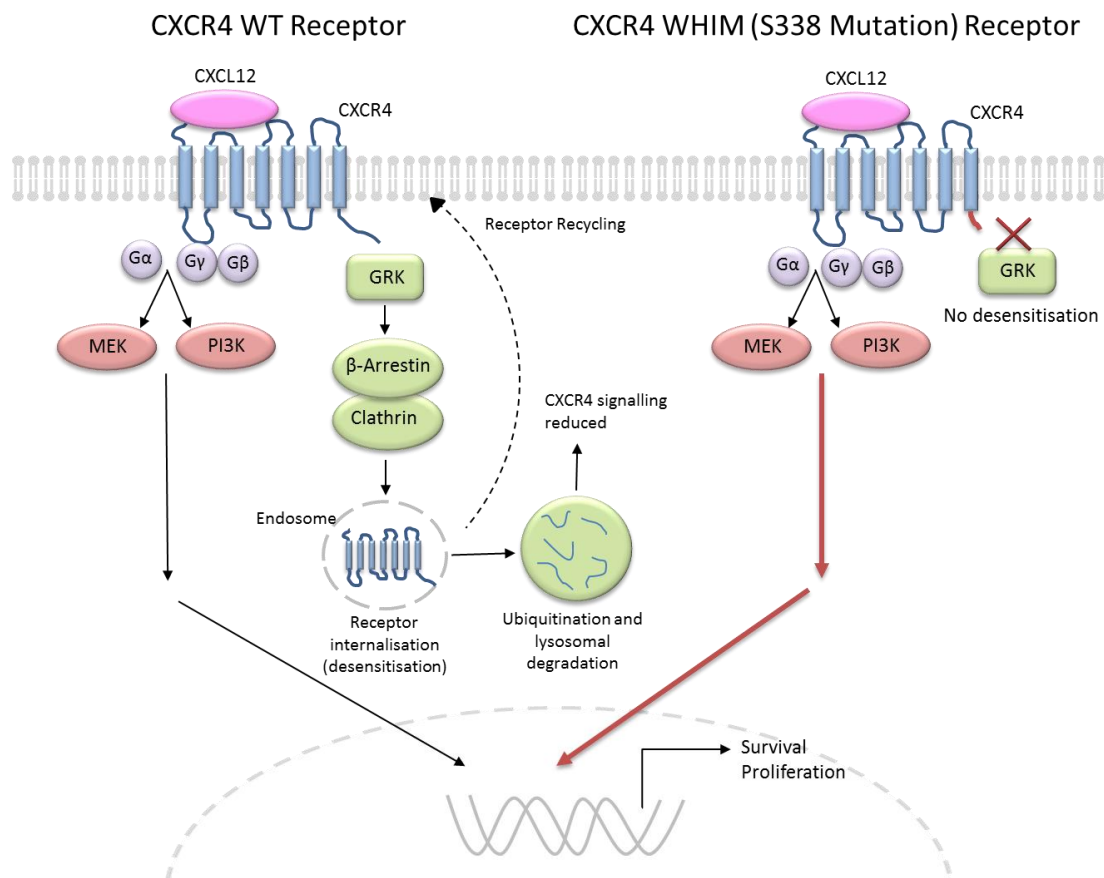
Figure 1.11 – CXCR4 receptor signalling in both wild type cells (left) and WHIM mutated cells (right). Once CXCL12 (SDF1) binds to CXCR4, survival signalling is activated. In wild type cells, GRK phosphorylates the C-terminal tail of CXCR4, inducing desensitisation of the receptor. At this point CXCR4 may be degraded by the lysosome or it may be recycled back to the membrane. In either case, CXCR4 signalling is tightly controlled. In cells expressing CXCR4 WHIM, the C-terminal tail is truncated, preventing phosphorylation by GRK. This prevents CXCR4 desensitisation, leading to prolonged CXCR4 survival and proliferative signalling. Figure adapted from Teicher and Fricker, 2010.

In B-cells, stimulation of the BCR can promote CXCR4 signal propagation and receptor recycling through BTK, confirmed by addition of Ibrutinib, which reduces surface levels of CXCR4 through blockage of BTK, thereby impeding phosphorylation and receptor signal transduction, preventing CXCR4 receptor recycling (Chen *et al.* 2016).

The CXCR4 desensitisation mechanism exists to switch off CXCR4 signalling when required; however, this regulation is lost in CXCR4 (S338X) WM cells. The occurrence of an early stop codon truncates the C-terminus of the CXCR4 receptor, preventing GRK mediated phosphorylation, and therefore recruitment of arrestins that mediated receptor internalisation (figure 1.10). This results in uninterrupted CXCR4 signalling. Consistent with this CXCR4 signalling enhances proliferative and survival signals, which increases malignancy.

Table 1.2 - CXCR4 mutations present in WM patients. Of these patients, they may harbour one of several somatic variants in CXCR4, a few of which a described here. Of these validated variants, each one induces an effect functionally similar to mutations associated with WHIM syndrome. The mutations described do not affect the transmembrane portion of CXCR4 and therefore do not affect ligand binding or G-protein signalling. Instead, they disrupt the C-terminal tail, specifically resulting in the loss of regulatory phosphor-serines involved in receptor internalisation. Often an insertion mutation may be present in addition to a S338X non-sense mutation.

CXCR4 Mutation	Mutation	Amino Acid change	Gene Change	Effect
CXCR4 **r.931_933insT**	Frameshift	T311fs	Insert T	Truncation of C tail
CXCR4 **r.952_954insA**	Frameshift	T318fs	Insert A	Truncation of C tail
CXCR4 **c.1013C<A**	*Nonsense*	S338X	C>A	Truncation of C tail
CXCR4 **c.1013C<G**	*Nonsense*	S338X	C>G	Truncation of C tail
CXCR4 **c. 1012_1013delT**	Frameshift	S338fs	Delete T	Truncation of C tail
CXCR4 **c. 1017_1018del T**	Frameshift	S339fs	Delete T	Truncation of C tail
CXCR4 **c. 1031_1033delCT**	*Nonsense*	S344X	Delete C/T	Truncation of C tail

The S388 mutation in WM patients is similar to those found in WHIM (warts, hypogammaglobulinemia, infection and myelokathexis) syndrome and is one of a number of mutations identified in CXCR4 (table 1.2) (Xu *et al.* 2016; Hunter *et al.* 2014; Poulain *et al.* 2016). WHIM syndrome is characterised by defects in marrow trafficking of CXCR4^{+} cells, notably neutrophils, which are retained in the bone marrow and depleted from the circulation (myelokathexis), leading to increased susceptibility to infection such as HPV, hence the increased incidence of warts in these patients. Furthermore, WHIM patients often experience hypogammaglobulinemia, a loss of circulating IgG, IgM and IgA, indicative of a low level of B-cells found in affected individuals (McDermott and Murphy 2019).

Similarly, an additional feature of WM B-cells is their abnormal accumulation in the BM, with CXCR4[WHIM] B-cells showing the highest bone marrow disease involvement (Treon *et al.* 2014). Additionally, long-lived PCs from mice expressing CXCR4[WHIM] fail to populate the BM, instead immature proliferating PBs accumulate in PC BM niches. Together this suggests that due to the perturbed WM B-cell trafficking, these cells obtain a unique environment for differentiation (Biajoux *et al.* 2016).

1.3.3 CXCR4 downstream signalling

Downstream targets of CXCR4 include several non-receptor tyrosine kinases. Once CXCL12 is bound, a conformational change activates the trimeric G protein by inducing the dissociation of the Gα subunit. Gα inhibits adenyl cyclase, which produces cAMP. cAMP stimulates the activity of these non-receptor tyrosine kinases. Notable signalling pathways include the activation of the Ras/Raf/MEK/ERK pathway which regulates proliferation. ERK signalling can further be activated through the Gβγ subunit. This subunit activates phospholipase C (PLC). PLC hydrolyses PIP2 into IP3 and DAG, which

can activate ERK signalling. Alongside this, Gα and Gβγ can activates PI3K. PI3K can phosphorylate AKT, which affects cell proliferation, survival, and migration (Pozzobon *et al.* 2016).

Throughout B-cell differentiation, AKT phosphorylation may become rewired as the cells enter the different stages. Notably it has been reported that GC B-cells express high levels of PDK1, which catalyses the phosphorylation of the T308 residue of AKT, whereas naïve B-cells express high levels of mTORC and PTEN which preferentially catalyses AKT at the S473 residue (Downward 1998; Luo *et al.* 2019)

1.3.4 Treatments for WM

First line therapy for WM includes rituximab, an antibody against the B-cell surface molecule CD20 that signals to natural killer (NK) cells and macrophages to induce antibody dependent cellular cytotoxicity (Yelvington 2018). This is often combined with bendamustine. Similarly to alkylating agents, it induces DNA crosslinking or double strand DNA breaks, thereby preventing protein synthesis through initiation of the p53 induced stress response, leading to apoptosis (Kalaycio 2009). Bendamustine also inhibits mitotic checkpoints leading to mitotic catastrophe and additionally it has anti-metabolite activity (Leoni *et al.* 2008). The overall response rate for this treatment was 95%, with an improved progression free survival compared to dexamethasone, rituximab, and cyclophosphamide (DRC) another routine regimen for WM (Paludo *et al.* 2018).

While agents conventionally used in WM such as purine analogues and monoclonal antibodies effectively deplete the B-cell component of the disease, the PCs are not targeted (Varghese *et al.* 2009). This has a direct effect on patient management particularly when the symptoms relate to the production of IgM. Alternative strategies that show some specificity to the secretory PCs as well as the B-cell component are therefore required.

Moreover, for relapsed patients who are not suitable for chemotherapy or immunotherapy, an alternative treatment utilises BTK inhibitors (Pal Singh, Dammeijer and Hendriks 2018), (Pal Singh, Dammeijer and Hendriks 2019). Phase 3 trials have shown the effectiveness of ibrutinib and rituximab in combination in relapsed patients, with a progression-free survival rate of 82% for ibrutinib–rituximab versus 28% with placebo–rituximab (Dimopoulos *et al.* 2018).

BTK is activated in the signal transduction pathway downstream of the BCR and TLRs. WM cells expressing the MYD88[L265P] somatic mutation promote survival through activation of BTK signalling and introduction of a BTK inhibitor prevents MYD88 binding to BTK leading to inhibition of NF-κB, inducing WM cell apoptosis (Yang *et al.* 2013). Additionally, CXCR4, through activation of G_i proteins, can

interact with BTK and promote survival signalling alongside non-BTK dependant mechanisms (Pal Singh, Dammeijer and Hendriks 2018), (Bence *et al.* 1997).

Patients expressing CXCR4^{WHIM}, however show an increased resistance to ibrutinib treatment. 80% of relapsed/refractory WM patients expressing CXCR4 WT achieve a major response from ibrutinib therapy, whereas only 30% of patients expressing CXCR4^{WHIM} reach the same response (Treon *et al.* 2013).

WM cells expressing CXCR4^{WHIM} have a hyper-activated alternate CXCR4 receptor signalling that compensates for the loss of BTK, thereby reducing the effectiveness of ibrutinib and other therapeutics. Indeed, inhibition of ERK and AKT signalling in WM cells potentiates ibrutinib induced apoptosis, therefore suggesting that these signalling events are a powerful survival factors that probably contribute to the clinical presentation of CXCR4^{WHIM} WM patients (Cao *et al.* 2015).

There is therefore a need for a more detailed understanding of the CXCR4 signalling pathways and its interaction with other surface receptors, such as the BCR and CD19 that promote survival and drug resistance. Additionally, mapping the most significant pathways would enable the formulation of alternate kinase inhibitor combinations that would best combat the cooperation between these receptors and potentially inform future therapeutics.

1.4 B-cell Co-stimulatory Receptors

1.4.1 CD19

Whilst surface immunoglobulin is the most notable receptor for driving B-cell differentiation, there are important accessory receptors that assist in modulation of signals involved in this process. B-lymphocyte antigen CD19 is a 95 kd type I transmembrane glycoprotein possessing two extracellular Ig like domains and a large cytoplasmic tail containing nine tyrosine residues that, when phosphorylated, enable docking of SH2 domain containing proteins (Fujimoto *et al.* 2000).

CD19 is expressed during all phases of the B-cell lineage, beginning at immunoglobulin gene rearrangement, and peaking on mature B-cells. This expression is maintained throughout the GC reaction. Expression however does decrease as the cells transition into PCs, but not entirely. CD19 is also expressed highly on many B-cell malignancies such as acute and chronic lymphoblastic leukaemias (ALL/CLL), and various B-cell lymphomas (Cooper *et al.* 2004; Aldoss and Forman 2020)

CD19 exists within a complex containing CD21, CD81 and CD225. This complex interacts with the BCR, helping to reduce the threshold for B-cell activation likely through the generation of an amplification loop. For the BCR to become activated, it requires protein tyrosine kinase activation. LYN, the main Src family protein kinase, is necessary for the initiation of BCR signalling and the formation of this

amplification loop. CD19 regulates this by utilising its cytoplasmic tail containing the 9 tyrosine residues to act as a scaffold, that when phosphorylated during BCR-ligand interactions, function as SH2-docking motifs that recruit regulatory BCR associated tyrosine kinases, such as LYN, thereby amplifying BCR signalling and activating downstream pathways involving PI3K, AKT and BTK (Fujimoto *et al.* 2000; Morbach *et al.* 2016; Tedder, Inaoki and Sato 1997).

Specifically, BCR and/or CD19 ligation induces CD19 phosphorylation by LYN at tyrosine 513, which then binds to this tyrosine via is SH2 domain, leading to recruitment of LYN and subsequent phosphorylation of tyrosine 482. This in turn leads to further LYN recruitment and phosphorylation at tyrosine 482. This phosphorylation, induces conformational changes in CD19, allowing tyrosine 391 to become phosphorylated, which recruits VAV, itself phosphorylated by LYN. At this point, LYN may lose its SH2 domain binding affinity and release CD19, allowing further LYN binding and activation, creating the amplification loop that initiates a cascade of signalling events involved in B-cell differentiation. Furthermore, release of CD19, may allow the tandem SH2 domains of PI3 kinase to interact with CD19 tyrosines 482 and 513. Therefore, CD19 plays a crucial role in recruiting protein tyrosine kinases required for BCR signalling (Fujimoto *et al.* 2000).

Additionally, CD19 interacts with other protein kinases, including other Src family kinases and RAS kinases (Sato, Jansen and Tedder 1997). BTK associates with CD19 following BCR ligation, though not via phosphorylated tyrosine residues on CD19, instead likely through associated molecules. It is thought that CD19 aids in activation and prolongation of BTK signalling. Whilst CD19 and BTK cooperation aids in BCR signalling, loss of CD19 or BTK alone only moderately affects signalling responses, whereas loss of both severely dampens responses. This data supports the notion that CD19 acts a signalling hub through collaboration with various receptors and protein kinases (Fujimoto *et al.* 2002).

CD19 expression has been experimentally depleted to observe defects in B-cell maturation. Mouse models deficient for CD19 show normal levels of B-cell resident within both the BM and peripheral circulation, however splenic B-cell numbers are diminished suggesting CD19 is not crucial for early B-cell development but is important for mature B-cell differentiation and potentially the GC reaction. Indeed CD27+ memory B-cell generation is diminished in CD19 deficient patients. Additionally, in response to both T-independent and T-dependant stimulation, a reduced rate of proliferation and immunoglobulin production has been observed. In contrast, overexpression of CD19 negatively affects immature B-cell maturation but enhances proliferation of mature B-cell populations (Engel *et al.* 1995; Rickert, Rajewsky and Roes 1995; van Zelm *et al.* 2006).

Within the context of CXCR4, on the surface of B-cells CXCR4 localises to the BCR on CD19-IgD islands within nanometre sized proximity and are functionally connected. Stimulation of either CXCR4 or the BCR induces phosphorylation of CD19 (Keppler *et al.* 2015). It has been proposed that CD19 can be redeployed as a transmembrane scaffold for additional receptor signalling, including CXCR4. Indeed, B-cells with altered CD19 membrane mobility that are stimulated with CXCL12 showed diminished AKT and FOXO phosphorylation, suggesting that CD19 malfunction results in failure of PI3K activation via CXCR4 (Keppler *et al.* 2015). Therefore, CD19 may act as a central hub for signalling within B-cells and may specifically aid in promoting CXCR4 mediated differentiation and survival signalling. In WM cells this may represent a unique mechanism which these cells may rely on to survive.

Additionally, the IgD-class BCR expression is crucial for functional CXCR4 function on mature B-cells that have not yet undergone class-switch recombination, indicated by calcium mobilisation disruption in CXCL12 stimulated IgD$^{-/-}$ B-cells. Furthermore, this crosstalk is mediated by CD19 via the actin cytoskeleton, which restores functional CXCR4 PI3K/AKT and ERK signalling in IgD BCR-deficient B-cells (Becker *et al.* 2017). Thus, CXCR4 deploys unique downstream signalling mechanisms in the B-cell lineage that are likely to be altered during differentiation and may exhibit additional adaptations in the context of WM.

1.4.2 IgD vs IgM signalling

The BCR is composed of a membrane bound immunoglobulin connected to a signal transduction region, itself composed of Igα and Igβ. All immunoglobulin isotypes have identical antigen specificity and are associated with the same signalling heterodimer (Igα and Igβ) and other signalling proteins such as SYK, LYN and BTK (Maity *et al.* 2018).

In naïve B-cells, the BCR is either an IgD or and IgM protein. Despite providing similar function for antigen binding and eventual GC generation, the IgD BCR and IgM BCR signalling differs. IgM is the predominant form of the BCR within the BM during B-cell development, but once the B-cells move from this environment and populates peripheral lymphoid organs, the B-cells are able to express the IgD phenotype.

It has been proposed that IgD plays a greater role in B-cell homeostasis and B-cell selection (Geisberger, Lamers and Achatz 2006). The BCR can induce constitutive tonic survival signalling in the absence of antigen stimulation and following antigen binding, signal transduction events that actively promote B-cell survival. Closer inspection shows cross-linking of the IgM BCR on murine splenic B-cells induces a strong survival signal, whereas the IgD BCR transmits a tonic survival signal, but cross-linking negatively affects survival. Stimulation through both BCRs induces a moderate survival signal; together this indicates opposing roles for both isotypes. IgD may diminish antigen-induced survival signalling

potentially for restricting non-specific or self-antigen generation (Yasuda *et al.* 2018). Opposingly, the pro-survival IgM signalling may play a crucial role in the maintenance of malignant WM cells.

1.4.3 Relationship between immunoglobulin Isotype and plasma cell fate

The WM cell of origin is a B-cell that has undergone somatic mutation but not isotype switch events. Since class-switched WM are extremely rare, there may be unique properties related to the IgM signalling. The switching event can modulate the fate of B-cells as the different classes of BCR can induce variability in signal transduction (Boothby, Hodges and Thomas 2019; Sahota *et al.* 2002).

For example, during the germinal centre reaction, IL-4 induces antibody class switching to either IgE or IgG1. IgG1 class switched cells are capable of maintaining long-term humoral memory whereas IgE-expressing cells frequently do not possess the same ability, potentially due to a self-limiting effect to prevent aberrant allergic responses (Yang, Sullivan and Allen 2012). Additionally, immunisation can induce the formation of GC centres comprising of clusters of either IgM+ or IgG+ B-cells. Subsequent challenge drives the IgG+ B-cells to differentiate to PCs, whereas IgM+ B-cells reinitiate a GC reaction to activate switching to IgG1, reinvigorating the memory pool (Dogan *et al.* 2009). Together this suggests that Ab class can influence the fate of B-cells.

TLR9 stimulation of transitional B-cells can induce terminal differentiation into IgM memory B-cells. These cells express AID and have undergone some somatic mutation. It has been proposed TLR stimulation generates primitive IgM memory cells that have low levels of SHM which increases the Ab repertoire generated from Ig gene rearrangement in the bone marrow (Aranburu *et al.* 2010). It is possible that WM cells arise from an innate memory cell, an IgM+ memory B-cell that is generated from a T-cell independent differentiation process. An innate IgM+ B-cells may then potentially originate from a TLR stimulated transitional B-cell possessing a MYD88 mutation that would go on to become a WM cell (Capolunghi *et al.* 2013)

It has been noted that patients deficient for MYD88 or IRAK4 have a diminished number of IgM memory B-cells, which is interesting in the context of WM, due to the presumed instigating MYD88 mutation and aberrant IgM secretion. This could suggest an origin of the high IgM secretion seen in WM cells (Weller *et al.* 2012).

Class switched memory B-cells are capable of activating and differentiating into PCs after antigen recall with or without co-stimulation by Tfh cells. In comparison, naïve IgM and IgD expressing B-cells are unable to differentiate into PCs without the aid of co-stimulatory signals induced by accessory receptors (Engels *et al.* 2009).

WM cells may recruit various surface receptors to enable their differentiation, which may translate to a greater sustained downstream activation of survival signalling pathways such as ERK, AKT, MYD88 and NF-κB. The requirement of these cells to utilise accessory receptors to survive compared to healthy B-cells and PCs implies a unique vulnerability to blockage of this receptor coordination and cessation of these survival signals. Together this may explain the unusual lymphoplasmacytic fate of IgM+ WM B-cells and PCs and the enhanced survival of normally short-term IgM B-cells/PCs and a potential target for therapeutics.

1.5 In vitro generation of PCs

Generally, there is a good understanding of the processes that drive PC maturation, however, until recently, there were few experimental models that allowed for the investigation of the entire human B-cell differentiation pathway, nor the various factors that drive this process and promote survival. Moreover, in the case of B-cell malignancies, this has prevented a full understanding of how specific B-cell and PC environmental niches affect the impact of disease specific mutations.

The multi-stage in vitro model used in this study, replicates the progression of B-cells to mature PCs and has allowed for an understanding of the key factors that may contribute to B-cell differentiation and PC survival and has been successfully used to differentiate WM B-cells (figure 1.12) (Cocco *et al.* 2012; Shrimpton *et al.* 2020).

The model utilises CD40L, IL-21, and IL-2 as they are known to play a role in adoption of the PC fate after T-cell dependant B-cell activation. In addition, F(ab')$_2$ anti-IgG/IgM is included to stimulate the BCR. IL-6, IL-21 and IFN-α are added at day 13, promoting acquisition of CD138, indicating the
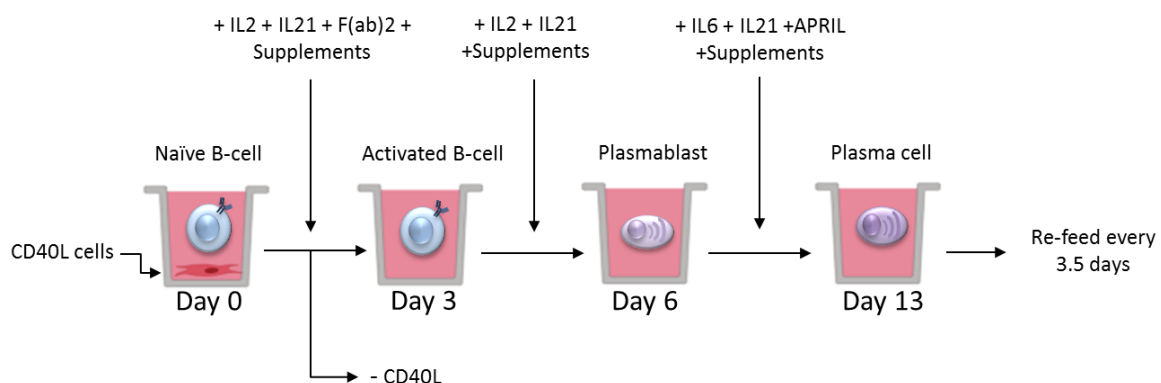
Figure 1.12 – B-cell differentiation model. PBMCs are collected from donors and B-cells purified. At day 0, B-cells are co-cultured with CD40L expressing cells. At day 3 CD40L cells are removed, and cytokines and supplements are added. After day 3 (activated B-cells) a new combination of cytokines is added alongside supplements. Finally, at day 6 (plasmablast stage), APRIL is added, helping drive cells to a PC phenotype (day 13).

development of a PC phenotype. The model was further updated to include the supportive role of the stromal niche, through addition of a stromal cell layer. Recent modifications have subsequently replaced the need for a late-stage stromal layer and IFN-α, with the addition of a proliferation-inducing ligand (APRIL) (figure 1.11) (Cocco *et al.* 2012; Stephenson *et al.* 2021).

1.6 Aims and Objectives

1.6.1 Aims

The overall aim of this project is to assess CXCR4 signal integration in ASCs, including the role of co-receptors and the impact of dysregulated CXCR4 in WM using a novel in vitro system of PC differentiation. This model has allowed a greater understanding into which factors may contribute to PC maturation and survival. Utilising this model, it will enable the investigation into the relationship between CXCR4 survival signalling, the WHIM mutation and CD19 collaboration. Specifically, we aim to define which signalling pathways regulate the differentiation and survival of WM ASCs and how CXCR4 in particular impacts on this process. Importantly, CXCR4 may signal through a variety of pathways at discrete stages of differentiation. In WM, eradication of both B-cells and PC are necessary for effective disease control and may require different types of therapies that exploit the unique characteristics of these cell populations.

1.6.2 Hypotheses

1. **ASCs generate unique CXCR4 signalling patterns depending on the stage of differentiation.**

    As B-cells are triggered to differentiate, they transition into a short lived proliferative PB stage. Following this they differentiate to a mature long-lived PC phenotype. How key signal transduction pathways are modulated may vary due to the different nature of the two cell populations that both secrete immunoglobulin.

2. **B-cells and ASCs expressing CXCR4^{WHIM} generate an enhanced survival signalling pattern.**

    The effect of the introduction of a WHIM mutation on B-cell/PC phenotype, viability and CXCR4 expression and signalling will be observed. The response of healthy primary B-cells and ASCs to CXCL12 will be determined and provide a control profile. From this the same cellular characteristics and signal transduction events will be established for WM^{WHIM} cells.

3. **B-cell and ASC surface receptors CD19 coordinates with CXCR4 to amplify survival signalling that is further enhanced in WM^{WHIM} B-cells and ASCs.**

The impact of co-stimulation of CXCR4 with CXCL12 and the aforementioned surface co-receptors will be assessed using the *in vitro* model. The response of healthy primary B-cells and ASCs to these stimuli will be determined. Specifically, the effect on cell phenotype and downstream signal propagation at both the PB and PC stage will provide a control profile. These stimuli will be assessed on PBs, and PCs transduced with the WHIM mutation.

4. **CD19 deficient B-cells and ASCs will generate a weaker response to CXCL12 stimulation and possess defects in normal B-cell differentiation.**

CD19 deficient B-cells will be cultured within the differentiation model. Acquisition of normal PB/PC phenotype will be assessed as well as CXCR4 expression. Additionally, these cells will be stimulated with CXCL12, and the aforementioned signal transduction pathways will be assessed to confirm CD19's role as a signalling hub for CXCR4.

2.1 Project aims

1) Assess the ability of partners of CXCR4 such as CD19 to propagate signal transduction at different stages of B-cell differentiation in both normal and WM cells.

2) Assess the mechanism of signalling through the defined partners with a focus on PI3K and MAPK pathways.

3) Assess the effect of mutant CXCR4 to alter collaborative signal integration.

4) Assess the differentiation and signalling capabilities of CD19 deficient B-cells.

2.0 Materials and Methods

2.1 Molecular techniques

2.1.1 Plasmids

A set of pIRES2 eGFP based mammalian expression plasmids encoding epitope-tagged human full-length CXCR4 with and without the WHIM mutation were obtained from the University of Dundee MRC-Protein Phosphorylation & Ubiquitination Unit (table 2.1).

Constructs	Plasmid vector
HA CXCR4 (WT)	pIRES2 eGFP (Clontech; University of Dundee MRC-Protein Phosphorylation & Ubiquitination Unit)
HA CXCR4 (WHIM)	pIRES2 eGFP (Clontech; University of Dundee MRC-Protein Phosphorylation & Ubiquitination Unit)

Table 2.1 –Plasmids for transfection

2.1.2 DNA digestion with restriction endonucleases

Restriction digests were performed on pIRES2 eGFP parent plasmids using the volumes and endonucleases detailed in table 2.2. Reaction mixtures were incubated for 1 hour at 37°C. Calf-intestinal alkaline phosphatase (CIP; New England Biolabs) was added and incubated at 37°C for 20 minutes to prevent the recircularization of the parent vector. Restriction digests were performed on the Dundee plasmids to confirm the presence of CXCR4 using the sites shown in table 2.3.

Reagent	Volume (µl)	Manufacturer
DNA	4µl	-
Buffer 10x	5µl	New England Biolabs
BSA	0.5µl	New England Biolabs
EcoRI	1µl	New England Biolabs
XhoI	1µl	New England Biolabs
dH$_2$0	38.5µl	Ambion

Table 2.2 - reaction mixture for DNA digestions

Enzyme	Restriction site 5'-3'	Manufacturer
XhoI	C*TCGAG	New England Biolabs
EcoRI	G*AATTC	New England Biolabs

Table 2.3 - Restriction endonucleases

2.1.3 Agarose gel electrophoresis

Digests were visualised using a 1% agarose gel and ethidium bromide (EtBr) staining. 1% (w/v) of agarose was dissolved in 1X TBE buffer (89mM Tris-base, 80mM boric acid, 2mM EDTA) with the addition of 2.5 µl of ethidium bromide (Fisher Scientific). DNA mixed with a buffer containing 40% sucrose, 30% (v/v) glycerol and food colouring was loaded onto a gel and run at 100V for 30-50 minutes. Molecular weight ladders (100bp or 1kb; New England Biolabs) were included for size comparison. Gels were imaged using the Geldoc XR system (Bio-Rad).

2.1.4 DNA extraction

DNA fragments were visualised using a transilluminator and excised from each gel using a scalpel. DNA elution was performed using QIAquick® Gel Extraction Kit following the manufacturer's instructions (QIAGEN).

2.1.5 Ligation

DNA generated from restriction digests was ligated into a new parent vector using T4 ligase (Invitrogen). The reaction mixture is outlined in table 2.4. The mixture was incubated at room temperature for 2 hours.

Reagent	Volume (µl)	Manufacturer
Vector	1µl	-
Insert	4µl	-
5X Ligase Buffer	1µl	Invitrogen
T4 Ligase	0.5µl	Invitrogen
dH$_2$0	3.5µl	Ambion

Table 2.4 - Reaction mixture for ligation

2.1.6 Transformation of bacterial cells

5µl of DNA was added to 50µl of competent DH5α and incubated on ice for 20 minutes. The reaction was heat shocked for 45 seconds at 42°C and then transferred to ice for 2 minutes. 200µl of super optimal culture medium (SOC) (Invitrogen) was added and the mixture was incubated for 1 hour at 37°C in an orbital shaker. 100µl of the medium 24 was subsequently streaked onto Lennox lysogeny broth-agar (LB) (Formedium) plates containing the appropriate antibiotic (50µg/ml kanamycin). The plates were left to incubate overnight at 37°C.

2.1.7 Plasmid purification

Single colonies were picked and transferred to 3ml of LB broth with kanamycin. Cultures were incubated overnight at 37°C in an orbital shaker. 500µl of the overnight culture was added to 50ml LB broth containing kanamycin and incubated overnight at 37°C in an orbital shaker. Following

incubation, a sample of the culture was taken for a glycerol stock and the remaining was centrifuged at 4000rpm for 30 minutes. The DNA was then purified using a midi-prep kit (Qiagen). DNA was quantified using a NanoDrop™ spectrophotometer (ND-1000; ThermoScientific).

2.1.8 RNA isolation

To collect RNA, Cell samples were obtained (~$5x10^5$ cells) and washed with PBS. 800µl of TRIzol™ was then added to the cell pellet. The cells were then stored at -80°C until required. To isolate the RNA, 160µl of chloroform was added to the lysed cells. Lysed cells and chloroform were the mixed through gentle inversion. Samples were then centrifuged at 12,000g at 4°C for 10 minutes. The sample is then separated into three phases, an organic phase, a middle phase and an upper aqueous phase containing the RNA. The clear aqueous phase is carefully removed and 5-10µg of RNAse free glycogen was added to act as a carrier. 400µl of isopropanol was added and the sample was incubated at room temperature for 10 minutes. The sample is then centrifuged at 12,000g at 4°C for 10 minutes. The supernatant was then removed and the pellet was washed by vortexing with 1ml of 75% ethanol. The ethanol was then removed and the sample was air dried for 5-20 minutes. Once the sample had dried, the sample was dissolved in 50ul of RNAse free water and heated to 55°C for 10 minutes. Finally, the RNA was treated with DNase I (Invitrogen) following the manufacturer's instructions. Concentration was then determined using a Nanodrop™ spectrophotometer.

2.1.9 Viral Constructs and Transductions

To insert the CXCR4 inserts into the MSCV viral constructs, the existing pIRES-eGFP-CXCR4 constructs were digested using the restriction digest protocol detailed in section 2.1.2. The specific reagents used are detailed in table 2.5

Reagent	CXCR4-WT (µl)	CXCR-WHIM (µl)	Control (µl) (CXCR4-WT)
DNA	1.4	1.25	1.4
Buffer	5	5	5
BSA	0.5	0.5	0.5
EcoRI	1	1	-
XhoI	1	1	-
dH$_2$O	41.1	41.25	43.5
Total	50	50	50

Table 2.5 - Restriction Digestion reagents for CXCR4 WT and CXCR4 WHIM constructs. A control digest was performed without restriction enzymes.

The digest mixes were incubated at 37°C for 1 hour and 1μl of CIP was added after for 20 minutes at 37°C. concurrently, the MSCV vector (provided by the Hodson group (Caeser *et al.* 2019)) was prepared for digestion. The reagents for this digest are listed in table 2.6

Reagent	MSCV vector	control
DNA	3	3
Buffer	5	5
BSA	0.5	0.5
EcoRI	1	-
XhoI	1	-
dH$_2$O	38.5	37
Total	50	50

Table 2.6 - Restriction Digestion reagents for MSCV vector. A control digest was performed without restriction enzymes.

A 1% agarose gel with ethidium bromide was prepared and GLB was added to each sample. The samples were loaded onto the gels. Bands were cut out using a scalpel and a gel purification was completed following the manufacturer's instructions (QIAquick® Gel Extraction Kit). Next the Ligation of the inserts and the MSCV vector was completed. The details of the ligation mixes are included in table 2.7

Table 2.7 - Ligation reactions for MSCV vectors and Gel purified CXCR4 (WT) and CXCR4 (WHIM) inserts.

Reagent	CXCR4-WT	CXCR4-WHIM	Control
MSCV vector	1	1	1
Insert	4	4	-
Ligase Buffer	1	1	1
T4 Ligase	0.5	0.5	0.5
dH20	3.5	3.5	3.5

The ligation reactions were left to run for 2 hours at RT. The ligated mixes were then prepared for transformation into competent bacteria. Stable competent *E.coli* (New England Biolabs) cells were thawed on ice for 10 minutes and mixed with 5μl of ligation. The control ligation was also mixed with bacteria. The cells were then mixed, and placed on ice for 30 minutes. The cells and ligation mixed was placed in a water bath set at 42°C for 30 seconds and then placed on ice for 5 minutes. 950μl of NEB 10-beta/stable outgrowth medium® (New England Biolabs) was then added into the mixture. The cells were placed in a shaking incubator at 30°C for 1 hour. 50-150μl of the cell suspension was then spread onto ampicillin plates and grown O/N at 37°C. Colonies were then picked from each plate and added to 3ml Ampicillin broth. These were then grown O/N at 37°C. A miniprep was then completed from 1.5ml of each sample according to the manufacturer's instructions (Invitrogen). Isolated plasmid DNA was then measured on the Nanodrop. Additionally a restriction digest was performed on the

plasmid DNA using the same conditions detailed in table 2.5 and visualised on an agarose gel to confirm which clones had successfully incorporated the plasmid DNA. Next, the +ve bacterial clones were scaled up in preparation for a Midiprep. 50ml of ampicillin LB broth was added into plastic conical flasks. 1ml of positive clones of CXCR4-WT and CXCR4-WHIM was added to broth. They were then grown overnight at 37°C. Glycerol stocks were prepared from the O/N cultures. A Midiprep was performed and the plasmid DNA was measured on the Nanodrop.

HEK-293T cells were cultured prior to transfection. 2×10^6 HEK-293T cells were seeded in 10cm petri dishes in 6ml DMEM (high glucose, 10% HIFBS, 5ml Pen/Strep, 5ml Glutamine) 24 hours in advance of transfection. 24 hours after seeding, cells were checked to verify attachment and viability. Existing DMEM was removed and 6ml of fresh DMEM was added. Per transfection, 1ml of Opti-mem (Thermofisher) and 18µl TransIT-293 (Mirus Bio) was prepared and mixed and incubated at RT for 10 minutes. Packaging plasmids and retroviral constructs were then prepared and incubated for 30 minutes at RT (table 2.7). Transfection mix was then mixed and gently distributed dropwise over the HEK293T cells in 10 cm plates. The plates was then shaken gently. HEK293T cells were incubated at 37°C in a Class II incubator for 48 hours. (Section 2.2.11 details the collection of viral supernatants and subsequent transduction of B-cells).

Reagent	WT CXCR4 HEK293T cells (µl)	WHIM CXCR4 HEK293T cells (µl)	Manufacturer
GALV-MTR	2.5	2.5	Provided by the Hodson group (Caeser *et al.* 2019)
pHIT60	2.5	2.5	Provided by the Hodson group (Caeser *et al.* 2019)
MSCV-CXCR4-WT	2.1	-	-
MSCV-CXCR4-WHIM	-	1.87	-

Table 2.8 - reagent mix for transfecting HEK293 cells with retroviral constructs containing either CXCR4-WT or CXCR4-WHIM. Volumes shown show mix required for transfecting one 10cm petri dish of HEK293T cells.

2.2 Cell Culture

2.2.1 Cell lines

Cell line	Origin	Media
HEK 293	Transformed human embryonic kidney cells	DMEM +10% HIFBS
CD40L murine Fibroblasts	NCTC clone 929 [L cell, L-929, derivative of Strain L] from *Mus musculus* stably transfected with human CD40L	IMDM media + 10% HIFBS

Table 2.9 - Cell lines

Cell lines were authenticated using standard short tandem repeat (STR) DNA profiling analysis (CRUK Cancer Centre Genomics Facility). CD40L expressing murine fibroblasts were obtained from Dr Sean Diehl, University of Amsterdam, Netherlands. MWCL-1 and BCWM-1 cell lines were obtained from Dr Steven Ansell, Mayo Clinic, USA. HEK 293 cell lines were obtained from ATCC and used for transfections. Cells were maintained at 37°C in a humidified atmosphere at 5% CO_2.

2.2.2 Population and ethics

Peripheral blood was obtained from healthy volunteers and collected in 9ml EDTA tubes following informed consent. Approval for this study was granted by the Leeds (East) NHS Research Ethics Committee, REC reference number 07/Q1206/47.

2.2.3 Irradiated CD40-L expressing murine cells

Murine fibroblasts transfected with human CD40L (CD154) were irradiated twice on ice using 50 Gray for 50 minutes in a gamma irradiator (NDT) with gentle mixing between doses. After irradiation, 100µl of cells were stained with an α-CD154 antibody and phenotype was assessed via flow cytometry to confirm expression. An aliquot of $2x10^6$ pre-irradiated CD40L-L cells was then prepared for freezing in cryovials and stored at -80°C. 24h prior to sample processing, an aliquot of CD40L cells was thawed and added to 10ml Iscoves Modified Dulbecco's Medium (IMDM) media + 10% HIFBS (Invitrogen) then centrifuged at 1500rpm for 5 minutes. CD40L-L cells were re-suspended in 24ml fresh IMDM + 10% HIFBS and 0.5 ml was plated per well of two 24-well plates (0.5ml/well; $4.16x10^4$/well) and incubated overnight at 37°C.

2.2.4 *In vitro* differentiation of human B-cells

2.2.4.1 Isolation of PBMCs

Peripheral blood was obtained from healthy donors with informed consent. Healthy donors were selected from the lab population and were defined as a volunteer with a good health status with no major active illness. Age range of donors varied between 20-60 years and there was no selection based on gender or any other category. 50ml peripheral blood mixed with an equal volume of sterile phosphate buffered saline (PBS) at room temperature (RT). 34ml of the blood/PBS mix was layered on top of 17ml Lymphoprep™ (Allere Ltd.). The blood/lymphoprep was centrifuged at 2400rpm/ 1114 x g for 20 minutes at RT (acceleration 5, brake 0). The mononuclear layer was removed and divided between two 50ml falcon tubes containing 10ml cold PBS. The volume was made up to 50ml with cold PBS, the peripheral blood mononuclear cells (PBMCs) were centrifuged at 1800 rpm for 15 minutes at 4°C. Cells were combined into one tube, washed with 50ml cold PBS and centrifuged at 1500rpm for 10mins at 4°C. This was repeated, and then the PBS was removed, and cells were washed with 15ml

ice-cold MACS buffer (PBS, 0.5% BSA) (Miltenyi). Cells were counted before being centrifuged at 1500rpm for 10mins at 4°C.

Due to the COVID-19 pandemic, WM patient samples were no longer available for study due to issues obtaining said samples via colleagues with access and the lack of patients coming on site for sample collection. The pandemic also restrained the number of volunteers available for use as healthy controls, due to the introduction of lockdowns, partime working and social distancing measures.

2.2.4.2 Magnetic labelling of cells

B-cell selection was carried out with a Miltenyi memory B-cell isolation kit for maximum 1×10^8 cells. The PBMC pellet was resuspended in 400µl of cold MACS buffer. 100µl B-cell Biotin-Antibody Cocktail was added and the mixture was incubated for 20 minutes at 4°C. Then 300µl of cold MACS buffer and 200µl anti-Biotin Microbeads were added, and incubated for 20-30 minutes at 4°C. 10ml cold MACS buffer was added to the cells, which were then centrifuged at 1500rpm for 10 minutes at 4°C. The cell pellet was re-suspended in 1ml cold MACS buffer.

2.2.4.3 Magnetic separation of cells

To negatively select for memory and naïve B-cells, an LD Column (Miltenyi) was placed in the magnetic field of a MACS separator and rinsed with 2ml of cold MACS buffer. The cell suspension was added to the column and the unlabelled cells passing through were collected in a fresh tube. The column was washed 3 times with 1ml of cold MACS buffer and the flow through collected in the same tube. The cells were counted and re-suspended in IMDM + 10% FBS at 5×10^5 cells/ml.

2.2.4.4 Culture conditions day 0

B-cells were cultured in 24-well plates at 1×10^5 cells/ml in IMDM + 10% HIFBS with MEM amino acid solution (1:50) (Sigma) and Lipid Mixture 1, chemically defined (1:200) (supplements) (Sigma) and the addition of human IL-2 (20 U/ml, Roche), human IL-21 (50 ng/ml, Peprotech) and F(ab')$_2$ goat anti-human IgM and IgG (10 µg/ml, Jackson Immunoresearch).

2.2.4.5 Culture conditions day 3

B-cells were removed from the CD40L-L cells by gentle pipette mixing. B-cells were reseeded at 1×10^5 /ml in IMDM + 10% HIFBS + supplements, with the addition of human IL-2 (20 U/ml) and human IL-21 (50 ng/ml).

2.2.4.6 Culture conditions day 6

Cells were collected and counted. Cells were seeded in a 24 well plate in IMDM + 10% HIFBS + supplements with the addition of human IL-6 (10 ng/ml, Peprotech), human IL-21 (50 ng/ml),

multimeric APRIL (100 U/ml, Adipogen) and gamma secretase inhibitor (GSI) inhibitor (100nm, Tocris). Cells were seeded at $1x10^6$/ml.

2.2.4.7 Culture conditions day 10

Cells were collected and a lymphoprep was performed to remove dead cells. Cells were layered onto lymphoprep and centrifuged at the settings detailed in 2.2.4.1. The mononuclear layer was removed, and cells were washed in cold PBS and centrifuged at 1800 RPM for 15 minutes, followed by a second wash in PBS and centrifuged again at 1500 RPM for 10 minutes. B-cells/PBs were then resuspended in fresh IMDM media containing + 10% HIFBS + supplements with the addition of human IL-6 (10 ng/ml), human IL-21 (50 ng/ml), multimeric APRIL (100 U/ml) and GSI (100nm).

2.2.4.8 Culture conditions day 13

PCs were collected as previously and counted. Human IL-21 was removed from the media + supplements + human IL6 + APRIL + GSI. Cells were re-fed every 3.5 days by replacing media with fresh media + supplements + day 13 cytokines.

2.2.4.9 Culture conditions for APRIL/TGFβ/IFNα

Once naïve and memory B-cells were isolated, cells were cultured in normal differentiation conditions up until day 6. Cells were then cultured in 3 different conditions: IL-6, Il-21, supplements and either APRIL+GSI, TGFβ (Peprotech) or IFNα (Peprotech). The cells were maintained in these culture conditions up until the plasma cell stage (day 13). Samples were taken for surface CXCR4 staining following the staining method specified previously and analysis via flow cytometry at day 10 and 13.

2.2.5 Cytokines and growth factors for generation of human plasma cells

Cytokine/ Growth Factor	Stock Concentration	Final Concentration	Supplier
hIL-2	10,000 units/ml	20 units/ml	Roche
hIL-21	100µg/ml	50ng/ml	Peprotech
F(ab')$_2$ anti-IgM/IgG	1.2mg/ml	10µg/ml	Jackson Laboratories
Amino Acids	50X	20µl/ml	Sigma
Lipid Mix	200X	5µl/ml	Sigma
hIL-6	100,000ng/ml	10ng/ml	Peprotech
APRIL	100µg/ml	100ng/ml	Adipogen
γ-secretase inhibitor L-685,458	1mg/ml	1µg/ml	Tocris
hIFN-α	1x107 units/ml	100 units/ml	Peprotech
hTGF-β	100 µg/ml	2.5µg/ml	Peprotech

Table 2.10 - Cytokines and growth factors required for in vitro B-cell differentiation

2.2.6 Plasmid transfection

For transient transfection of HeLa and HEK 293 cells, 100 ng/μl of plasmid DNA was prepared. 10μl (1μg) of this was added to GeneJuice® transfection reagent (Milipore) and Opti-MEM serum free media (Thermofisher). Reaction mixture was incubated for 20 minutes and then added dropwise onto cells. Cells were incubated overnight at 37°C. Transfection efficiency was determined by GFP expression analysed under fluorescent microscopy and flow cytometry. Lysates were then taken for protein evaluation as described in section 2.4.1.

2.2.7 Nucleofection

18-24 hours before nucleofection, 1-2x10^6 cells were plated into wells. Cells were incubated overnight at 37°C. An appropriate amount of cells were harvested and centrifuged. Cells were suspended in Ingenio® electroporation solution (Mirus Bio). 20μg of plasmid DNA was added to the mixture. An electrical current was applied to the cells using an Amaxa Nucleofector™ (programme X-001) and then they were transferred to a 12 well culture dish containing RPMI media supplemented with 10% FCS.

2.2.8 G418 antibiotic kill curve

MWCL-1 and BCWM-1 cells were seeded into wells and incubated at 37°C for 24 hours. The selection antibiotic G418 (Geneticin) was then added dropwise at different concentrations for each well. Each concentration was done in duplicate. Cells were left for 24 hours. Viability was determined using trypan blue exclusion counts.

2.2.9 Cell counting

At each time point of the differentiation, cell counts were performed to determine the cell density for reseeding into differentiation conditions and for sample collection for flow cytometry and stimulation experiments. 10μl of cells was mixed with 10μl of Trypan blue (Sigma) and counted manually using a haemocytometer and a cover slip. Cell count per ml was determined using the following equation

$$Cell\ number\ per\ ml = \frac{ml = average\ cell\ count}{number\ of\ haemocytometer\ squares\ counted}\ x\ 10^4\ x\ dilution\ factor$$

Cell number per ml was multiplied by the total volume to calculate the total cell count.

2.2.10 Cell freezing and thawing

To freeze cells, the cell suspension is centrifuged at 1500 RPM and resuspended at 1x10^6 cells/ml in cold freezing mix (90% FCS and 10% DMSO). 1ml of the cell suspension is then transferred to a cryovial and stored at -80°C for a minimum of 24 hours. Cryovials were then transferred to the liquid nitrogen storage bank for long-term storage. To thaw cells, cryovials were removed from either the -80°C or liquid nitrogen and warmed until thawed. Cells were then transferred to fresh media and spun by

centrifugation to remove the freezing mix. Cells were then resuspended in fresh media at the preferred density and seeded into flasks or wells.

2.2.11 Viral supernatants

Viral supernatants from HEK-293T cells were collected using a 10ml syringe. The supernatants were then filtered through 0.22μm filters into fresh falcon tubes. Viral supernatants were then frozen at -80 °C for storage or prepared for transduction of B-cells by adding 25μM HEPES (Thermofisher) and polybrene (Santa Cruz Biotechnology) (10μg/ml) to the viral titer mix and gently mixing.

2.2.12 B lymphocyte transductions

At Day 2 of the B-cell differentiation, B-cells-CD40L co-cultures were centrifuged in 24 well plates at 400g for 4 minutes at RT. 90% of the supernatant was removed leaving approximately 100μl of media per well. 1ml of previously prepared viral supernatant was added to each well of the B-cell CD40L co-culture. The cells were then mixed gently five times. The plates were the sealed with parafilm® (Bemis) and spun at 1500g for 90 minutes at 32°C. After centrifugation, approximately 70% of the viral supernatant was removed (700μl) and replaced with 800μl fresh D0 cytokine mix without F(Ab')$_2$. Cells were left to incubate at 37°C for 24 hours before a sample was collected for flow cytometry evaluation of transduction. Remaining cells were collected, and day 3 media was prepared. These cells were then cultured in the *in vitro* differentiation system as normal.

2.3 Flow cytometry

2.3.1 Flow cytometer

Flow cytometry was performed using a CytoFLEX S or CytoFLEX LX (Beckman Coulter). Analysis was performed using FlowJo v10 (Treestar).

2.3.2 Antibodies for Immunophenotypic analysis

Antibody	Volume used (μl)	Manufacturer	Isotype control
CD19-PE	20	BD Pharminogen	Mouse IgG1-PE
CD20-V450	25	Invitrogen	Mouse IgG2b κ
CD27-FITC	20	BD Pharminogen	FITC Mouse IgG1 κ
CD38-PECγ7	5	BD Pharminogen	Mouse IgG1-APC
CD138-APC	20	BD Pharminogen	Mouse IgG1-APC
CD79b-PE	10	BD Pharminogen	Mouse IgG1-PE
CD19-vioblue	5	Miltenyi Biotec	Mouse IgG1-VioBlue
hCXCR4	10	R&D Systems	Mouse IgG2A - PE
7AAD	5	BD Pharmingen	N/A
anti-Akt (pT308)	20	BD Phosflow	Mouse IgG1, κ
CXCR4	5	R&D Systems	Mouse IgG2A-PE
CD2	1	BD Biosciences	Mouse IgG1 κ
Live/dead fixable	100	Biolegend	N/A

Table 2.11 - Antibodies used for immunophenotype analysis – Normal B-cell/PC flow panel was selected for identification of these cell populations by previous analysis completed by the Doody/Tooze group, itself based on a standard B-cell/PC detection panel used in clinical immunological assessment of these cell populations.

2.3.3 Immunophenotypic analysis of differentiating B-cells

1×10^5 cells were resuspended in FACs buffer (PBS, 0.5% BSA, 0.05% sodium azide) and centrifuged. 500ul of blocking buffer containing normal mouse serum (25µl), human IgG (8.35µl) and FACs buffer (466.65µl) was prepared and added to the cells. The cells were then incubated on ice for 15 minutes. The appropriate primary antibodies/isotype was then added to the cells and left on ice for 15 minutes. Cells were then centrifuged and resuspended in FACs buffer. Samples were run on a Beckman Coulter CytoFLEX S High Throughput (13 colour laser) flow cytometer. Cells are analysed through use of various gates including FSC/SSC, FSC/FSH (singlet/doublet discrimination), 7AAD (live/dead), CD19, CD20, CD27, CD38 and CD138.

2.3.4 Gating strategy for flow cytometry

B-cells were first gated on their forward vs side scatter phenotype to obtain population P1 (figure 2.1). Utilisation of this B-cell selection process reliably generates an easily detectable B-cell population that under flow cytometry analysis is located within gate P1. Doublets were then excluded for forward scatter by plotting forward area scatter against forward height scatter (P2). This forms a cohesive population that allows for discrimination of clumps of cells. Doublet have double the area values of
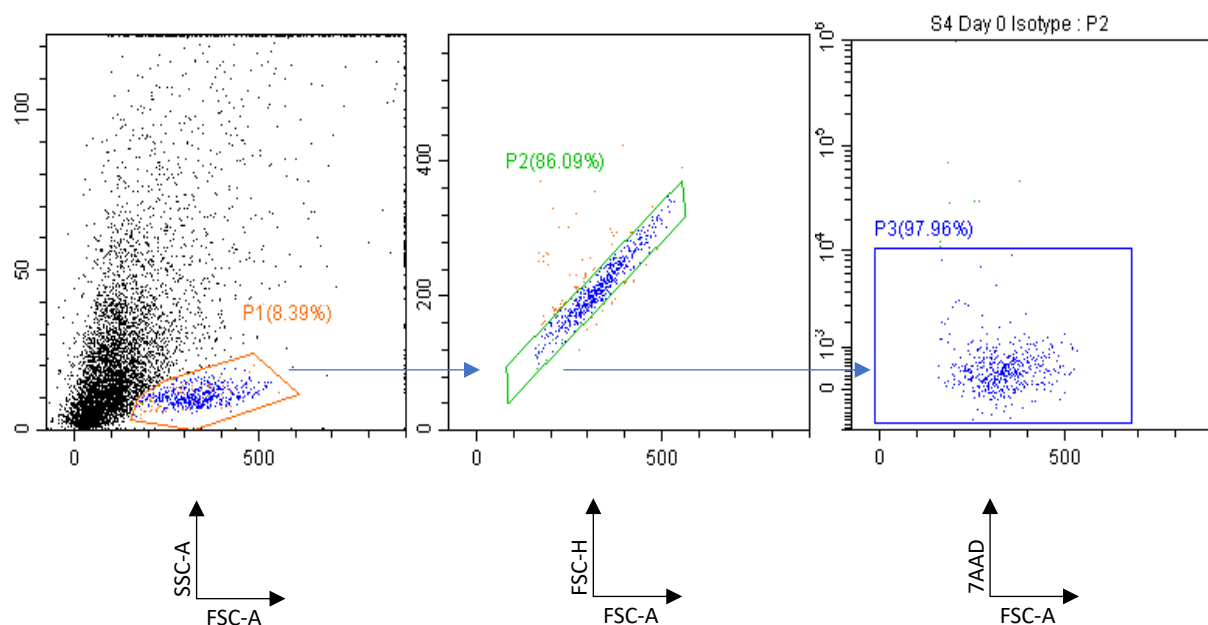
Figure 2.1 – Gating strategy for immunophenotype analysis. Cytexpert was used to generate the gating strategy. Forward and side scatter were used to identify the B-cells and PCs. Following this doublet discrimination was used via assessing forward scatter area vs forward scatter height. Finally dead cells were excluded using 7AAD.

single cells, and an equivalent height. It was necessary to remove these, as a doublet composed of a

fluorescent positive and negative cell will generate a false positive result. A live dead discrimination was then performed, with living cells determined using 7AAD staining against forward scatter (P3). Dead cells will take up the 7AADc stain, whereas live cells will exclude it, and therefore can be identified.

Following initial analysis through Cytexpert, all flow cytometry results were further analysed using FlowJo software. All dot plots and histograms were generated through FlowJo using the gating described in this section previously. Following live dead discrimination, cells were analysed using B-cell and PCs phenotypic markers as well as CXCR4 (table 2.12). Percentage positive and MFI was calculated. GraphPad Prism was used for quantitative analysis and creation of scatter graphs and bar charts for displaying expression levels between sampes/donors and conditions.

2.3.5 Fluorescence compensation protocol

A compensation protocol was utilised to correct for emission spectra overlap. Compensation beads (BD Biosciences) were individually stained with antibodies detailed in table 2.12 described in section 2.3.2. The volume of antibody added was the same as used for cell staining. One tube was left unstained and cells were used for 7AAD staining. Cells were let to incubate for 5 minutes at RT. Beads/cells were then resuspended in 300µl of FACs buffer. Samples were then run on the CytoFLEX using a compensation programme.

2.4 Protein analysis

2.4.1 SDS polyacrylamide gel electrophoresis (PAGE) and immunoblotting

Cells were resuspended from well plates using a cell scraper, transferred to falcon tubes and centrifuged. The cells were washed in ice-cold PBS and the centrifuged again to remove leftover PBS. Ice-cold RIPA buffer with protease inhibitors was added to the cells and they were incubated for 10 minutes on ice. Cells were transferred to an Eppendorf and centrifuged at 4°C for 10 minutes. Lysates were mixed with 5X GLB (4% SDS (Sigma), 20% glycerol (Sigma), 10% 2-mercaptoethanol (Sigma), 0.004% bromophenol blue (Sigma) and 0.125 M Tris HCl). Western images were generated using Amersham Hyperfilm™ ECL (GE Healthcare) and processed in an X-ray developer (SRX-101A). Alternatively, Westerns were imaged using the Chemidoc MP Imaging system (BioRad).

2.4.2 Antibodies for immunoblotting

Antibody	Dilution	Manufacturer	Host	Secondary Antibody
P-Akt (T308)	1:1000	Cell Signalling	Rabbit	Goat Anti-Rabbit H+L (HRP)
P-Akt (S473)	1:1000	Cell Signalling	Rabbit	Goat Anti-Rabbit H+L (HRP)
Akt (Pan)	1:1000	Cell Signalling	Rabbit	Goat Anti-Rabbit H+L (HRP)
Anti-β-Actin	1:10000	SigmaAldrich (Merck)	Mouse	Goat anti-Mouse H+L (HRP)
pERK	1:1000	Cell Signalling	Rabbit	Goat Anti-Rabbit H+L (HRP)

Total ERK	1:1000	Cell Signalling	Rabbit	Goat Anti-Rabbit H+L (HRP)
CXCR4	1:1000	Proteintech	Rabbit	Goat Anti-Rabbit H+L (HRP)
CXCR4	1:500	Abcam	Goat	Mouse anti-Goat H+L (HRP)
ICSBP(E-9) – (IRF8)	1:100	Santa Cruz Biotechnology	Mouse	Goat anti-Mouse H+L (HRP)
p-CD19	1:1000	Cell Signalling	Rabbit	Goat Anti-Rabbit H+L (HRP)
CD19	1:2000	Proteintech	Mouse	Goat Anti-Mouse H+L (HRP)
AKT isoform 1	1:1000	Cell Signalling	Rabbit	Goat Anti-Rabbit H+L (HRP)
AKT isoform 2	1:1000	Cell Signalling	Rabbit	Goat Anti-Rabbit H+L (HRP)
AKT isoform 3	1:1000	Cell Signalling	Mouse	Goat Anti-Mouse H+L (HRP)

Table 2.12 - Antibodies for immunoblotting

2.4.3 Polyacrylamide gels

Gel	Tris Buffer	polyacrylamide	dH$_2$0	10% APS	Tetramethylethylenediamine
10% resolving	2.5 ml	3.3 ml	4.1ml	100µl	10µl
7.5% Resolving	2.5 ml	2.5 ml	4.92ml	100µl	10µl
7.5% Stacking	2.5 ml	1 ml	6.5ml	100µl	10µl

Table 2.13 - Polyacrylamide gel recipe (for 10ml)

2.4.5 Enzyme-linked immunosorbent assay (ELISA)

Serum and conditioned media samples were obtained from healthy control and patient samples. These samples were then diluted to an appropriate concentration (1:100). Reagents and antibodies were prepared according to the manufacturer's instructions (Bethyl). 1µl of purified coating antibody was diluted in 100µl coating buffer and 100µl of diluted antibody was added to the required number of wells. These wells were incubated for 1 hour at RT. The antibody was removed by washing with wash buffer 5 times. 200µl of blocking solution was added to the wells and left to incubate for 30 minutes at RT or overnight at 4°C. Blocking buffer was removed, and the plate was washed five times with wash buffer. Standards were prepared as per the manufacturer's instructions. 100µl of sample or standard was added to the wells and the plate was incubated at RT for 30 minutes. After incubation, the samples/standards were removed from the wells and the plate was washed five times using wash buffer. The HRP detection antibody was diluted in sample/conjugate diluent at a recommended dilution of 1:150,000. 100µl of diluted detection antibody was added to each well. The plate was left to incubate for 60 minutes at RT. Following incubation, the detection antibody was removed, and the plate was washed five times with wash buffer. TMB substrate was prepared according to manufacturer's instructions (Bethyl). 100µl of TMB substrate was into each well and the enzymatic colour reaction was allowed to develop at RT for 15 minutes in the dark. After 15 minutes, the reaction was stopped by adding 100µl ELISA stop solution (0.18M H$_2$SO$_4$). The plate was tapped gently to mix. The plate was then run on a plate reader at 450nm (BioTek Citation 5 Imaging Reader).

2.5 Cell signalling analysis

2.5.1 Cell preparation

Cells were washed, counted, and re-suspended at 1-$2x10^6$ in 0.5% serum IMDM containing IL-6/IL-21/APRIL. Cells were incubated for 12-20 hours at 37°C. Following this, cells were placed in a 37°C water bath.

2.5.2 CXCL12 stimulation of B-cells and PCs

An unstimulated sample of cells was taken and added to 2x sample buffer. Stimulus was added (CXCL12/F(Ab')$_2$) and after 1 minute a sample was taken. Samples were then taken after 5 and 10 post stimulation. Each tube was mixed thoroughly. Samples were loaded onto an SDS-polyacrylamide gel and phosphorylated and total protein was analysed as detailed in 3.3.1.

2.5.3 αCD19 bead preparation

Anti-biotin beads were vortexed. An aliquot of biotinylated αCD19 and was added to a 2ml tube and 500µl of anti-biotin beads ($1x10^8$) was added to the aliquot. The volume was adjusted up to 1ml by adding cold PBS (0.5% BSA, 2mM EDTA). The mixture was then incubated for 2 hours at 2-8°C under gentle rotation. After incubation the bead mix was stored at 2-8°C. The loaded bead mix was then resuspended and a 25µl aliquot was transferred to a separate Eppendorf. 100-200µl of culture medium (phenol red free, 0.5% serum IMDM) was added to the beads. The mixture was centrifuged at 300x*g* for 5 minutes. Following centrifugation, the supernatant was removed, and the antibody-bead mix was resuspended in the same media at the same concentration as previously. The loaded antibody-bead mixture was ready for stimulations.

2.5.4 αCD19 and F(Ab')$_2$ stimulation of B-cells and PCs

Cells were counted and re-suspended at 1-$2x10^6$ in 0.5% serum IMDM containing IL-6/IL-21/APRIL. Cells were incubated for 12-20 hours at 37°C. Following this, cells were placed in a 37°C water bath. An unstimulated sample of cells was taken and added to 2x sample buffer (for immunoblot). D6 B-cells and D13 PCs were stimulated with αCD19 bound beads at a bead-to-cell ratio of 1:2. Sample collection was completed as described in section 2.4.1.

2.6 Statistical Analysis

The number of repeats for each experiment is detailed in the figure legends. Comparison of means was carried out using the student t-test. Error bars indicate standard deviation (SD). Statistical analysis was performed through GraphPad prism software.

3.0 – CXCR4 signal propagation changes during terminal B-cell differentiation

3.1 Introduction

CXCR4 is a chemokine receptor present on numerous cell types, including lymphocytes. It binds to the chemokine CXCL12 to induce the migration of target cell populations towards specific tissues and also has been shown to promote survival through the activation of PI3K and MAPK signalling pathways, leading to down regulation of pro-apoptotic factors and the transcription of pro-survival genes, alongside genes involved in cell adhesion and migration (Suzuki, Rahman and Mitsuya 2001). During the initial stages of B-cell development, CXCL12-CXCR4 maintains precursor B-cell populations in the bone marrow, but as they mature, the cells lose responsiveness to CXCL12 and are exported to the periphery upon completion of antigen receptor rearrangement and selection (Egawa *et al.* 2001). Although circulating mature B-cells have diminished responses to CXCL12 (McHeik *et al.* 2019; Fedyk *et al.* 1999; Honczarenko *et al.* 1999), once they have entered secondary lymphoid organs, B-cells can regain sensitivity. This is best illustrated in the migration of B-cells towards the GC, and working in opposition to the CXCR5-CXCL13 axis to bring B-cells from light zone, into the dark zone to undergo further rounds of SHM, before cycling back into the light zone. After successful generation of high-affinity clones during the germinal centre response, CXCR4 then aids in the migration of PBs towards survival niches such as the BM (Biajoux *et al.* 2016).

CXCR4 surface expression is known to vary as B-cells differentiate from the immature and pre-B-cell stage to the mature B-cell and PB/PC stage (Nie *et al.* 2004). In particular, it has previously been shown that human naïve and memory B-cells stimulated in vitro with either T-D (IL-2 + IL-10 + CD40L) or T-I (IL-2 + IL-10 + SAC or CpG) type stimuli upregulate CXCR4 on the resulting plasmablasts (Muehlinghaus *et al.* 2005) and that the potential niche signal TGFβ3 can further enhance CXCR4 expression on in vitro generated PBs (Stephenson *et al.* 2019).

 Not only does CXCR4 vary in expression throughout B-cell ontogeny, it also possesses distinct signalling effects at different stages. Indeed, pre- and pro- B-cells are capable of migration towards CXCL12 and intracellular calcium mobilisation after stimulation, whereas mature B-cells fail to generate these responses, indicating a rewiring of CXCR4 signalling as the B-cells mature. Additionally, B-cell lines representing circulating B-cells lack essential CXCL12 mediated G protein subunit disassociation that leads to migration seen in B-cell precursors (Neptune and Bourne 1997). Additional investigation revealed circulating B-cell chemotaxis and calcium mobilisation is blocked despite

detectable CXCR4 internalisation, G-protein activation and ERK1/2 phosphorylation (Palmesino *et al.* 2006)

It has been suggested that the external environment may modulate the functionality of CXCR4 on B-cells at all stages of the differentiation. Indeed, TGFβ can alter the expression of CXCR4 and has been identified as a pro-survival factor for PBs. Previous work has shown that pre-treatment of TGFβ generates a more sustained ERK activation in response to CXCL12 (Stephenson *et al.* 2019), leading to an enhanced expression of immediate early response genes EGR1 and cFOS, EGR1 being particularly relevant in malignant PC function (Mikulasova *et al.* 2017). However the effects of ligation were only assessed in day 7 PBs, and therefore the relationship between CXCR4 expression and ERK signal transduction in PCs and the effect of other niche signals is unknown.

3.2 In vitro B-cell differentiation model

Previous work in the lab has utilised a model of B-cell differentiation using negatively selected B-cells isolated from PBMCs that mature in response to T-dependant stimulation (CD40L and F(ab')$_2$ anti-IgG/M) and plasma cell maturation/survival factors such as IFNα and TGFβ. Negative selection was chosen to minimise the likelihood of unintended stimulation of the B-cells that can occur through positive isolation and therefore potentially affect downstream experiments. Positive selection kits generally yield purer samples, however a purity of >95% B-cells is often achieved with negative selection.

From this, cells can be obtained and stimulated to understand the signal transduction events in response to various stimuli, including CXCL12. Moreover, the model system allows the analysis of cells at each of the key stages of differentiation and the opportunity to alter conditions. Importantly, ongoing work in the lab has examined the impact of substituting the PC survival factor APRIL for IFNα and TGFβ as the cells transition from PBs to PCs (Stephenson *et al.* 2021). Therefore, the initial aim was replicate these new conditions with the goal of studying CXCR4 signalling in these cells.

Figure 3.1 visualises the B-cell phenotype during differentiation. At day 0 the B-cells are quiescent and express high levels of both CD19, a pan B-cell marker that is expressed on all cells belonging to the B-cell lineage, and the marker CD20. A fraction of the B-cells also shows positivity for CD27, a marker associated with the memory B-cell population. CD38 is used as a marker of antibody secreting cells but is generally expressed at a low level at day 0. By day 6 the cells have been activated and most will have reached the PB phenotype. Here CD20 begins to decrease and CD38 is homogeneously induced.

High CD38 is maintained from this point and the PC marker CD138 begins to be expressed on a small fraction of the cells. A gain of CD27 expression relates to the transition to mature ASCs. By day 13 the cells have mostly reached the PC stage and the majority will express CD138, which diverges from the previously published conditions where day 13 cells presented a more uniform expression of CD138 (Cocco et al 2012). All cells should express CD38 at this point. CD20 expression is almost completely lost and CD19 expression is reduced slightly in some of the cells, similar to what has been observed in IFNα conditions, although to a lesser extent (Arumugakani *et al.* 2017).
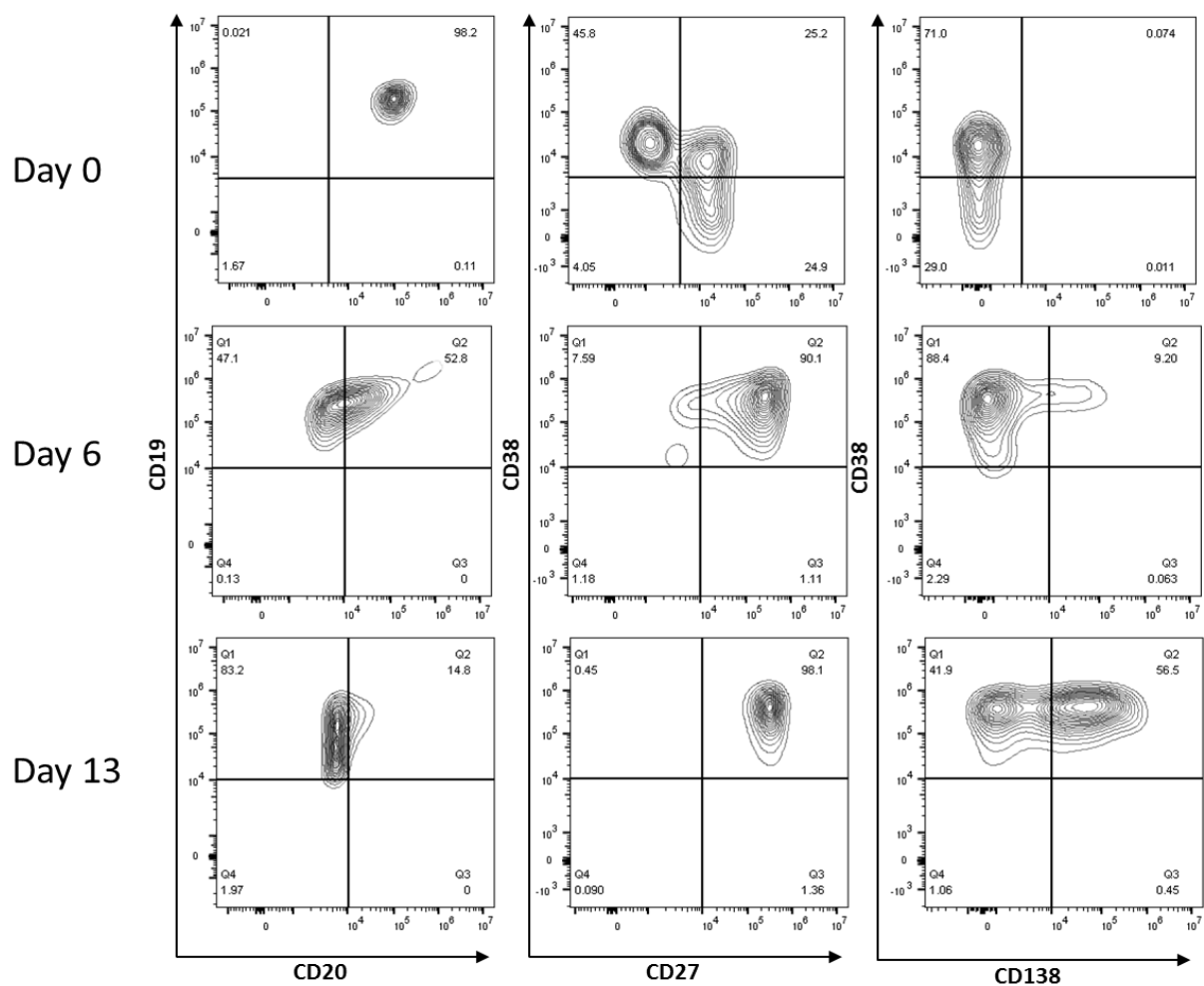
Figure 3.1 - Assessment of cell surface phenotype throughout the in vitro differentiation model via flow cytometry. B-cells isolated from PBMCs are activated with CD40L and F(ab')$_2$ anti-IgG/M at day 0 and left until day 3 where cytokines are added to induce differentiation. At day 6 APRIL is added to support survival signalling. By day 13 PCs have formed. At day 0, 6 and 13 samples are taken and stained with B-cell markers and the phenotype is then analysed by flow cytometry. This is a representative plot from an individual donor.

3.3 Cell viability during the differentiation response

As B-cells become activated, they leave the quiescent state and begin rapid proliferation and generate a large cell population. Within the GC, B-cells undergo rounds of affinity maturation and selection, with the population of cells dropping drastically after eliminating B-cells with an inefficient antibody binding capability. Therefore, in a normal T-dependent immune response the cells destined for terminal differentiation are only a small population. In the in vitro model, this effect of expansion and contraction is also observed, despite the lack of selective pressure that would normally take place in the light zone of a GC. Once the day 0 are stimulated, they proliferate rapidly and by day 6 have reached peak numbers. Following this, the cell population begins to drop continually up to day 13. Figure 3.2 shows the cell numbers determined by manual counting using a haemocytometer and trypan blue live/dead exclusion.

3.3.1 Cell count during the differentiation
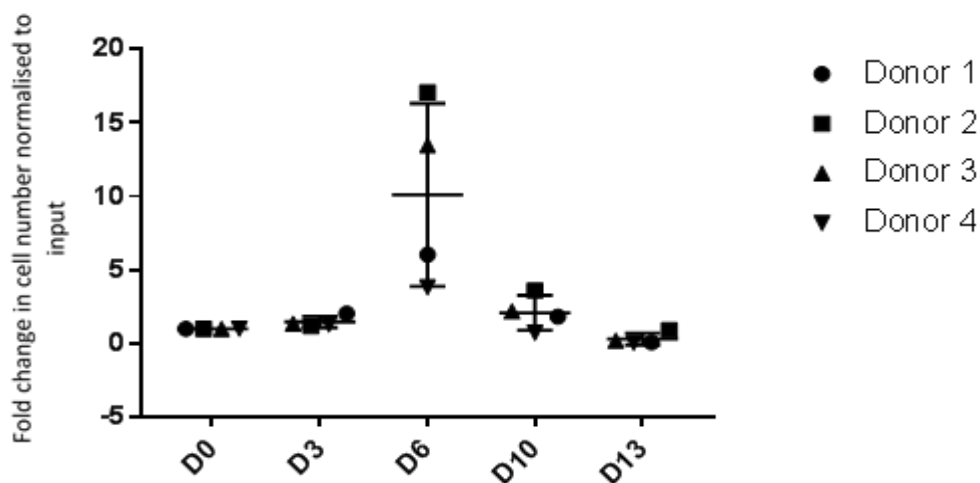
Figure 3.2 – Fold change in cell numbers during the differentiation. PBMCs were isolated from donors and B-cells were selected for. Cells were then cultured within the differentiation model. Cell numbers were determined at each time point of the differentiation and then normalised to the input cell count at day 0 (D0) to calculate fold change. Cell numbers were determined using a haemocytometer and trypan blue live dead exclusion N=4.

There is some variability in cell count over the time course. B-cell numbers generally increase a small amount between day 0 and day 3 but the main effect at this point is activation and preparation for cell division. The major proliferative stage occurs between day 3 and 6, at which point the cells are removed from CD40L and cell count increases by a large amount with a potential fold increase of up to 17x. There is some variability in cell counts by day, due to numerous potential factors including donor response variability and the proportion of starting memory vs naïve cells. From day 6 proliferation decreases and eventually stops, with the cells having committed to the PC programme. By day 13 cell count reaches similar levels seen at day 0.

3.3.2 Plasma cell phenotype attainment

Despite some variability in cell counts at day 6, the in vitro system is able to model the differentiation of B-cells accurately, with the majority of cells reaching the PC phenotype by day 13 (figure 3.3) indicated by the phenotypic marker CD138. CD138 begins to appear as early as day 6, but the percentage positivity is miniscule. Significant CD138 expression appears at day 10 with between 30-60% of cells expressing CD138. By day 13 expression increases and between 55-85% of cells are CD138 positive.
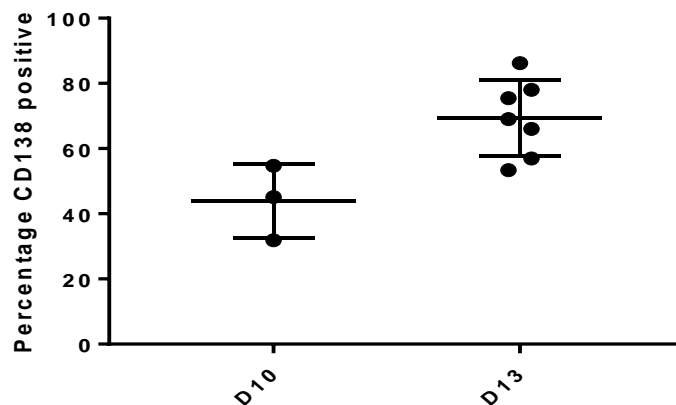
Figure 3.3– Percentage positivity of CD138 of healthy Day 10 and Day 13 plasmablasts/plasma cells. Day 10 and 13 cells obtained from the differentiation model were assessed for successful differentiation of plasma cell phenotype utilising CD138 as a marker via flow cytometry. Cells were taken at day 10 and 13, washed, blocked, and stained with antibodies targeting CD138. Cells were then assessed for CD138 expression via flow cytometry. (Day 10 N=3, day 13 N=7).

3.4 CXCR4 expression of differentiating B-cells from healthy control donors

3.4.1 CXCR4 surface expression flow data

Next it was necessary to determine the normal CXCR4 expression levels throughout the differentiation response. Determining expression levels is important for subsequent interpretation of signalling experiments. For example, an observation of lower MAPK activation may reflect either a lower degree of receptor engagement or altered signalling capacity. Expression of CXCR4 was analysed by flow cytometry throughout the differentiation at day 0, 6 and 13 (figure 3.4).
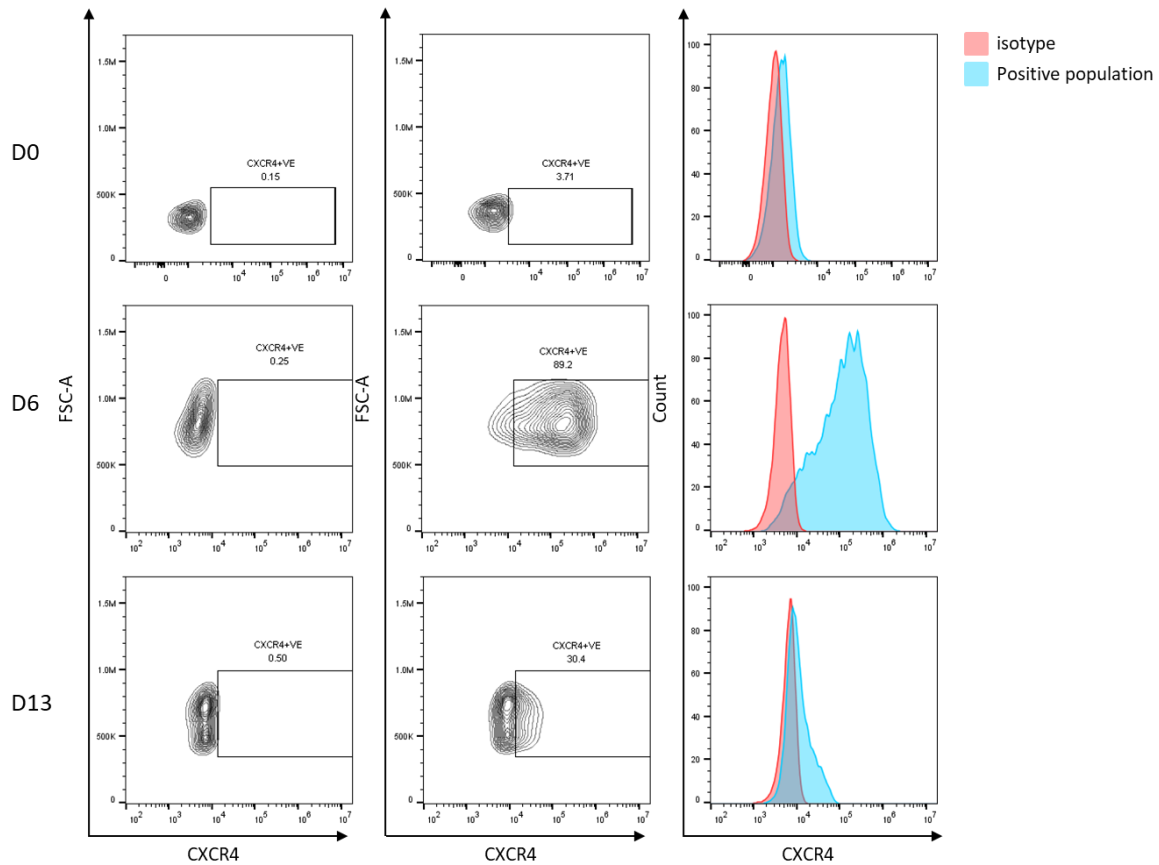
Figure 3.4 – Surface CXCR4 expression during the B-cell differentiation analysed by flow cytometry. Day 0, 6 and 13 B-cells/ASCs were cultured within the differentiation model and samples from the aforementioned days were collected, washed, blocked and finally stained with either a CXCR4 detection antibody or a mouse IgG isotype antibody and surface expression was measured (blue) compared to isotype control (red).Associated contour plots showing CXCR4 expression are also shown.

The expression was compared against an isotype to compensate for background staining from the antibodies. The day 0 flow data indicate very low levels of CXCR4 expression on resting B-cells. By day 6 CXCR4 expression is at its peak, which may reflect the role of CXCR4 in directing movement of PBs from the GC to the bone marrow. This is followed by a decrease in CXCR4 expression by day 13 despite the importance of CXCR4 for PC retention in the BM.

3.4.2 Quantification of CXCR4 expression

To compare the CXCR4 surface expression between samples, the surface expression was quantified as MFI. Delta MFI was then determined by subtracting the MFI of the isotype expression values from the MFI of the positively stained populations (figure 3.5). This confirmed that the pattern of expression was consistent across multiple donors.
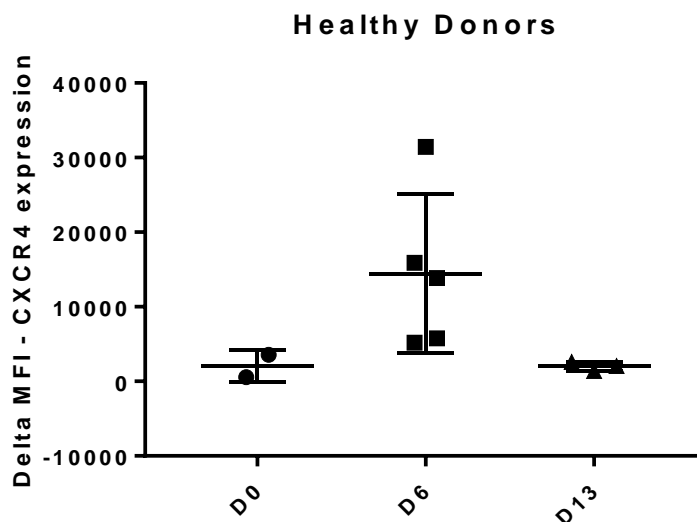
Figure 3.5 - ΔMFI of the surface CXCR4 expression of differentiating cells within the in vitro system. PBMCs were obtained and B-cells isolated. Cells were cultured in the in vitro B-cell differentiation system until they reached the plasma cells stage at day 13. Cells were collected at days 3, 6 and 13 for assessment of CXCR4 surface expression by flow cytometry. ΔMFI obtained from cells obtained from separate donors at day 0 (n=2), 6 (n=5) and 13 (n=3) and plotted.

3.5 Expression of CXCR4 in different culture conditions

The reduction in surface CXCR4 at the later stages of culture was unexpected, given the importance of this receptor in maintaining cells within a supportive niche. This may reflect a change in signalling requirements since the cells cease to migrate and instead may utilise CXCR4 for positioning or activation of survival pathways. Alternatively, it may be related to the culture conditions. To confirm that the culture conditions do not affect CXCR4 expression this was assessed at both mRNA and protein level.

3.5.1 *CXCR4* mRNA expression using different niche culture conditions

As mentioned in the Introduction, a benefit of the system is the ability to modulate conditions that a differentiating B-cell may encounter in vivo. Thus, PBs encountering APRIL and TGFβ in the niche are likely to be different from those generated under inflammatory conditions, mimicked by exposure to IFNα. Previous work in the lab has shown that short-term exposure to TGFβ led to a transient increase

of *CXCR4* (Stephenson et al). To determine whether these factors might influence the level of CXCR4 at later time points, available gene expression data sets were examined. Firstly, the microarray data indicate there are no major differences in *CXCR4* expression in differentiating B-cells cultured in either TGFβ, IFNα or APRIL conditions (figure 3.6). Under all conditions, *CXCR4* expression follows the same trend of peak expression at day 6, followed by a decrease until day 13.

To confirm the loss of mRNA expression of CXCR4 was not due to the increased cell death beyond day 6, mRNA expression for genes with expression that remains constant and genes that increase across the differentiation were assessed. mRNA levels for various housekeeping genes, such as TATA box binding protein (TBP), stayed constant across the differentiation. However, some housekeeping genes, such as β-actin (ACTB) and Glyceraldehyde-3-phosphate dehydrogenase (GAPDH) showed slight decreases by day 13. mRNA for expression for *PRDM1* (BLIMP1) expression increased to day 13, as expected. Together this indicates cell death may slightly affect the mRNA expression data, but generally indicates that the CXCR4 mRNA expression is real.
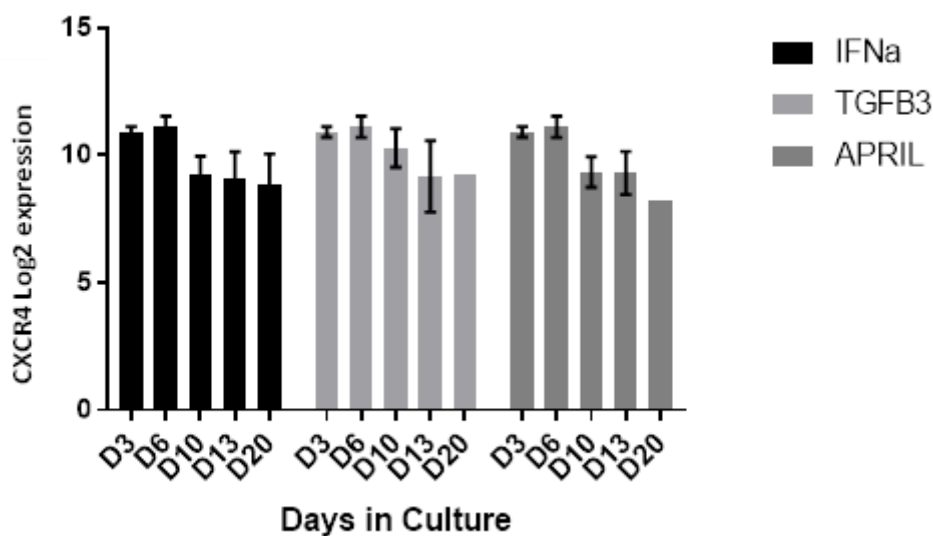
Figure 3.6 - CXCR4 mRNA levels in B-cells differentiated in 3 different culture conditions. B-cells were cultured as normal until day 6. From day 6 the cells were split and cultured in either IFNα, TGFβ3 or APRIL survival conditions, alongside normal cytokines and growth factors. RNA was collected at each of the specified time points and amounts quantified by microarray. Each bar represents CXCR4 mRNA expression levels at each time point for each culture condition These results are derived from 3 donors. Data from Sophie Stephenson and Matt Care. (N=3)

4.5.2 Surface phenotype analysis of culture conditions

Next, surface expression of CXCR4 was analysed via flow cytometry. B-cells were cultured as normal until day 6. From day 6 cells were cultured in the three different conditions, IFNα, TGFβ or APRIL alongside normal cytokines and supplements. Flow samples were analysed at day 6 (figure 3.7) and

day 9 (figure 3.7) for CXCR4 expression. Additionally, B-cell marker expression was determined for all conditions. At day 6, CXCR4 expression shows the expected upregulation and is consistent between donors. CXCR4 expression at day 6 was used to evaluate change in CXCR4 expression at day 9 under the different culture conditions.
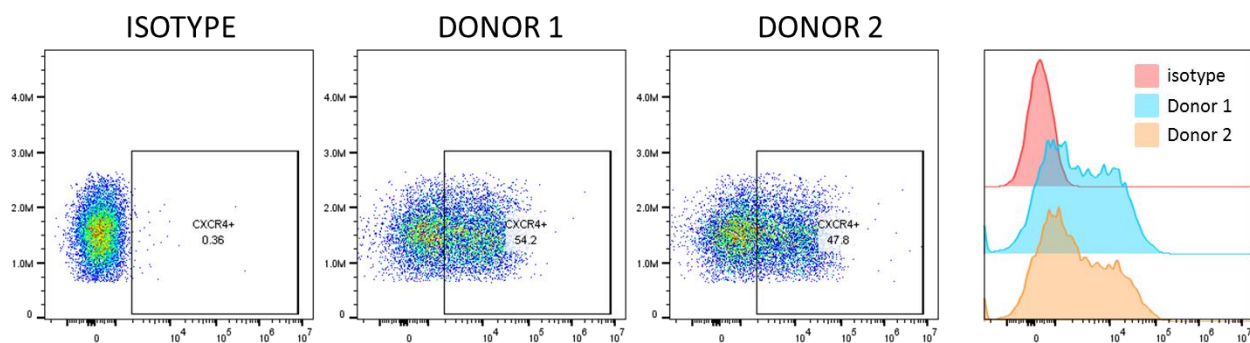
Figure 3.7 – CXCR4 expression on in vitro generated plasmablasts. B-cells were obtained from two donors and differentiated up to day 7 where CXCR4 expression was analysed to establish the starting point in surface expression as the cells differentiate under the three different culture conditions. Surface expression determined by flow cytometry using a CXCR4 detection antibody. N=2

Day 6 cells were then split into the three culture conditions (APRIL, IFNα and TGFβ) in addition to the normal differentiation cytokines and supplements given at day 6. CXCR4 surface expression was then analysed (figure 3.7). The day 9 CXCR4 expression data show only a small decrease in CXCR4 expression under APRIL and TGFβ conditions with a drop of less than 8% CXCR4 positive cells. Under IFNα conditions however, CXCR4 expression reduced by 16%. For donor 2, APRIL conditions actually maintained CXCR4 expression with only a 1.7% decrease in positive cells. TGFβ did show a greater decrease in CXCR4 expression compared to donor 1 (26.9%). Finally, IFNα conditions show a moderate decrease in expression of 14.7% (figure 3.8) Together this data indicate that, whilst there is some variation between donors, APRIL conditions maintained the greatest CXCR4 surface expression with only a slight change between day 6 and 9. Meanwhile, IFNα showed a somewhat greater loss of CXCR4 but was again consistent between donors (figure 3.9). TGFβ showed a much greater CXCR4 surface expression variation between donors. This could indicate a donor specific response to TGFβ, as previously an assessment of CXCR4 expression 24 hours after TGFβ exposure at day 6 showed enhanced expression (Stephenson *et al.* 2019) and may reflect the degree of differentiation in the two

cultures. Therefore B-cell and PC makers were assessed at day 9 (Badr *et al.* 2005; Muehlinghaus *et al.* 2005).
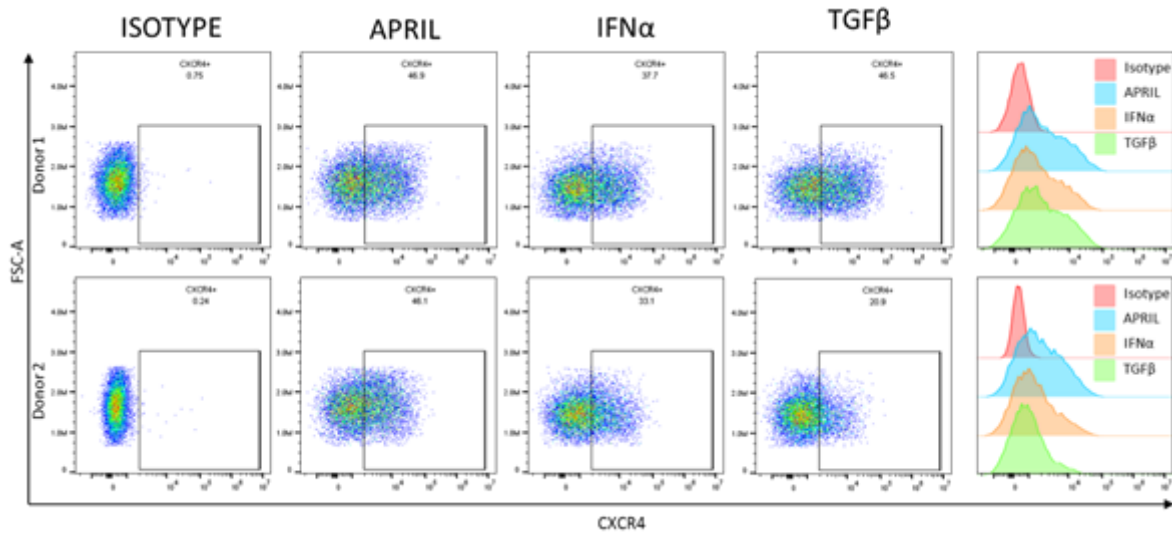
Figure 3.8 - CXCR4 surface expression of two donor B-cells/PBs under three culture conditions (APRIL, IFNα and TGFβ). Donor B-cells were differentiated past day 7 (**figure 3.**7) and CXCR4 surface expression determined by flow cytometry at day9 and analysed using FlowJo software. Dot plots indicate spread of population and histograms are included for direct comparison of populations (N=2).

At day 6 donor 2 had a larger percentage of CD19/CD20 double positive cells, indicative of a less differentiated population as B-cells downregulate CD19 and CD20 as they become PCs (figure 3.10). By day 9, this had equalised and the percentage of CD19/CD20 positive cells was similar between donors. However, TGFβ conditions showed a larger double positive population, suggesting this condition helps retain this phenotype, despite this condition also promoting the highest percentage
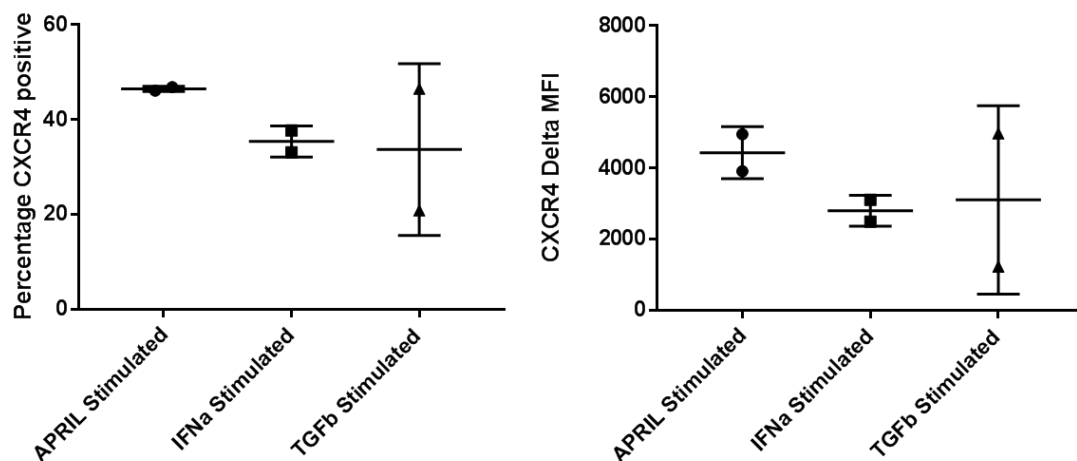
Figure 3.9 - Quantification of CXCR4 surface expression data for different culture conditions at day 9. Percentage CXCR4 positive population of cells assessed at day 9 (**figure 3.8**) were quantified and plotted for each culture condition (APRIL, IFNα and TGFβ). Delta MFI of CXCR4 surface expression for different culture conditions at day 9. MFI was determined using FlowJo software and delta MFI was calculated by subtracting the MFI of the isotype data (N=2)

of PC generation. This would help to explain the lower level of CXCR4 expression in donor 2. APRIL conditions generate the lowest percentage of PCs, which would match the generally higher CXCR4 percentage positivity seen in this condition. CXCR4 surface expression was mot measured beyond day 9 due to high cell death rates in these experiments. However, it is expected CXCR4 expression would be maintained at a low level, as seen in the mRNA data.
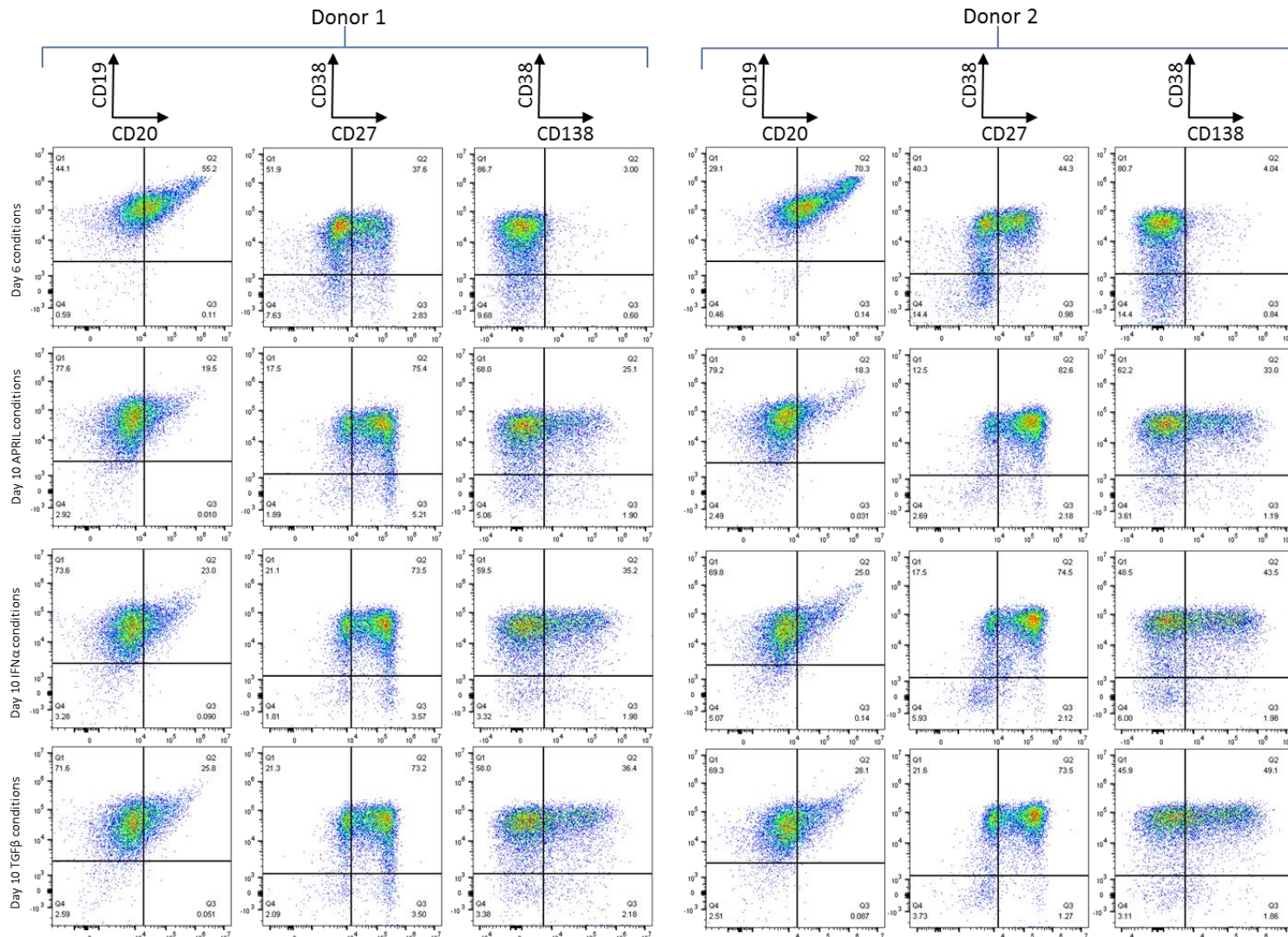
Figure 3.10 – Flow cytometry analysis of B-cell/PC phenotypic surface expression markers under three culture conditions (APRIL, IFNα and TGFβ). B-cells were isolated and cultured up to day 6 under normal conditions before separation into either APRIL, IFNα and TGFβ conditions. Day 6 B-cell/PC surface phenotype was determined before separation into culture conditions. Day 9 phenotype was analysed for each culture condition to determine effects on B-cell differentiation and associated changes to CXCR4 surface expression (N=2))

3.6 CXCR4 signalling response in B-cells and ASCs

During the process of PC differentiation, the B-cell intermediates use similar signalling pathways to integrate external information and produce potentially distinct outcomes. This can arise through collaborations between receptors and fine-tuning of signal strength and duration. To understand how CXCR4 signal propagation might influence developmental programs, initial investigation looked at the signalling in different populations of ASCs. To do this, the activation of key protein kinases regulating proliferation and survival were assessed in response to CXCL12 stimulation.

3.6.1 Impact of pre-stimulation conditions on the ability to detect pathway activation

Withdrawal of serum or survival factors can lead to the inactivation of PI3K and ERK1/2 signalling pathways (Ley *et al.* 2003). Therefore, transient depletion could enhance the detection of a response to CXCL12. Based on this reasoning, lowering the level of foetal calf serum (0.5%) either alone or combined with removal of the various cytokines and APRIL was trialled. Day 6 cells were cultured for 24 hours in depleted media and then stimulated by the addition of CXCL12. Lysates generated after 1, 5 and 10 minutes were analysed for the presence of ERK1/2 phosphorylation by Western blotting (figure 3.11). In the samples cultured in low serum there was no detectable pERK1/2 at time 0. Upon stimulation there was an increase in phosphorylation at 1 minute that diminished over time.
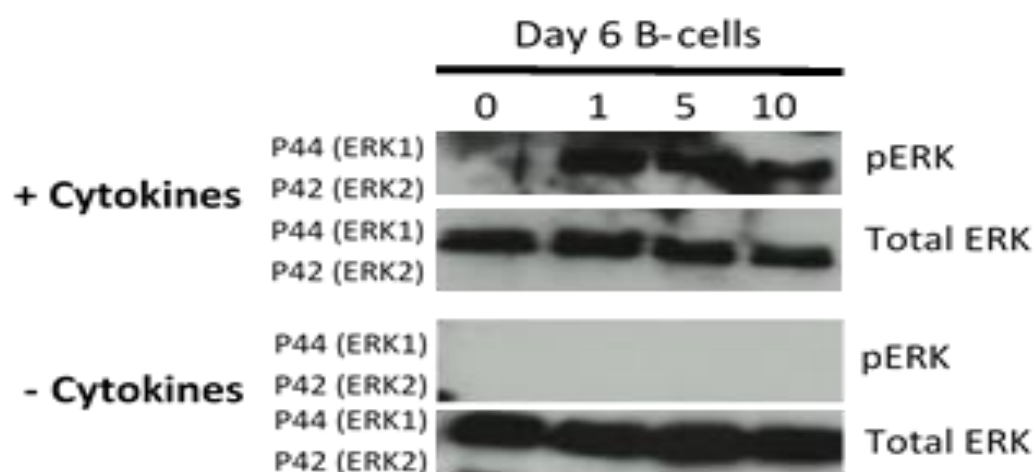
Figure 3.11 – Western blot analysis of ERK phosphorylation in day 6 B-cells stimulated with CXCL12 and cultured overnight with or without cytokines. Protein was obtained from day 6 B-cells and serum starved overnight with or without IL-21, IL-6, and APRIL. Amino acids and Lipids were omitted in both conditions. Protein was loaded onto SDS page gel and ran before being transferred to a nitrocellulose membrane and probed for detection of phosphorylated and total ERK protein using HRP-bound secondary antibodies bound to primary antibodies targeting these proteins. One representative blot shown (N=2).

In contrast, omission of day 6 reagents (IL-21, IL-6, APRIL) lead to a loss of inducible ERK1/2 phosphorylation. This could indicate significant stress and possibly cell death during the overnight deprivation. Subsequent experiments were therefore performed using the low serum only pre-incubation.

3.6.2 Impact of γ-secretase inhibitor (GSI) on CXCR4 and downstream signalling

At day 6 of the B-cell differentiation, APRIL was included to promote survival of ASCs. APRIL exerts its effect though interaction with B-cell maturation antigen (BCMA), which can upregulate expression of anti-apoptotic proteins, such as BCL-XL. APRIL was included in the serum starve prior to stimulation to both maintain as close to normal culture conditions as possible and to prevent excessive cell death. It has been suggested that BCMA can be cleaved from the cell surface by γ-secretase. Therefore, a γ-secretase inhibitor (GSI) was included in the in vitro model to prevent release of soluble BCMA, which would act as a decoy to neutralise APRIL. Previous experiments have shown that this strategy enhances the response to APRIL and leads to the production of a greater number of PCs (Belnoue *et al.* 2008; Benson *et al.* 2008; Laurent *et al.* 2015; Stephenson *et al.* 2021).

However, treatment of both B-CLL and myeloma cells with GSI was shown to downregulate CXCR4 expression and associated CXCL12 mediated cellular migration. Conversely, robust CXCR4 activation can overcome the cell cycle blockade and apoptosis induced by GSIs (Secchiero *et al.* 2017; Mirandola *et al.* 2013). Therefore, it was necessary to discern how best to maintain cells within low-serum conditions whilst minimising the impact on CXCR4 expression. Initially, CXCR4 expression was assessed from PCs taken directly from the in vitro differentiation culture when cultured with or without GSI and the ΔMFI was determined (figure 3.12).
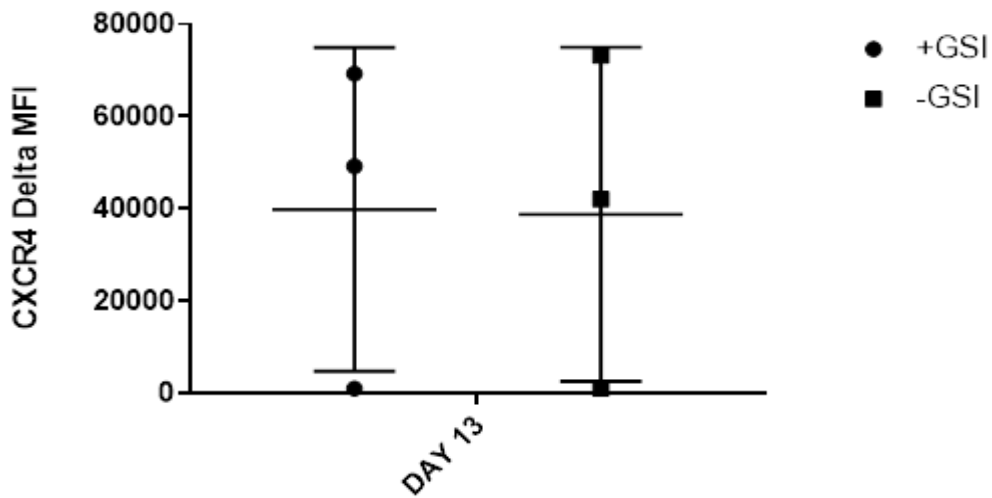
Figure 3.12 - ΔMFI of CXCR4 surface expression for day 13 PCs cultured with or without GSI. B-cells were isolated from 3 donors and differentiated in vitro. At day 6 B-cells/PBs were split into two culture conditions, with or without GSI. All other cytokines and supplements were added to both conditions. PCs were collected and stained for CXCR4 with a CXCR4 detection antibody and phenotype was assessed by flow cytometry. Surface expression was determined using FlowJo and ΔMFI was calculated by subtracting MFI values of isotypes. The data was plotted using graphpad prism software (N=3).

The data indicate that CXCR4 surface expression is unchanged by the presence of the GSI. To confirm that GSI does not modulate CXCR4 functionality, the effect of GSI on CXCR4 signalling was assessed. To do this, day 6 and 13 cells were serum starved overnight with or without the inclusion of GSI. The activation of ERK1/2 and AKT in response to CXCL12 was then assessed via Western blot (figure 3.13)
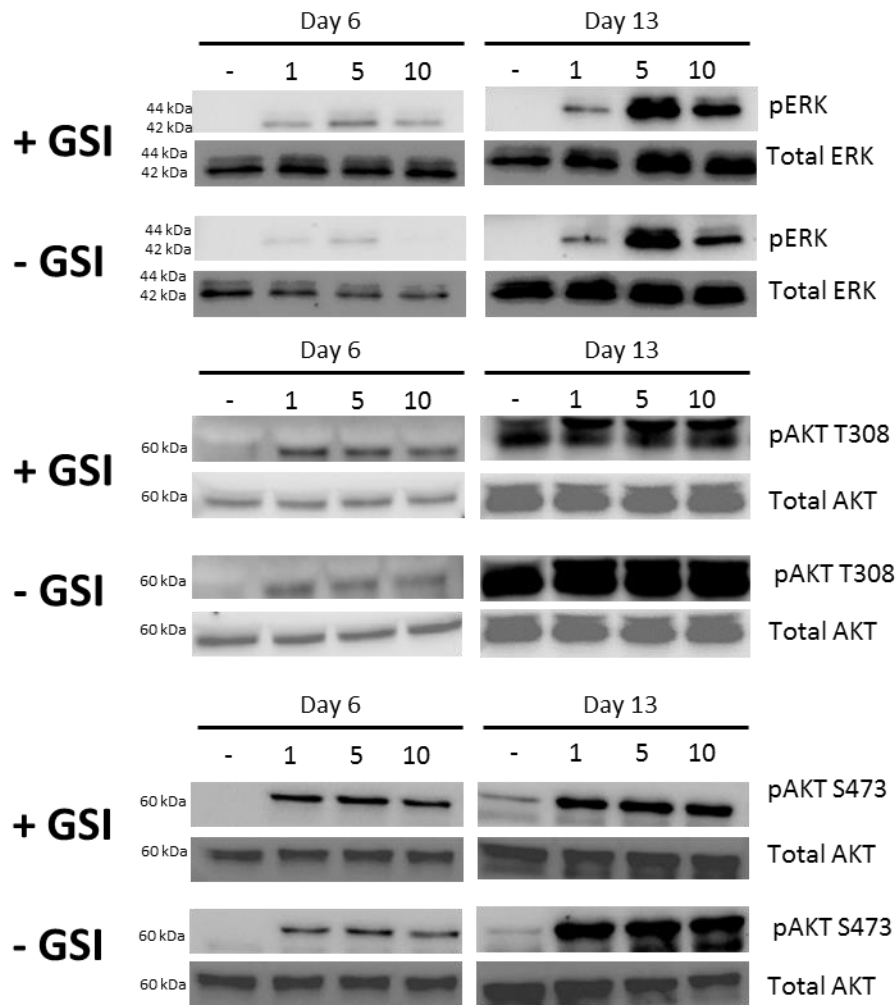
Figure 3.13 - Western blot analysis of phosphorylated and total ERK1/2, AKT T308, and AKT S473 protein in day 6 or 13 cells with or without GSI and stimulated with CXCL12. Protein was obtained from day 6 or 13 cells that had been serum starved overnight with or without GSI. Protein was loaded onto gels and SDS page was performed. Gels were transferred to blots and were probed for phosphorylated and total ERK and AKT protein. (N=2).

Based on the similarity of the total ERK1/2 detected between the conditions, there is likely very little difference in the ERK1/2 phosphorylation response. Indeed, the rate of phosphorylation is unchanged, however it is possible ERK1/2 phosphorylation is switched off quicker without the presence of GSI. At day 13 ERK1/2 activation is similar between both conditions. At both day 6 and 13, in both conditions, the AKT activation pattern at the T308 and S473 residues indicates a similar level of phosphorylation. From these data, there is reasonable evidence to confirm that GSI has a minimal effect on CXCR4 expression and signalling capabilities in this differentiation model and was therefore included in subsequent experiments.

3.6.3 Plasma cells generate a stronger ERK1/2 signalling response than plasmablasts

Previous work has shown CXCL12 stimulation of PBs generates a transient pulse of MAPK kinase signalling, inducing genes related to classic growth factor responses (Stephenson *et al.* 2019). The Ras/Raf/MEK/ERK1/2 pathway is important for proliferation and has been linked to cell cycle entry (Zwang *et al.* 2011). MAP kinase signalling has been associated with chemotaxis in leukocytes (Cara *et al.* 2001) however the effects of CXCL12 on these signalling pathways in PCs is as of yet undetermined.

Peripheral blood B-cells were isolated and cultured in APRIL conditions. At day 6, 10 and 13 a sample of cells was collected, serum starved overnight and stimulated with CXCL12. A pre-stimulatory sample was taken. Stimulated cells were added to sample buffer, 1, 5 and 10 minutes after stimulation. These samples were then analysed by Western blot (figure 3.14). Stimulation with CXCL12 activates ERK1/2 phosphorylation as early as 1 minute after stimulation in all cell populations. Additionally, peak ERK1/2 phosphorylation occurs at 5 minutes post stimulation at the various stages of PC maturation. Notably, day 6 PBs have the weakest activation of ERK1/2 signalling, whilst day 13 cells have the strongest ERK1/2 phosphorylation, despite the decline in cell surface expression of CXCR4. Data for day 10 varies
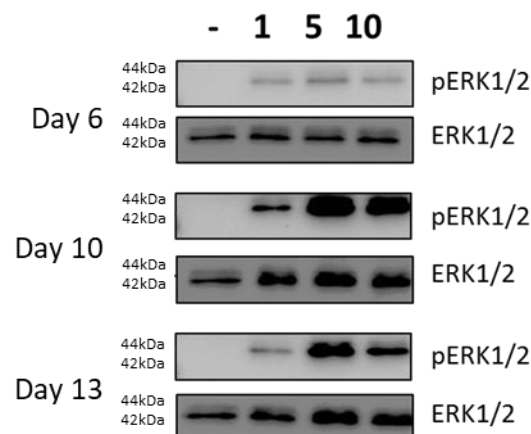
Figure 3.14 - Western blot analysis of phosphorylated and total ERK protein in day 6, 10 and 13 cells stimulated with CXCL12. A pre-stimulatory sample was taken before addition of CXCL12. Cells were added to sample buffer to obtain protein and then run on a SDS gel before being transferred to a blotting membrane and probed for phospho-ERK and total ERK. A Representative donor is shown (n=3)

significantly between donors. This is likely due to variation in donor differentiation rates and the population at day 10 being a transitional time point with more of a mix of PBs and PCs. Image lab software was used to quantify ERK1/2 phosphorylation for each donor (figure 3.15). Quantification of ERK1/2 phosphorylation confirms at both day 6 and day 13 cells, peak phosphorylation occurs at 5 minutes post stimulation, before decreasing at 10 minutes. The data suggests that PCs generate a stronger ERK1/2 signalling cascade compared to day 6 PBs and retain a higher signal for longer. Indeed, at day 13 there may still me some phosphorylation after 10 minutes. This suggests altered signalling

capabilities in response to CXCL12 as the cells mature and change from a proliferative, migratory population to a quiescent one that takes up residence in a survival niche (Bianchi and Mezzapelle 2020).
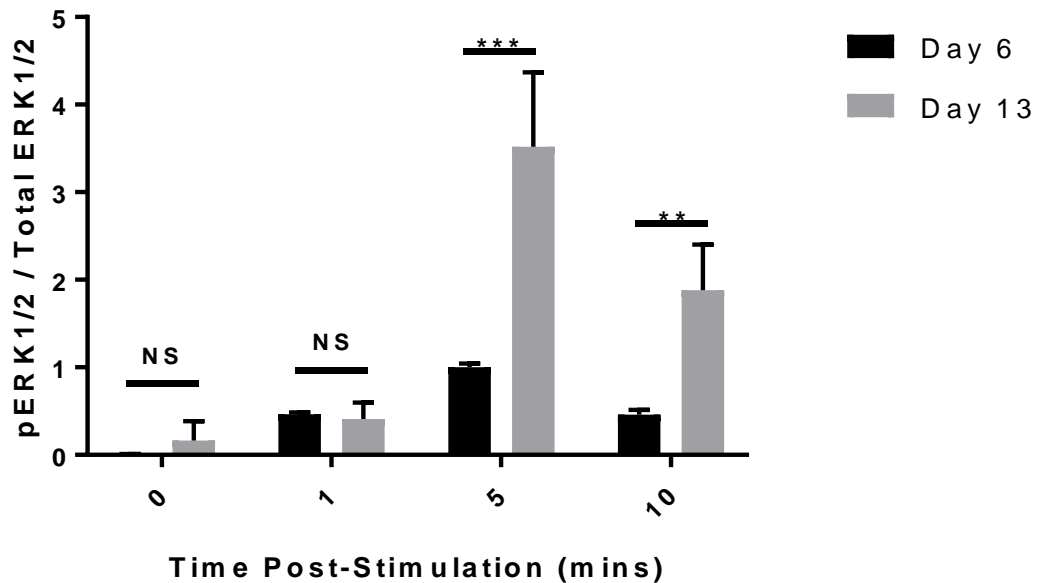
Figure 3.15 – Quantification of pERK signals in cells stimulated with CXCL12. ERK phosphorylation from 3 donors was quantified using Image Lab software. Additionally, total ERK protein levels were also quantified for each time donor at all-time points. Quantified pERK values were normalised to total ERK protein levels. The average of normalised values ± SD were then plotted for each donor. Each bar represents the pERK signal strength at the indicated time point after stimulation for both day 6 and 13 cells. Statistical significance was determined using a student multiple t-test between day 6 and 13 at each time point (n=3) (* = p<0.05; **=p<0.01, ***=P<0.001.)

3.6.4 AKT signalling response in PCs is enhanced compared to PBs

Alongside the MAPK signalling pathway, another notable non-receptor kinase target of CXCR4 signalling is the PI3K-AKT pathway. This signalling pathway is involved in survival mechanisms, proliferation, and migration. Notably, at different stages of the B-cell life cycle, AKT activation may become rewired to shift the selection of downstream targets and change the signalling response (Luo *et al.* 2019). It has been reported that GC B-cells express high levels of PDK1, which catalyses the phosphorylation of the T308 residue of AKT, whereas naïve B-cells express high levels of mTORC and PTEN which preferentially leads to the phosphorylation of AKT at the S473 residue. The balance of the phosphorylation at these two sites is thought to determine target specificity and differential signalling. Therefore, AKT phosphorylation was analysed at residues S473 and T308.
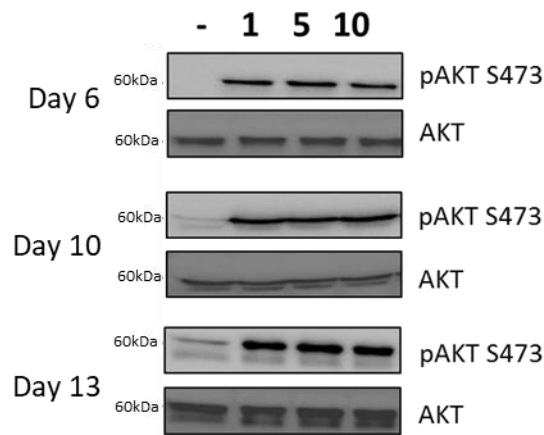
Figure 3.16 – pAKT S473 Western blot analysis of Day 6, 10 and 13 cells stimulated with CXCL12. A pre-stimulatory sample was taken before addition of CXCL12. Cells were added to sample buffer and run on a SDS gel before being transferred to a blotting membrane and probed for phospho-AKT S473 and total AKT. A Representative donor is shown (n=3)

Similarly, to ERK1/2, CXCL12 induces a stronger pAKT response in day 13 PCs compared to day 6 cells (figure 3.16). However, the peak phosphorylation lasts from 1 minute to 10 minutes, indicating an extended period of pAKT at all time points, suggesting less of a feedback mechanism to turn off AKT activation (figure 3.16). However, quantification of pAKT S473 activation normalised to total AKT shows that peak AKT phosphorylation at S474 occurs at 5 minutes but remains activated to a greater extent than ERK1/2. The general pattern shows that AKT phosphorylation at S473 is greater in day 13 cells, however there is a much greater variation between donors (figure 3.17).
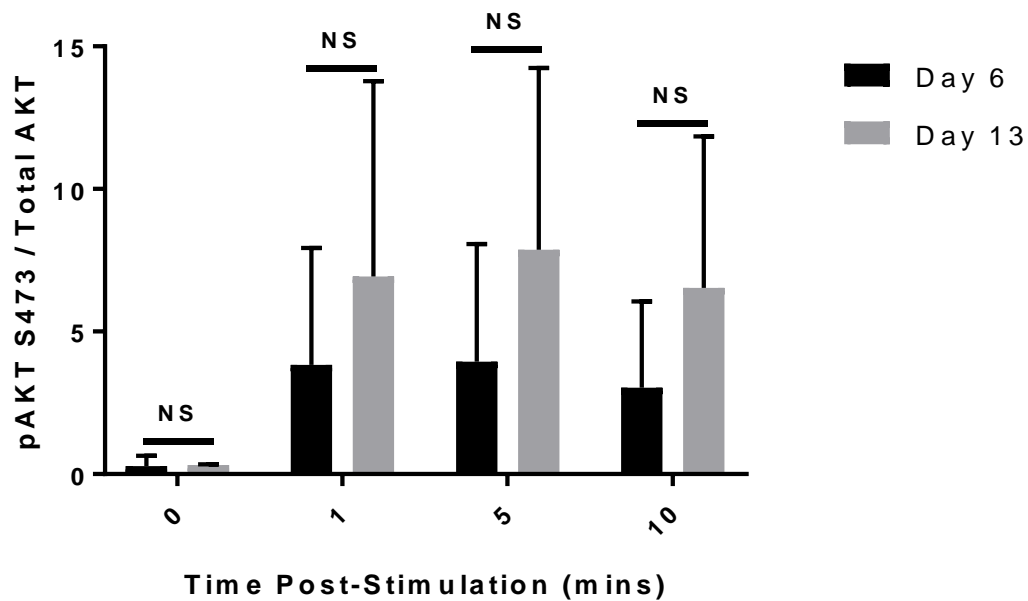
Figure 3.17 - Quantification of pAKT signals at residue S473 after CXCL12 stimulation. AKT phosphorylation from 3 donors was quantified using Image Lab software. Additionally, total AKT protein levels were also quantified for each time donor at all time points. Quantified pAKT values were normalised to total AKT protein levels. The average of normalised values ± SD were then plotted. Each bar represents the pAKT signal strength at the indicated time point after stimulation for both day 6 and 13 cells. Statistical significance was determined using a student multiple t-test between day 6 and 13 for each time point. (N=3).

Next, AKT phosphorylation was then analysed at the T308 residue (figure 3.18). At day 6, there is a clear activation of AKT at T308 that peaks 1 minute post stimulation. At day 13 there is a stronger activation of AKT, however the peak activation does not occur until much later during the stimulation, at about 5-10 minutes. Finally, in PCs AKT phosphorylation at this residue is much stronger and peak activation seems to occur at about 1-5 minutes after stimulation. Before stimulation there is a higher constitutive level of phosphorylation at this residue compared to day 10 and day 6.
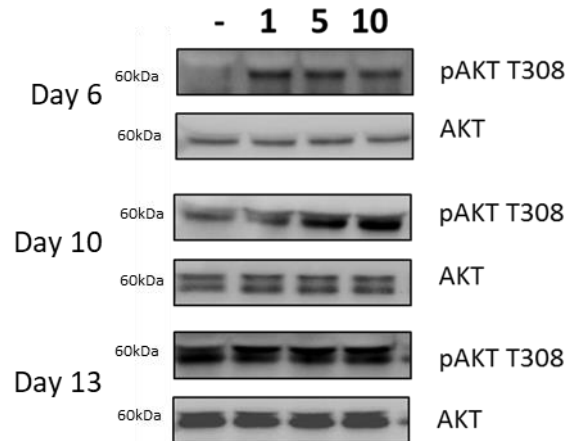
Figure 3.18 - pAKT T308 Western blot analysis of day 6 and 13 stimulated with CXCL12. A pre-stimulatory sample was taken before addition of CXCL12. Cells were added to sample buffer and run on a gel before being transferred to a blotting membrane and probed for phospho-AKT T308 and total AKT. A Representative donor is shown (n=3).

The pAKT T308 activation results were then quantified across all donors (figure 3.19). Day 6 cells exhibit only a low level of pAKT T308 phosphorylation in response to CXCL12 but is rapidly activated and short lived. In comparison, day 13 PCs generate a stronger, extended phosphorylation response. Additionally, there is a high level of variation between donors at day 13.

Analysis of the CXCL12 stimulation data indicate that at day 13, the cells are more responsive to CXCL12 signals, shown by a stronger and more sustained AKT response at both residues and a much stronger ERK1/2 phosphorylation. This likely ties in with changing requirements for migration of PBs to and retention of PCs within survival niches.
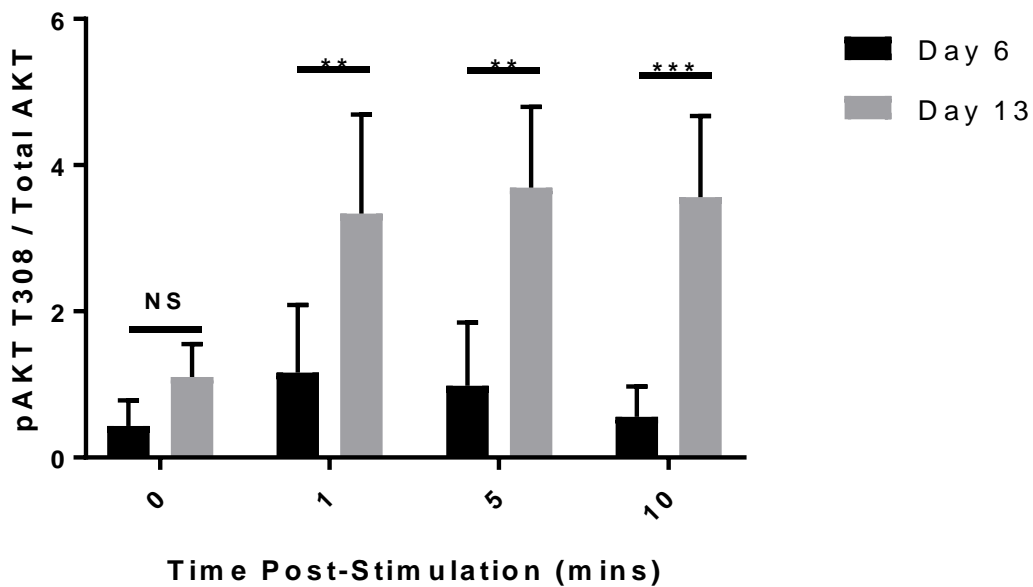
Figure 3.19 - Quantification of pAKT signals at residue T308 after CXCL12 stimulation. AKT phosphorylation from 3 donors was quantified using Image Lab software. Additionally, total AKT protein levels were also quantified for each time donor at all time points. Quantified pAKT values were normalised to total AKT protein levels. The average of normalised values ± SD were then plotted. Each bar represents the pAKT signal strength at the indicated time point after stimulation for both day 6 and 13 cells. Statistical significance was determined using a student multiple t-test between day 6 and 13 at for time points. N=3 (* = p<0.05; **=p<0.01, ***=P<0.001.)

3.6.5 Expression pattern of AKT isoforms

There are 3 isoforms of AKT: AKT1, AKT2 and AKT3. Structurally, they are very similar, yet they mediate different functions, both in health and disease settings. Particularly relevant to this study is the finding that AKT1/2 are involved in GC formation. B-cells deficient for AKT1/2 fail to survive or proliferate upon BCR stimulation and fail to form a GC, however this can be restored through CD40 ligation. Additionally, AKT1/2 activation inhibits FOXO1 activity, allowing upregulation of IRF4, therefore inducing PC differentiation (Zhu *et al.* 2019).

It was noted that two molecular weight AKT species were consistently detected on day 13 cells, which may indicate another means of rewiring the signalling output in PCs. AKT isoform expression was therefore assessed throughout the differentiation to determine to what degree AKT is expressed and whether particular isoforms dominate at different stages. Cell lysates generated from multiple stages of differentiation were assessed for AKT1 and AKT2 expression via Western blot (figure 3.20). Samples were also analysed for total AKT. Both donors showed a moderate level of AKT1 expression at day 0, but a lower expression level of AKT2. By day 3 expression of AKT1 and 2 increased. By day 6 expression of both isoforms had dropped slightly but were still highly expressed. At day 10 expression of the 60kDa form of AKT1 and had dropped notably. Instead, prominent bands were detected at a smaller size of 50 kDa. These bands were also detected at day 6 for both isoforms and day 3 for AKT 2. Additionally, 40 kDA bands were detected at day 10 for both isoforms. The high expression of AKT1 and 2 is likely related to the enhanced proliferation and survival signalling needed for activated B-cells. The pattern of fragmented AKT, notably at day 10 may be indicative of caspase-mediated cleavage (Wu *et al.* 2011) (Penela *et al.* 2019) that may accompany the high level of cell death between days 6 and 10.
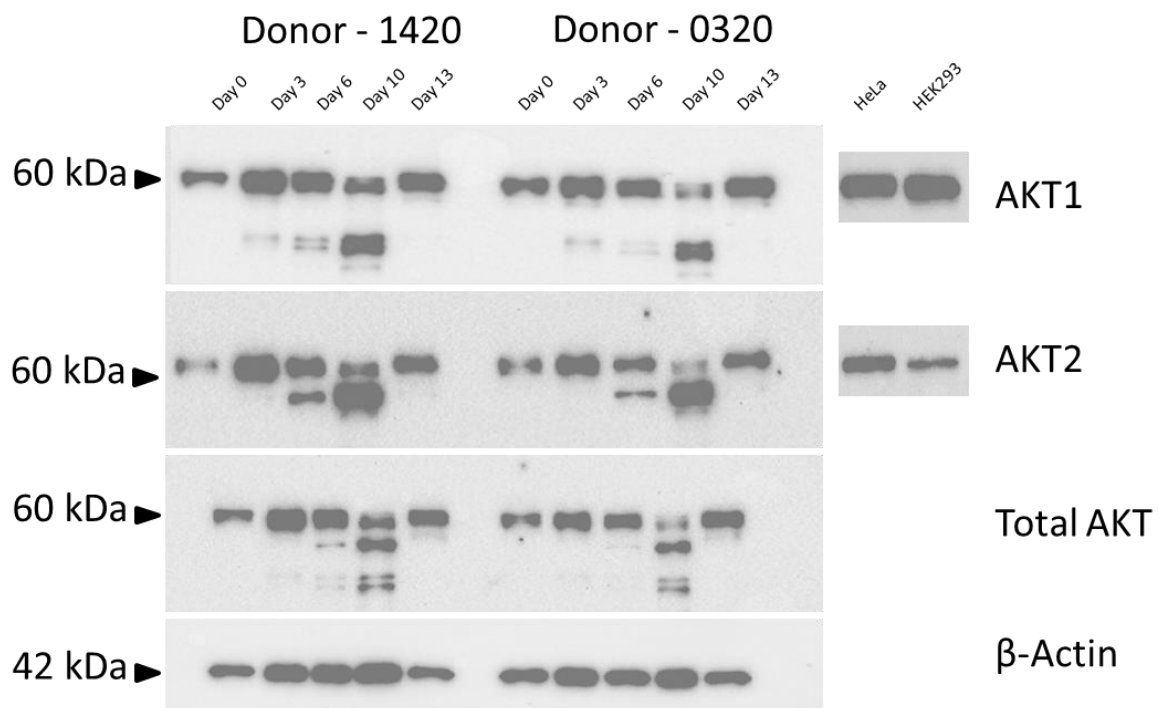
Figure 3.20 - Western blot analysis of AKT isoform expression in differentiating B-cells. Protein lysates from two donors and positive control cell lines HeLa and HEK293 were run on a SDS gel before being transferred to a blotting membrane and probed for AKT1, AKT2 and pan AKT expression. β-Actin was used as a loading control. N=2

3.7 Discussion

The work presented in this chapter was developed from the need to understand how CXCR4 signalling is altered during the differentiation of B-cells within an in vitro culture system, in particular during the transition from PB to mature PC. Several publications have documented how CXCL12 triggers different responses in early B-lymphopoiesis vs mature B-cells (McHeik *et al.* 2019; Egawa *et al.* 2001; Fedyk *et al.* 1999). It is also clear that PBs and PCs require CXCR4 to home to and take up residence in the bone marrow (Cheng *et al.* 2018), but the details of the signalling at these later stages remains unknown. Previous work in the lab has provided some initial insight into the signalling events downstream of CXCR4 in PBs, particularly those that have been generated in the presence of TGFβ. However, whether the effect of CXCL12 is the same in PCs has not been determined.

The flow cytometry analysis indicates that day 0 B-cells express the some of the lowest levels of CXCR4 surface expression, indicating that this protein in actuality may provide very little function for resting B-cells and is in agreement with the lack of response observed elsewhere (list of ref below). Although an intermediate time point was not assessed, by day 6, high levels of CXCR4 surface expression had been reached. The intervening activation stage is comparable to a germinal centre reaction, which is characterised by the cyclic movement of B-cells from the dark zone to the light zone and back again. This level of movement requires the control of specific chemokine-chemokine receptor interactions such as CXCR5 and CXCL13 and most importantly, CXCR4 and CXCL12. It would be of interest to monitor the precise pattern of upregulation at the earlier time points, but the prediction is that the high levels of CXCR4 seen at day 6 are the result of cells preparing to exit from a GC-like activation phase. Beyond day 6, the cells are phenotypically PBs, which then quickly develop into PCs. By day 13 these ASCs have a diminished CXCR4 surface expression which is slightly higher than that seen at day 0. This potentially indicates that PCs can cope with minimal CXCR4 once they have arrived at their survival niche, as other trophic factors may take over as the major contributors to long term PC survival. However, there are some limitations of this model. Additional environmental cues generated from a survival niche, such as was shown with TGFβ, may influence the expression of CXCR4 in PCs generated in vitro.

Despite this, generation of PBs and PCs of healthy donors within the differentiation model shows a consistent pattern of surface expression of key B-cell lineage markers in response to CD40L and BCR stimulation, with a maintenance of CD19, loss of CD20 and gradual upregulation of CD38, CD27 and CD138. Additionally, all samples show that the B-cells, once activated, undergo rapid proliferation up to day 6, followed by a contraction of cell numbers by day 13. Together, this is indicative of the

acquisition of a PC phenotype. Therefore the in vitro model is a robust and capable model sufficient for investigation of CXCR4 signalling mechanics in ASCs.

There are several advantages of utilising an in vitro model over an in vivo model. Firstly, in this type of study, ease of access to cells is crucial. B-cells can be isolated from PBMCs from multiple donors quickly. The in vitro model allows for collection and analysis of cells and their responses at various points during the differentiation without difficulty. Additionally, it allows for easy manipulation of the culture conditions. Further work envisioned for this project was to assess BM conditions and the signalling responses of B-cells and PCs. This flexibility provides an excellent model that cannot as easily be replicated in animals. There are however some drawbacks to using the in vitro model. An animal model would provide a more realistic response and is therefore more representative. A true GC does not form in the in vitro model. Instead, the presence of AID and relevant cytokines allows for affinity maturation without the need for a GC. Whilst this is sufficient for the generation of PCs, it does not truly reflect what occurs naturally, whereas an animal model would provide this. Mice models also provided a variety of tissues that can be analysed beyond PBMCs alone, including BM, spleen and thymus.

Subsequently, some investigation into the effects of different niche conditions on CXCR4 surface expression was completed. Microarray analysis was utilised to compare the *CXCR4* mRNA expression of differentiating B-cells cultured in with either APRIL, TGFβ or IFNα culture conditions. APRIL is a crucial survival factor that is secreted from CD68+ macrophages, which closely associate with BM resident PCs. It binds to BCMA on cells and has been shown to induce expression of the anti-apoptotic protein BCL-XL in CD138+ve PCs (Belnoue *et al.* 2008; Gabay *et al.* 2009).

TGFβ affects B-cells in many different areas of the differentiation process, such as isotype switching (van Vlasselaer, Punnonen and de Vries 1992). TGFβ has also been implicated in regulation of B-cell survival and proliferation but is often very context dependant in its effects. TGFβ has anti-proliferative effects, including inhibition of TFs associated with cell growth, such as c-MYC and the expression of CDK inhibitors (Zhang, Alexander and Wang 2017). The effects of TGFβ are less well described in PCs. As PCs are quiescent, it is unlikely TGFβ plays an anti-proliferative role. Indeed, previous work from our group has shown that proteomic analysis of the secretome of a BM stromal cell line was highly enriched for TGFβ (Stephenson *et al.* 2019). Subsequent studies revealed TGFβ acts as a pro-survival factor in PCs. Additionally, PCs pre-treated with TGFβ generate a sustained ERK1/2 activation signal after CXCL12 stimulation. Interestingly, the combined treatment of these cells also maintained an increased expression of c-FOS, which suggests a convergence of the TGFβ and CXCR4 signalling pathways. This sustained pERK1/2 signal stabilises c-FOS, which is associated with survival signalling

(Murphy *et al.* 2002). Interferons have a wide range of effects in B-cells including proliferative and anti-apoptotic roles. IFNα aids in the survival of myeloma cells (Ferlin-Bezombes *et al.* 1998) and has been shown to assist in generation of short lived plasma cells (Mathian *et al.* 2011).

Assessment of the microarray data show that under each condition, *CXCR4* mRNA expression peaks at day 3 and day 6 before dropping. TGFβ3 conditions retained *CXCR4* expression to the greatest extent after day 6 and up to day 20, followed by IFNα, but overall, the effect of each condition was comparable. Protein analysis indicates that APRIL conditions retained the highest CXCR4 surface expression. IFNα retained the least. TGFβ conditions generated a varied response, with some cells maintaining a high level of CXCR4 expression and some expressing much less. The variance between the two samples may be due to donor variation, perhaps relating to the differences in differentiation rate. Error in reagent preparation is unlikely due to both samples receiving the same TGFβ stimulating media. Additional repeats would determine if this was a random event. The average ΔMFI however was again similar between each condition. It is likely that there are multiple other BM trophic factors that can influence CXCR4 expression. To build on this data, a more faithful simulation of a BM environment should be utilised at specific points in the differentiation. Factors to assess would include components such as MIF, anti-CD44 and CD40L. Similar to the results obtained with TGFβ3 and CXCL12, these trophic factors may modulate the signal transduction events downstream of CXCR4 and should be assessed. Additionally, a range of samples should be used, including MGUS, smouldering MM, symptomatic WM, relapsed WM, and refractory WM. This would enable a more complete understanding of the relationship between CXCR4 expression and its role in different types of ASC populations.

In addition to CXCR4 expression, cell surface phenotype was assessed for each condition. Phenotypic analysis indicates that cells from all three conditions generated a robust PC population, shown by CD138 expression. However, APRIL conditions generated the smallest CD138+ve population, whereas IFNα and TGFβ conditions generated more comparable percentages of CD138+ve cells at the day 13 time point. Together this indicates a slower rate of differentiation in APRIL stimulated cultures. Moreover, the signalling dynamics may vary between these cell populations, further highlighting the importance of investigating the effects of the bone marrow niche.

Evaluation the signal transduction events downstream of CXCR4 are crucial for understanding the nature of CXCL12-induced survival mechanisms in long-lived PCs and their malignant counterparts. PI3K and MAPK kinase signalling are major pathways utilised by both healthy and malignant B-cells (Leleu *et al.* 2007) and are both activated by CXCL12. Initial analysis indicates that day 6 PBs show a weaker phosphorylation of ERK1/2 in response to CXCL12 stimulation than in day 13 PCs. Additionally,

PI3K/AKT signalling is amplified in PC compared to PBs, however there is some variation between donors. Given that PBs and PCs exhibit distinct differences in cell cycle status, longevity, and location in vivo, it is reasonable to suggest that they are potentially wired differently for downstream signalling events. Indeed, downstream of CXCR4 there a various Gα, Gβ and Gγ proteins, PI3Ks and PLCs, and a variety of scaffold proteins and modulators that will affect signalling cascade, kinases interactions and post-translational modifications that could contribute to the observed patterns (Bianchi and Mezzapelle 2020). For example, in the in vitro system, *PIK3CD* is highly expressed in resting and activated B-cells, but the mRNA is repressed as the cells differentiate (Cocco *et al.* 2012). In contrast, *PIK3CA* mRNA is maintained throughout differentiation and *PIK3CG* mRNA is induced at the PB stage and maintained at high levels in PCs. Also, there is evidence that AKT signalling is rewired during different stages of B-cell activation, with changes in the relative levels of T308 and S473 phosphorylation in GC and naïve B-cells (Downward 1998; Luo *et al.* 2019), and the data presented here are also consistent with such a change as the cells undergo terminal differentiation. Additionally, analysis of AKT isoforms revealed fragmentation of AKT protein at day 10 of the differentiation, possibly consistent with caspase-mediated degradation (Jahani-Asl, Basak and Tsang 2007). Day 10 is characterised by a continuing contraction of the cell population. Thus, the loss of AKT signalling may contribute to the death of PBs within the model which may be overcome by the inclusion of caspase inhibitors. Analysis of the CXCL12 stimulation data indicate that at day 13, the cells are more responsive to CXCL12 signals, shown by a stronger and more sustained AKT response at both residues and a much stronger ERK1/2 phosphorylation.

Changes between a transient and a sustained signalling response likely leads to different biological outcomes, indeed PCs by nature develop into long lived PCs within a BM niche, whereas PBs are a transient stage and therefore short lived. Here, identification of differences in both AKT and ERK signal intensity and duration may be key factors that define these traits. Additional studies investigating the role of niche environment on these signal pathways may help provide clarity (Mendoza, Er and Blenis 2011). A future study could assess TGFβ pre-treatment of PBs and PCs and looking to see how PI3K and MAPK signalling impacts expression of immediate early response genes such as EGR1 and c-FOS and also functional effects such as motility and survival (Stephenson *et al.* 2019; Murphy *et al.* 2002).

4.0 CD19 as a signalling hub in antibody secreting cells

4.1 Introduction

CD19 is a B-cell lineage surface receptor expressed highly in B-cells and also in PCs. The primary role of CD19 is to reduce the threshold for BCR activation, by acting as a scaffold, forming an active SH2-recognition domain for effector molecules e.g., VAV, important for signal transduction downstream of the BCR (Depoil *et al.* 2008). In B-cells, CD19 has been shown to act as a scaffold for receptor coordination for other receptors including CXCR4 (Keppler *et al.* 2015). Furthermore, the authors suggest that CXCR4 utilises CD19 as a means of recruiting PI3K as other receptors do, including BAFFR, CD40, TLR and the BCR. The ability of CD19 to act as a central hub of PI3K signalling may be important in instances of low signalling input requiring amplification as might occur during tonic BCR signalling. The choice of co-receptors used by B-cells can potentially alter the types of PI3K employed and therefore the coupling to downstream pathways. As such, the role of CD19 and CXCR4 co-stimulation was assessed here. Furthermore, the role of CD19 as a signalling hub has been described only in B-cell populations, where the cells possess a BCR. The relationship between the aforementioned surface receptors on PBs and PCs has yet to be investigated.

4.2 Stimulation of antibody secreting cells by CD19 ligation

CD19 amplifies signalling downstream of the BCR through the formation of a complex with CD21 and the BCR. Tyrosines within the cytoplasmic domain of CD19 acts as scaffold proteins that, when phosphorylated due to BCR interaction with antigen, function as SH2 motifs that recruit regulatory BCR associated tyrosine kinases. CD19 can then bind and amplify the activity of these tyrosine kinases such as LYN, leading to recruitment of PI3K. PI3K can then promote activation of AKT and BTK. Moreover, CD19 has been shown to enhance the activation of MAPK pathways in BCR-activated cells, and in some instances CD19 ligation alone is sufficient to activate ERK activity (Li and Carter 2000; Morbach *et al.* 2016; Tedder, Inaoki and Sato 1997).

Similarly, CD19 may act as a signalling hub to amplify CXCR4 related survival signalling through association with both the BCR and CXCR4 in B-cells. To observe how CXCR4 and CD19 interaction may modulate downstream signalling at later time points during differentiation, stimulations were to be prepared to assess co-stimulation of CXCR4 with CXCL12 and CD19 with an anti-CD19 coupled to beads. Initially however, direct stimulation of CD19 alone was investigated to see what intrinsic capabilities CD19 activation has on these pathways (figure 4.1), (figure 4.2).

4.2.1 αCD19 induced ERK signalling

Analysis of ERK signalling following CD19 ligation (figure 4.1) shows a notable absence of ERK phosphorylation at both day 6 and day 13 for all samples. For two samples, there was no detectable ERK activity at both day 6 and day 13. The final sample shows a faint band that looks to be non-specific. There are variable levels of total ERK protein in each sample, likely due to the effects of stripping buffer, however at day 13 in all samples there is a high level of ERK detected.
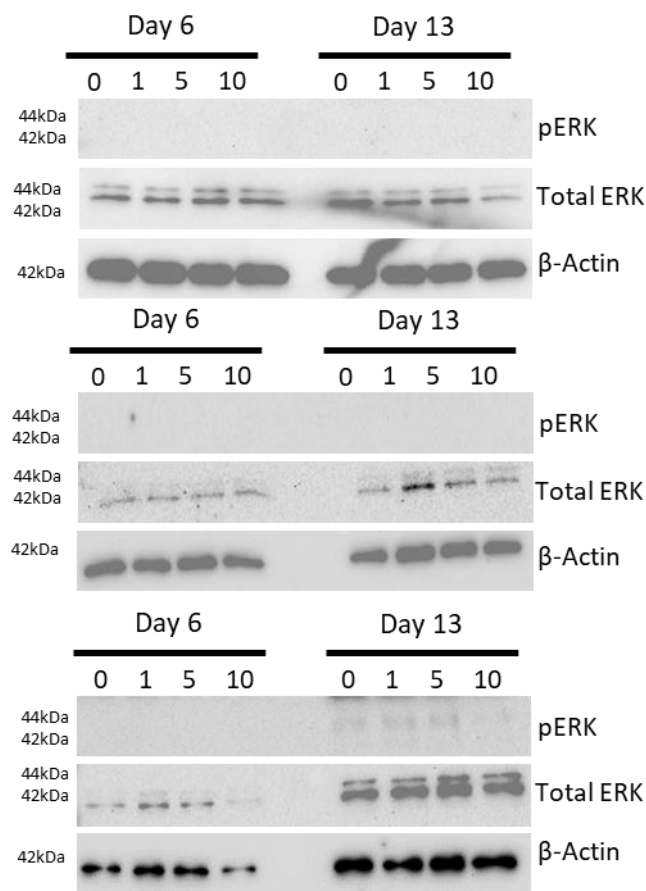
Figure 4.1 - Western blot visualising phosphorylated ERK of day 6 plasmablasts and day 13 plasma cells stimulated with αCD19 microbeads. B-cells were cultured in normal differentiation conditions. At day 6 and day 13, a sample of cells were transferred to 0.5% serum conditions overnight. Following overnight starvation, cells are stimulated with αCD19 microbeads, with samples taken pre-stimulation, 1, 5 and 10 minutes after stimulation and mixed with sample buffer immediately. Samples are then analysed by gel electrophoresis, before transfer to a blotting membrane and probed for phosphorylated and total ERK protein. Actin was used as a loading control. (N=3)

The data suggests that CD19 stimulation has a very small effect on inducing ERK signalling, especially compared to CXCR4 activity. Therefore, it is likely that the proposed signalling hub role of CD19 does

not involve contributions to MAPK activation, but instead is restricted to PI3K. It was important to assess CD19 stimulation on AKT phosphorylation to confirm this theory.

5.2.2 αCD19 induced AKT activity

Following from the ERK signalling analysis, AKT phosphorylation was assessed after αCD19 stimulation (figure 4.2). The Western blots show no visually detectable AKT phosphorylation at day 6 for all samples at both the S473 and T308 residue, despite detectable total AKT levels. Non-specific bands can be detected for one sample at day 13 at the T308 residue for most samples. These bands are smaller than the expected molecular weight and do not show a clear pre-stimulatory sample band, however they may mask the presence of a fainter band. Together this suggests there is little to no AKT
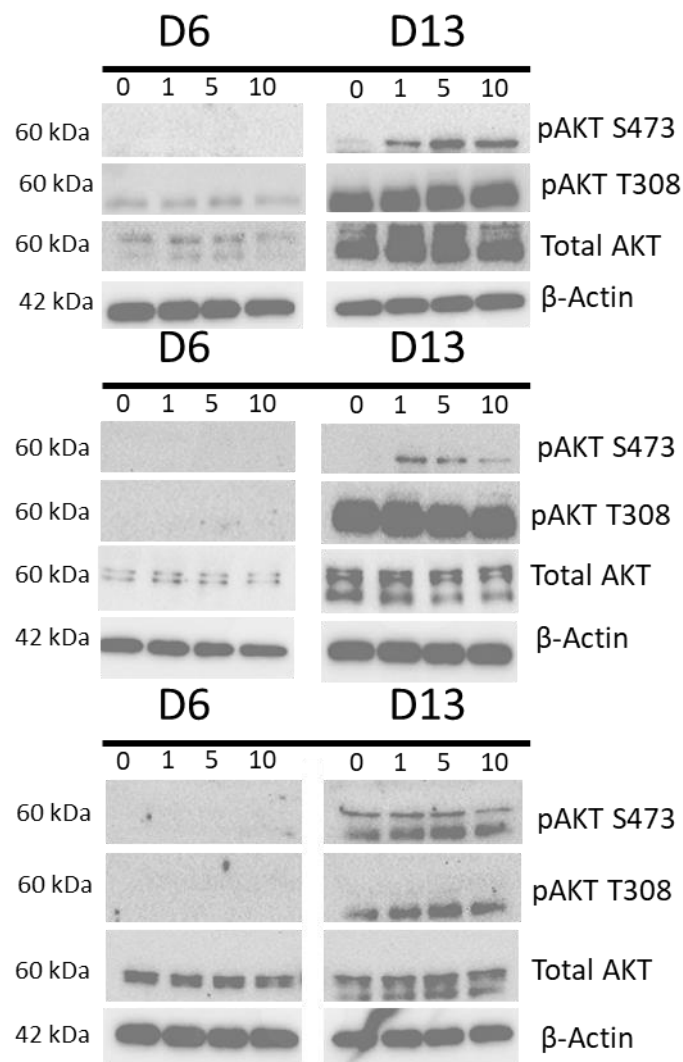
Figure 4.2 - Western blot visualising Phosphorylated AKT activity of D6 B-cells and D13 PCs Stimulated with αCD19 microbeads. B-cells were cultured in normal differentiation conditions. At day 6 and day 13 cells are cultured in 0.5% serum conditions overnight. Following overnight starvation, cells are stimulated with αCD19 microbeads, with samples taken pre-stimulation, 1, 5 and 10 minutes after stimulation and mixed with sample buffer immediately. Samples are then analysed by gel electrophoresis before transfer to a blotting membrane and probed for phosphorylated and total ERK protein. Actin was used as a loading control. (N=3)

phosphorylation at T308. At day 13, there are bands detected indicating phosphorylation at residue S473. These bands are clear and show convincing evidence for CD19 induced activity.

This western blot data set was then quantified (figure 4.3). Quantification of the AKT blots confirms the failure of CD19 to activate AKT phosphorylation in day 6 cells at the S473 residue, whilst generating a moderate phosphorylation response at day 13. A comparable level of phosphorylation can be detected at both day 6 and 13 at the T308 residue, however this may be affected by the non-specific bands and therefore this result should be taken with caution. Furthermore, the unusual pattern of phosphorylation does not match that seen previously of a peak at 1 or 5 minutes, followed by a decrease by 10 minutes, further suggesting that the bands quantified are overshadowed by the presence of non-specific bands.
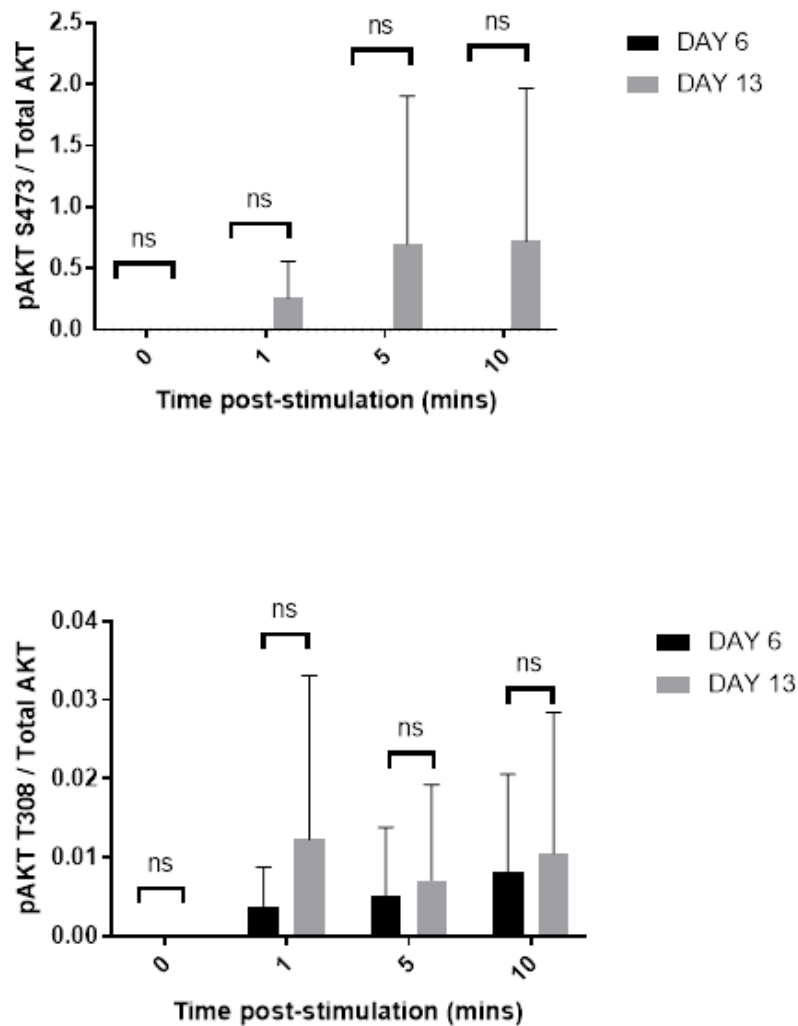
Figure 4.3 - Quantifications of AKT phosphorylation westerns shown in figure 4.2. Day 6 and day 13 cells were stimulated with αCD19 microbeads, with samples taken pre-stimulation, 1, 5 and 10 minutes after stimulation and mixed with sample buffer immediately. Samples are then analysed by gel electrophoresis before transfer to a blotting membrane and probed for phosphorylated and total AKT protein. Densitometry was performed on the western blots of both pAKT at residue S473 (upper) and T308 (lower). Day 6 and day 13 Western data for 3 donors was quantified using the Image Lab software. Each bar represents the pAKT signal strength at 1,5 and 10 minutes post stimulation for both day 6 and 13 cells. (N=3). Significance was determined using multiple Wilcoxon tests.

Next, this data set was compared with the quantified Western data of cells stimulated with CXCL12 (figure 4.4). At the S473 residue, the data show a similar pattern of stimulation between day 6 and 13 of both αCD19 stimulation and CXCL12 stimulation. At day 6, both stimulations induce a weaker phosphorylation pattern, though αCD19 stimulation induces a weaker response at both time points compared to CXCL12 stimulation, most notably at day 13. Additionally, as seen in figure 4.3, there is almost no phosphorylation occurring at day 6 after αCD19 stimulation. There is a high degree of variability at day 13 for CXCL12 stimulations, shown by the large error bars, which may reflect the variable percentage of cells that have attained a plasma cell phenotype. The error bars for the αCD19

stimulated cells at day 13 are smaller, suggesting αCD19 stimulation may generate a more consistent response.

At the T308 residue, CXCL12 stimulated cells generate a much stronger phosphorylation signal at both time points. The detected phosphorylation pattern seen in figure 4.2 for αCD19 stimulation is far smaller than that by CXCL12 stimulation, suggesting αCD19 likely does not induce significant phosphorylation at this residue.
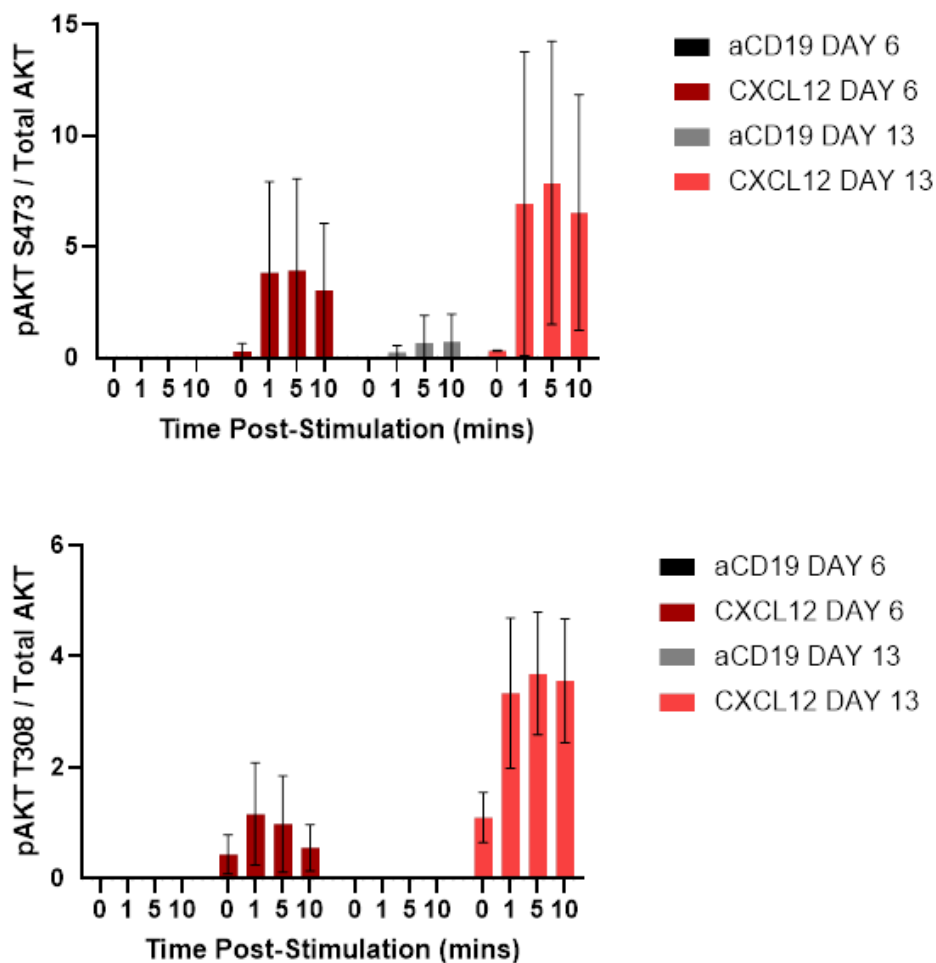
Figure 4.4 - (A) Comparison of the quantifications of the AKT S473 phosphorylation western blots shown for CXCL12 and αCD19 stimulated cells. Protein from day 6 and 13 cells stimulated with either CXCL12 or αCD19 beads was obtained and loaded onto SDS gels before transference to a blotting membrane. Blots were assessed for phosphorylated AKT at serine S473. The day 6 and day 13 western data of cells stimulated with either CXCL12 (figure 3.18) or αCD19 beads (figure 4.3) was quantified using Image Lab software and compared. **(B) Comparison of the quantifications of the AKT T308 phosphorylation western blots shown for CXCL12 and αCD19 stimulated cells.** Protein from day 6 and 13 cells stimulated with either CXCL12 or αCD19 beads was obtained and loaded onto SDS gels before transference to a blotting membrane. Blots were assessed for phosphorylated AKT at serine T308. The day 6 and day 13 western data of cells stimulated with either CXCL12 (figure 3.18) or αCD19 beads (figure 4.3) was quantified using Image Lab software and compared. Each bar represents the pAKT signal strength at the indicated time point after stimulation with either CXCL12 or aCD19 stimulating beads for both day 6 and 13 cells. (N=3)

Collectively, these data show CD19 stimulation with a CD19 cross-linking antibody generates a weaker ERK and AKT response compared to cells stimulated by CXCL12. However, the pattern of

phosphorylation is similar for both stimulations, with day 13 cells showing stronger AKT and ERK activation compared to day 6 cells.

4.3 Effects of long term CD19 stimulation

Stimulation of plasmablasts with αCD19 beads did not generate a notable signalling response, suggesting that direct ligation of CD19 is unlikely to have a biological impact at this stage of differentiation. To test this, plasmablasts were cultured in the presence of the antibody-coupled beads and assessed after an extended period.

4.3.1 Cell viability

Cells from 3 donors were cultured as normal up to day 6. At day 6, the cells were split between three conditions, normal day 6 conditions including APRIL, day 6 conditions with αCD19 stimulating beads and finally day 6 conditions without APRIL or αCD19 beads. Cells were maintained in culture from day 6 until day 10. At day 10 a cell count was performed using absolute counting beads (figure 4.5). As expected, inclusion of APRIL enhanced cell viability. In contrast, CD19 stimulation had no effect.
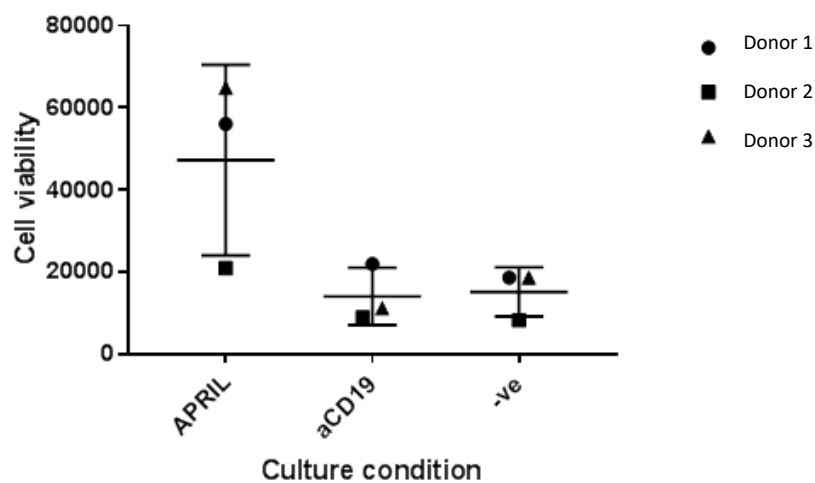
Figure 4.5 - Cell viability of D10 PB/PCs cultured in either APRIL, αCD19 or control conditions. B-cells obtained and isolated from peripheral blood were cultured within the *In vitro* model up to day 6. At day 6 cells were split into three culture condtions; APRIL, αCD19 beads or neither (-ve) and maintained until day 10. At day 10, cell viability was determined via cell counts using counting beads and flow cytometry (N=3)

4.3.2 B-cell and PC phenotype

The phenotype of each sample was then assessed to determine how CD19 stimulation may affect B-cell differentiation (figure 4.6). The flow data indicate CD19 expression is maintained in all conditions, with the majority of cells CD19+ve (>97%) (5.7.1). There are no notable differences at this level

between the conditions, indicating that the beads do not affect surface levels after 3 days of contact. However, there is variability in the proportion of CD19+ CD20 -ve population (figure 4.7).
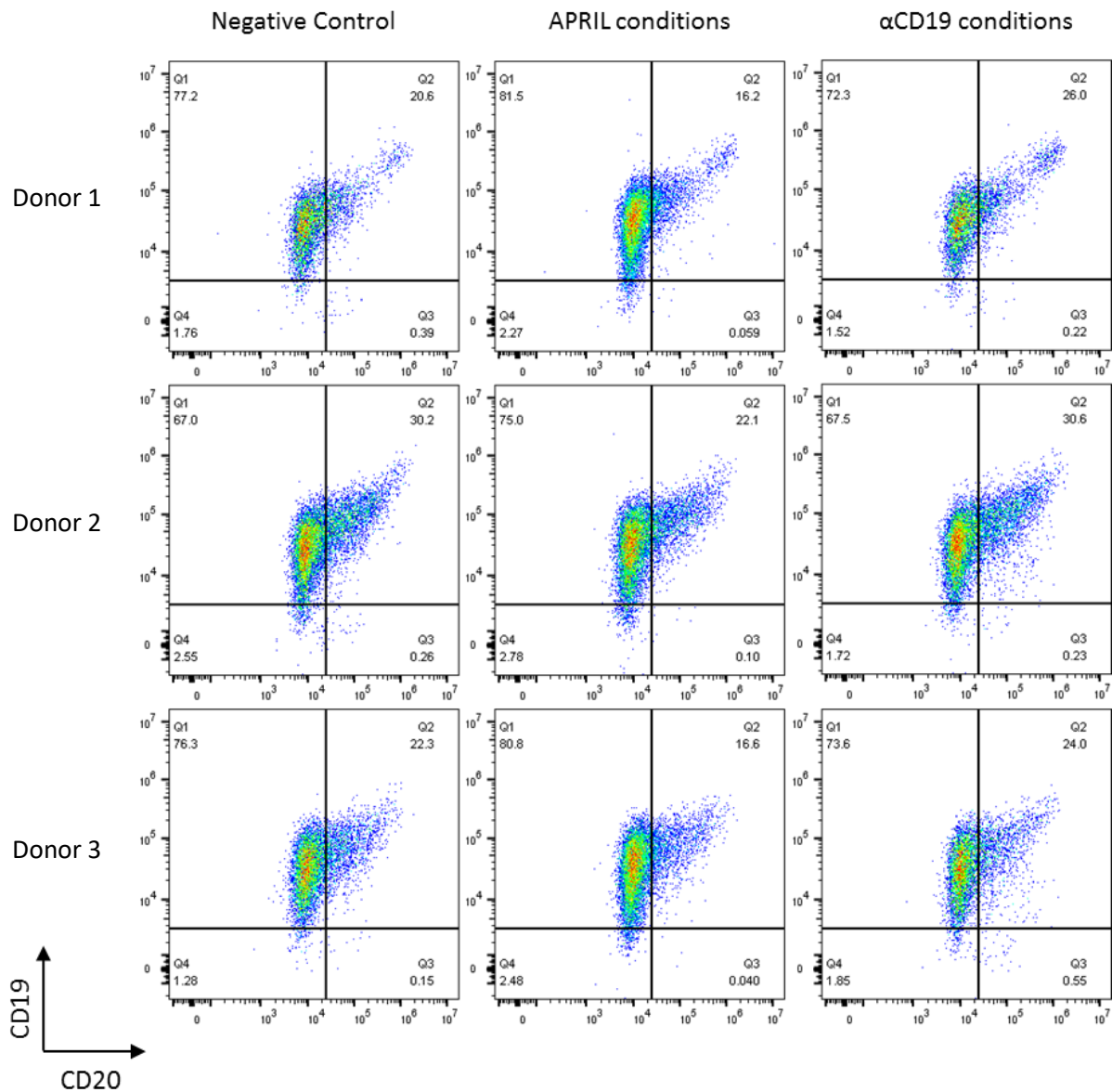
Figure 4.6 – Impact of APRIL or αCD19 on CD19/CD20 surface expression. B-cells obtained and isolated from peripheral blood were cultured within the In vitro model up to day 6. At day 6, cells were split into three culture conditions; APRIL, αCD19 beads or neither (negative control) and maintained until day 10. Flow samples were obtained and stained with antibodies against CD19 and CD20 and the phenotype as assessed. Results from 3 independent donors are shown.
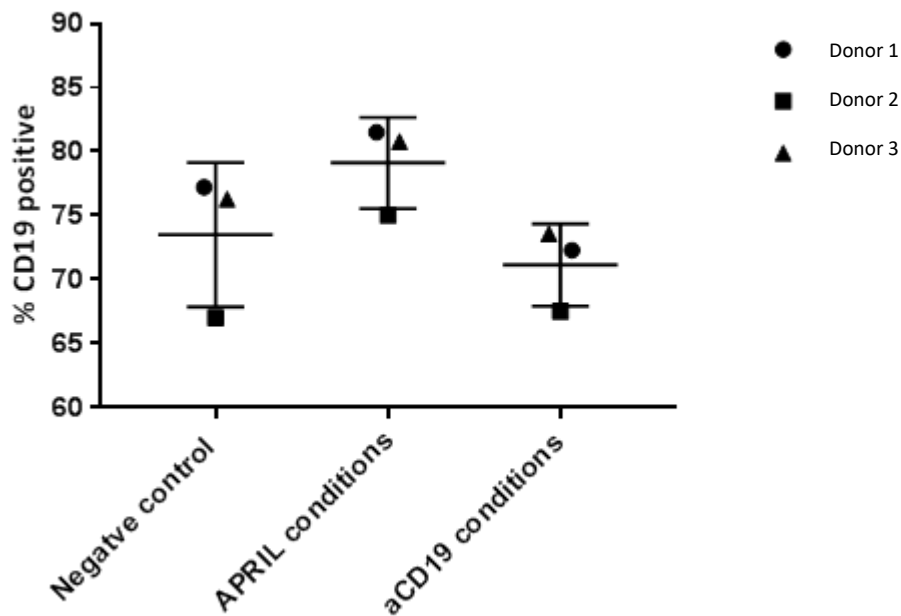
Figure 4.7 - Percentage of CD19+ CD20- day 10 PB/PC from three donors cultured in either APRIL or αCD19 conditions. . B-cells obtained and isolated from peripheral blood were cultured within the In vitro model up to day 6. At day 6, cells were split into three culture conditions; APRIL, αCD19 beads or neither (negative control) and maintained until day 10. Flow samples were obtained and stained with antibodies against CD19 and CD20 and the phenotype as assessed. The percentage of cells that are positive for CD19 but negative for CD20 (Q1 from figure 4.6) was quantified and plotted in graphpad prism.

The loss of CD20 is indicative of transitioning to the plasma cell state. To confirm this, plasma cell generation was assessed via CD138 expression (4.8). The data show that, under all three conditions, plasma cell differentiation is generally comparable. However, to confirm that there are no trends, the percentage CD138 expression was assessed (figure 4.9).
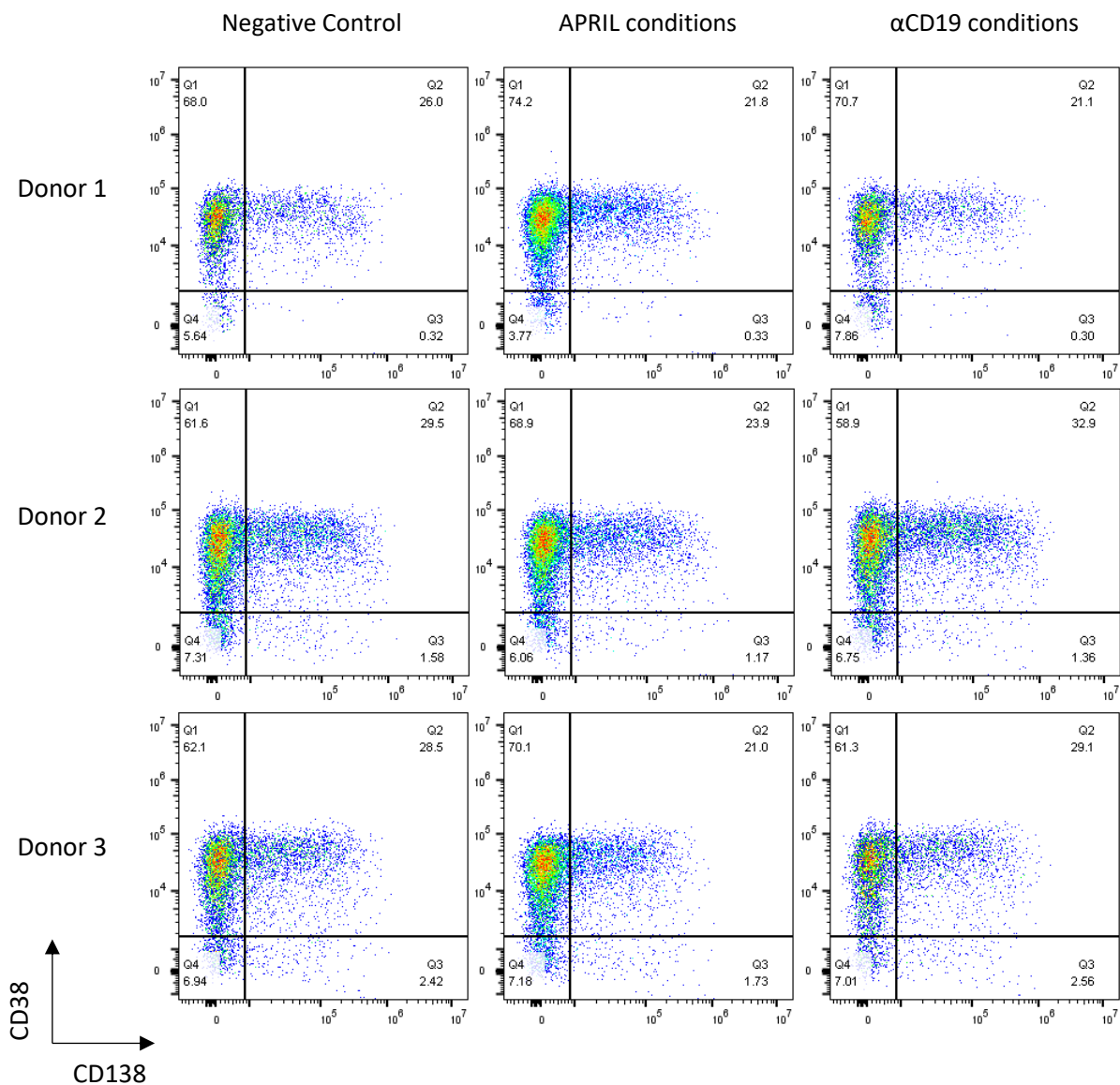
Figure 4.8 - CD38/CD138 surface expression of day 10 PB/PCs from three donors cultured in either APRIL or αCD19 conditions. B-cells obtained and isolated from peripheral blood were cultured within the In vitro model up to day 6. At day 6, cells were split into three culture conditions; APRIL, αCD19 beads or neither (negative control) and maintained until day 10. Flow samples were obtained, and stained with antibodies against CD38 and CD138 and the phenotype as assessed. Results from 3 independent donors are shown.

The analysis of CD138 expression indicates that APRIL conditions promote the lowest attainment of plasma cell phenotype, potentially due to the retention of proliferative cells that have survived compared to untreated or αCD19 treated cells. The differences between each condition are small, however.
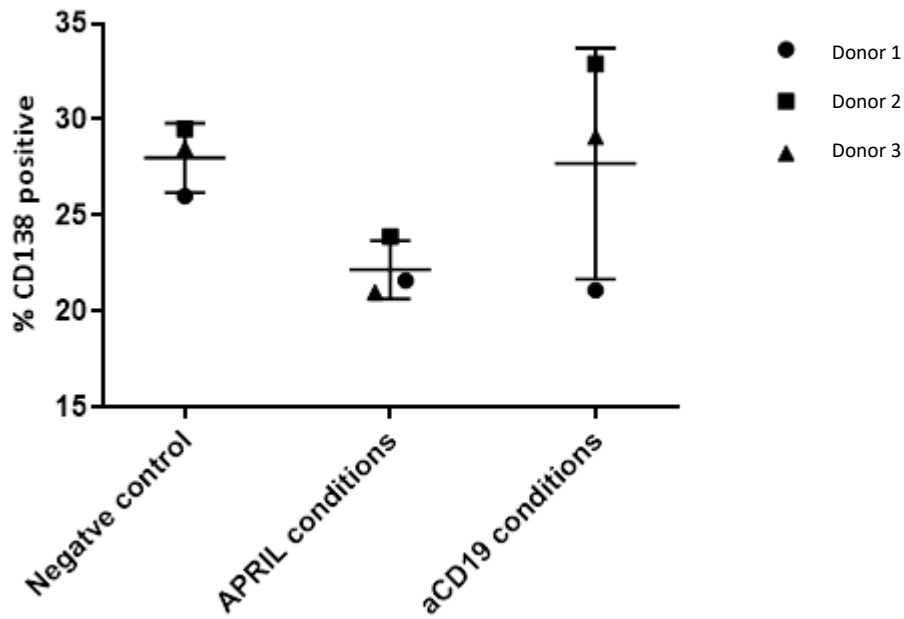
Figure 4.9 - Percentage of CD138 +ve day 10 PB/PC from three donors cultured in either APRIL or αCD19 conditions. B-cells obtained and isolated from peripheral blood were cultured within the In vitro model up to day 6. At day 6, cells were split into three culture conditions; APRIL, αCD19 beads or neither (negative control) and maintained until day 10. Flow samples were obtained and stained with antibodies against CD138 and the phenotype as assessed. The percentage of cells that are positive for CD138 (Q2 from figure 4.8) was quantified and plotted in graphpad prism.

Together, this data indicate that long term αCD19 stimulation has a minimal effect of PB/PC phenotype. There are slight differences seen with PC cell generation (CD138), however the observed differences are small and require a larger sample set to provide full confidence of any significant differences.

4.3.3 CXCR4 expression

CXCR4 surface expression was also analysed for the long-term stimulation with CD19 bound beads. As CD19 acts as a signalling hub for various surface receptors including CXCR4, long term stimulation may affect subsequent CXCR4 signalling. Despite the minimal activity seen in short term stimulation with CD19, there may be an accumulative effect seen over a long-term stimulation that may have effects on B-cell differentiation. CXCR4 surface expression was assessed for all three conditions and showed a comparable surface expression for all three (figure 5.7.6). BC1 showed the highest CXCR4 expression of the 3 donors for all conditions, notably αCD19 stimulation. Despite this, figure 4.10 confirms the similarity between the three conditions.
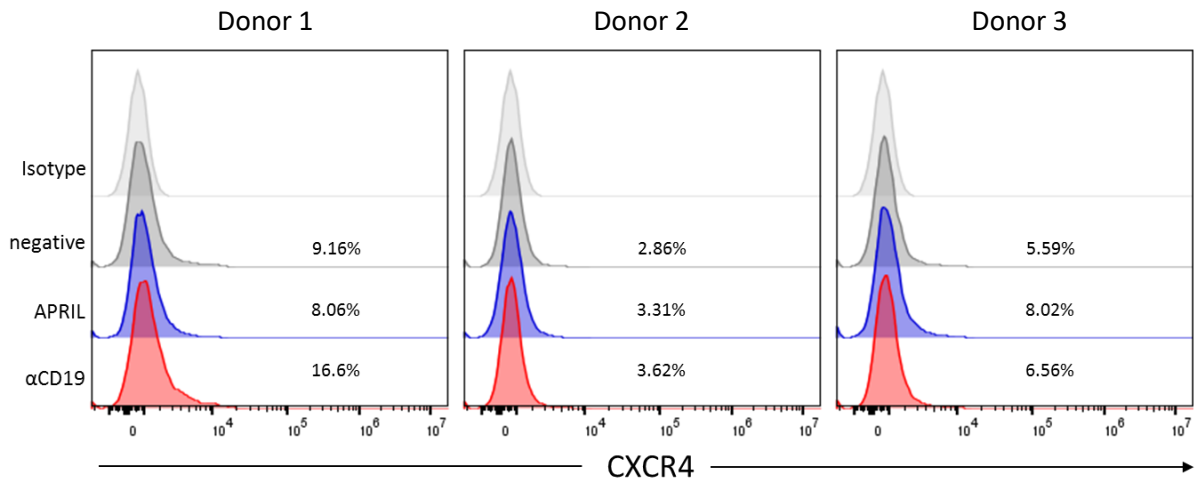
Figure 4.10 – CXCR4 surface expression for D10 PBs/PCs cultured in either APRIL conditions or αCD19 conditions. . B-cells obtained and isolated from peripheral blood were cultured within the In vitro model up to day 6. At day 6, cells were split into three culture conditions; APRIL, αCD19 stimulating beads or neither (negative) and maintained until day 10. Flow samples were obtained and stained with antibodies against CXCR4 and the phenotype was assessed. The percentage of cells that are positive for CXCR4 are indicated for each condition. An isotype control is included. (N=3)

Figure 4.11 shows the ΔMFI values for CXCR4 surface expression for each donor and condition. The data indicate there are no notable differences between each condition and therefore CXCR4 surface expression is maintained at a comparable level even after stimulation with αCD19.
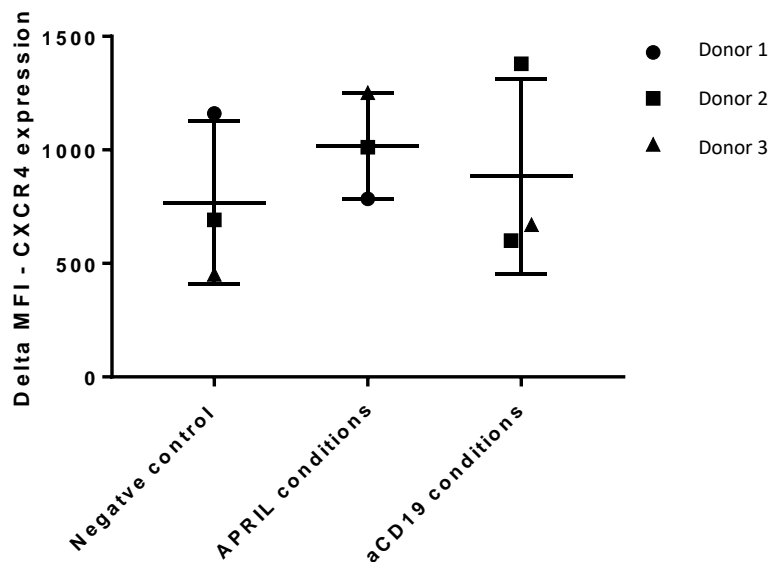
Figure 4.11 –CXCR4 ΔMFI for ASCs cultured in APRIL or αCD19 bead conditions.

B-cells obtained and isolated from peripheral blood were cultured within the In vitro model up to day 6. At day 6, cells were split into three culture conditions; APRIL, αCD19 stimulating beads or neither (negative) and maintained until day 10. Flow samples were obtained and stained with antibodies against CXCR4 and the phenotype was assessed. CXCR4 MFI was determined using the Flowjo software and the MFI of the isotype CXCR4 expression values was subtracted to determine ΔMFI.

Although the range of assays to test the ligation of CD19 at the plasmablast stage were limited, the data support the idea that it is unlikely to play a major role through direct ligand encounter. Since CD19 also functions to aid BCR and other surface proteins by acting as a signalling scaffold, it was therefore necessary to investigate whether its main role in antibody secreting cells was more likely to reflect its ability to boost signals following ligation of other receptors.

4.4 Co-stimulation of antibody secreting cells by an anti-CD19 and CXCL12

Previous work has shown that stimulation with an antibody to CD19 increases CXCL12-mediated responses in murine B-cells (Becker et al., 2017). To determine whether a similar response could be observed in human ASCs, plasmablasts and plasma cells were stimulated with both CXCL12 and αCD19.

4.4.1 αCD19 and CXCL12 induced ERK signalling

Initially, ERK signalling was assessed after stimulation with CXCL12 and αCD19. Cells were serum starved as previously prior to stimulation. Cells were collected at 1, 5 and 20 minutes after stimulation
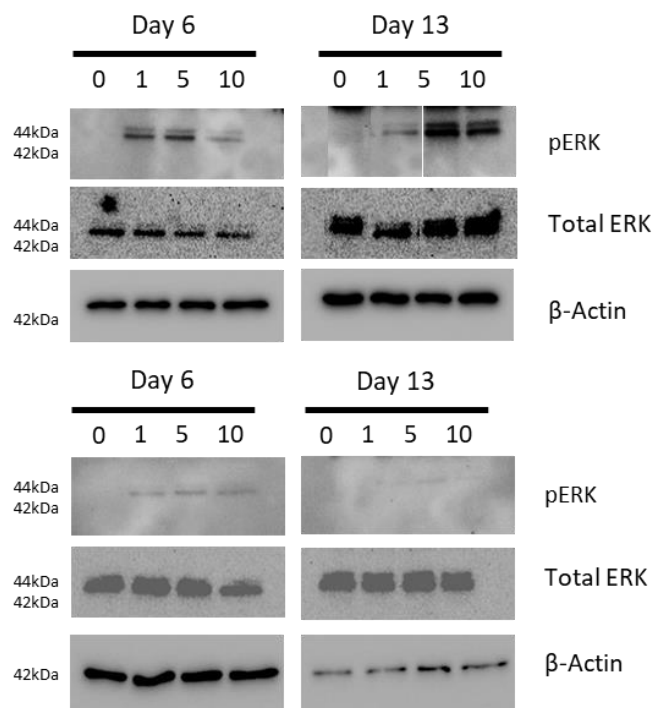
Figure 4.12 - Western blot visualising phosphorylated ERK from cells stimulated with αCD19 microbeads and CXCL12. B-cells were cultured in normal differentiation conditions. At day 6 and day 13, cells were cultured in 0.5% serum conditions overnight. Following overnight starvation, cells were stimulated with αCD19 microbeads and CXCL12, with samples taken pre-stimulation, 1, 5 and 10 minutes after stimulation and mixed with sample buffer immediately. Samples are then loaded on a blot for gel electrophoresis before transfer to a blotting membrane. Blots are probed for phosphorylated and total ERK protein. Actin was used as a loading control. (N=2)

and a pre-stimulatory sample was also taken. Protein was collected and analysed via Western blot (figure 4.12).

After co-stimulation with CXCL12 and αCD19, day 6 cells show a stimulation response similar to that seen from CXCL12 stimulated cells. Between day 6 and 13, the blots suggest day 6 cells generate a stronger ERK phosphorylation. The loading varies between day 6 and day 13 for one of the samples, therefore the samples were quantified to confirm the true phosphorylation pattern (figure 4.13).
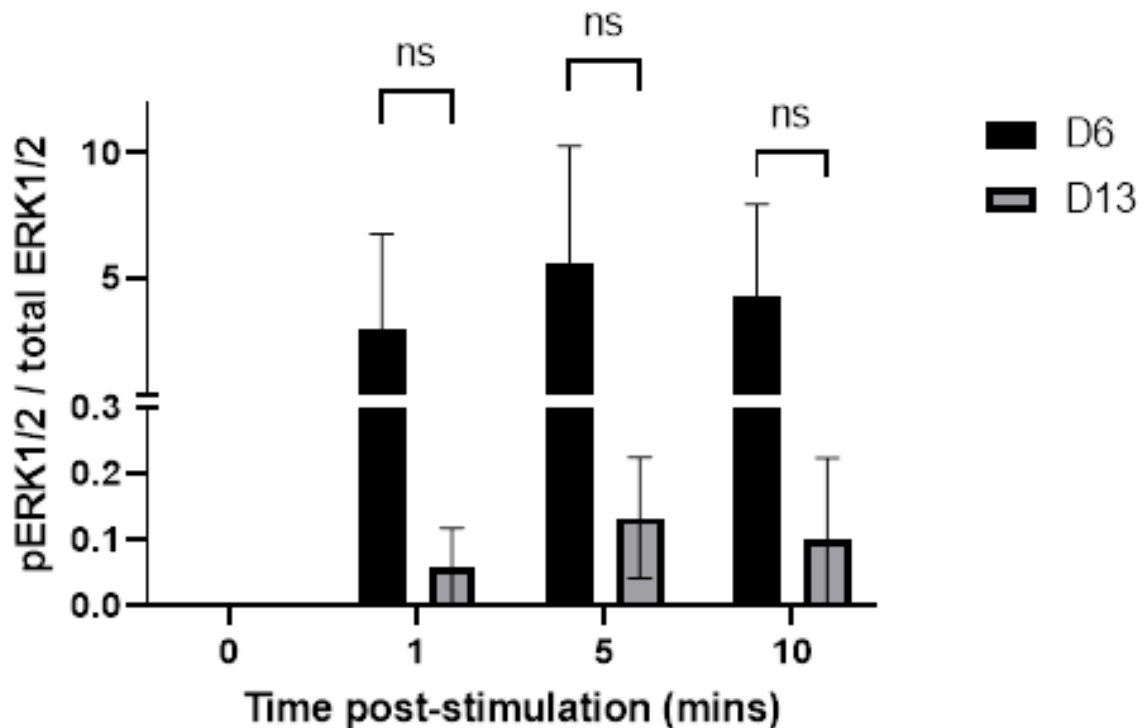
Figure 4.13 – Quantification of Western blots visualising phosphorylated ERK from cells stimulated with αCD19 microbeads and CXCL12. B-cells were cultured in normal differentiation conditions. At day 6 and day 13, cells were cultured in 0.5% serum conditions overnight. Following overnight starvation, cells were stimulated with αCD19 microbeads and CXCL12, with samples taken pre-stimulation, 1, 5 and 10 minutes after stimulation and mixed with sample buffer immediately. Samples are then loaded on a blot for gel electrophoresis before transfer to a blotting membrane. Blots are probed for phosphorylated and total ERK protein. Densitometry was conducted using Image Lab software. Each bar represents the pERK signal strength at the indicated time point after stimulation for both day 6 and 13 cells. (N=2). Significance was calculated using a student t-test.

Quantification and normalisation of the pERK western blot data show a notable difference in ERK phosphorylation at day 6 and 13. Compared to day 13 stimulation, day 6 cells generate a far stronger phosphorylation pattern. To understand how this stimulation has affect ERK activity, they were compared with CXCL12 treated cells alone (figure 4.14).

Figure 4.14 – Comparison of pERK signal from day 6 and day 13 ASCs stimulated with either αCD19 microbeads and CXCL12 or CXCL12 only. B-cells were cultured in normal differentiation conditions. At day 6 and day 13, cells were cultured in 0.5% serum conditions overnight. Following overnight starvation, cells were stimulated with αCD19 microbeads and CXCL12, with samples taken pre-stimulation, 1, 5 and 10 minutes after stimulation and mixed with sample buffer immediately. Samples are then loaded on a blot for gel electrophoresis before transfer to a blotting membrane. Blots are probed for phosphorylated and total ERK protein. Densitometry was conducted using Image Lab software. pERK quantification values was compared between each stimulating condtions and graphed using Graphpad Prism software. Each bar represents the pERK signal strength at the indicated time point after stimulation with either CXCL12 or CXCL12 with αCD19 beads for both day 6 and 13 cells (N=3 CXCL12 stimulation, N=2 dual stimulation).

Quantification shows co-stimulated day 6 cells produce the strongest level of ERK phosphorylation, closely followed by that seen from day 13 PCs stimulated by CXCL12 alone. These data suggest that CD19 may have an effect of amplifying CXCR4 signal transduction in day 6 cells but reduces the CXCL12-induced ERK signalling in PCs. All the stimulations on each day show a peak phosphorylation at 1 or 5 minutes and a decreasing level by 10 minutes.

4.4.2 αCD19 and CXCL12 induced AKT signalling

Next, AKT signalling induced by co-stimulation by CXCL12 and αCD19 was analysed (figure 4.15). Phosphorylation at the S473 residue shows variable activity for day 6 and day 13 cells, but generally showing a strong response. Additionally, highly phosphorylated bands can be detected for up to 10 minutes in the second sample, suggesting that co-stimulation may prolong signalling. At the T308 residue, phosphorylation appears slightly less, but more comparable between day 6 and 13. Again the second sample shows a strong response up until 10 minutes, suggesting this particular sample may have a more sensitive reaction to these stimuli. To confirm the above analysis, the blots were quantified (figure 4.16).
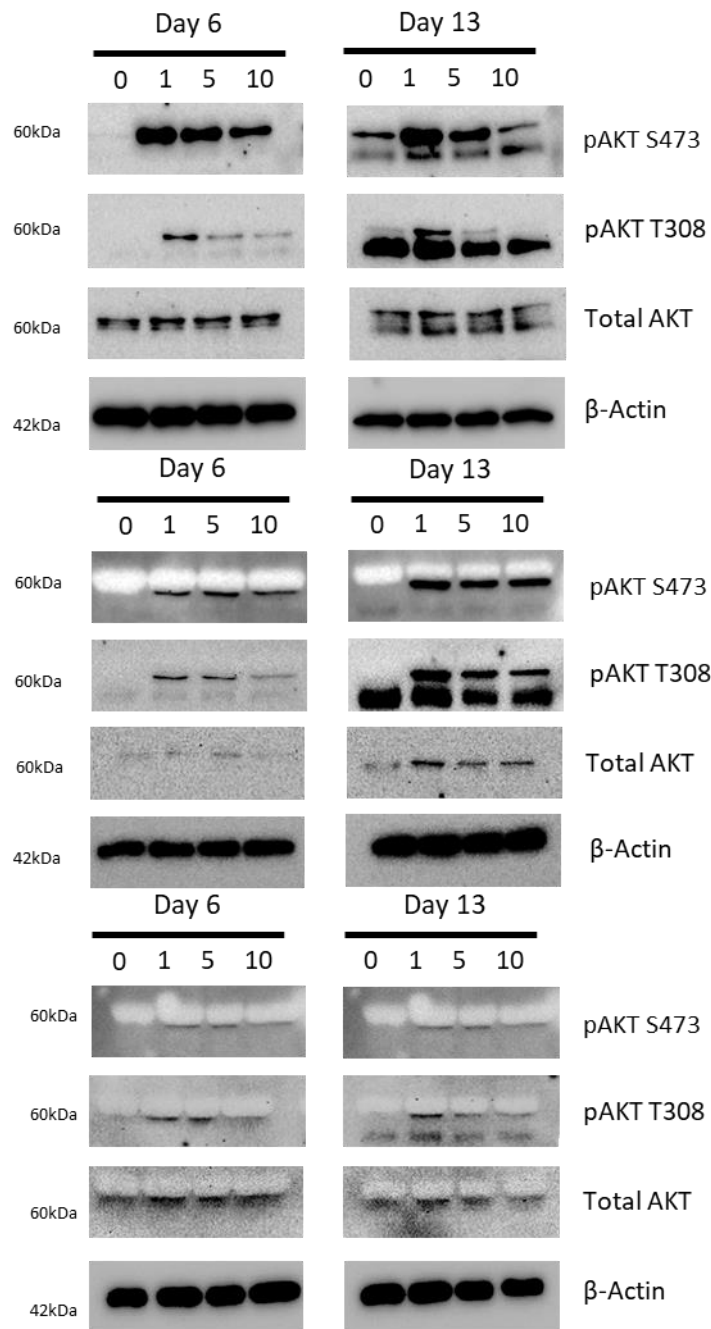
Figure 4.15 - Western blot visualising phosphorylated AKT from cells stimulated with CXCL12 and αCD19 microbeads. B-cells were cultured in normal differentiation conditions. At day 6 and day 13 cells were cultured in 0.5% serum conditions overnight. Following overnight starvation, cells were stimulated with either αCD19 microbeads and CXCL12, with samples taken pre-stimulation, 1, 5 and 10 minutes after stimulation and mixed with sample buffer immediately. Samples are then loaded on a blot for gel electrophoresis before transfer to a blotting membrane. Blots are probed for phosphorylated (at residues S473 and T308) and total AKT protein. Actin was used as a loading control. (N=3)

The densitometry analysis confirms that, at the S473 residue, there is a similar level of phosphorylation at both time points, but day 13 cells maintain activity more than day 6 cells. At the T308 residue, day 13 cells generate a greater phosphorylation signal that again is maintained to a higher degree than
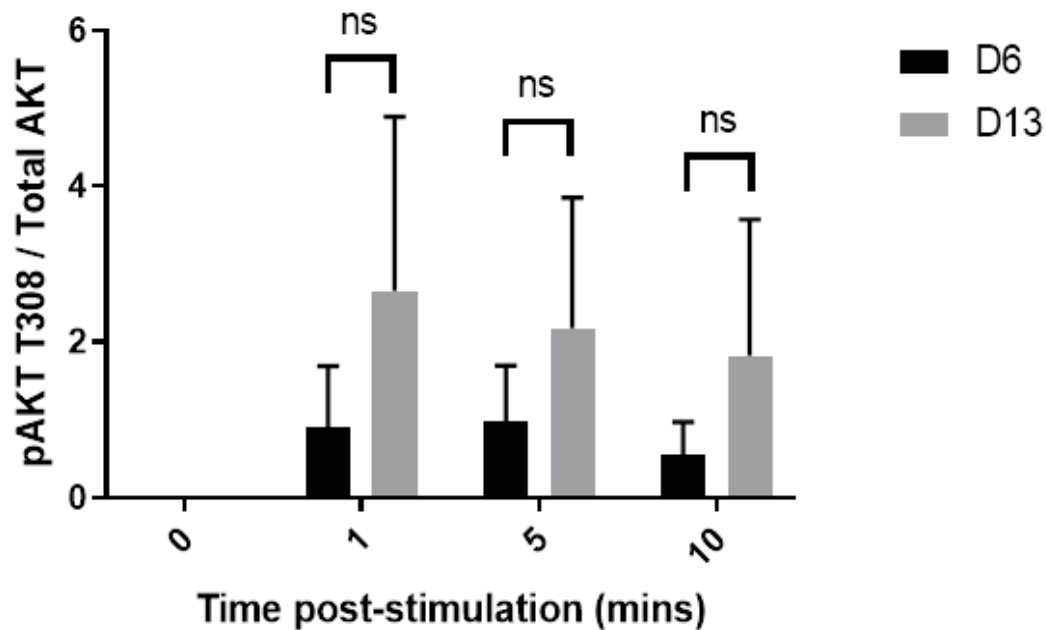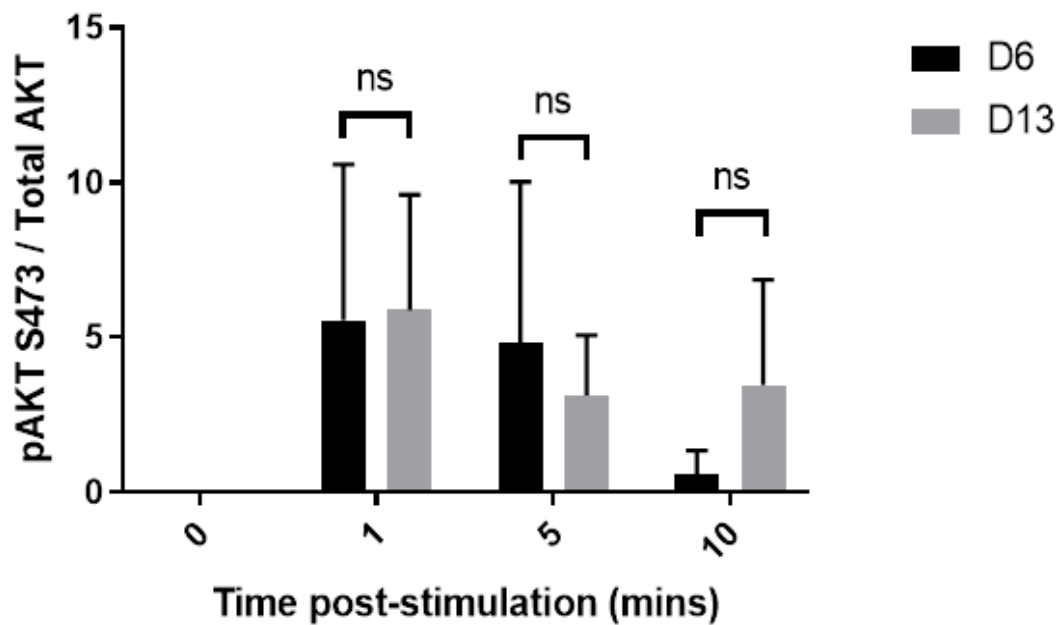
Figure 4.16 - Quantification of Western blots visualising phosphorylated AKT from cells stimulated with αCD19 microbeads and CXCL12. B-cells were cultured in normal differentiation conditions. At day 6 and day 13, cells were cultured in 0.5% serum conditions overnight. Following overnight starvation, cells were stimulated with αCD19 microbeads and CXCL12, with samples taken pre-stimulation, 1, 5 and 10 minutes after stimulation and mixed with sample buffer immediately. Samples are then loaded on a blot for gel electrophoresis before transfer to a blotting membrane. Blots are probed for phosphorylated (At residues S473 and T308) and total AKT protein. Densitometry was conducted using Image Lab software. Each bar represents the pAKT signal strength at the indicated time point after stimulation for both day 6 and 13 cells. (N=3). Significance was calculated using a Students t- test.

day 6 cells. Together these data suggests that co-stimulation may also enhance PB signalling through S473 to comparable levels seen at day 13. It was therefore crucial to compare with the CXCL12 stimulation alone (figure 4.17).

Comparisons of co-stimulation with CXCl12 stimulation alone reveals a similar level of activity between both conditions. At day 6 co-stimulation may generate a marginally stronger phosphorylation pattern compared to CXCL12 alone, however the range of variation in donor response to both stimulations show that both generate a comparable level of activity. By day 13 CXCL12 stimulation may generate a stronger response, but again the donor variation indicates both stimulations create a comparable signalling pattern. Both stimulations maintain some signalling by 10 minutes. CD19 stimulation may have a negative effect at the PC stage, reducing phosphorylation at S473, however the variation in donor responses makes this conclusion difficult to confirm.
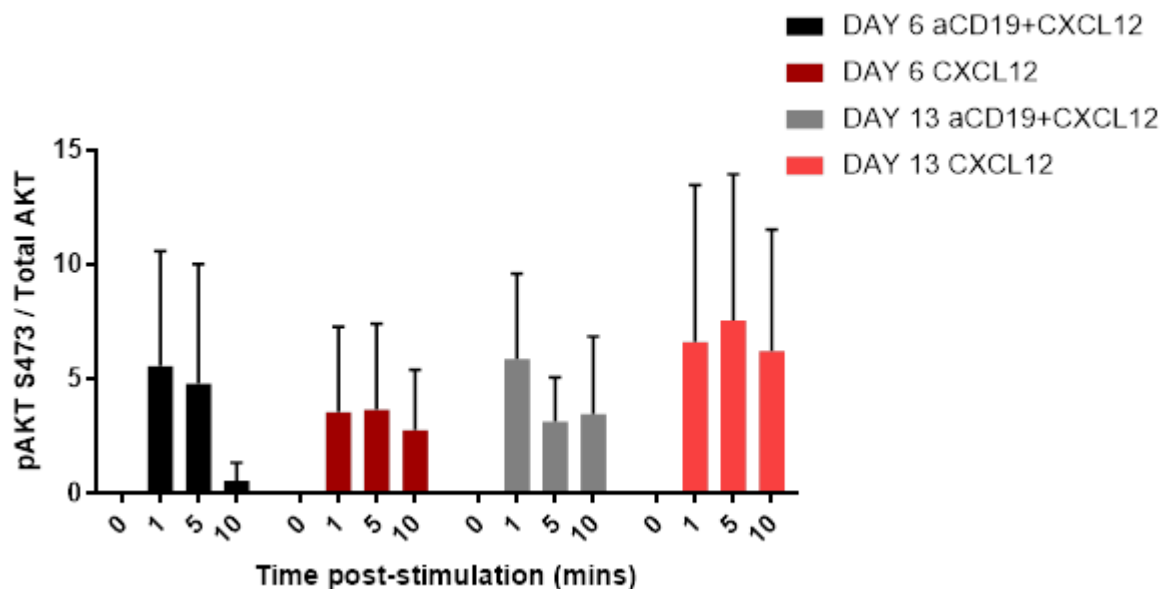
Figure 4.17 - Comparison of pAKT S473 signal from day 6 and day 13 ASCs stimulated with either αCD19 microbeads and CXCL12 or CXCL12 only. B-cells were cultured in normal differentiation conditions. At day 6 and day 13, cells were cultured in 0.5% serum conditions overnight. Following overnight starvation, cells were stimulated with αCD19 microbeads and CXCL12, with samples taken pre-stimulation, 1, 5 and 10 minutes after stimulation and mixed with sample buffer immediately. Samples are then loaded on a blot for gel electrophoresis before transfer to a blotting membrane. Blots are probed for phosphorylated (at residues S473) and total AKT protein. Densitometry was conducted using Image Lab software. pAKT S473 quantification values were compared between each stimulating condition and graphed using Graphpad Prism software. Each bar represents the pAKT S473 signal strength at the indicated time point after stimulation with either CXCL12 or CXCL12 with aCD19 beads for both day 6 and 13 cells (N=3).

The phosphorylation pattern at AKT reside T308 was also compared for both types of stimulations (figure 4.18). At day 6, both stimulations generate a weaker response compared to day 13. Additionally, the phosphorylation activity is very similar, with a comparable peak activity and rate of decay. At the PC stage, again the two stimulations generate a comparable pattern of phosphorylation.

CXCL12 stimulation alone may maintain activity for an extended period, however a longer assessment would be required. Co-stimulation peak activity occurs earlier than CXCL12 stimulation alone. Together, this data indicate that both stimulations generate a comparable phosphorylation pattern at both time points with only minor differences in rate of activation. CD19 stimulation therefore appears to have little effect at this residue.
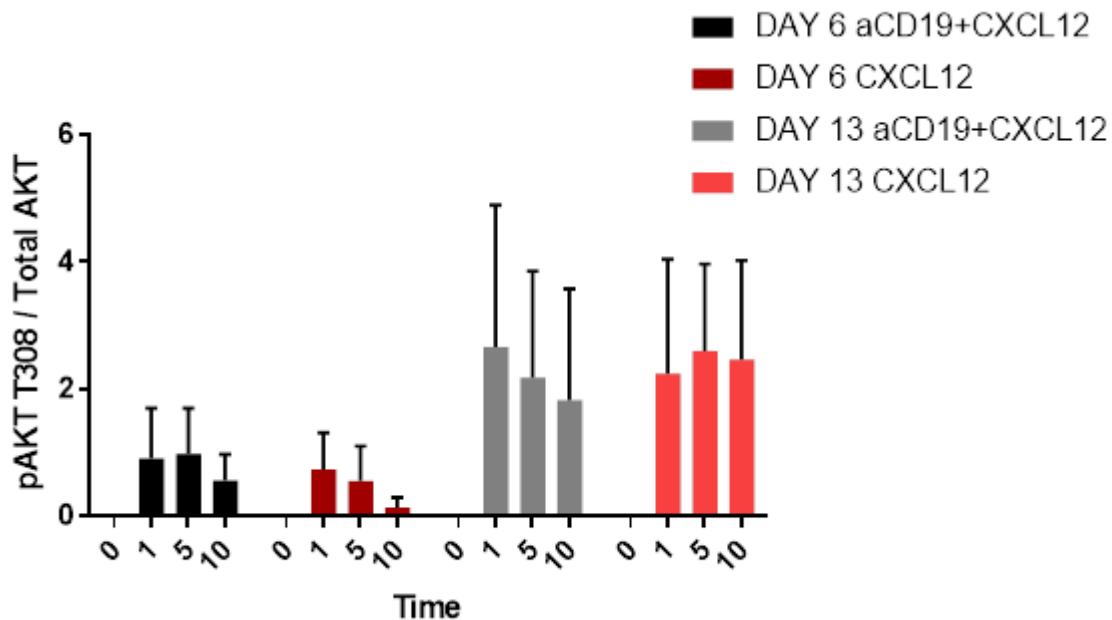
Figure 4.18 - Comparison of pAKT T308 signal from day 6 and day 13 ASCs stimulated with either αCD19 microbeads and CXCL12 or CXCL12 only. B-cells were cultured in normal differentiation conditions. At day 6 and day 13, cells were cultured in 0.5% serum conditions ove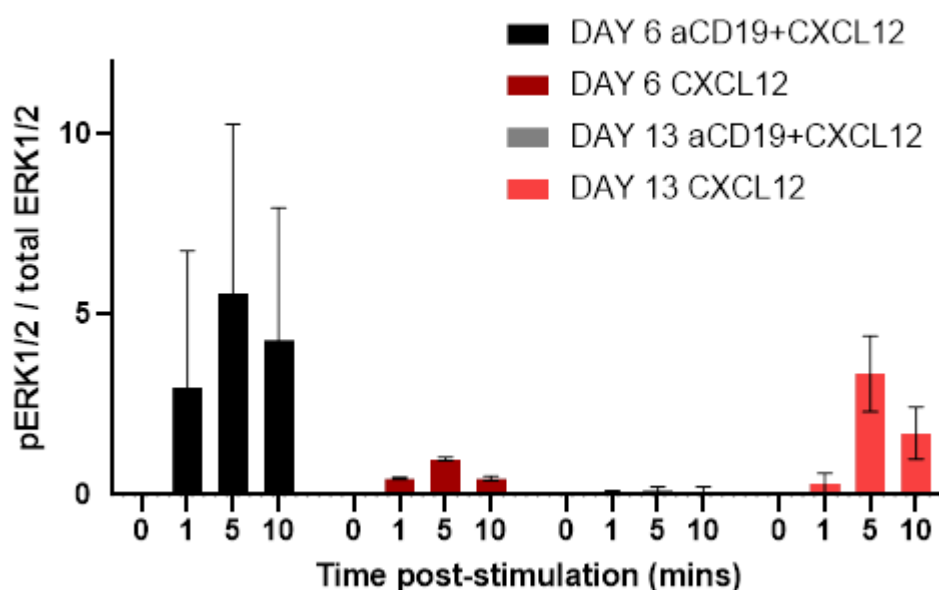rnight. Following overnight starvation, cells were stimulated with αCD19 microbeads and CXCL12, with samples taken pre-stimulation, 1, 5 and 10 minutes after stimulation and mixed with sample buffer immediately. Samples are then loaded on a blot for gel electrophoresis before transfer to a blotting membrane. Blots are probed for phosphorylated (at residue T308) and total AKT protein. Densitometry was conducted using Image Lab software. pAKT T308 quantification values were compared between each stimulating condition and graphed using Graphpad Prism software. Each bar represents the pAKT T308 signal strength at the indicated time point after stimulation with either CXCL12 or CXCL12 with aCD19 beads for both day 6 and 13 cells (N=3).

4.5 CD19 deficient signalling dynamics

Previous studies suggest CD19 can promote survival and proliferative signals though its function as a signalling hub for both the BCR and CXCR4 in mature B-cells. The function of CD19 however is less clear in ASCs. Direct ligation of CD19 alone yields very limited effects on the tested signal transduction events, but the combined CXCL12 and anti-CD19 stimulations indicated a potential shift in response, particularly in the degree of ERK phosphorylation. To clarify how CXCR4 signalling is impacted by CD19, B-cells isolated from a newly identified CD19 deficient individual were assessed using the differentiation model and signal transduction events downstream of CXCR4.

4.5.1 Ex-vivo generation of mature CD19 deficient plasma cells

To date there have only been 10 documented cases of CD19 deficiency (Wentink *et al.* 2018). Previous literature has documented a reduction in the development of B-cell numbers and an impaired response to vaccination, however, there is notable variation in patient disease presentation and ex-vivo B-cell function. Therefore, the ability of CD19 deficient B-cells to generate ASCs in response to T-dependant response was assessed. Initially, PBMCs were isolated from peripheral blood and B-cells were selected as normal. CD19-ve B-cells were cultured within the B-cell differentiation model and at days 0, 6 and 13, the phenotype was assessed (figure 4.19)

The CD19 deficient B-cells, as expected do not express CD19 throughout the differentiation. As the cells differentiate, the cells begin to lose CD20 expression as seen on healthy cells. By day 13 all the cells have downregulated CD20, suggesting normal PC development. CD19 deficient cells also acquire normal CD38 expression, suggesting normal B-cell activation and differentiation. Additionally, at day 6 the cells also begin to express CD27 and by day 13, almost all the cells are positive for CD27, a marker highly expressed on PCs. Finally, the majority of the cells express CD138 by day 13. This suggests the B-cells are fully capable of differentiating into plasma cells.
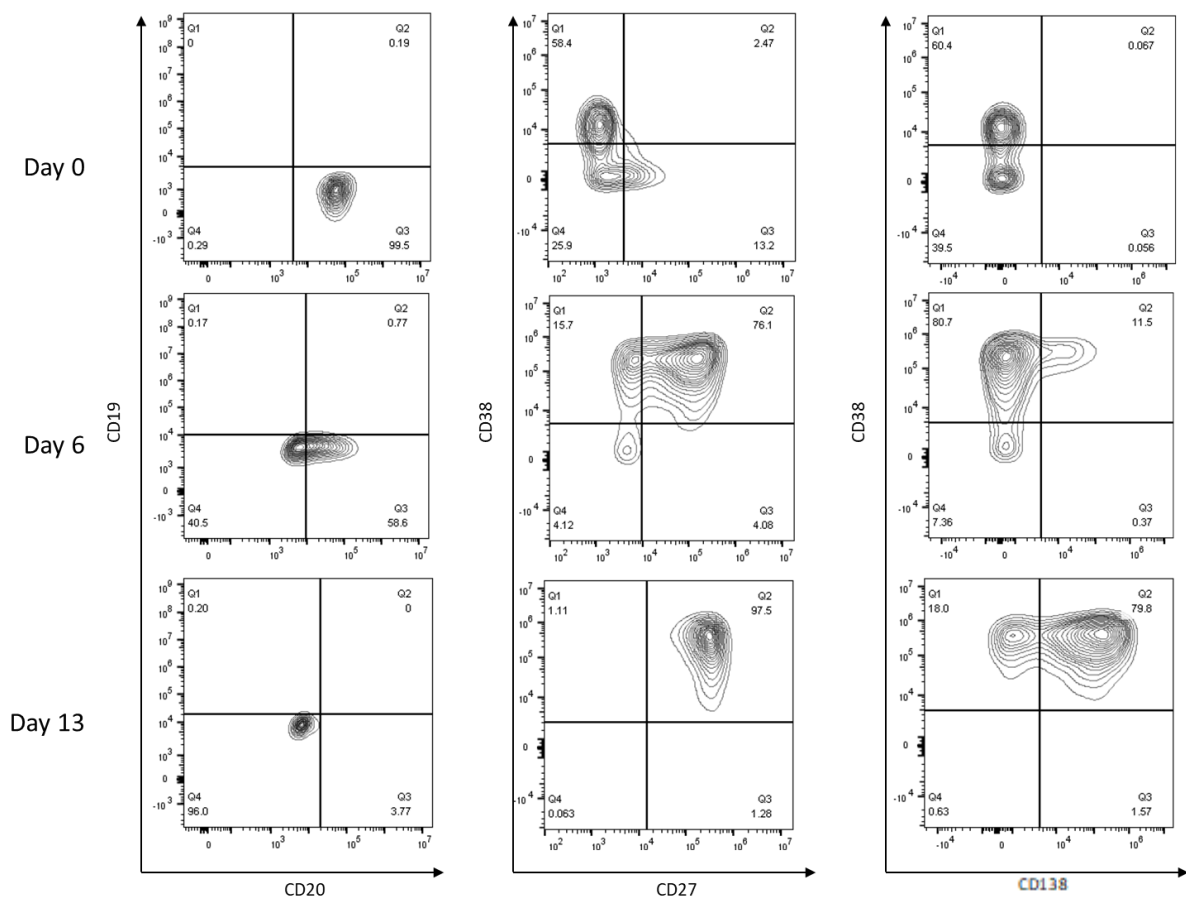
Figure 4.19 - Representative flow cytometry analysis of CD19-deficient patient day 0 and 6 cells and D13 plasma cells. PBMCs were obtained from peripheral blood and CD19 deficient B-cells were isolated via negative selection. B-cells were maintained within the *in vitro* differentiation model, following T-cell dependant stimulation, up to day 13. B-cells and PCs were collected for assessment of phenotype at day 0, 6 and 13 by flow cytometry. CD19 deficiency was assessed and attainment of plasma cell generation by loss of surface CD20 and gain of CD38/CD138 after stimulation with T-dependent stimulation conditions.

Next, B-cell and PC surface markers were compared between CD19-ve cells and healthy controls. Figure 4.20 shows the percentage positive expression of CD20, CD38 and CD138 between healthy control cells and CD19-ve cells. The data indicate both healthy and CD19-ve cells express a comparable level of CD20 and CD138 at all time points, indicating normal attainment of a PC phenotype. CD38 expression in CD19 deficient cells also matches that of healthy controls, albeit at moderately slower rate, i.e., at day 0, the B-cells express a lower level of CD38, indicating a slight delay, which is repeated at both day 6 and, to a lesser degree day 13, however, the majority of the CD19-ve cells express CD38 by day 13, indicating normal acquisition. CD27 expression is more varied, however CD19-ve cells express CD27 within the range seen in healthy controls at all timepoints, again confirming normal B-cell differentiation.
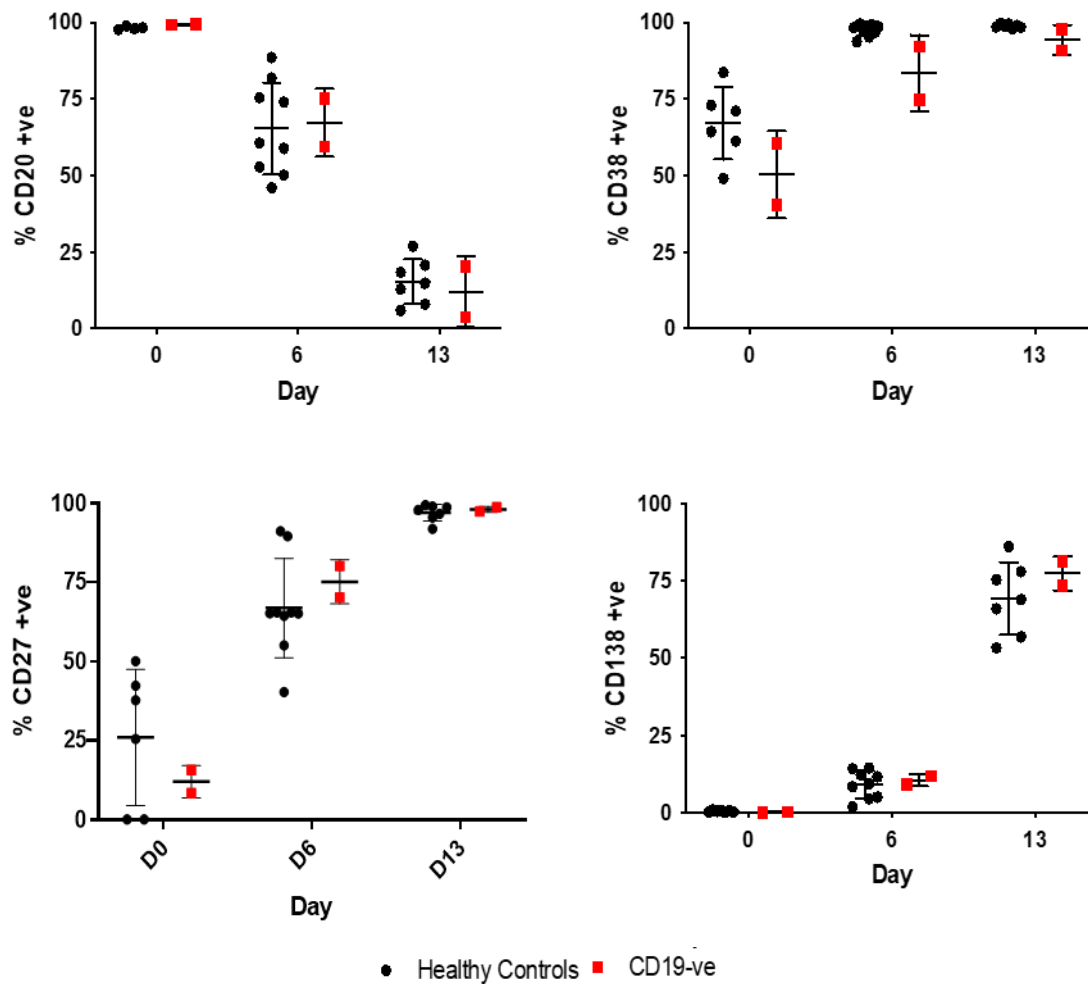
Figure 4.20 - **Quantification of the percentage of cells expressing indicated markers at day 0, 6 and 13 of the differentiation.** PBMCs were obtained from peripheral blood and CD19 deficient B-cells were isolated via negative selection. B-cells were maintained within the in vitro differentiation model, following T-cell dependant stimulation, up to day 13. B-cells and PCs were collected for assessment of phenotype at day 0, 6 and 13 by flow cytometry. Cell phenotype at D0, 6 and 13 was quantified as percentage positive for both healthy controls and CD19 deficient cells. Black indicates healthy controls and red indicates CD19 deficient cells. Healthy Controls, n= 9; CD19-ve, n=2 independent differentiations performed 5 months apart.

Phenotypically, the CD19 deficient B-cells are comparable to healthy B-cells and plasma cells at all time points, indicating the B-cell differentiation in these cells is maintained.

4.5.2 CD19 deficient B-cell viability

While the CD19-ve cells appeared to acquire a normal PC phenotype, there may be defects in the relative survival of cells following stimulation. During the differentiation of CD19-ve B-cells, the cell viability was measured at each time point and compared to that of healthy controls (figure 4.21)
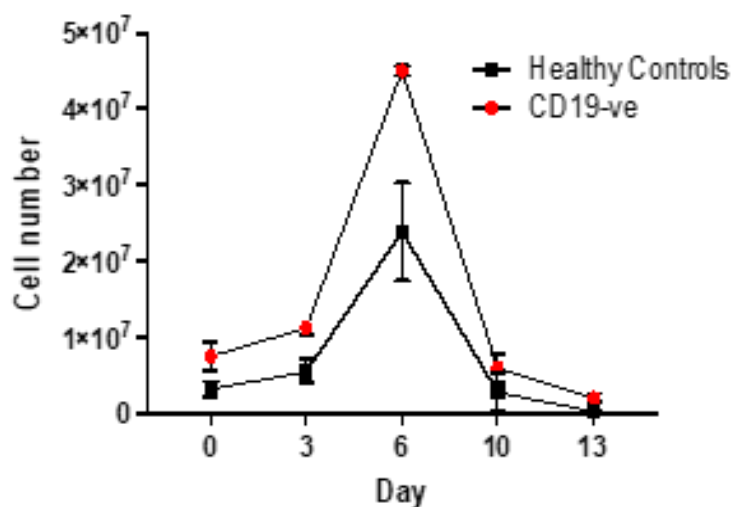
Figure 4.21 - Evaluation of viable cell number of CD19 deficient and healthy B-cells and ASCs during the differentiation assay. PBMCs were obtained from peripheral blood and CD19 deficient B-cells were isolated via negative selection. B-cells were maintained within the in vitro differentiation model, following T-cell dependant stimulation, up to day 13. Cell counts performed at day 0, 3, 6, 10 And 13 and assessed by haemocytometer and trypan blue stain. Healthy Controls, n=4; CD19-ve, n=2.

CD19 deficient cells exhibit a typical pattern of initial expansion from day 0 and reach a maximum cell count at day 6 during the PB stage. From day 6, the cell count diminishes as mature PCs emerge. The deficient cell viability during the differentiation mirrors the healthy control viability, indicating no defects. The CD19 deficient cells generated a notably high population of PBs by day 6 compared to the healthy controls.

4.5.3 Immunoglobulin production

Data from previous studies show CD19 deficient or diminished B-cells respond poorly to BCR stimulation, leading to a weak antibody production in response to vaccination (van Zelm *et al.* 2006). Again, to analyse how this mutation affects PC function, media samples were collected from cells during the differentiation and assessed for both IgM and IgG production (figure 4.22). Levels of IgM and IgG produced from CD19-ve cultures were relatively low at day 6, the levels increased to become more comparable to those of healthy controls at day 13. This data indicate that the defects in antibody production seen here are closer to that seen in the literature for day 6. By day 13, at the PC stage, where CSR has already occurred, immunoglobulin production shifts to increase IgG production, and

CD19 deficient cells are able to secrete immunoglobulin to a similar level seen in the healthy controls, indicating that PC Ig secretion is maintained.
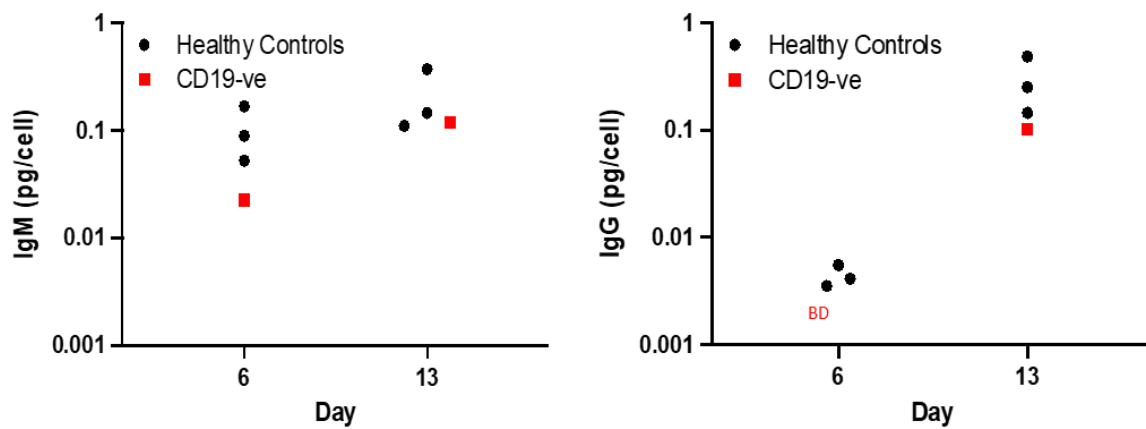
Figure 4.22 - Quantification of secreted IgM and IgG at days 6 and 13. PBMCs were obtained from peripheral blood and CD19 deficient B-cells were isolated via negative selection. B-cells were maintained within the in vitro differentiation model, following T-cell dependant stimulation, up to day 13. Cell supernatant samples were collected at both day 6 and 13 and immunoglobulin secretion was assessed by ELISA. Healthy Controls, n=3; CD19-ve, n=1. BD, below detection.

4.6 – Transcriptome analysis of differentiating CD19 deficient cells

To determine whether the apparently normal differentiation of CD19-ve B-cells was accompanied by more subtle changes in the underlying gene expression programme, RNA sequencing was performed on material collected from differentiating cells at all key phases of the differentiation model. Healthy controls and CD19 deficient cells were collected at days 0, 3, 6, 10 and 13, allowing for assessment of gene regulation in resting B-cells, activated B-cells, PBs and PCs. Due to the rarity of CD19 deficient patients, only one donor was available. Cells from 3 donors were used for the healthy controls.

4.6.1 CD19 expression

Initially, *CD19* expression was assessed in healthy controls and the CD19 deficient patient sample (figure 4.23 A). RNA sequencing data indicate that, whilst the scales are not equivalent, the overall pattern of *CD19* expression is similar between the two groups. Both populations express high levels of *CD19* at day 0. As the cells differentiate, expression decreases until by day 13 and day 20, expression has dropped to its lowest point. Firstly, this matches the pattern seen in the protein expression of healthy differentiating cells, as CD19 decreases slightly by the time the cells reach day 13. Secondly, despite the CD19 deficient patient expressing no surface CD19 protein throughout the differentiation, as determined by flow cytometry, yet still shows high gene expression during the commitment and expansion phases, suggest that at the mRNA level, there are no defects in the regulation of *CD19*

expression. The defect was identified as c.622del in *CD19* exon 4 and classified as pathogenic (Appendix, data from Chris Watson). This variant results in a frameshift translation that was predicted to result in nonsense mediated decay resulting in the loss of CD19 expression; however, preservation of the mRNA levels would suggest another mechanism leads to loss of protein.
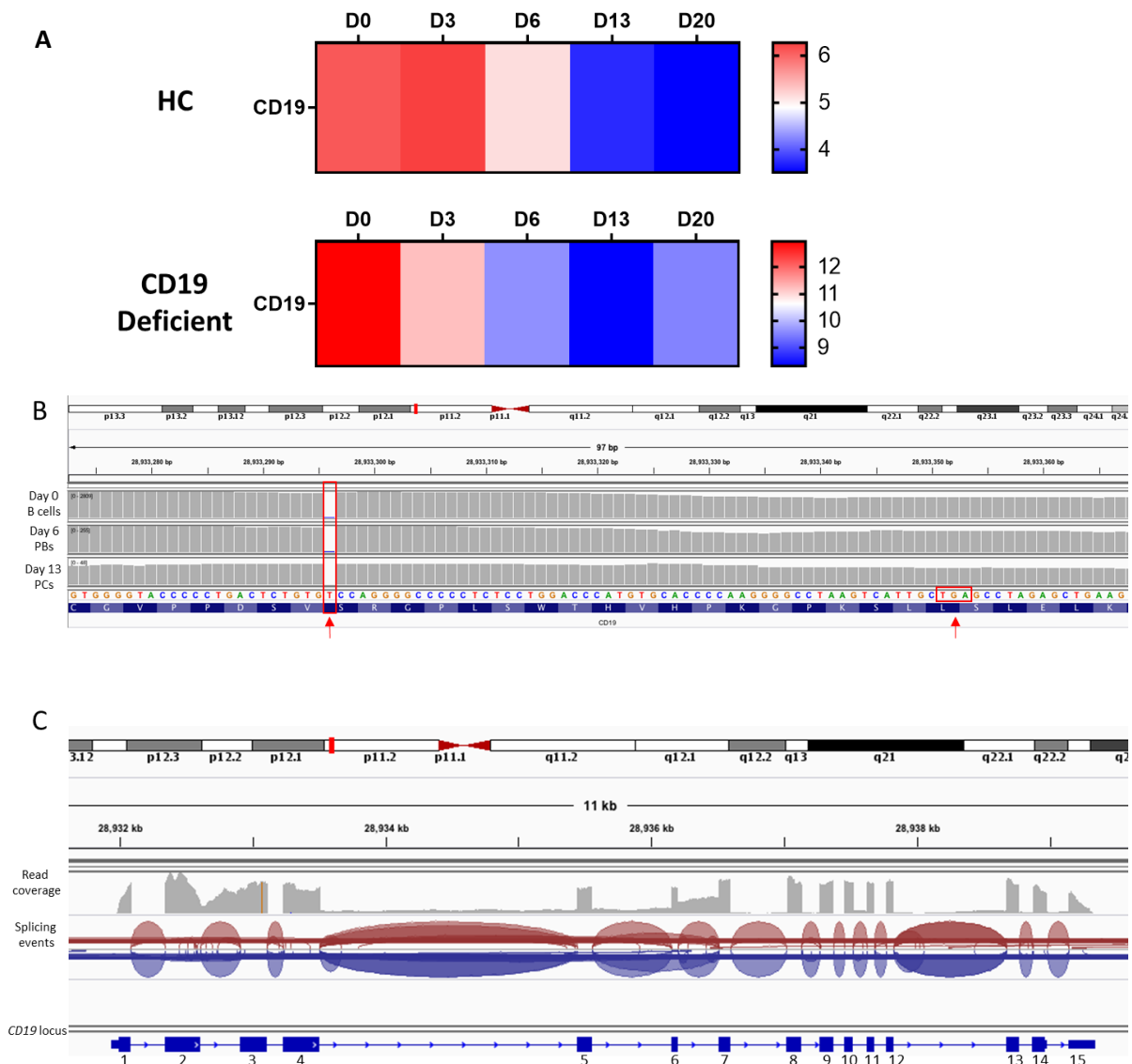
Figure 4.23 – Heatmap of normalised expression of CD19 (VST) in CD19-ve and healthy differentiating B-cells (A). Loss of CD19 is not attributable to NMD or exon skipping (B and C). PBMCs were obtained from peripheral blood and CD19 deficient B-cells were isolated via negative selection. B-cells were maintained within the in vitro differentiation model, following T-cell dependant stimulation, up to day 13. RNA was isolated from B-cells, PBs and PCs at the main time points during the differentiation. RNA sequencing was performed, and CD19 expression data set was analysed. **Loss of CD19 is not attributable to NMD or exon skipping.** (B) Presence of exon 4 mutation in CD19 reads from RNA-seq in differentiation samples from all time points predicted to lead to a truncated protein lacking the transmembrane domain (highlighted by arrows). (C) Reads for all CD19 exons were observed uniformly across the locus with normal splicing patterns, apart from some evidence for skipping of exon 6 encoding the membrane-proximal region of the cytoplasmic domain. Representative results from day 0 sample is shown.

Additional analysis of the CD19 deficient transcript using DEXseq analysis confirmed the presence of the mutation in exon 4 (figure 4.23 B), resulting in the generation of an early stop codon and therefore predicted generation of a truncated protein product lacking the transmembrane region, in day 0,6 and 13 cells. Despite this, investigation of the splicing pattern showed uniform expression of all 15 CD19 exons, however there is evidence of skipping of exon 6, which encodes the membrane-proximal region of the cytoplasmic domain (figure 4.23 C).

4.6.2 Comparison of differentiation associated genes

The phenotype of differentiating CD19-ve cells suggested a normal pattern of differentiation. To confirm that the underlying gene expression matched this, mRNA analysis was completed for differentiation-associated genes to examine how this deficiency may affect genetic control of key proteins associated with commitment of and progression through each phase of B-cell differentiation (figure 4.24)
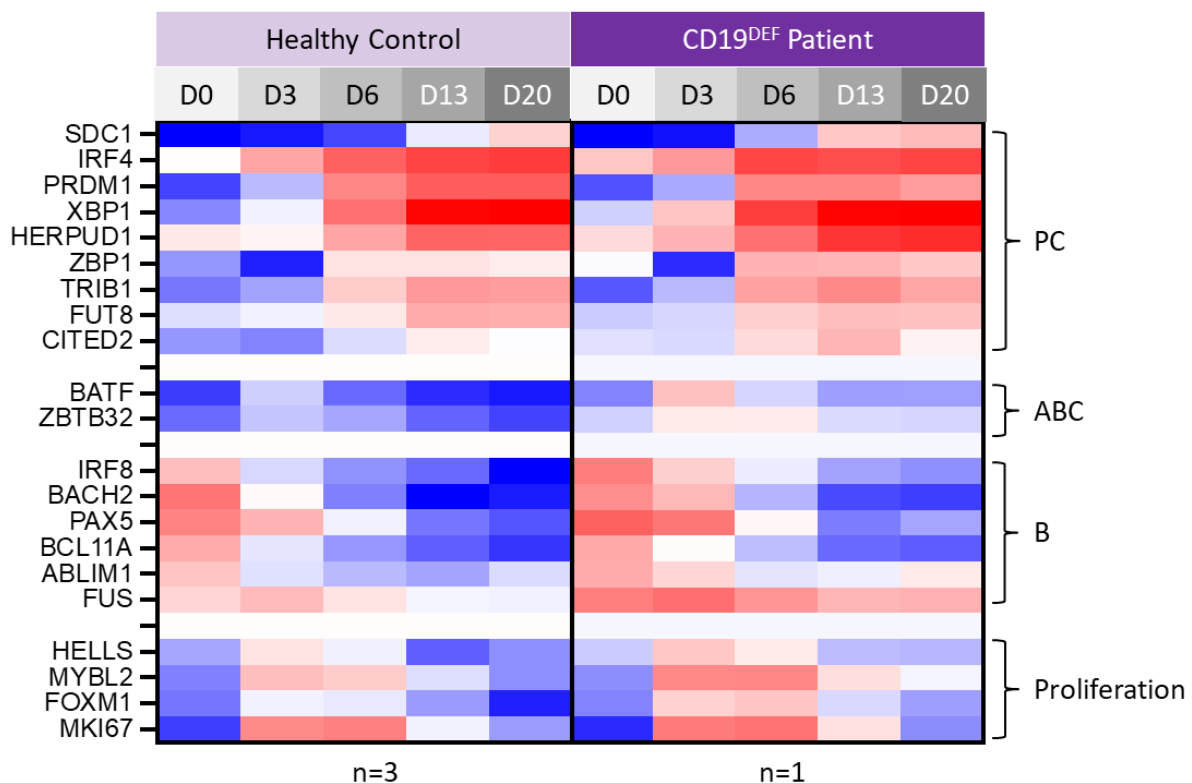
Figure 4.24 – Heatmap of normalised expression of genes (VST) associated with B-cell differentiation. PBMCs were obtained from peripheral blood and CD19 deficient B-cells were isolated via negative selection. B-cells were maintained within the in vitro differentiation model, following T-cell dependant stimulation, up to day 13. RNA was isolated from B-cells, PBs and PCs at the main time points during the differentiation. RNA sequencing was performed, and expression data for several genes associated with B-cell differentiation were analysed.

Components of the B-cell programme (B) programme such as *IRF8*, *BACH2* and *PAX5* are equally expressed at each time point for both HCs and CD19 deficient cells, where expression is high during day 0-3 and then decreases after this point. The CD19-ve cells show an appropriate upregulation of the genes *BATF* and *ZBTB32* indicative of activation at day 3 (ABC). Additionally, genes associated with the PC programme are comparable, for example *IRF4*, *PRDM1* and *XBP1* are lowly expressed before day 6, but from day 6 expression is high when the majority of the cells will be PBs. Together this shows that differentiation control in the CD19 deficient B-cells is conserved, which is consistent with the flow cytometry data that show these donor cells differentiated normally. Also included are several genes associated with proliferation in B-cells. The deficient cells match the expression of that seen in the healthy controls, will enhanced expression during the expansion phases during days 3-6. This implies these cells are fully capable of rapid proliferation induced by strong T-dependent activation.

4.6.3 Comparison of signalling associated genes

Next, relevant genes associated with B-cell signalling were assessed for differential expression (figure 4.25). In this instance genes that were common between the HCs and CD19-ve were compared by calculating the standard deviation of each gene across the time series, then ranking the genes from highest to lowest variance. The ranking of the genes was then compared between the two groups. Genes that changed rank by > 5000 may indicate abnormal regulation.
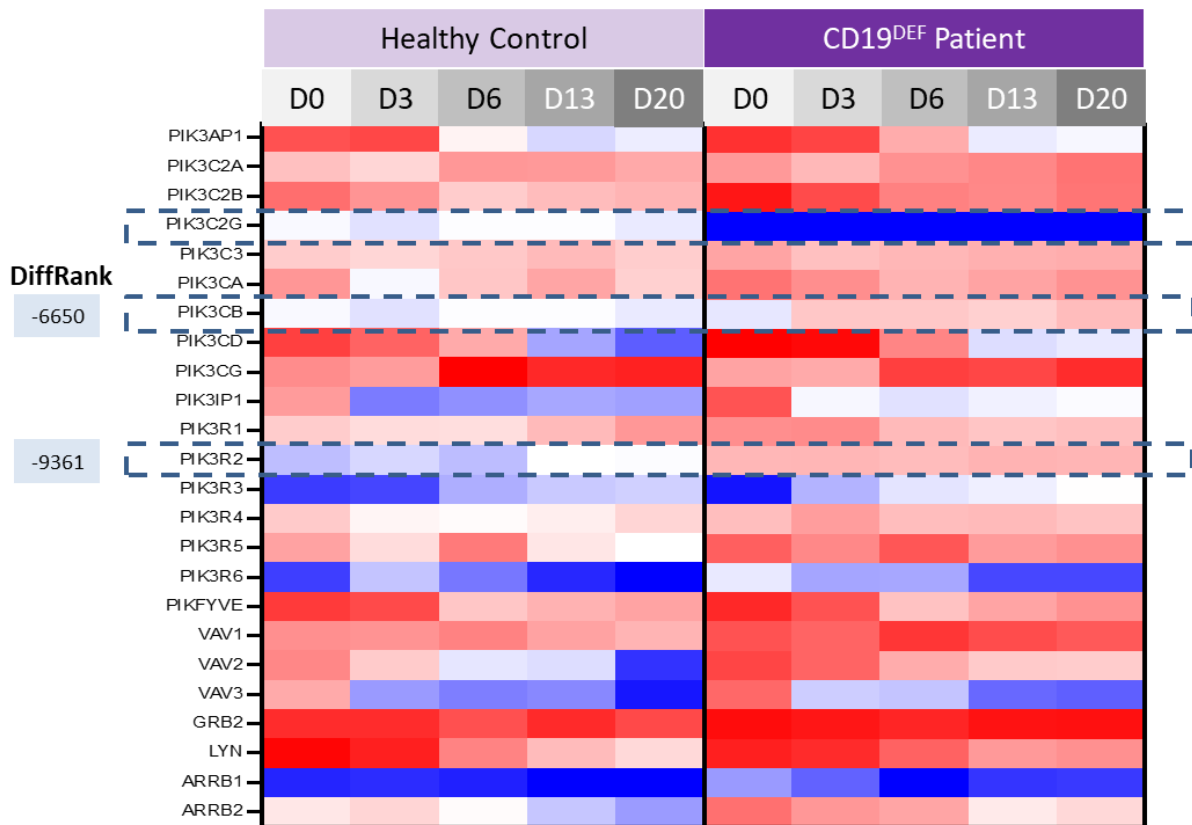
Figure 4.25 - Heatmap of normalised expression of genes (VST) associated with B-cell signalling. PBMCs were obtained from peripheral blood and CD19 deficient B-cells were isolated via negative selection. B-cells were maintained within the in vitro differentiation model, following T-cell dependant stimulation, up to day 13. RNA was isolated from B-cells, PBs and PCs at the main time points during the differentiation. RNA sequencing was performed, and expression data for several genes associated with B-cell signalling were analysed. Genes highlighted indicates a significant differential rank (Analysis performed by Matthew Care).

Overall, the expression of signalling associated genes is comparable between healthy and CD19-ve differentiating B-cells/PCs, however highlighted are 3 genes which show an altered expression pattern in CD19 deficient cells. The most significantly differentially expressed genes are PI3K genes, specifically *PIK3CB* and *PIK3R2*, which have a differential rank that changed substantially between the two groups. PI3K are signalling molecules associated with both CD19 and CXCR4. CD19 deficient cells show overall stronger expression of *PIK3CB* from day 3 of the differentiation and an increase in *PIK3R2* from day 0. *PIK3C2G* expression is far lower throughout the differentiation in deficient cells, however the differential ranking is greater than -5000. Other CD19 associated signalling molecules assessed include *VAV*, *GRB2* and *LYN*, however these are comparable between the two populations. Arrestins are associated with G-protein coupled receptor regulation, including CXCR4 desensitisation. Expression of the *ARRB1* and *ARRB2* genes are comparable between the controls and deficient cells, however there is slightly lower expression in healthy PCs, suggesting there could be some potential role in deficient cells that dampen CXCR4 signals, however further samples would be required to evidence this.

4.6.4 CXCR4 expression

We have established that CD19 deficient B-cells are capable of undergoing differentiation to the ASC stage and possess a typical phenotype, viability, and immunoglobulin secretion over the 13 days. Next it was necessary to understand how the deficiency may or may not affect CXCR4 surface expression as this may have repercussions for signalling downstream of CXCR4 (figure 4.26).
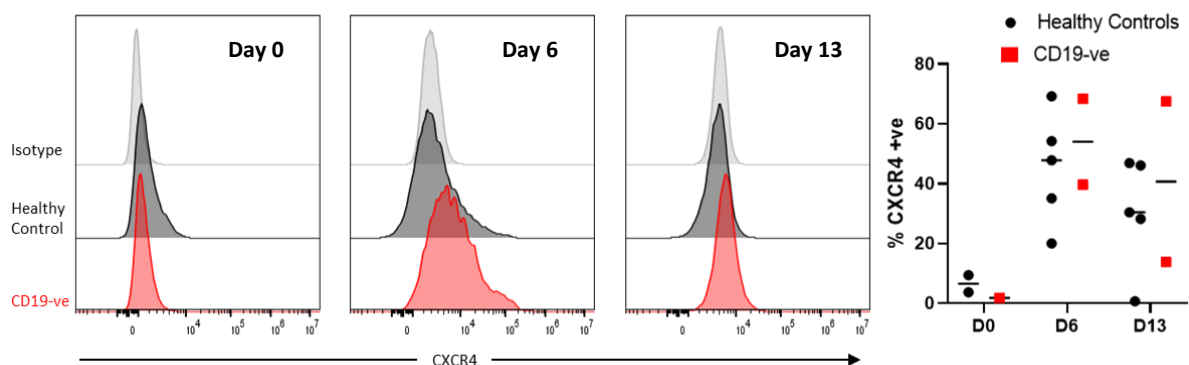
Figure 4.26 - Expression of cell surface CXCR4 was evaluated on day 0 B-cells, day 6 plasmablasts and day 13 plasma cells. PBMCs were obtained from peripheral blood and CD19 deficient and healthy B-cells were isolated via negative selection. B-cells were maintained within the in vitro differentiation model, following T-cell dependant stimulation, up to day 13. B-cells and PCs were collected for assessment of CXCR4 phenotype at day 0, 6 and 13 by flow cytometry. A representative plot is shown. Cells were blocked and stained with αCXCR4-PE and surface expression was analysed using flow cytometry. Plots were prepared using FlowJo software. Quantification of percentage CXCR4+ve cells in Healthy Controls (n=5) and CD19-ve (n=2 independent differentiations). CXCR4 positive cells were quantified and plotted for both healthy controls and CD19 deficient cells.

CXCR4 expression is maximally expressed at day 6 during the plasmablast stage for both healthy controls and CD19-ve cells. From day 6, CXCR4 surface expression decreases but is maintained at a low level in both cell types. Notably, CXCR4 expression was very highly maintained in day 13 CD19-ve PCs in one of the differentiations, but generally, CXCR4 expression is comparable between the deficient and healthy cells.

4.6.5 CXCR4 signalling

CD19 forms a complex on the surface of B-cells that acts as co-stimulatory element to amplify antigenic signalling via the B-cell receptor to promote activation of various signalling pathways, notably PI3K signalling. To determine whether CXCR4 signal propagation is affected by the loss of CD19, PBs and PCs were exposed to CXCL12 and the phosphorylation of PI3K and MAPK intermediates AKT and ERK were assessed (figure 4.27).
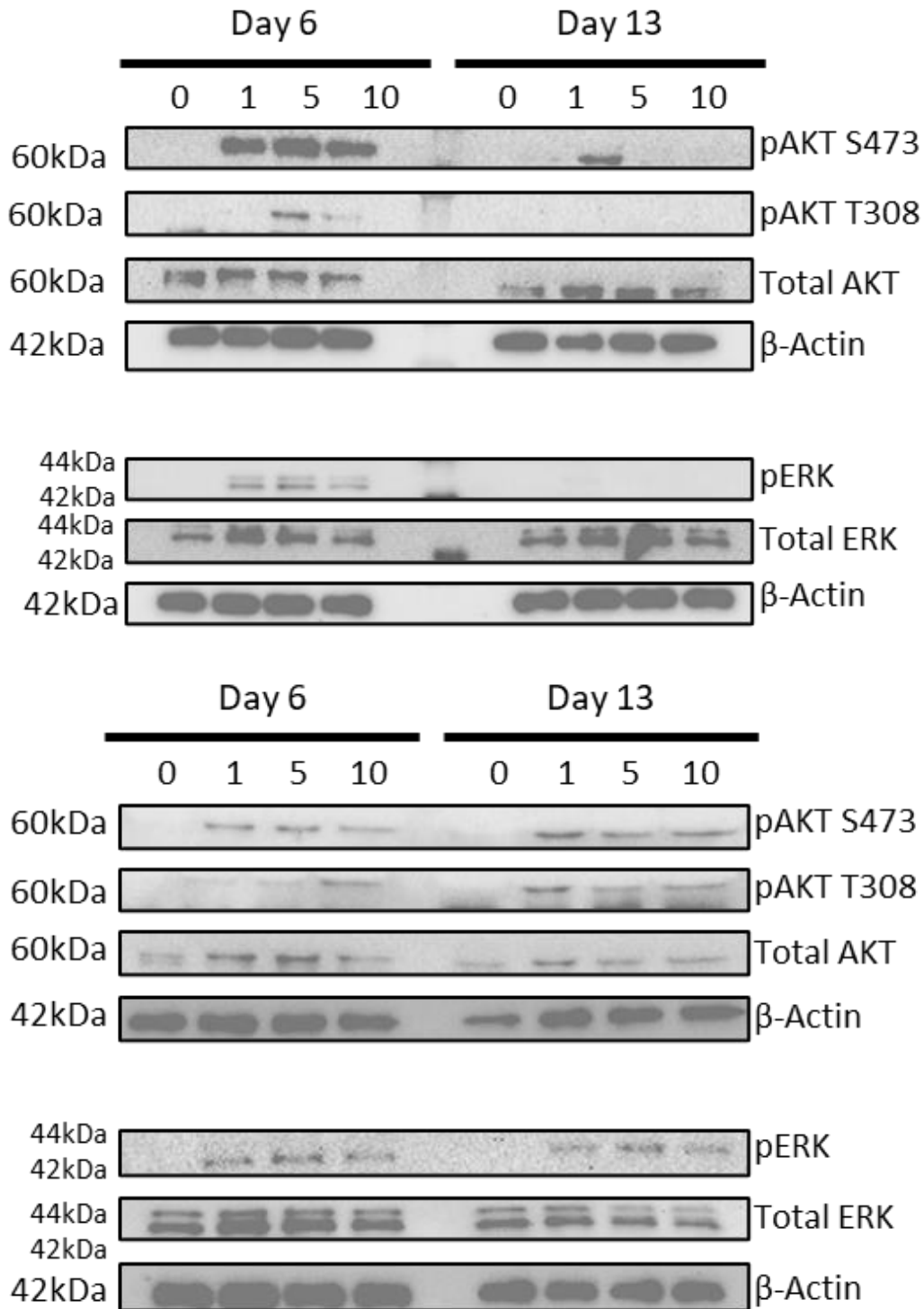
Figure 4.27 – Western blot analysis of pAKT S473, pAKT T308 and pERK at total AKT or ERK protein levels from day 6 and 13 CD19 deficient cells stimulated with CXCL12. PBMCs were obtained from peripheral blood and CD19 deficient B-cells were isolated via negative selection. B-cells were cultured in normal differentiation conditions. At day 6 and day 13 cells were cultured in 0.5% serum conditions overnight. Following overnight starvation, cells were stimulated with CXCL12, with samples taken pre-stimulation, 1, 5 and 10 minutes after stimulation and mixed with sample buffer immediately. Samples are then analysed by gel electrophoresis and western blot. Blots are probed with detection antibodies for phosphorylated ERK and AKT protein (N=2), Upper and lower figures indicate two independent differentiations from the same donor performed 5 months apart.

In healthy controls, both day 6 PBs and day 13 PCs showed a rapid induction of AKT and ERK phosphorylation. The response to CXCL12, in CD19-ve PBs, signalling was generally preserved, with a moderate day 6 ERK phosphorylation response and detectable pAKT response at both residues, though phosphorylation at the T308 residue was only detectable at 5 and 10 minutes whereas in control samples, phosphorylation could be detected earlier at 1 minute (figure 3.18). There is some variation between detection in PBs at the S473 residue between the two stimulations, with signal strength being weaker in the second differentiation, however the signalling pattern is conserved.

CD19-ve PCs exhibited striking defects, particularly in the lack of ERK phosphorylation. In the first differentiation, ERK phosphorylation cannot be detected indicating a complete failure to activate MAPK signalling. The second stimulation, however, shows that there is some ERK phosphorylation, however the signal strength is comparable to that seen in day 6 PBs. In HCs, ERK signalling in PCs consistently exhibit a far stronger response to CXCL12 stimulation (figure 3.14). Therefore, this suggests that ERK signalling is depleted in CD19 deficient cells.

AKT signalling is also altered in CD19 deficient PCs. Phosphorylation at the S473 residue is decreased, with phosphorylation only being detectable at one minute in the first stimulation. The second stimulation shows a stronger signal detectable from 1 minute to 10 minutes, however the signal strength is similar to the signal seen at day 6, suggesting some depletion in these cells. The pAKT T308 signalling at day 13 is absent in the first stimulation but detectable in the second. However, in both circumstances, detection is lower than that seen in HCs (figure 3.18).

To fully assess how CD19 deficient cell signalling compares to healthy controls, densitometry was performed for both stimulations. From this, the phosphorylated protein was quantified and normalised to total protein. The quantified values were then directly compared to healthy controls (figure 4.28). At day 6, the data show a similar yet somewhat diminished pAKT S473 response, however, the signalling response is generally maintained in PBs. At day 13, AKT phosphorylation in healthy cells varies between donors, with one donor with the weakest phosphorylation signal being comparable to the CD19-ve samples. Despite this, the CD19-ve samples show a notably lower average phosphorylation at day 13, indicating a defect in AKT signalling. This defect is more apparent at the T308 residue. At day 6, phosphorylation is comparable between healthy donors and CD19 deficient samples. By day 13, there is a clear loss of signalling through this residue. Together this suggest that there is impaired AKT signalling in CD19-ve PCs.

For ERK signalling, the densitometry analysis shows ERK signalling in PBs is similar comparable, suggesting that ERK activation remains intact. By day 13 however, it is clear the CD19-ve cells have

failed to generate an ERK signal. Whilst HCs show a strong peak phosphorylation 5 minutes after stimulation, CD19-ve cells maintain minimal signalling at all time points following stimulation.
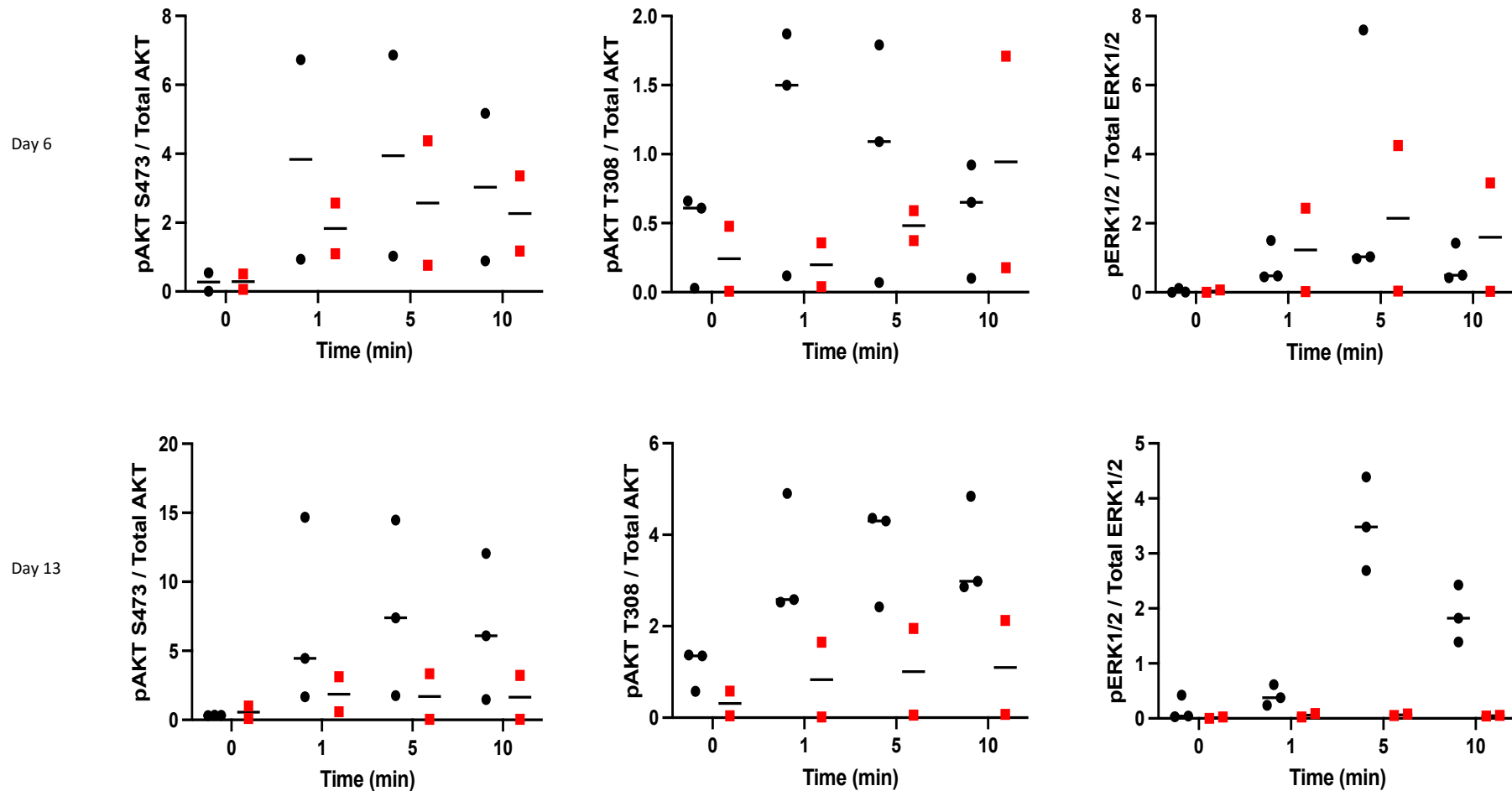
Figure 4.28 - Quantification of relative phosphorylation from Healthy Controls (n=3) and CD19-ve (n=2 - two independent differentiations from the same patient). PBMCs were obtained from peripheral blood and CD19 deficient B-cells were isolated via negative selection. B-cells were cultured in normal differentiation conditions. At day 6 and day 13 cells were cultured in 0.5% serum conditions overnight. Following overnight starvation, cells were stimulated with CXCL12, with samples taken pre-stimulation, 1, 5 and 10 minutes after stimulation and mixed with sample buffer immediately. Samples are then analysed by gel electrophoresis and western blot. Blots are probed with detection antibodies for phosphorylated ERK and AKT protein. Phosphorylation of ERK and AKT from each sample was quantified using Image Lab software. Additionally, total protein levels were also quantified for each time donor at all time points. Quantified phosphorylated protein values were normalised to total protein levels. Normalised values were then plotted for each donor. (Red = CD19-ve, Black = HC)

4.7 – Impact of CXCL12 stimulation of CD19-ve cells during culture

The change in proximal CXCR4 signalling in CD19-ve cells is likely to result in a change in cell behaviour. In addition to short term CXCL12 stimulation, CD19-ve B-cells were also subject to long-term stimulation of CXCL12 via inclusion of the cytokine within the culture media. Cells were isolated and activated as normal and maintained until day 6. At day 6 the cells were split and either cultured with or without CXCL12.

4.7.1 Cell viability

Long-term exposure of these cells to CXCL12 may show defects in survival compared to healthy cells treated similarly. Initially, cell counts were carried out to assess any changes in defects in the ability
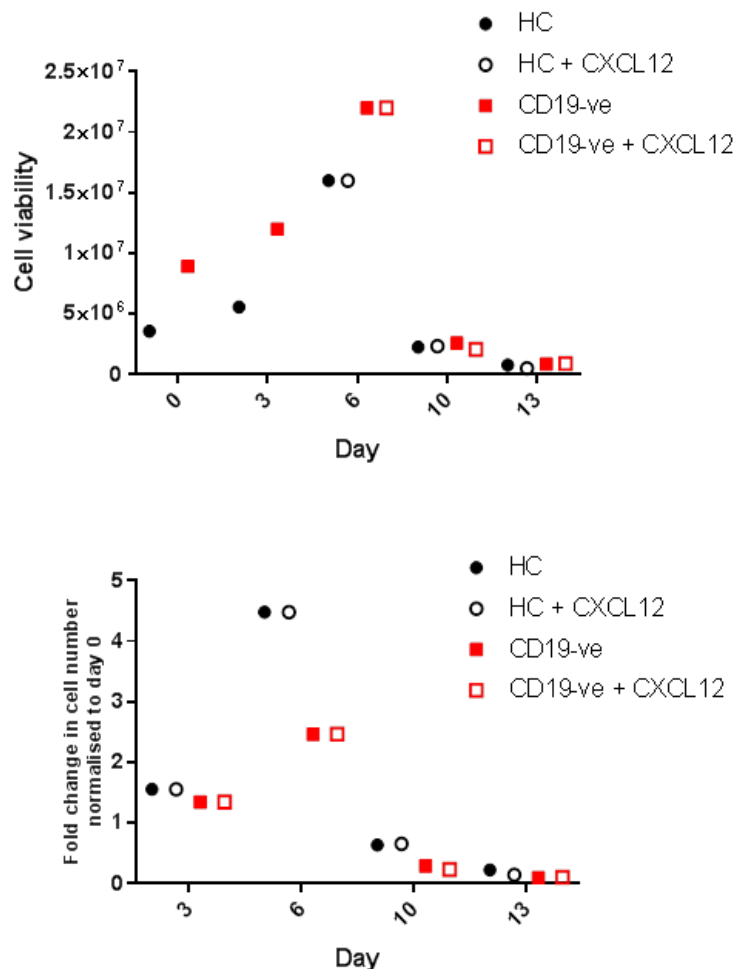
Figure 4.29 - Cell viability of B-cells/PCs cultured in either APRIL or APRIL+CXCL12 conditions (Top). PBMCs were collected from peripheral blood and B-cells were isolated via negative selection. B-cells were maintained in the differentiation culture following T-cell dependant stimulation until day 6. At day 6, cells were split into either normal APRIL conditions or APRIL + CXCL12 conditions. Cell counts were taken at day 0, 6, 10 and 13 from the different culture conditions. Cell counts were determined using haemocytometer and trypan blue staining **(upper)**. Fold change in cell number was determined via normalisation to the day 0 count and plotted **(Lower)**.

to respond to CXCL12 (figure 4.29). If CXCL12 induces enhanced survival signalling, this may be detected in the cell counts of PBs and PCs during the maintenance phase starting after day 6, where we would expect to see an improved cell count at this stage.

The cell viability data indicate that, again the CD19-ve B-cells do not have detectable defects in proliferation during the expansion phase of the differentiation post activation at day 3. Also, the CD19-ve cell counts after day 6 during the maintenance phase of the differentiation are comparable to the HC, both populations experience a rapid contraction of viable cells. Cell viability measures between APRIL treated and APRIL with CXCL12 treated samples show, that from day 10 onwards, a comparable cell count. This suggests that, in the presence of APRIL at least, that CXCL12 provides no measurable benefit to PB and PC survival.

4.7.2 B-cell and PC phenotype

B-cell and PC phenotype was assessed to determine of the impact of inclusion CXCL12 (figure 4.30). As expected, the CD19 deficient patient expressed no CD19 surface protein. This was unchanged when CXCL12 was included in the culture media. Inclusion of CXCL12 had no impact on CD19 expression in healthy controls. CD27 expression is comparable across all samples and conditions.

CD38 expression is slightly lower in the CD19-ve samples, however the range of the difference is small, suggesting that CD38 acquisition is unaffected by both the CD19 deficiency and the inclusion of CXCL12. In both samples, there are CD38+ve cells in the CXCL12 stimulated conditions, however these variations are minute.

At day 6, both healthy controls and CD19-ve cells expressed high levels of CD20, with about 70% of cells CD20 positive. By day 13, the two populations diverge in their expression of CD20. CD19-ve cells more rapidly downregulate CD20. In the CXCL12 treated population, this downregulation is slightly less than in the APRIL only treated population. The two populations of healthy control cells share a more slightly comparable CD20 expression, but both express about 20% more CD20 than the CD19 deficient samples. The quicker downregulation of CD20 in the CD19 deficient cells suggests they more rapidly generate a PC-like population, however as shown in figure 4.19, the CD20 expression in the first CD19-ve differentiation is comparable to healthy controls. In addition to this, whilst the CD138 expression of the deficient cells shown here is far higher compared to the healthy controls, again figure 5.7.2 shows that attainment of a PC phenotype is comparable to that seen in HCs. It is possible then that this HC differentiates much slower than average. CD138 expression is similar between the APRIL and APRIL/CXCL12 conditions.
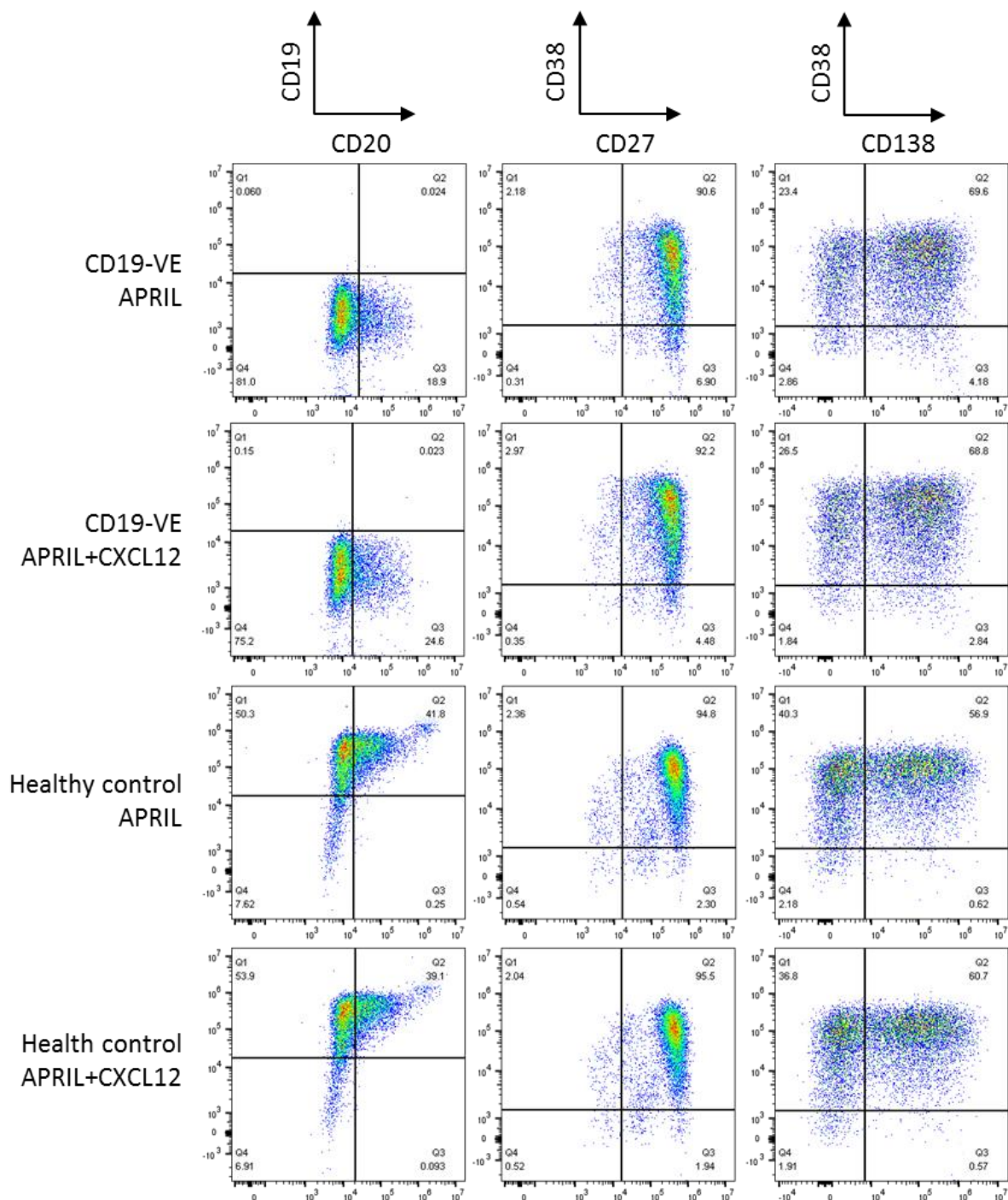
Figure 4.30 – B-cell/PC surface phenotype of day 13 PB/PCs from CD19-ve B-cells or healthy control cultured in either APRIL or APRIL+CXCL12 conditions. PBMCs were isolated from healthy and Cd19 deficient donors and B-cells were isolated. B-cells were maintained within the differentiation culture system until day 6. Day 6 cells were split into either normal APRIL conditions or APRIL with CXCL12 and maintained until day 13. At day 13, samples were taken for phenotypic analysis. Cells were blocked and stained with antibodies targeting B-cell/PC markers (CD19, CD20, CD27, CD38 and CD138). Surface expression was analysed using FlowJo software (N=1)

To summarise, the inclusion of CXCL12 in the culture media has a minimal effect on B-cell differentiation, CD19-ve cells do not shown any defects in PC phenotype attainment, and CXCL12 does

modulate any characteristics of these cells, as confirmed by the phenotype percentage positivity data (figure 4.31).
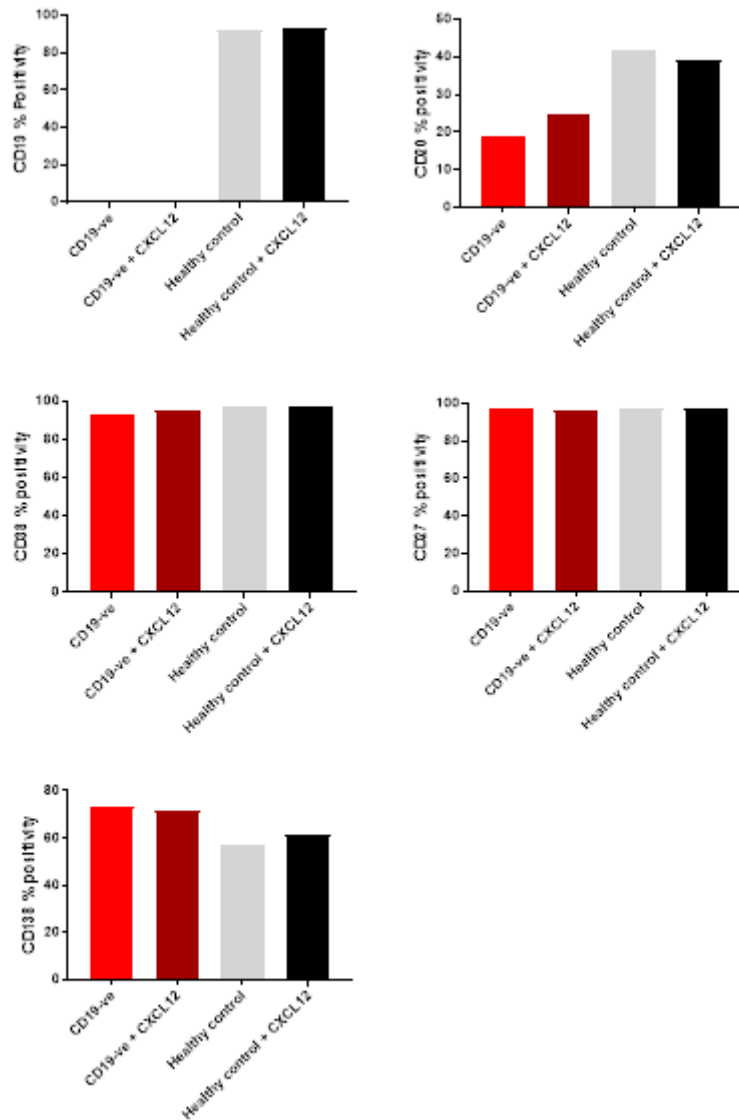
Figure 4.31 - Quantification of the percentage of cells expressing indicated markers at day 13 of the differentiation. PBMCs were isolated from healthy and Cd19 deficient donors and B-cells were isolated. B-cells were maintained within the differentiation culture system until day 6. Day 6 cells were split into either normal APRIL conditions or APRIL with CXCL12 and maintained until day 13. At day 13, samples were taken for phenotypic analysis. Cells were blocked and stained with antibodies targeting B-cell/PC markers (CD19, CD20, CD27, CD38 and CD138). Cell phenotype at D13 (figure 4.30) was quantified as percentage positive for both healthy controls and CD19 deficient cells cultured in either APRIL conditions or APRIL+CXCL12 conditions. Bright red indicates Cd19 deficient cells in APRIL conditions and dark red in CXCL12 conditions. Grey represents healthy cells in APRIL conditions and black indicates cells in CXCL12 conditions. Bars represent percentage positivity of the indicated Cell surface marker (n=1).

4.7.3 CXCR4 expression

To confirm that the lack of observable changes in the above assays were not due to abnormal levels of CXCR4, its expression was monitored. CXCR4 expression followed the expected pattern of peak expression at day 6 before decreasing between day 6 and 13 (figure 4.32). The majority of the CD19-ve day 6 cells expressed CXCR4, whereas the healthy control had a particularly low peak CXCR4 expression in comparison. These further cements the finding that the CD19-ve cells are largely phenotypically normal. Additionally, in this differentiation the CXCR4 surface expression was maintained at day 13 more than seen previously.

Inclusion of CXCL12 in the culture media had little impact on CXCR4 expression. In both the CD19-ve and HC, there is a slight decrease in surface CXCR4 expression. As both cell populations were affected similarly, this effect is possible a result of normal reduction of CXCR4 in the presence of CXCL12. The data here suggest that long term CXCL12 does not impact CXCR4 protein levels. ΔMFI was calculated in addition to the percentage positivity to confirm the above results (figure 4.33).
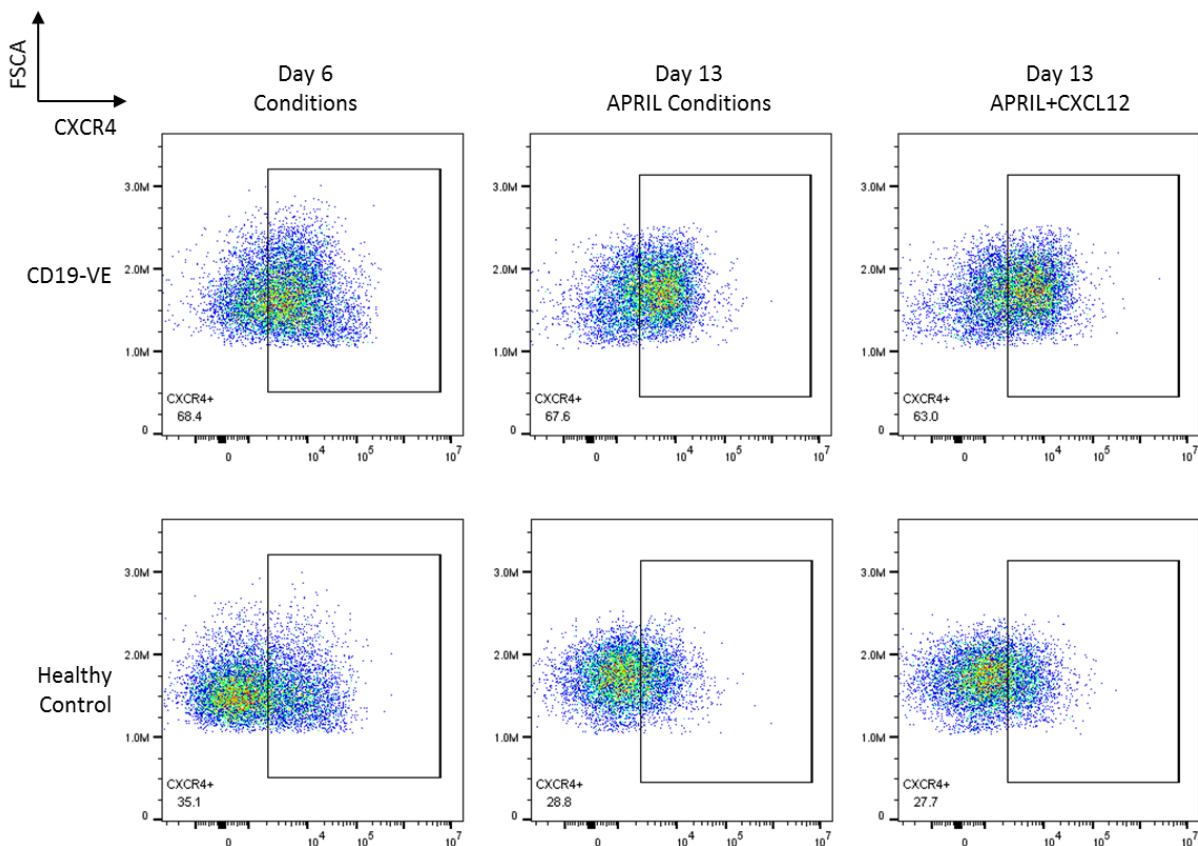
Figure 4.32 - Expression of cell surface CXCR4 was evaluated on day 6 and day 13 cells cultured in either APRIL or APRIL+CXCL12 conditions. PBMCs were isolated from healthy and Cd19 deficient donors and B-cells were isolated. B-cells were maintained within the differentiation culture system until day 6. Day 6 cells were split into either normal APRIL conditions or APRIL with CXCL12 and maintained until day 13. Cells were stained with αCXCR4-PE and surface expression was analysed using flow cytometry. Percentage of CXCR4 positive cells are indicated. Plots were prepared using FlowJo software
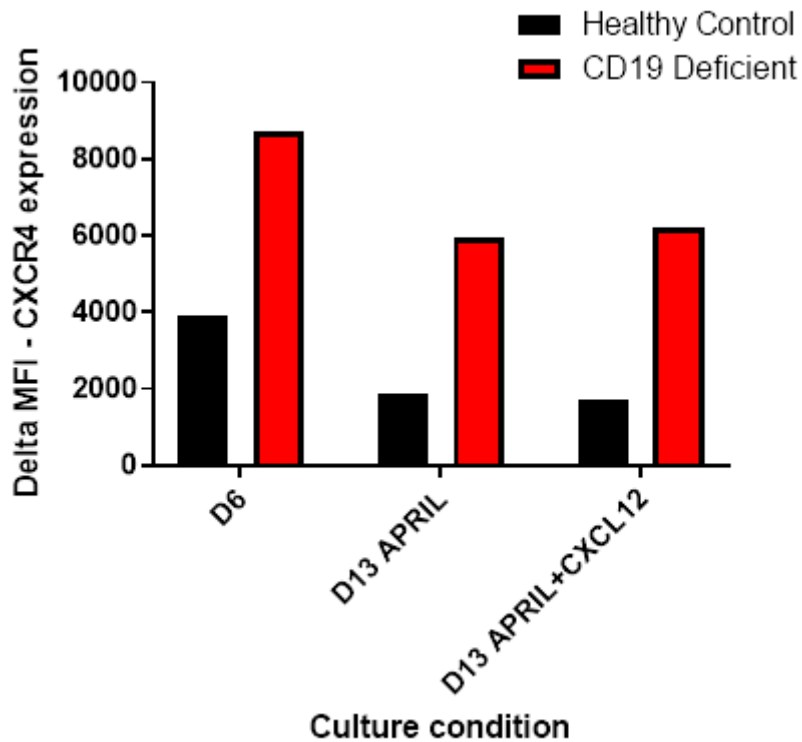
Figure 4.33 – Calculated ΔMFI for surface CXCR4 expression of day 6 and day 13 cells cultured in either APRIL or APRIL+CXCL12 conditions. PBMCs were isolated from healthy and Cd19 deficient donors and B-cells were isolated. B-cells were maintained within the differentiation culture system until day 6. Day 6 cells were split into either normal APRIL conditions or APRIL with CXCL12 and maintained until day 13. MFI values were determined for CXCR4 expression for each condition and sample. ΔMFI was then calculated by subtraction of isotype MFI values from sample MFI values. ΔMFI was then plotted using graphpad prism software. Each bar represents ΔMFI values for CXCR4 expression for each timepoint and each culture condition (N=1).

As expected, the ΔMFI values confirm the previous results, that CXCR4 expression is mostly unaffected by the inclusion of CXCL12 in the differentiation model. This could indicate CXCR4 signalling is not a major driver of survival in PCs, However, removal of APRIL may reveal a role for CXCL12, as APRIL likely provides sufficient survival signalling for these cells.

4.8 Discussion

These analyses provide insight into the role that CD19 plays in the convergence of CXCR4 signalling on differentiating B-cells. Previous findings indicate that CD19 can act as a signalling hub to amplify BCR and CXCR4 receptor signalling (Depoil *et al.* 2008; Becker *et al.* 2017; Keppler *et al.* 2015). However, the role of CD19 in PC signalling is less clear. CD19 surface expression is maintained throughout the differentiation however a subset of PCs has been identified within the BM that are CD19-ve, CD38+ve and CD138+ve. This subset possesses reactivity against viral antigens that have be stored for

immunological memory over 40 years and a distinct PC gene expression pattern that was surmised to reflect the long-lived nature of these cells (Halliley *et al.* 2015). However, subsequent studies have shown that long-term immunity can be provided by both CD19+ and CD19- PC fractions (Groves *et al.* 2018; Brynjolfsson *et al.* 2017). Thus, the importance of the differential loss of CD19 in PCs remains unknown. To understand how CD19 might play a role in ASCs, this chapter aimed to understand what signalling events downstream of CD19 as well as how CXCR4 signalling is impacted by CD19 ligation and CD19 depletion.

Evaluation of CD19 was to be completed firstly by direct stimulation of CD19. Cells were stimulated with CD19 antibody conjugated to biotin that was mixed with avidin beads to enable cross-linking of CD19 on the surface of cells in a manner analogous to bead-mediated crosslinking of CD28 and TCR to activate T cells. Day 6 PBs and day 13 PCs were stimulated with αCD19 bound beads alone. It was expected that direct stimulation of CD19 in the absence of co-stimulation may only have a moderate effect on downstream signalling as CD19 stimulation is usually associated with BCR signalling. Stimulation of both PBs and PCs showed a complete lack of ERK signalling indicating that CD19 requires co-ligation with another surface receptor to generate an ERK signal, namely the BCR (Li and Carter 2000; Li and Carter 1998).

AKT signalling was assessed for phosphorylation at two residues, S473 and T308. Activation of AKT at T308 was not clearly detected in either PBs or PCs, but this may have been hampered due to the presence of non-specific bands. Additionally, quantification proved that in comparison to CXCL12 stimulated cells, it is likely the bands detected were due to background. Interestingly, there was detectable phosphorylation at the S473 residue in PCs only. The quantification data show that whilst this activity is far weaker than that seen in CXCL12 stimulated PCs, it shows that PC are responsive to CD19 stimulation. AKT activity could not be detected at day 6, when the cells are mostly PBs, however most PBs at day 6 are usually more CD19 positive than PCs, indicating that there is an intrinsic property of PCs enabling sensitivity to CD19 ligation that is not present in PBs.

The low level of kinase activation could be related to the method of CD19 activation used. Therefore an alternative mechanism for CD19 could be utilised. It is well studied that the complement system can activate B-cell signalling, as shown by the presence of receptors for complement proteins C3b on the surface of B-cells (Ross et al., 1973). CD19 associates with CD21 which allows binding of the complement C3d fragment of activated C3 that is attached to targets of complement activation (e.g. foreign or self-antigens). CD19, in complex with CD21 can co-stimulate signalling through the BCR, thereby linking recognition of foreign antigens by complement to B-cell activation (Fearon and Carroll 2000; Eden, Miller and Nussenzweig 1973; Ross *et al.* 1973). From this, a new experiment could be

developed whereby complement protein C3d is used to bind to CD21 in complex with CD19, activating the signalosome complex. This way CD19 can be activated whilst mitigating the problem of a lack of a natural ligand for CD19.

Co-stimulation of PBs and PCs with CXCL12 and αCD19 generated a unique signalling pattern not seen in CXCL12 stimulation alone. Under CXCL12 conditions, day 13 PCs generate a strong ERK signalling pattern whereas day 6 PBs show a weaker induction of ERK phosphorylation. In contrast, PBs exposed to co-stimulation generate a far stronger phosphorylation of ERK compared to PCs. This dichotomy implies αCD19 dampens CXCR4 mediated ERK signalling in PCs and enhances it PBs. While a potential negative regulatory role for CD19 is unexpected, it is worth noting that multiple myeloma cells are consistently CD19 negative. It is conceivable that a loss of CD19 is compatible with the altered signalling found in malignant plasma cells.

There is significant variation in the AKT S473 phosphorylation responses between donors, however in general stimulation of CXCL12 or CXCL12 with αCD19 in PBs was comparable as was stimulation in PCs. Overall the trend indicates that either form of activation was stronger in PCs compared to PBs. AKT signalling is an important regulator or survival in multiple cell types. At the T308 residue, this pattern was repeated, with a starker contrast showing a weaker response to both stimuli in PBs compared to PC. Additionally, the responses to CXCL12 or dual-stimulation in PCs was similar. PCs may be more responsive to CXCR4 signalling due to their requirement to survive in a particular niche. Enhanced PI3K signalling may be intrinsic for this function. CD19 ligation does not seem to amplify this and therefore, in healthy PCs at least, does not improve PC survivability. Furthermore, the downregulation of surface CXCR4 after stimulation may limit the ability of CD19 to function as a signalling hub.

Because CD19 itself can promote AKT signalling, it was thought that long term stimulation of differentiating PBs may promote survival. Initially, CD19 was included in normal differentiation conditions, however changes in cell phenotype and viability could not be detected (data not shown). it was therefore assumed that APRIL itself may mask any effect of αCD19 beads as APRIL is a potent survival factor. Therefore, the cells may not have required the use of CD19 induced signalling. The experiment was repeated with three culture conditions to enable a greater understanding of CD19 activation of B-cells and PCs in the in vitro differentiation model. Despite this, αCD19 stimulating conditions failed to promote a survival benefit. Cell viability under these conditions was comparable to conditions without either αCD19 or APRIL indicating no improved survival signalling was generated. Additionally, the phenotype of these cells at day 10 was similar. All conditions allowed for normal attainment of CD38 and loss of CD20, showing normal progression towards to PC cell state. CD138 expression was different between the conditions. APRIL conditions generated the lowest proportion

of CD138+ cells suggesting that either there was a slower generation of mature PCs or due the lower cell viability in αCD19/untreated conditions, there was a greater proportion of CD138+ long-lived PCs at this time point.

As short-term CD19 stimulation was only able to generate a signal in day 13 PCs, it may be that as long-term stimulation only assessed up to day 10, where only about 20% of the cells had attained a CD138+ phenotype, that the effect of long-term αCD19 was not yet active until more cells reached a PC phenotype at day 13 and beyond. CXCR4 surface expression was similar between all conditions, further supporting the idea that direct stimulation of CD19 by cross-linking generates only a weak signal transduction pattern in PCs but not PBs.

One caveat of these studies was the lack of confirmation that the αCD19 beads were having an effect on the cells. Whilst some AKT phosphorylation activity is detectable, additional experiments could have been included to ascertain the efficacy of the beads. Further optimisation to fully determine the bead-to-cell ratio could have been completed, where different bead to cell ratios would be assessed via e.g. calcium flux. A small calcium flux can be detected in B-cells stimulated with anti-CD19 (Dasu *et al.* 2009). Additional controls would include beads unconjugated to the CD19 antibody and FC receptor control. A positive control could be F(ab)2 , as this would induce a strong calcium flux. Additionally, stimulated and unstimulated cells could be assessed for CD19 phosphorylation via western blot analysis.

To further assess how CD19 can affect signalling, B-cells from a CD19 deficient patient were obtained. The patient B-cells express no surface CD19 however under optimized conditions are capable of undergoing BCR stimulation and generating a strong proliferative response. Earlier reports describe CD19 deficient B-cells as incapable of mounting a normal B-cell response and fail to activate, causing an absence of class switched memory B-cells (van Zelm *et al.* 2006; Warnatz *et al.* 2002), however additional studies have indicated a spectrum of mutation and disease severity, revealing capability of some patients B-cells to successfully activate but fail to mount a substantial immunoglobulin response (Kanegane *et al.* 2007).

The patient utilised in this study showed mild pan-hypogammaglobulinemia, particularly affecting the IgG subclass and a detectable CD20+ CD19- B-cell population. The patient also possessed a reduced memory B-cell population. It may also be possible that in this model, significant B-cell stimulation is provided that may circumvent the requirement for CD19 to reduce the threshold for B-cell signalling, therefore the CD19 deficient cells do not experience defects in differentiation and survival as seen previously in the literature.

Under B-cell activating conditions, the CD19-ve cells undergo all the normal phenotypic changes seen in healthy B-cells, including CD20 downregulation, CD27 and CD38 acquisition by day 6 and finally the majority of cells becoming CD138+ by day 13, indicating a functional adaptation to the PC programme. Additionally, cell viability matches the pattern seen in healthy controls. Together this indicates, that for this mutation, B-cell activation and maturation to PC is maintained under *in vitro* conditions. IgM and IgG production was relatively low at day 6 however by day 13, they were comparable to those seen in healthy controls. This data indicate that the defects in antibody production seen here somewhat match that seen in the literature for day 6. At the plasma cell stage, where CSR has already occurred, immunoglobulin production shifts to increase IgG production, and CD19 deficient cells are able to secrete immunoglobulin to a similar level seen in the healthy controls, indicating that plasma cell Ig secretion is maintained. CXCR4 expression also followed the normal pattern, peaking at day 6 to levels comparable to HCs and reducing to low levels by day 13. Whilst CXCR4 expression was maintained higher than normal at day 13 in one of the differentiations, the other differentiation showed a more expected result of very low levels. Further assessment of CD19 differentiations would be required to understand if CXCR4 expression is actually retained to this level.

CD19-ve PBs seem to be capable of generating a weak AKT and ERK signal in response to CXCL12, however once the cells become majority PCs, ERK signalling is almost completely lost and AKT phosphorylation is severely reduced. The signalling data suggests that CD19 on PCs does have potential to function as a signalling element. Loss of these pathways would imply significant defects to downstream gene transcription, leading to flaws in activation crucial pathways regulating survival, migration, and adhesion. It could indicate that loss of CD19 in PCs cells is less to do with survival but may be more important migration/adhesion. Alternatively, it could be that inclusion of APRIL, as a potent survival factor maintains PC survival irrespective of ERK signalling defects. APRIL binds to BCMA on PCs, this induces activation NF-κB signalling and MAPK signalling (Hatzoglou *et al.* 2000; Mackay *et al.* 2003).

Inclusion of NF-κB inhibitors, such as IKK complex inhibitors or NF-κB translocation inhibitors may reveal a potent flaw in CD19-ve PC survival, therefore an experiment could be designed, firstly confirming that inclusion of NF-κB inhibitor induces severe defects in cell viability. Next addition of CXCL12 and the NF-κB inhibitor may force healthy B-cells to become reliant on ERK signalling induced by CXCL12, and therefore CD19- PCs would be unable to be rescued by CXCL12. Inclusion of ERK inhibitors and AKT inhibitors could be included for validation.

Analysis of the RNA sequencing revealed a normal expression of CD19 throughout the differentiation of the CD19 deficient cells. It was predicted that the introduction of a frame shift mutation seen in the

CD19 deficient patient would induce nonsense-mediated decay (NMD) due to the generation of an early stop codon within exon 4, and therefore there would be no translation of CD19 mRNA to generate protein. However, RNA seq analysis indicates CD19 expression is maintained at normal levels. Exons 2 and 4 encode the Ig like domains, exon 5 encodes the transmembrane region and exons 6-14 encode the cytoplasmic domains responsible for the signalling function of CD19 (Zhou *et al.* 1992). The truncation in this patient occurs within exon 4. It is possible that the extracellular component is translated but without the membrane spanning region and cytoplasmic tail region, the protein is not presented on the cell surface and therefore cannot be detected by flow analysis, nor can it provide function as a signalling hub for e.g. the BCR or CXCR4. Indeed, Data from other CD19 deficient patients have also shown normal levels of CD19 transcripts despite truncations in exons associated with the cytoplasmic domains (van Zelm *et al.* 2006). It has therefore been suggested that the reduction in protein is rather a result of the instability of the truncated CD19 proteins. It has been observed that truncated yet stable CD19 proteins, where up to 95% of the cytoplasmic domain of CD19 is deleted, can associate with CD81 and CD225 on the B-cell surface. However deletion of the transmembrane and cytoplasmic domain, prevents CD19 complex formation and therefore surface expression, yet mRNA expression is normal (Bradbury, Goldmacher and Tedder 1993). How these transcripts are able to avoid NMD however is unclear, though some mechanisms have been described (Ge *et al.* 2016).

Additional analysis of the exon pattern of this patient revealed no major defects. There is some evidence of exon skipping at exon 6, which codes for the transmembrane proximal region of the cytoplasmic domain. However, this occurs in addition to the normal expression pattern, and therefore could not account for the loss of CD19 expression. Indeed analysis of genetic mutations of CD19 in ALL have shown how variants in exons 2-5 can lead to a truncated protein lacking membrane anchorage. They also state that there was no evidence of NMD and that alternate splicing occurs at very low frequencies (0-2.7%) and therefore accounts for an insignificant fraction of tumour cells lacking CD19 (Orlando *et al.* 2018) .The literature shows that even in the presence of a nonsense mutation in CD19 that leads to a truncated protein, mRNA expression is maintained and neither NMD nor alternate splicing account for the loss of CD19 surface expression. This indicates some other mechanism controls the loss of CD19 expression. However, it supports the data collected here, where CD19 RNA expression is maintained despite the confirmed presence of a nonsense mutation in exon 4.

RNA sequencing analysis of differentiation genes indicate a lack of defects in the control of B-cell differentiation, and this supports the phenotypic data that indicate the same. Assessment of signalling related mRNA expression in these deficient cells suggest there may be some alterations in PI3K gene

expression. Increased expression of these genes could indicate a decision by the cells to attempt to mitigate the failure to activate ERK signalling through CXCL12 signalling.

CD19-ve cells treated with APRIL and CXCL12 within the differentiation model have comparable cell counts to the HCs. Additionally, healthy cells cultured with APRIL or APRIL with CXCL12 also show similar cells counts throughout the differentiation. This suggests that CXCL12 does not confer a survival advantage in PBs and PCs in APRIL conditions as APRIL may provide sufficient survival signalling that further CXCR4 activation cannot improve upon, implying CXCR4 surface protein is being cycled to prevent excessive signalling. A follow up experiment should be completed assessing the impact of either APRIL or CXCL12 or neither to fully show if long term CXCL12 stimulation can affect PC survival.

In conclusion, these results indicate that CD19 participates in signal transduction events in fully mature PCs. Although the significance of direct CD19 ligation on these cells remains unknown, the findings in this chapter provide a strong basis for further investigation.

5.0 – Signalling in CXCR4^{WHIM} antibody secreting cells

5.1 Introduction

The data presented in the previous chapters provide evidence that CXCR4 signalling changes as B-cells differentiate, with mature PCs displaying enhanced activation as well as a greater dependence on CD19. Waldenström macroglobulinemia (WM) is a unique B-cell malignancy whereby malignant transformation is linked to the capacity to complete terminal differentiation to the immunoglobulin-secreting PC stage (Owen *et al.* 2003). Whilst there is not complete understanding of the mechanisms that drive WM, mutations in MYD88 have been identified in over 90% of patients that result in dysregulated NF-κB signalling (Treon *et al.* 2012). In addition to this, there have also been CXCR4 mutations identified in about 30% of WM patients. These mutations are characterised by the inability of afflicted cells to induce ligand mediated receptor internalisation and therefore cease signal transduction, leading to enhanced signalling associated with proliferation, survival, and migration (Lagane *et al.* 2008). Assessment of this WHIM mutation has identified an enhanced activation of AKT and ERK signalling and an associated decrease in levels of apoptosis in WM B-cell lines. This indicates these pathways are key regulators of WM cell survival (Cao *et al.* 2015).

The analysis of CXCR4 signalling in PB and PCs presented here has identified a specific pattern of phosphorylation, showing enhanced MAPK/ERK and PI3K/AKT signalling in mature PCs compared to PBs. PB/PCs utilise the CXCR4-CXCL12 axis for migration towards survival niches, including the BM. WM cells are characterised by their unique ability to undergo B-cell differentiation within the BM, implying that there is an altered chemotactic homing potential of the malignant cells. Additionally, the presence of the CXCR4^{WHIM} mutation likely enhances this effect (Bidkhori *et al.* 2021)**.** Indeed, in mice engineered to express CXCR4^{WHIM}, PC trafficking is perturbed, as long-lived antigen specific PCs fail to populate the BM, whereas immature proliferating PBs quickly accumulate in this niche (Biajoux *et al.* 2016). Data provided here has shown proliferating PBs express higher levels of CXCR4 than mature PCs, suggesting a potentially higher response to CXCL12 signals, however in a healthy setting, the PCs generate a stronger response. It could then be assumed that WHIM mutated PBs are a significant driver of disease.

The impact of the loss of CD19 in these cell populations indicates a major role in its regulation of CXCR4 signalling and we have shown some evidence that crosslinking of CD19 does impact CXCR4 signalling. However, the impact in association with the CXCR4^{WHIM} mutation has yet to be explored. Therefore, this chapter will detail the assessment of the expression of CXCR4^{WHIM} utilising retroviral transduction and the downstream signal transduction pathways generated in response to CXCR4 and CD19 stimulation.

5.2 – Development of primary CXCR4^WT^ and CXCR4^WHIM^ over-expressing cells

To assess the effects aberrant CXCR4 signalling in ASCs, a study was planned to introduce B-cells with the CXCR4^WHIM^ mutation, which is created by changing S338 (TCA) in the intracellular C-terminal tail to a stop codon (TGA). This would enable mutant CXCR4 signalling in differentiating B-cells. Retroviral transduction of vectors containing CXCR4^WHIM^ and CXCR4^WT^ were to be introduced into the B-cells. Initially however, pIRES-EGFP vectors containing either *CXCR4*^WT^ or *CXCR4*^WHIM^ were obtained (Figure 5.1).
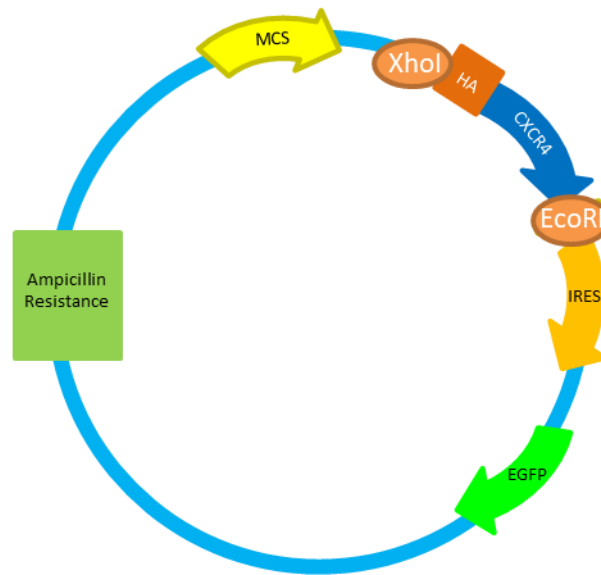
Figure 5.1 – pIRES-EGFP CXCR4 vector map – For transient transfection, plasmids were designed to include **a** HA tag was added before the CXCR4 sequence within the MCS to allow for identification of CXCR4 protein. The HAtag-CXCR4 sequence was flanked by restriction sites for XhoI and EcoRI to allow for removal of sequence and insertion into other plasmids. eGFP is included to visualise successful transfection using microscopy or flow cytometry. Ampicillin resistance was also included for selection.

An HA tag was included for detection of CXCR4 by Western blot analysis in transduced cells. Constructs were transformed into competent bacteria and plasmid DNA was purified for transfection into the relevant cells.

5.2.1 Restriction digests

Initially the CXCR4 expression constructs were checked to confirm that the CXCR4 protein could be detected in cells. Prior to transfection, a restriction digest using XhoI and EcoRI to liberate the insert was performed on the vectors (figure 5.2).
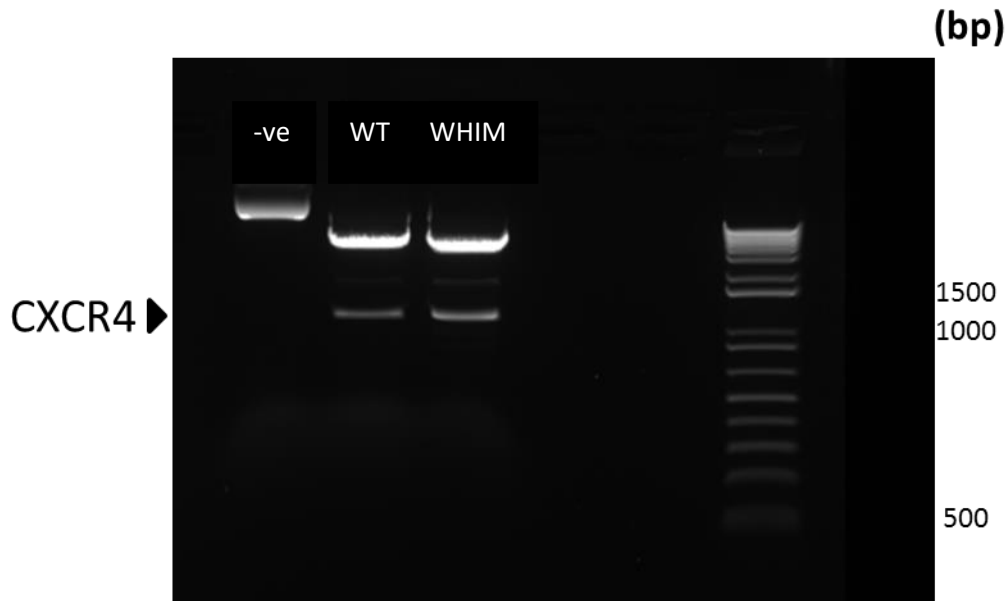
Figure 5.2 - Restriction digest confirming the presence of *CXCR4* inserts in piRES-eGFP vector. Digest reactions were performed on both the WT and WHIM constructs and a negative control digest was included with no restriction enzymes included in the digest mix. Digests were run at 37°C for 1 hour before gel loading buffer was added and mixes were loaded onto a 1% agarose gel. A DNA ladder was included to confirm the sizse of excised bands.

The presence of an insert of the appropriate size for *CXCR4* was confirmed by gel electrophoresis. Undigested plasmid was compared to the digested samples and showed that the digested samples released an insert of approximately 1000bp matching the expected size of 1060bp. Both WT and WHIM constructs released an insert of equal size.

5.2.2 Expression HA-tagged CXCR4

Next, HEK293 cells were cultured and prepared for transient transfection utilising the Gene Juice DNA transfer method. The CXCR4^{WT} and CXCR4^{WHIM} transfections were then assessed by flow cytometry to observe the expression of GFP, to determine successful uptake of constructs (figure 5.3). CXCR4 surface expression was also assessed. First, GFP was assessed in combination with a CXCR4 isotype antibody. This confirms the presence of GFP with the HEK293 cells for both the CXCR4^{WT} and CXCR4^{WHIM} constructs, where about 40% of the cells express GFP. The untransfected sample does not express any GFP. Next, CXCR4 expression was assessed alongside GFP expression. In the untransfected sample, a very sample amount of CXR4 was detected (4-7% of cells). In the transfected samples, CXCR4 expression is highly detectable, indicating successful expression of CXCR4 in these samples.
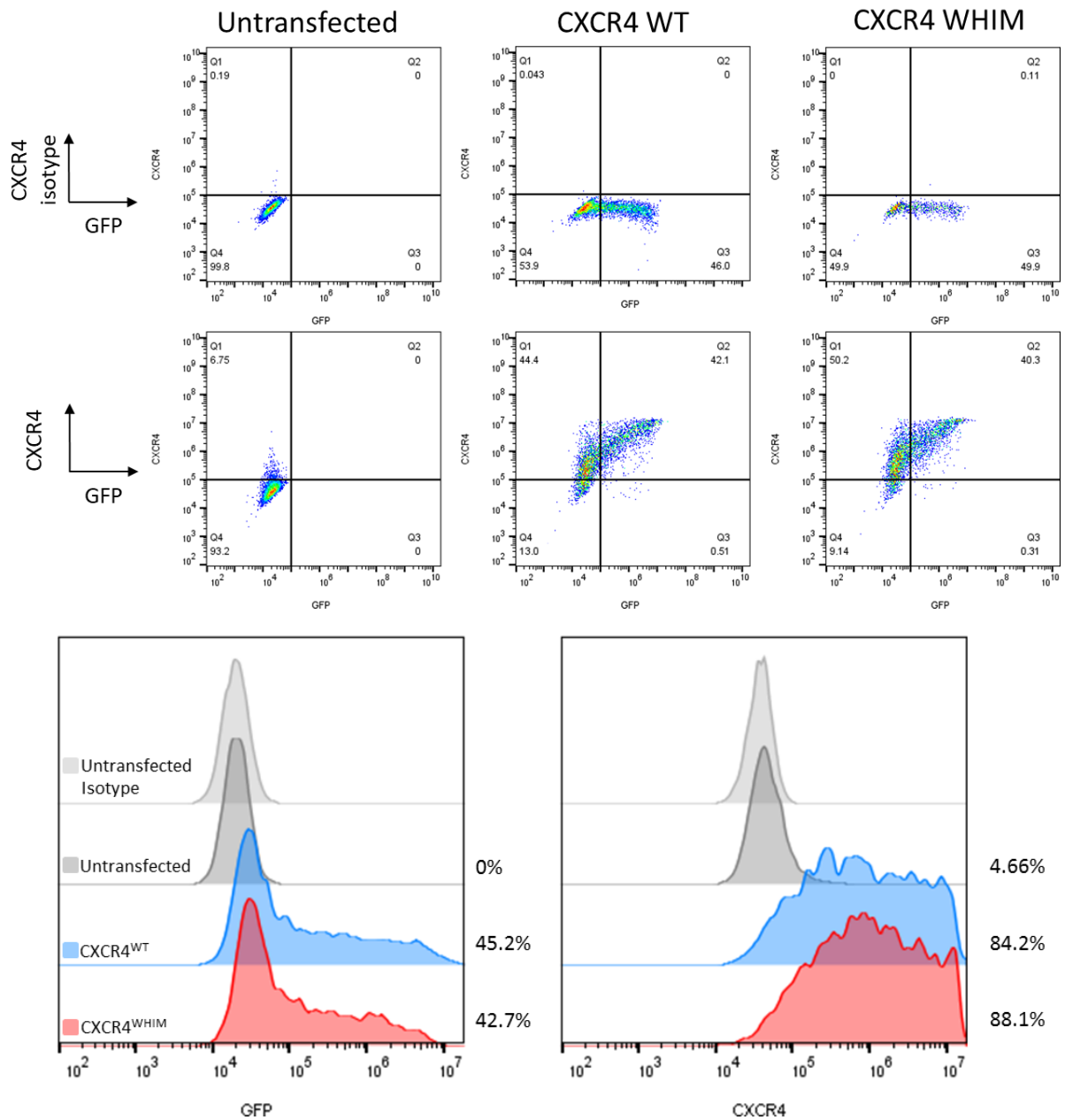
Figure 5.3 – Flow cytometry analysis for detection of GFP and CXCR4 in untransfected and transfected HEK293 cells. HEK293 cells were transiently transfected with either the CXCR4^{WT} or CXCR4^{WHIM} constructs using gene juice, or left untransfected. Cells were then stained with either a CXCR4 isotype antibody or CXCR4-PE antibody for assessment of CXCR4 expression. GFP expression generated from the eGFP gene within the construct was detected though the FITC channel. Histograms are included (lower panels).(N=1).

Following flow analysis, protein samples were collected from the HEK293 cells and protein extraction was performed utilising RIPA buffer lysis method. Extracted protein was prepared with sample buffer and loaded onto gels. A Western blot was completed, and expression of HA tag was assessed (figure 5.4).
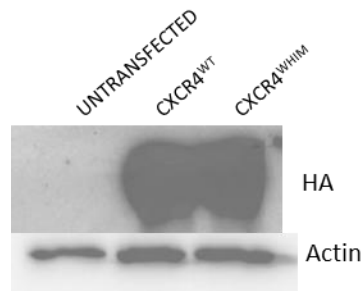
Figure 5.4 – Western blot analysis of HA expression in untransfected and CXCR4 transfected HEK293 cells. HEK293 cells were transiently transfected with either the CXCR4^{WT} or CXCR4^{WHIM} constructs using gene juice or left untransfected. Protein was isolated from these cells and loaded onto an SDS page gel before being transferred to a blotting membrane for western blot analysis of CXCR4 protein via detection of HA. Blots were blocked and then probed for HA using a HA detection antibody. Actin detection was used as a loading control.

HA expression was detected in transfected cells but at size much larger than expected (>250 kDa), suggesting that the CXCR4 protein had extensive post-translational modifications or has aggregated during lysis. A membrane isolation buffer/kit for extracting CXCR4 may have enabled for better isolation of CXCR4. Despite this, the lack of bands present in the untransfected sample and surface expression detected by flow cytometry indicate successful expression of CXCR4.

5.3 – Development of retroviral vectors

Following successfully heterologous expression from the pIRES vectors containing *CXCR4*^{WT} and *CXCR4*^{WHIM}, retroviral vectors were also developed to enable improved transduction of the CXCR4 constructs into differentiating B-cells (figure 5.5). CD2 was present within the viral vector to allow for identification of successful transduction.
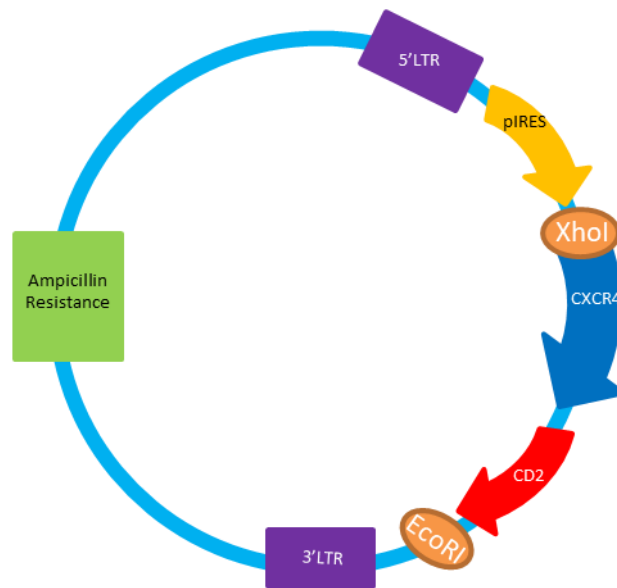
Figure 5.5 – Retroviral MSCV vector map containing CXCR4 insert, antibiotic resistance gene (Ampicillin), CD2 identification and restriction sites XhoI and EcoRI. For retroviral transfection, plasmids contained the same restriction enzymes shown in the pIRES-eGFP vector (figure 5.1) therby allowing insertion of CXCR4 sequence into the MSC vector. A CD2 sequence was also included as a marker for successful transduction, detectable via flow cytometry. Ampicillin resistance was also included for selection.

5.3.1 Restriction digests

Generation of retroviral constructs required the removal of the *CXCR4* inserts from the pIRES vectors and the digestion of the MSCV viral vector (figure 5.6). The gel shows successful removal of *CXCR4* inserts from the pIRES vector. Negative controls are indicated for pIRES and MSCV constructs.
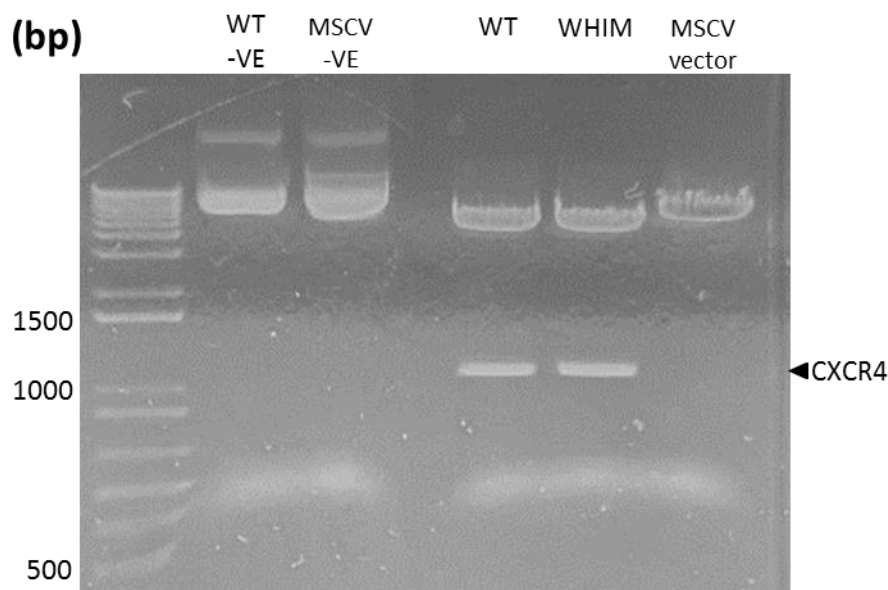
Figure 5.6 – Restriction digest of pIRES-eGFP-CXCR4^{WT} /CXCR4^{WHIM} and MSCV retroviral vector. . pIRES and MSCV constructs were digested with EcoRI and XhoI for 1 hour at 37°C. The digested MSCV was treated with CIP for 20 minutes to prevent re-ligation. WT and WHIM CXCR4 and digested MSCV vector bands were excised and later purified for ligation. Undigested negative controls for pIRES-eGFP CXCR4^{WT} and MSCV viral vector were included.

Following digestion, the *CXCR4* fragments and MSCV vector were gel purified and the isolated DNA were then ligated together. Next, the ligation mixes were transformed into competent NEB C3040 bacteria and grown on ampicillin plates from which 8 colonies from the CXCR4^WHIM and 7 colonies from the CXCR4^WT samples were picked. These colonies were added to LB-AMP broth mixtures and grown at 37°C. Finally, a miniprep was completed. A digest was performed to confirm that the *CXCR4* insert had successfully ligated into the MSCV vector (figure 5.7)
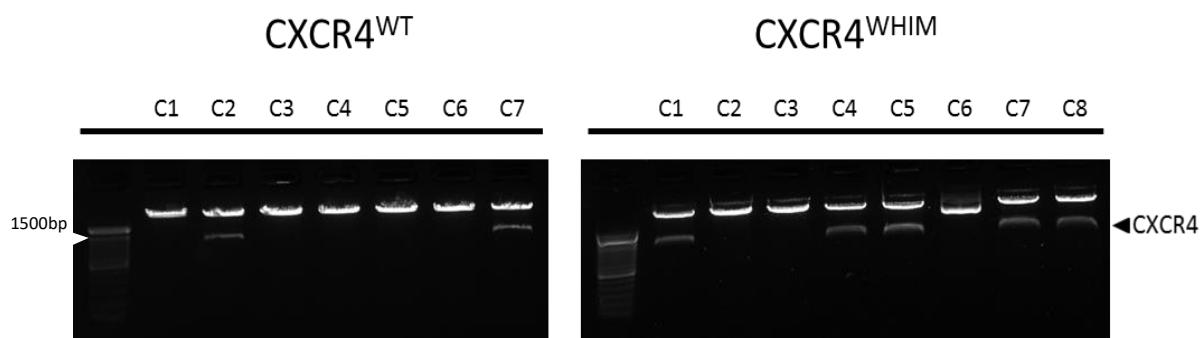
Figure 5.7 – Gel images representing restriction digests confirming presence of *CXCR4* inserts within MSCV vector. MSCV vectors and CXCR4 constructs were ligated together. Following this ligated mixes were transformed into competenet bacteria and colonies were grown. Colnies were picked and grown up in larger cutlrues ans a miniprep was completed. Isolated DNA was digested with XhoI and EcoRI restriction enzymes and mixes wwere run on agarose gels. CXCR4 bands were detected and are indicated, showing successful incorporation of CXCR4 inserts into retroviral vectors.

The DNA gel shows the successful ligation of the *CXCR4* insert and MSCV vector for two CXCR4^WT and five CXCR4^WHIM clones. Selected successful clones were then chosen for amplification of DNA via midiprep and the isolated DNA was utilised for retroviral transduction into HEK293 cells. The virus containing media was then applied to differentiating B-cells. These data confirm the successful acquisition of CXCR4^WT/WHIM retroviral constructs required to transduction of B-cells.

5.4 Transduction of differentiating B-cells

Current data suggests that the presence of the CXCR4^WHIM mutation identifies an adverse risk group and confers a resistance to targeted therapies. WHIM mutated CXCR4 lacks a complete C-terminal tail, preventing receptor internalisation and ligand binding, leading to maintained CXCR4 signalling. So far, key molecular responses downstream of CXCR4 in healthy B-cells and PCs have been defined. Building from this, we can elucidate how these responses are modulated in the presence of CXCR4^WHIM. To

assess the specific impact of CXCR4^{WHIM}, a gain-of-function approach was developed utilising retroviral vectors to transduce differentiating B-cells encoding both WT and WHIM mutated CXCR4.

5.4.1 CD2 expression

At day 2 of the B-cell differentiation, B-cells were inoculated with virus-containing media taken from transduced HEK293 cells. Cells were assessed for CD2 expression throughout the differentiation to confirm uptake of plasmid (figure 5.8).
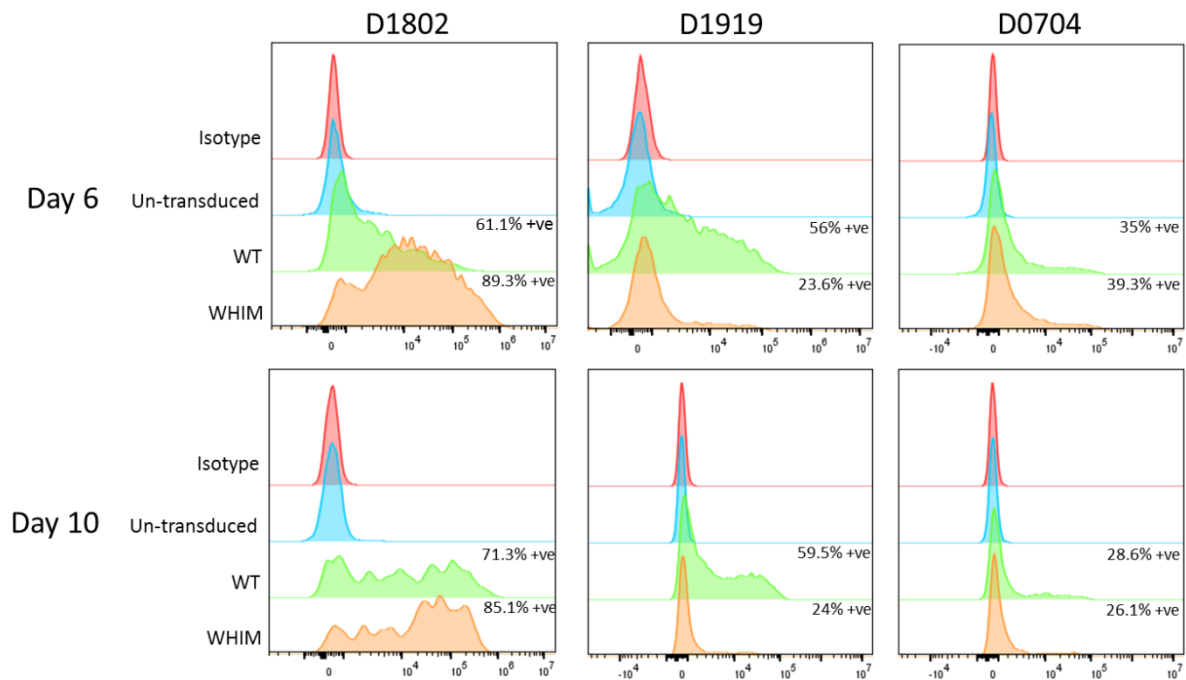
Figure 5.8 – Histograms showing CD2 expression in un-transduced and CXCR4^{WT} and CXCR4^{WHIM} transduced cells. Day 2 B-cells were transduced with CXCR4 constructs via viral media. Cells are then maintained through to day 6 and 13. At both these timepoints, a sample of cells was taken for flow cytometry analysis. Surface expression of CD2 was assessed by flow cytometry and analysed by FlowJo software. Isotype controls included. Anonymised donor sample numbers are shown at the top (N=3).

CD2 expression was variable amongst the three donors. Sample 1802 showed the strongest expression of CD2 at day 6 and a retained high expression by day 10. Transduction of CXCR4^{WT} was strong in sample 1919, with about half of the cells expressing CD2. Expression of CXCR4^{WHIM} is much less, however, and this pattern is repeated at day 10. Finally, sample 0704 shows expression of CD2 in over 30% of cells at day 6 for both constructs, however this decreases to about a quarter of the cell population at day 10.

5.4.2 CXCR4 expression

CXCR4 surface expression was assessed in each sample to determine how CXCR4 protein levels were affected by the transduction. Cells were assessed at day 6 and day 10. CXCR4 expression can be variable in day 6 cells, however, it is usually the peak level of expression throughout the differentiation. Transduction of CXCR4 should increase expression. By day 10 expression drops significantly, often as low as 10% of cells retain CXCR4 by this time point, however there can be some disparity in surface expression even at day 10.

Analysis of the N=1 sample (1802) shows strong upregulation of the CD2 marker (figure 5.8) in both WT and WHIM transduced cells. The CXCR4 flow data (figure 5.9) show, for sample 1802, that in untransduced cells, the base percentage of cells expressing CXCR4 is 44.5%. The CXCR4^{WHIM} cells show an enhanced expression of CXCR4 with 76.5% expression, correlating with the high CD2 expression seen in these cells. The WHIM mutation may have enabled these cells to maintain a much higher CXCR4 expression due to the inability to internalise the protein for degradation. This expression decreases by day 10 but is maintained above the control. The day 6 CXCR4^{WT} expression however is much lower than the untransduced control, despite the majority of this cell population being positive for CD2 expression. This could indicate that either there is a flaw with the WT construct or there is a feedback mechanism controlling CXCR4 expression such as the cells may be degrading CXCR4 to control signal transduction. CXCR4 expression increases in this cell population by day 10 to comparative levels to that seen in the CXCR4^{WHIM} cells.
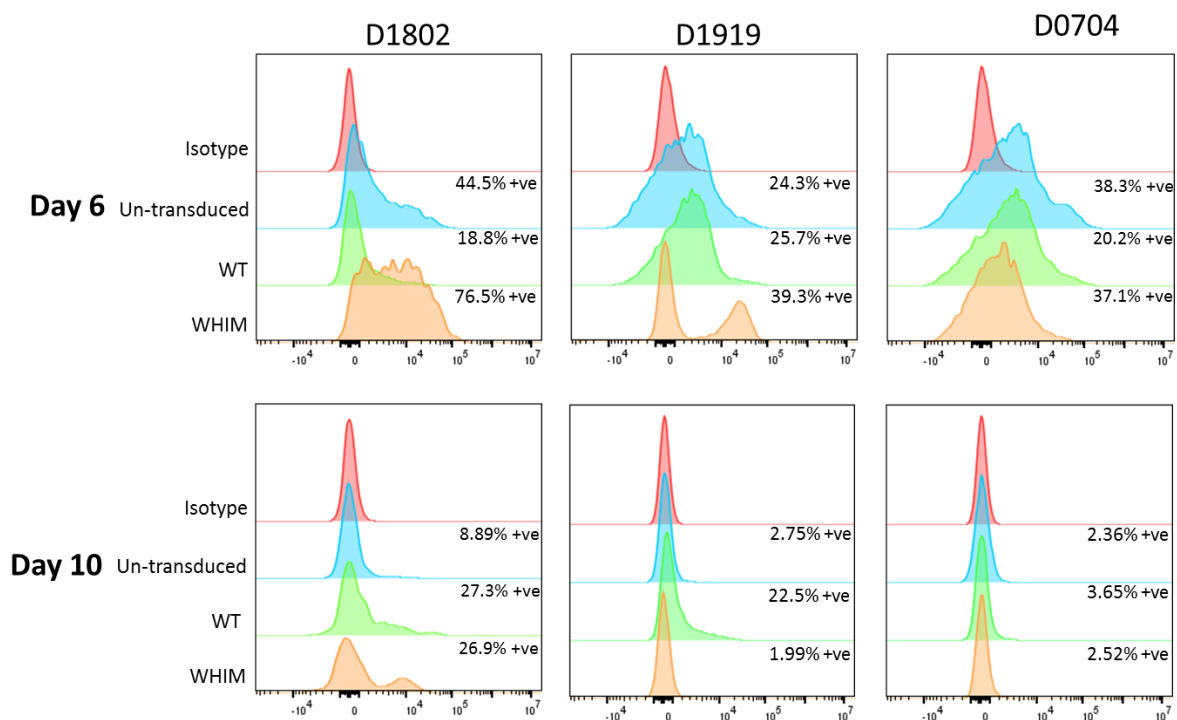
Figure 5.9 - Histograms showing CXCR4 expression in un-transduced and CXCR4^{WT} and CXCR4^{WHIM} transduced cells. Day 2 B-cells were transduced with CXCR4 constructs via viral media. Cells are then maintained through to day 10. At day 6 and 10, samples are taken for flow analysis. Cells were blocked and then stained with a CXCR4 detection antibody. Surface expression of CXCR4 was assessed by flow cytometry and analysed by FlowJo software. Isotype controls included. (N=3).

This could suggest an intrinsic difference in the regulation of CXCR4 in PB and PC populations. Expression of CXCR4 in sample 1919 at day 6 is similar to the control, suggesting only a weak increase in CXCR4 expression, more so in the WHIM transduced cells. By day 10 expression in these WHIM cells has decreased to levels seen in the control, however WT expression is maintained. Together with sample 1802, this affirms some mechanism to maintain CXCR4^{WT} in PCs. CXCR4 in the final sample (N=3, 0704) shows a comparable level of CXCR4 expression between the three conditions. CXCR4^{WT} cells show the lowest expression, suggesting the cells may be degrading CXCR4 protein. The WHIM transduced cells had a moderate level of CD2 expression, but a CXCR4 expression similar to the untransduced cells. While this may be indicative of a failed transduction, instead the transduction may have been successful and CXCR4^{WHIM} expression has simply peaked at 37.1%. By day 10 however, all the cells have very low levels of CXCR4 expression. Whilst D6 and D10 transduced 0704 cells failed to show enhanced CXCR4 expression in comparison to the control, CD2 expression indicates about 25% of these cells have taken up the viral construct, therefore It could indicate that whilst the expression is low, a proportion of this expression could be due to the transduction, rather than natural CXCR4 expression. CXCR4 percentage positivity was quantified and plotted to allow for easier comparison (figure 5.10)
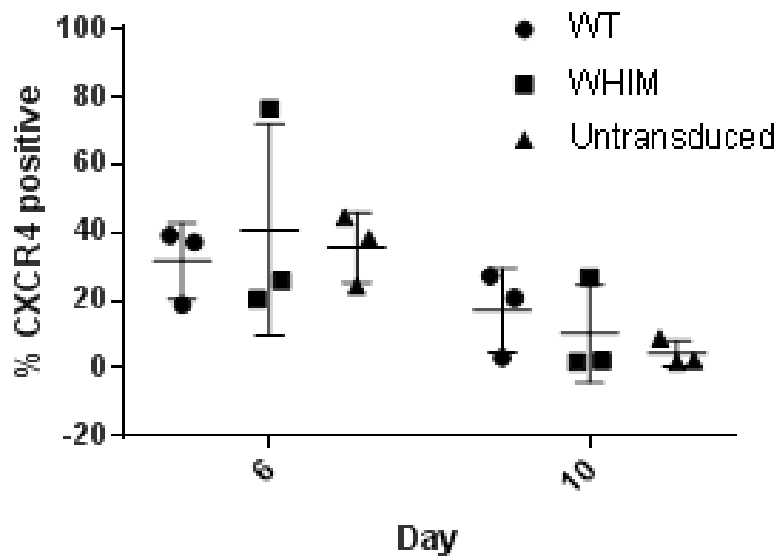
Figure 5.10 – Quantification of CXCR4 surface expression for untransduced, CXCR4^{WT} and CXCR4^{WHIM} ASCs. Day 2 B-cells were transduced with CXCR4 constructs via viral media. Cells are then maintained through to day 10. At day 6 and 10, samples are taken for flow analysis. Cells were blocked and then stained with a CXCR4 detection antibody. Surface expression of CXCR4 was assessed by flow cytometry. Percentage positivity of CXCR4 was plotted for each sample and each condition. N=3

The data confirms that CXCR4 expression was similar for each condition and transduction of CXCR4 was only partially successful. Also, despite high CXCR4 expression in some samples, CXCR4 expression followed the usual pattern of decreasing from day 6.

5.4.3 B-cell and PC phenotype

As previously, B-cells were isolated from PBMCs and cultured with CD40L stromal cells to induce B-cell activation. At day 2, cell media was removed and replaced with viral media before being centrifuged and replaced with fresh media. After confirmation of transduction at day 3, cells were maintained in culture as normal. First, B-cell and PC phenotype was assessed at day 6 and 13 (figure 4.8.1), (4.8.2) and (4.8.3). Work previously done in our lab suggests that WM cells may retain a larger CD19+ PC population than healthy cells and can generate a population of PCs that do not express CD38 (Shrimpton *et al.* 2020)**.** Although these features were not restricted to CXCR4 mutated samples, it was important to understand how the CXCR4^{WHIM} mutation in isolation may affect the phenotype of differentiating B-cells. Figures 5.11, 5.12 and 5.13 show the flow panels for transduced day 6 and day 10 cells for each sample.

Flow analysis indicate a high level of cell death in the transduced samples at day 10, either a by-product of the increased CXCR4 expression, or due to the transduction itself. There is also more cell

debris as seen in the CD19-CD20 panels. Attainment of CD27 and CD38 is comparable between all populations however, CD138 expression may be enhanced in the WHIM samples at day 6.

Phenotypic analysis shows downregulation of CD20 in all conditions for all samples, indicating normal exit from the B-cell programme. Additionally, at day 6, all samples express high levels of CD19, but by 10, all samples show a loss of CD19 expression, again a normal pattern seen in healthy B-cells shifting to a PC phenotype. Donor 1919 cells transduced with CXCR4^{WT} show a lack of CD27 expression at day 6 (figure 4.8.2) which suggests some failure in differentiation, however expression of CD27 is detected by 10, suggesting there is some delay in this condition in maturation, as the untransduced cells have strong expression of CD27 at day 6 (37.5%). The WHIM cells show the opposite, with 68% of day 6 cells showing CD27 expression. From day 6 to day 10, CD38 expression is attained and maintained in all samples under all conditions, again indicating no defects in differentiation to the ASC stage. Donor 1919 CXCR4^{WT} (figure 4.8.2) and donor 1802 CXCR4^{WHIM} (figure 4.8.1) show higher CD138 expression than the untransduced controls at day 6. This could indicate defects in normal differentiation regulation. Donor 1802 (figure 4.8.1) has more cellular debris in the transduced populations, indicating high levels of cell death, compared to the untransduced. To investigate further, percentage positivity for each B-cell/PC marker was quantified and compared for each sample.
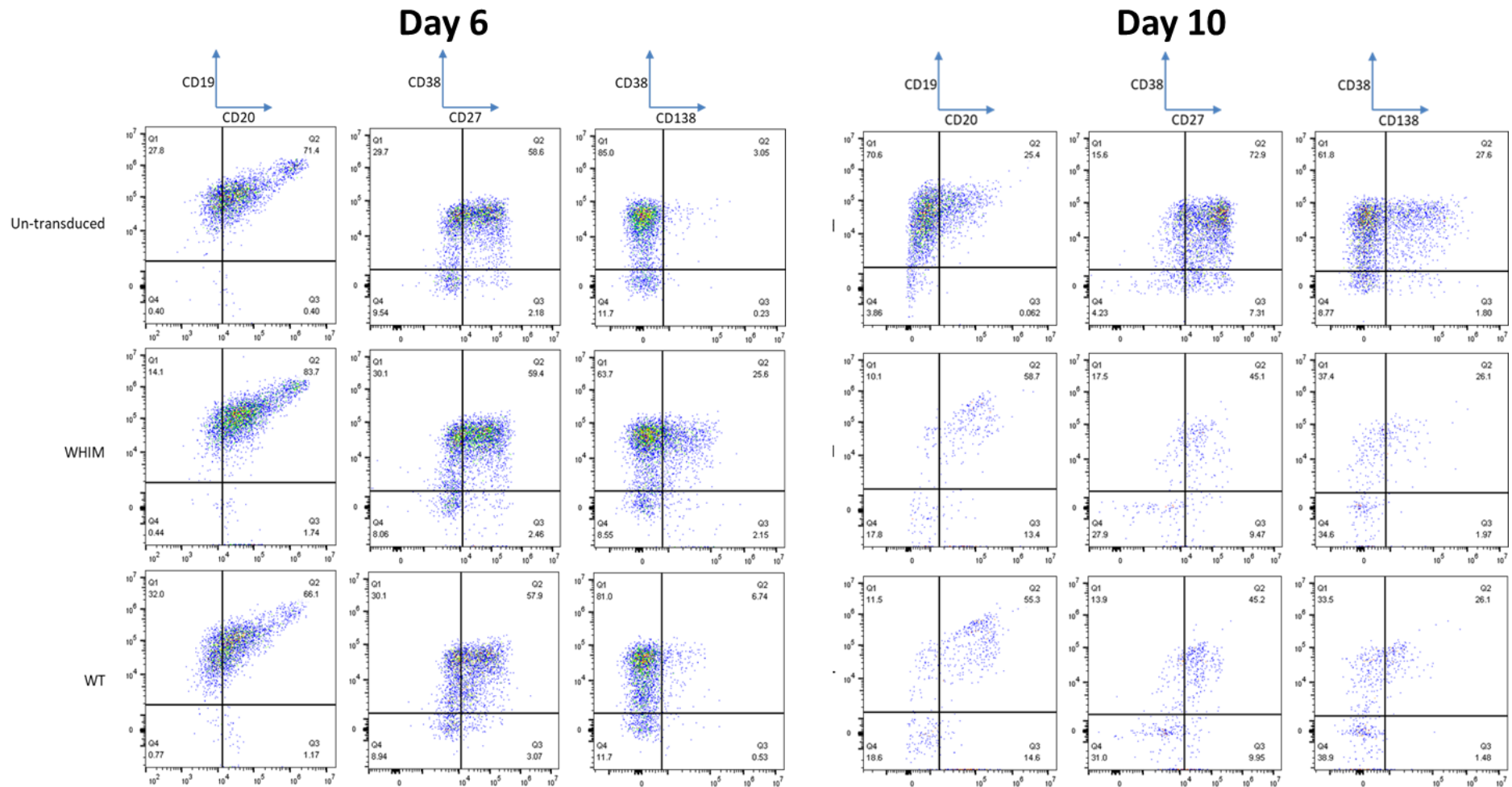
Figure 5.11 – Donor 1802 –Day 6 and 10 B-cell/PC phenotypic surface expression markers (CD19/CD20, CD38/CD27 and CD38/CD138) assessed by flow cytometry. Day 2 B-cells were transduced with CXCR4 constructs via viral media. Cells are then maintained through to day 10. At day 6 and 10, samples are taken for flow analysis. Cells were blocked and then stained with detection antibodies (CD19, CD20, CD27, CD38 and CD138). Surface expression of these markers was assessed by flow cytometry and analysed by FlowJo software.. (N=3, data for Donor 1802 shown).
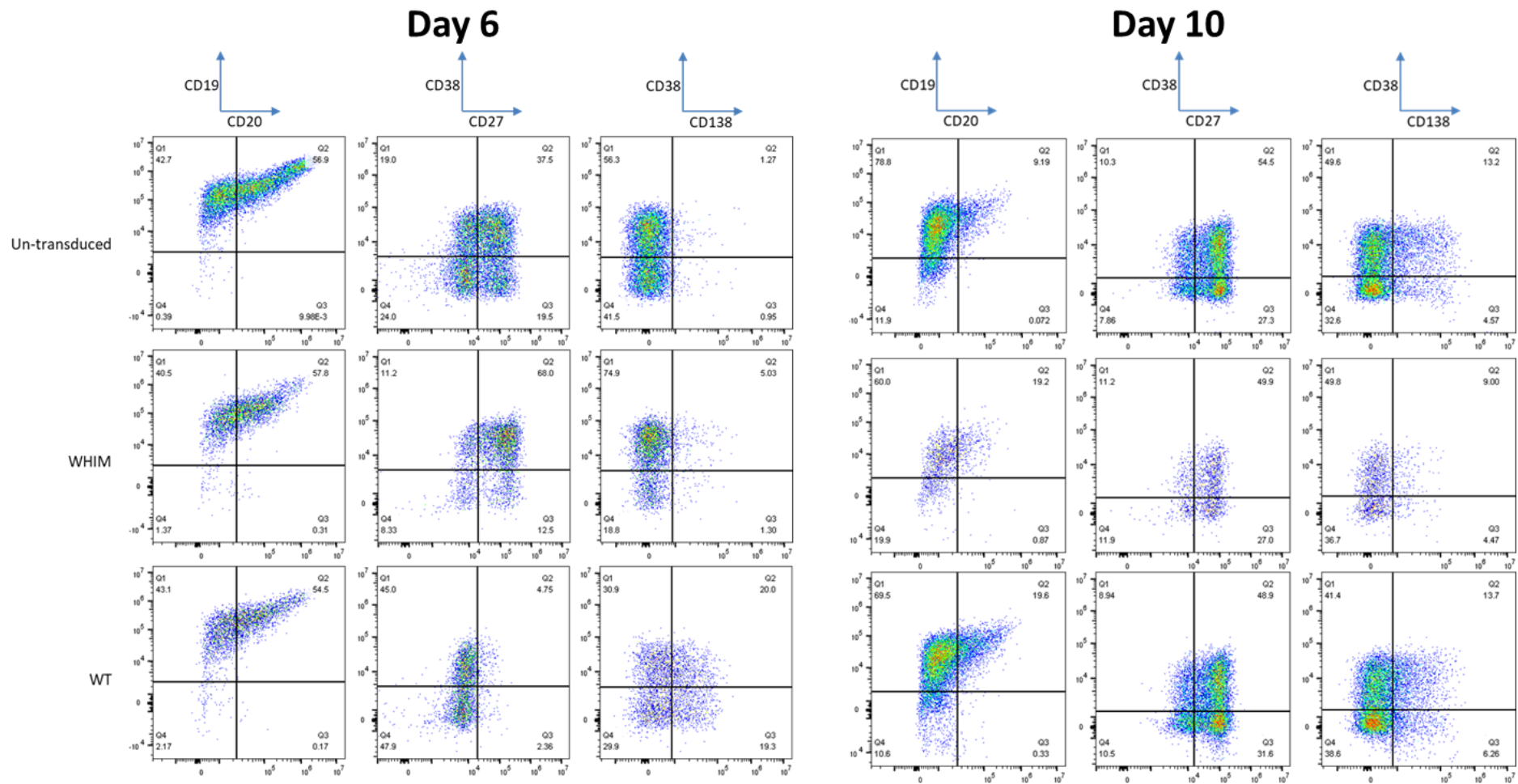
Figure 5.12 – Donor 1919 - Day 6 and 10 B-cell/PC phenotypic surface expression markers (CD19/CD20, CD38/CD27 and CD38/CD138) assessed by flow cytometry. Day 2 B-cells were transduced with CXCR4 constructs via viral media. Cells are then maintained through to day 10. At day 6 and 10, samples are taken for flow analysis. Cells were blocked and then stained with detection antibodies (CD19, CD20, CD27, CD38 and CD138). Surface expression of these markers was assessed by flow cytometry and analysed by FlowJo software.. (N=3, data for Donor 1919 shown).
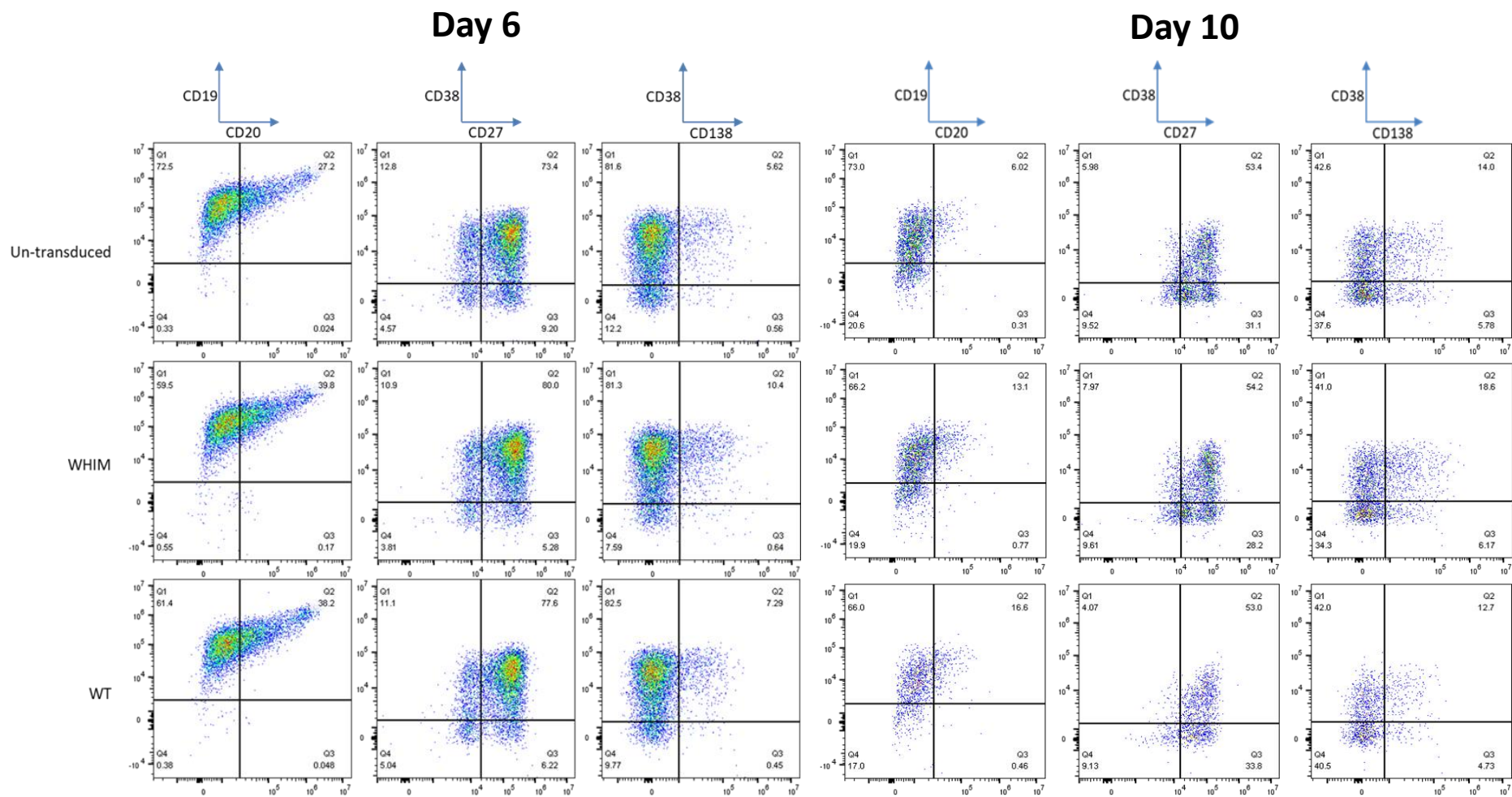
Figure 5.13 - Donor 0704 - Day 6 and 10 B-cell/PC phenotypic surface expression markers (CD19/CD20, CD38/CD27 and CD38/CD138) assessed by flow cytometry. Day 2 B-cells were transduced with CXCR4 constructs via viral media. Cells are then maintained through to day 10. At day 6 and 10, samples are taken for flow analysis. Cells were blocked and then stained with detection antibodies (CD19, CD20, CD27, CD38 and CD138). Surface expression of these markers was assessed by flow cytometry and analysed by FlowJo software.. (N=3, data for Donor 0704 shown).
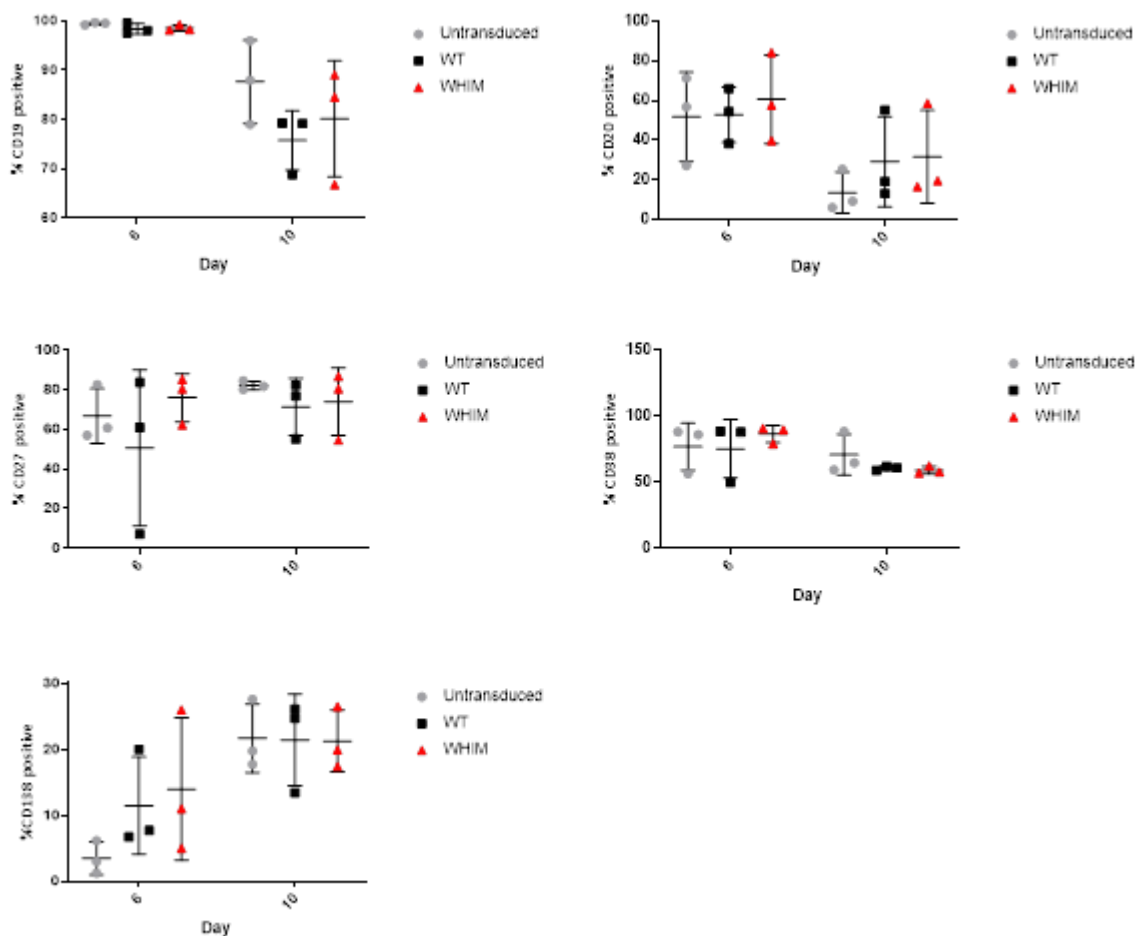
Figure 5.14 – Percentage positivity for each B-cell/PC surface marker for untransduced, CXCR4^{WT} and CXCR4^{WHIM} transduced day 6 and day 10 cells. Day 2 B-cells were transduced with CXCR4 constructs via viral media. Cells are then maintained through to day 10. At day 6 and 10, samples are taken for flow analysis. Cells were blocked and then stained with detection antibodies (CD19, CD20, CD27, CD38 and CD138). Surface expression of these markers was assessed by flow cytometry and analysed by FlowJo software. Percentage positivity for each marker was then plotted using graphpad prism software (N=3).

Inspection of cell phenotype indicates that at day 6 CD19 expression is consistent in all cell populations. Figure 5.14 suggests an enhanced CD19- population in WT and WHIM cells, however analysis of the flow plots for 1802 indicate it may have a greater amount of cell debris due to more cell death. The other samples show a comparable CD19- population. CD20 levels at day 6 are high for all samples, however as the cells transition to the day 10 stage, the transduced samples retain a larger CD20+ population compared to HCs, highlighting a potential link between CXCR4 and CD20 in PBs (Pavlasova *et al.* 2016).

CD38 expression is high at day 6 and this is retained through to day 10. The quantification highlights the intriguing CD138 expression seen in the CXCR4^{WT} transduced 1919 and CXCR4^{WHIM} transduced 1802 samples at day 6. CD138 expression is lowest in the untransduced cells, with sample 1802 CXCR4^{WHIM}

showing early acquisition of CD138 at day 6, this expression is retained through to day 10, and potentially suggesting strong expression of CXCR4^{WHIM} may enhance CD138 attainment in PBs. By day 10, CD138 expression is comparable in all cell populations.

CD27 expression is similar at day 6 for all samples, except for Sample 1919 CXCR4^{WT} where there is an almost complete loss of CD27 expression, which is recovered by day 10 to normal levels. CXCR4 expression was high as normal as was CD2 expression, however other samples did not manifest this phenotype. This sample did however express a higher level of CD138 at day 6 in both the CD38+ and CD38- samples. Furthermore at day 10, this sample had a much reduced CD138 expression compared to the untransduced sample, showing a loss of PC phenotype. These early PCs may have died quickly due to the presence of CXCR4^{WT} whereas sample the CXCR4^{WHIM} early CD138+ cells survived better.
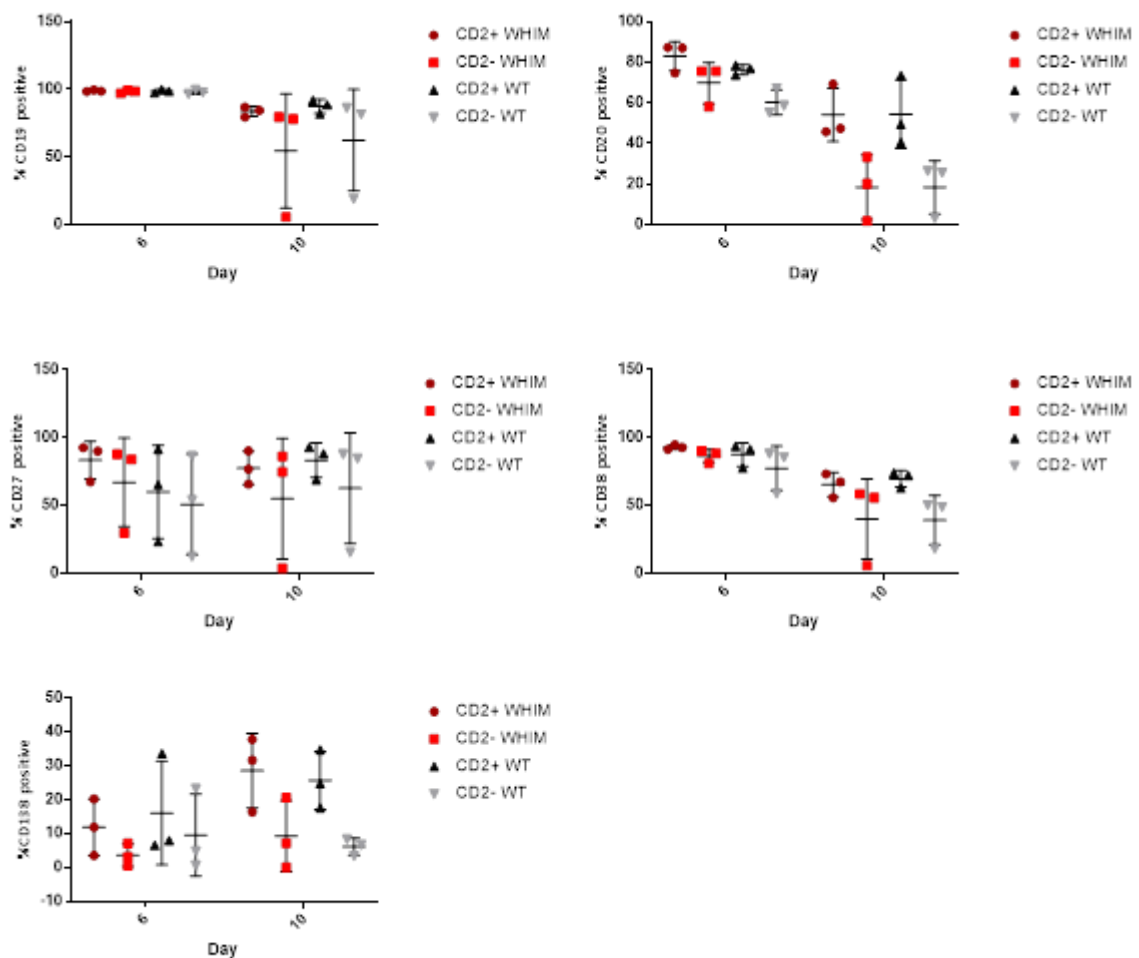
Figure 5.15 - Percentage positivity for each B-cell/PC surface marker for CD2+ and CD2- transduced day 6 and day 10 cells. Day 2 B-cells were transduced with CXCR4 constructs via viral media. Cells are then maintained through to day 10. At day 6 and 10, samples are taken for flow analysis. Cells were blocked and then stained with a detection antibodies (CD2, CD19, CD20, CD27, CD38 and CD138). Surface expression of these markers was assessed by flow cytometry and analysed by FlowJo software. Surface expression was assessed in either CD2 positive or CD2 negative cells to assess the impact of CXCR4 WT or WHIM expression on the phenotype of the ASCs. (N=3).

To further understand how the introduction of the CXCR4 mutation affected cell phenotype, cells were gated based on CD2 expression and surface expression was compared between the populations (figure 5.15).

Analysis of the CD2 positive and CD2 negative populations highlights the greater depletion of CD20 in CD2+ cells, confirming the potential link between CD20 and CXCR4. Additionally, CD138 expression is similar at day 6 however, it is generally greater for the CD2+ cells by day 10. This indicates an enhanced ability of CXCR4^{WHIM} cells to attain a PC phenotype. The potential functions of earlier and more intense CD138 expression may relate to some survival advantage (Teng, Aquino and Park 2012).

5.4.4 Viability counts

Additionally, cell viability was assessed throughout the differentiation. Introduction of the CXCR4 constructs may have variable effects on cell survival, namely due to high viral titres, production of toxic by-products or over-expression of CXCR4 itself may have detrimental effects on cell survival. Indeed based on the flow data, there were more viable cells generally in the untransduced cells (Figure 5.16)
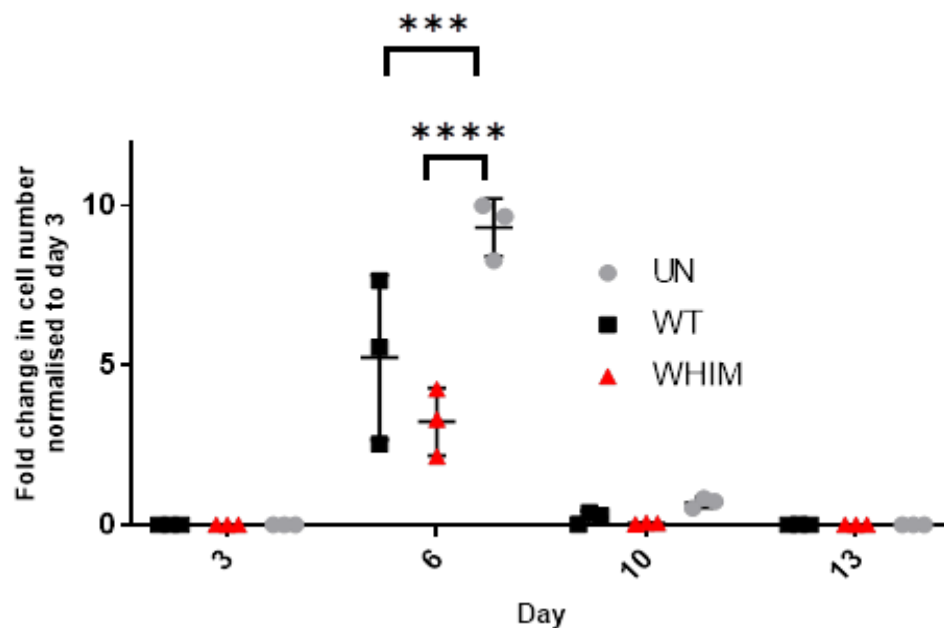
Figure 5.16-fold change in cell counts of CXCR4^{WT} and CXCR4^{WHIM} transduced cells and untransduced controls normalised to day 3 count. Day 2 B-cells were transduced with CXCR4 constructs via viral media. Cells are then maintained through to day 13. At day 3, 6, 10 and 13 cell counts done using a haemocytometer and trypan blue was used to exclude dead cells. Cell number was then normalised to the day 3 count. N=3. Statistical significance was determined using a Tukey's multiple comparisons test. (* = p<0.05; **=p<0.01, ***=P<0.001, ****=p<0.0001).

The cell counts confirm that the untransduced cells fared much better than the transduced cells from day through to day 10. The WT transduced cells showed the most variability in viability with some samples reaching similar levels of proliferation seen in the untransduced samples. WHIM mutated

samples had the worst proliferation on average. By day 10, untransduced cells maintained a slightly higher cell count, whereas both transduced cell types showed a stronger collapse in cell viability. By day 13, all WHIM mutated samples showed no viable cells remained. Only one WT and one untransduced sample made it to day 13, with similar counts of viable cells.

5.5 Signal transduction events in transduced B-cells and PBs

The CXCR4 surface expression data indicate that there was limited success in CXCR4 transduction, however CD2 expression was more successful indicating there are some transduced cells as part of the total population. Therefore, stimulations were conducted to assess signal transduction in these cells. Ideally, the transduced cells would be isolated for assessment, but this initial experiment was carried out on the bulk population. Samples of the day 6 transduced cells were collected, and serum starved as previously. By day 10, all samples had too great a reduction in cell viability that not enough cells could be used for stimulation. Therefore, analysis on signal transduction has been limited to day 6 PBs (figure 5.17).
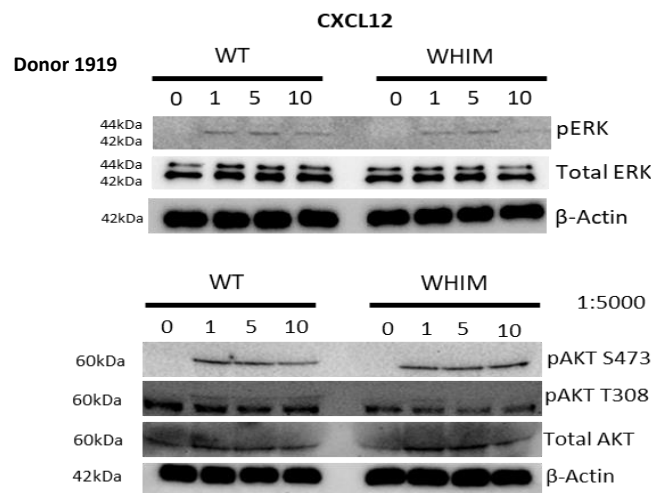
Figure 5.17 – Representative Western blots showing phosphorylation of ERK and AKT at S473 and T308 residues in response to CXCL12 stimulation. Day 2 B-cells were transduced with CXCR4 constructs via viral media. Cells are then maintained through to day 6. Analysis of D1919 day 6 cells cultured in APRIL conditions, serum starved and stimulated with CXCL12. A pre-stimulatory sample was taken before addition of CXCL12. Cells were added to sample buffer and run on a gel before being transferred to a blotting membrane and probed for phospho-ERK and phospho-AKT S473/T308. Total protein was also detected. Actin was assessed as a loading control. The analysis was performed on N=3 transduced sets of samples.

CXCL12 stimulation induces detectable phosphorylation in day 6 cells. Based on the flow data, 56% of the CXCR4^{WT} and 23.6% of the CXCR4^{WHIM} cells from this sample show CD2 expression. ERK activation in both WT and WHIM cells appears moderate and similar to that seen in HC at day 6 (figure 3.14). WT and WHIM cells show similar levels of ERK phosphorylation, and Actin detection shows comparable loading. Bearing in mind the limitations of this experiment, together this indicates that CXCR4^{WHIM} does not notably amplify ERK signalling compared to CXCR4^{WT}.

Assessment of the AKT signalling patterns shows that AKT phosphorylation at the T308 residue could be detected in both CXCR4^{WT} and CXCR4^{WHIM} cells, however the bands are faint. WT cells may show a prolonged signalling compared to WHIM mutated cells. Phosphorylation at the S473 shows bands from 1 minute after stimulation, through to 10 minutes after stimulation. Compared to HC's, the
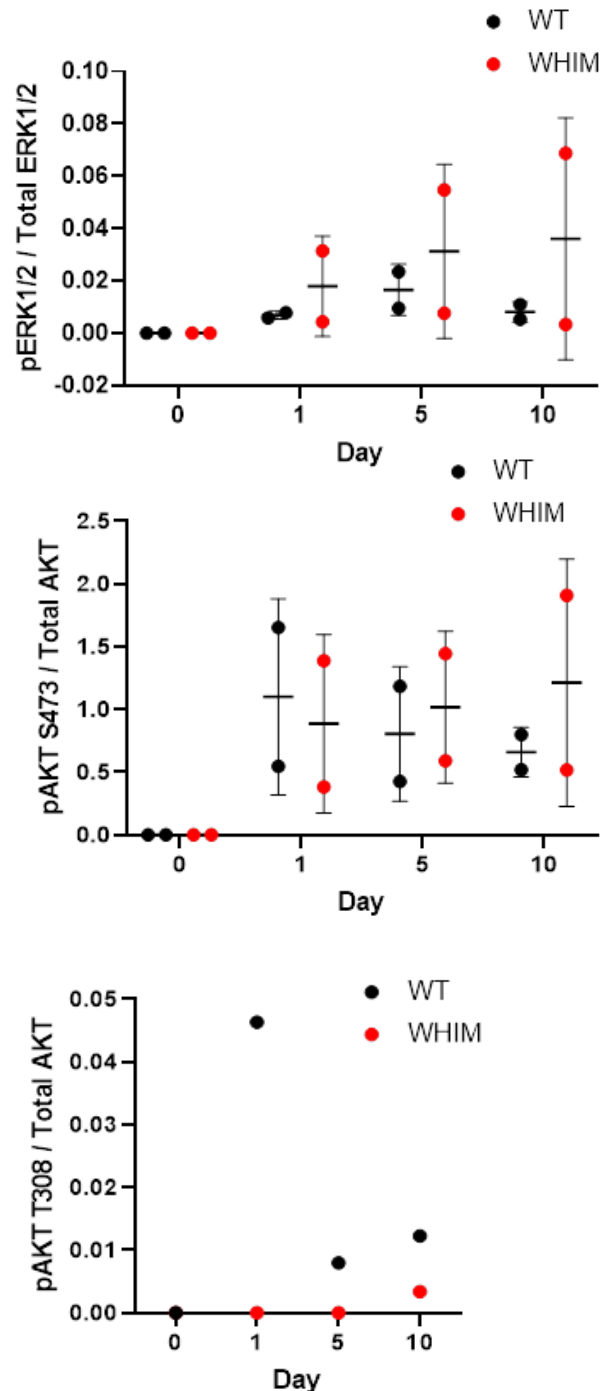
Figure 5.18 – Densitometry of phosphorylation events of CXCR4^{WT} and CXCR4^{WHIM} transduced day 6 cells stimulated with CXCL12. Day 2 B-cells were transduced with CXCR4 constructs via viral media. Cells are then maintained through to day 6. Analysis of D1919 day 6 cells cultured in APRIL conditions, serum starved and stimulated with CXCL12. A pre-stimulatory sample was taken before addition of CXCL12. Cells were added to sample buffer and run on a gel before being transferred to a blotting membrane and probed for phospho-ERK and phospho-AKT S473/T308 and total ERK/AKT protein. Western bands were quantified using Image Lab software (N=2).

phosphorylation seems comparable (figure 3.16). The Western blot data was quantified to confirm the signalling patterns between WT and WHIM cells (figure 5.18).

Quantification of the Western data show ERK phosphorylation is comparable between WT and WHIM mutated cells. WHIM mutated cells however have a slightly stronger average phosphorylation. These differences are however not statistically significant. Phosphorylation of AKT at the S473 residue is similar for both conditions with some activation beginning one minute after stimulation, which is generally maintained through to 10 minutes post stimulation. Phosphorylation of AKT at the T308 residue is very weak for both conditions. Activity is maintained until 10 minutes post stimulation; however, it is a very low level of detection.

To determine how signalling in the transduced cells compares to HC, densitometry was performed from the Western blots, and plotted against the densitometry values taken for the HCs (figure 5.19). Comparison of the HCs and transduced cells shows that overall, the HCs generated a much stronger phosphorylation response for all phosphorylation targets. To generate a detectable pAKT signal in the transduced cells, the pAKT S473 and T308 antibody was diluted to 1:5000 rather than 1:1000, due to excessive background and the presence of white bands suggesting the antibody concentration was too high. This may have contributed to the poor detection. Alternatively, the transduction may have impaired cell survival during the overnight serum starvation, reducing the number of cells capable of responding to CXCL12.

The pERK signal in the WHIM cells is maintained to a higher degree at 10 minutes compared to HCs. The HC signal drops after 5 minutes whereas the WHIM signal is maintained relative to the overall signal strength, indicating signalling may be prolonged compared to HCs. This effect is also seen in the pAKT S473 signal pattern for both WT and WHIM transduced B-cells/PBs. The pAKT T308 signal does follow a similar pattern in all cell types, suggesting there is no prolongation of the signalling at this residue.
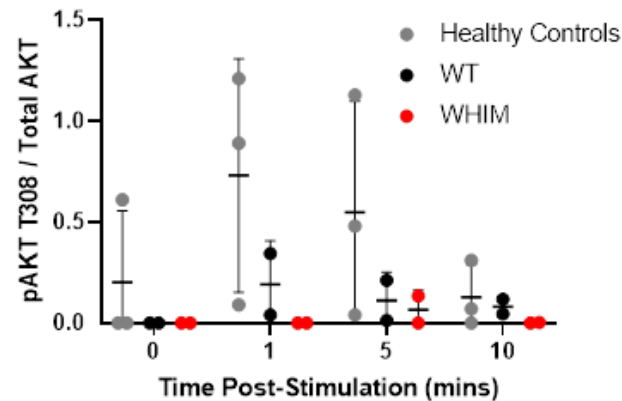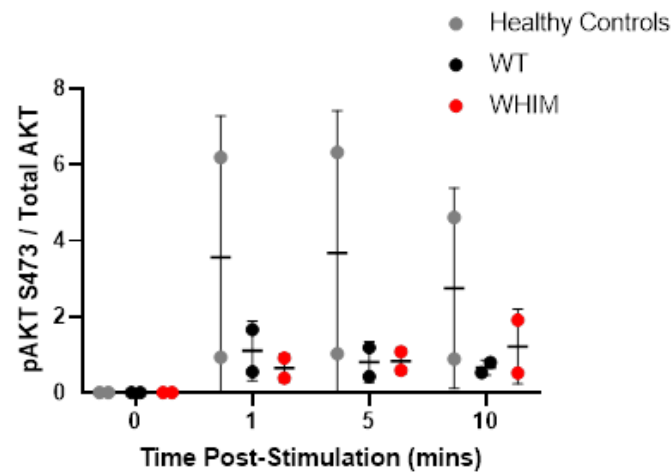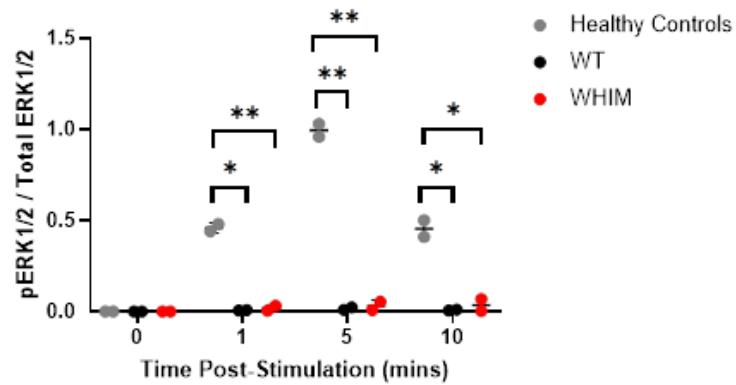
Figure 5.19 – Comparisons of phosphorylation events of CXCR4^{WT} and CXCR4^{WHIM} transduced day 6 cells and healthy controls stimulated with CXCL12. Day 2 B-cells were transduced with CXCR4 constructs via viral media. Cells are then maintained through to day 6. Analysis of D1919 day 6 cells cultured in APRIL conditions, serum starved and stimulated with CXCL12. A pre-stimulatory sample was taken before addition of CXCL12. Cells were added to sample buffer and run on a gel before being transferred to a blotting membrane and probed for phospho-ERK and phospho-AKT S473/T308 and total ERK/AKT protein. Western bands were quantified using Image Lab software. Densitometry calculated using Image Lab software. Calculated values were compared to densitometry values of healthy cells stimulated with CXCL12 (HC N=3, WT/WHIM N=2). Statistical analysis was performed using a student multiple T-tests, Only significant results are indicated. (* = $p<0.05$; **=$p<0.01$.)

5.6 Signalling in transduced cells stimulated with CXCL12 and αCD19

In addition to the signalling responses to CXCL12, the response to co-stimulation of CXCL12 and αCD19 stimulating beads was also assessed. WM cells have shown to retain a larger CD19+ population into PC stage, suggesting a role in WM PC function. Combined with the role of CD19 as a signalling hub, this could indicate CD19 stimulation may have further effects in WM cells expressing the CXCR4^{WHIM} mutation. Initially, transduced cells were collected at day 6 and the phosphorylation pattern at ERK and AKT was established (figure 5.20).
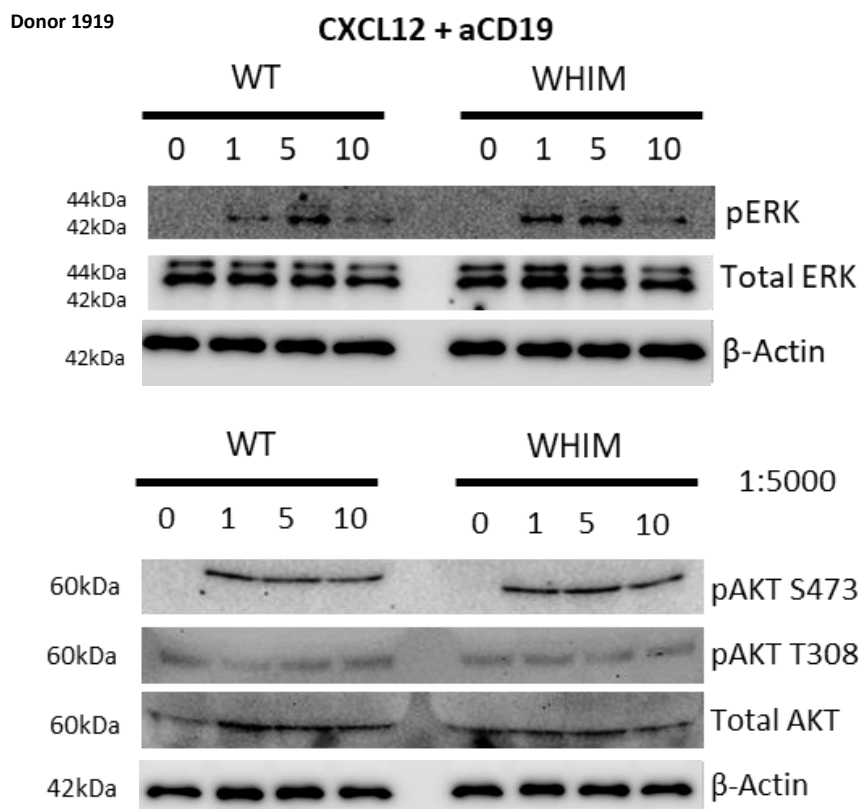
Figure 5.20 - Representative Western blots showing phosphorylation of ERK and AKT at S473 and T308 residues in response to CXCL12 and αCD19 stimulating beads. Analysis of Donor 1919 transduced day 6 cells cultured in APRIL conditions, serum starved and stimulated with CXCL12 and αCD19. A pre-stimulatory sample was taken before addition of stimulants. Cells were added to sample buffer and run on a gel before being transferred to a blotting membrane and probed for phospho-ERK and phospho-AKT S473/T308. Total protein was also detected. Actin was assessed as a loading control. (N=3).

Comparing WT and WHIM ERK phosphorylation, the blots indicate a similar response to dual stimulation, but WHIM mutated cells seem to generate stronger signalling earlier at 1 minute with
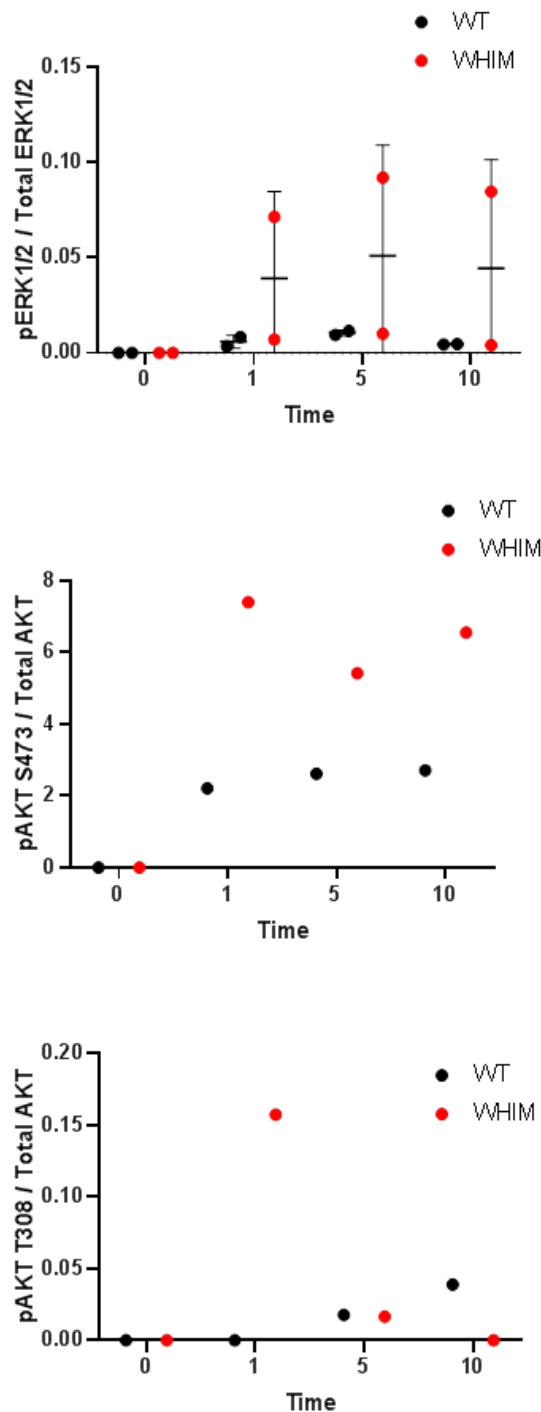
Figure 5.21– Densitometry of Western blot analysis of CXCR4^WT and CXCR4^WHIM transduced day 6 plasmablasts signalling in response to CXCL12 and αCD19 beads. Transduced day 6 cells cultured in APRIL conditions, serum starved and stimulated with CXCL12 and αCD19. A pre-stimulatory sample was taken before addition of stimulants. Cells were added to sample buffer and run on a gel before being transferred to a blotting membrane and probed for phospho-ERK and phospho-AKT S473/T308. Total protein was also detected. Image Lab software was used to quantify the Western blot bands of transduced cells stimulated with CXCL12 and αCD19 beads. Ratio of phosphorylated ERK, AKT S473 and AKT T308 to total protein was quantified. (N=2)

peak phosphorylation occurring at 1 and 5 minutes, suggesting there is a stronger phosphorylation pattern for longer. WT cells which have a weaker activation 1 minute after stimulation and only reach peak phosphorylation 5 minutes after stimulation. Loading between the two cells is comparable

indicating that this pattern is genuine, suggesting that the WHIM mutated cells may generate a stronger signal.

AKT phosphorylation at S473 is comparable between CXCR4^{WT} and CXCR4^{WHIM} with both cell populations generating a moderate response to stimulus that is maintained up to 10 minutes after stimulation. AKT phosphorylation at the T308 residue could be detected, however, the bands are incredibly faint at 1 and 5 minutes, potentially indicating these transduced cells are less able to signal through this residue, whereas HCs are capable of doing so. There are strong white bands (background) above the AKT T308 bands that obscure the bands of interest. The bands detected were then quantified as previously (figure 5.21).

Analysis of the ERK data indicate some variation between the WT and WHIM transduced cells. One sample of the WHIM mutated cells generates an ERK response that is comparable to the WT transduced cells for one sample, whereas another sample shows much greater signalling through ERK in response to co-stimulation. The most responsive sample had a greater CD2 expression, indicating a more successful induction, so that by day 6 this cell was expressing a larger proportion WHIM mutated CXCR4. This could explain the dichotomy in the responses of the two samples. In any case, successful transduction of CXCR4^{WHIM} looks to generate a stronger ERK signal in response to CXCR4 and CD19 co-ligation. Additionally, AKT signalling through the S473 residue was stronger in WHIM transduced cells. Peak activation is detected at 1 minute in the WHIM cells and 5 minutes in WT cells, suggesting activation of this pathway occurs faster in WHIM cells. Additionally, the phosphorylation signal remains maintained at a higher level 10 minutes post stimulation. This could indicate that the WHIM cells can maintain a CXCR4 signal for a longer period of time. The AKT T308 signalling pattern is also stronger in WHIM transduced cells. Signalling however is almost diminished by T=10, suggesting that the WHIM mutation does not support extended signalling at this residue. Additional repeats would be required to validate these results and would be improved by selective evaluation of transduced cells.

Next the signalling response to both CXCL12 and CXCL12 with αCD19 in transduced cells was compared (figure 5.22). The ERK signalling response indicates a clear enhancement of phosphorylation strength in WHIM mutated cells compared to WT. As shown previously, the phosphorylation pattern is similar between WT stimulated with CXCL12 and CXCL12 + αCD19. Dual stimulated WHIM mutated cells generate a slightly stronger response than CXCL12 stimulated WHIM mutated cells but are generally comparable. This suggests that addition of αCD19 has a minimal effect on the generation of an ERK signal in PBs.

The phosphorylation of AKT S473 is comparable between WT and WHIM cells stimulated with only CXCL12, however WHIM cells may generate a prolonged signal compared with WT transduced cells.

The dual stimulated cells however show a much stronger signalling response. CXCR4^{WT} cells stimulated with both CXCL12 and αCD19 show a stronger signalling response to CXC12 stimulated cells and the signal peaks 10 minutes after stimulation, indicating a prolonged signal. Finally, the dual stimulated CXCR4^{WHIM} cells generate a very strong AKT signalling pattern. This could suggest that in WHIM mutated cells, activation of CD19 promotes enhanced signalling that may induce enhanced survival signalling. Whilst long term CD19 stimulation did not confer a survival advantage in healthy cells, (figure 5.16), CD19 activation in WHIM mutated cells could promote improved survival signalling.

Signalling through AKT T308 is strongest in CXCR4^{WT} cells stimulated with CXCL12 only. There is notable variation between the samples, however they both follow the same pattern if peak activation at 1 minute after stimulation. WT cells that are dual stimulated only generate a weak phosphorylation. The signalling pattern is however does not peak until 10 minutes after stimulation.
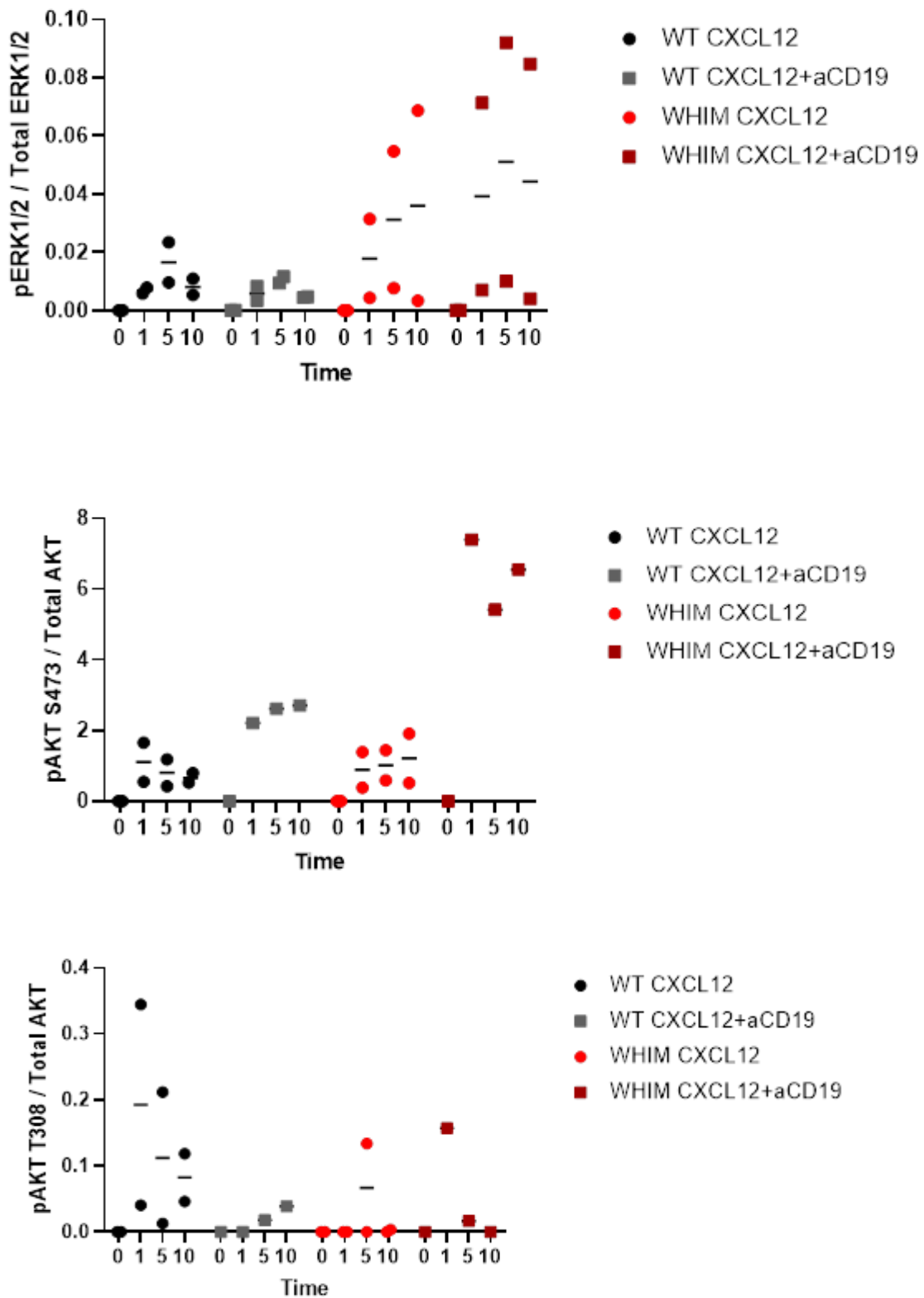
Figure 5.22 - Densitometry of Western blot analysis of CXCR4^{WT} and CXCR4^{WHIM} transduced day 6 plasmablasts signalling in response to CXCL12 or CXCL12 with αCD19 beads. A comparison of the densitometry values for ERK and AKT signalling in CXCR4 WT or WHIM transduced cells stimulated with either CXCL12 or CXCL12 with αCD19 stimulating beads was conducted. Image Lab software was used to quantify the Western blot bands of stimulated transduced cells Ratio of phosphorylated ERK, AKT S473 and AKT T308 to total protein was quantified.

In WHIM cells the signalling pattern is comparable between both conditions, however signalling peaks earlier in dual stimulated cells. There is no clear pattern of AKT phosphorylation at T308, therefore additional repeats will be necessary to elucidate the signalling pattern here.

5.7 Discussion

Key molecular responses downstream of CXCR4 in healthy ASCs have been defined. From this we can determine how these events are changed in the presence of CXCR4^{WHIM}. To assess the specific impact of CXCR4^{WHIM}, an approach was developed utilising retroviral vectors to transduce differentiating B-cells with vectors encoding both WT and WHIM mutated CXCR4.

Retroviral expression vectors were developed from mammalian expression vectors as initially, nucleofection was the original method to be used to develop CXCR4^{WHIM} expressing B-cells and PCs. However retroviral transfection was chosen instead due to the enhanced uptake of the viral vector seen in our group previously. CD2 expression was an efficient method of assessing vector uptake. There was some variability in the level of CD2 expression between the transduced samples, indicating some transductions were more successful than others. Due to this, further repeats will be required to build a better model of WHIM signalling.

Initial investigation of the B-cell/PC phenotypes of these transduced cells indicate a generally normal acquisition of a PB/PC phenotype by day 10. However, the more efficiently transduced sample, showed a somewhat lower level of CD19 expression at day 10, which is in conflict with the suggestion that WM may retain a higher CD19+ population.

CD27 expression is comparable across all cell populations, except for the exceptional loss in sample CXCR4^{WT} transduced sample 1919 at day 6. This pattern is not apparent in any other population/sample and CD2 expression is similar to other samples. The loss of CD27 in this sample may relate to the unusual CD38/CD138 expression pattern, where there is a similar sized population of CD38+CD138+ and CD38-CD138+ population. Low CD27 would normal be indicative of a reduced ability to reach the PC stage.

CD138 acquisition was detected by day 6, far earlier than expected, in a subset of day 6 cells transduced with CXCR4 (both WT and WHIM). Earlier acquisition of a PC phenotype may confer some survival enhancements, as seen by greater ERK and AKT signalling, however, this was not reflected in the viability measurements, where transduced cells experienced low peak cell count at day 6 compared to untransduced controls. This however may be due to effects of the actual transduction.

Of note, a subset of the transduced cells, both WT and WHIM mutated showed a retention of CD20 expression by day 10. Healthy B-cells downregulate CD20 as they transition to the PC programme.

Indeed CXCR4/CXCL12 signalling does play a role in the regulation of CD20 surface expression, as shown by the increase in CD20 expression in response the CXCL12 (Pavlasova *et al.* 2016). Additionally, enhanced levels of CD20 have been detected in WM cells. Together this could indicate a disease role for CD20, mediated in part by CXCR4 signalling.

Indeed, CLL cells within the BM are CXCR4^{dim} and express high levels of CD20. There is evidence showing CXCL12 can upregulate CD20 expression on chronic lymphocytic leukaemia (CLL) B-cells. However, here we see PBs overexpressing CXCR4 upregulate CD20, therefore perhaps expression of CXCR4 upregulates CD20 expression. This may be related to the propensity of WM to be retained within BM, thereby contributing to WM characteristics (Kriangkum *et al.* 2004; Pavlasova *et al.* 2018).

The apparent increased expression of CD138 in transduced PBs and PCs may relate to an increased ability to reside within the bone marrow. CD138 is important for cell-matrix interactions and therefore, increased CD138 expression in these cell populations may allow for improved survival with BM, and possibly relate to the ability of WM B-cells to undergo all their differentiation in the BM. Indeed, there is evidence that high CD138 expression is associated with the MYD88 mutation, and therefore, enhanced CXCR4 expression may contribute to this relationship (Kyrtsonis *et al.* 2011; Gayet *et al.* 2022; Teng, Aquino and Park 2012).

Only two of the transduced samples indicated a significant increase in CXCR4 surface expression compared to the untransduced controls. This effect was most notable in sample 0704 at day 6, however by day 10 there was still more CXCR4 detected compared to the controls. Despite the enhanced levels of CXCR4 detection at day 6, AKT and ERK phosphorylation events were minimal in comparison to healthy controls. However, relative to the peak ERK and AKT S473 phosphorylation, the drop in activity seemed reduced in the transduced cells, suggesting a prolonged level of signalling in these cells.

Indeed, WHIM transduced lymphoblastoid cells show a greater and more prolonged calcium flux in response to CXCL12 (Hernandez *et al.* 2003). Furthermore, the WHIM mutation generates an enhanced chemotactic response to CXCL12 and again maintained for longer, compared to healthy donor cells (Liu *et al.* 2012). The data obtained here may not show a stronger signalling response in WHIM mutated cells, but it does corroborate with the literature, showing a prolongation of activity in response to CXCL12.

The paucity of cells from the transduced samples prevented the analysis of phosphorylation events beyond day 6 of the differentiation. Whether this was due to the effects of the transduction itself or because of the overexpression of CXCR4 is not clear. Time constraints prevented further optimisation

of the transduction protocol and downstream studies, notably the signalling experiments and that selection of transduced cells was not completed. Therefore, further investigation of the effects of the CXCR4 WHIM mutation on PC function will require follow up investigation (Biajoux *et al.* 2016)

These results suggest that the gain of CXCR4 function may not modify signalling through the BCR per se but may enhance signalling through a pathway shared by both CXRC4 and the BCR converging on AKT. As seen in chapter 4, loss of CD19 affects signalling through both ERK and AKT in response to CXCL12, however healthy cells have a similar AKT response to both CXCL12 and CXCL12/αCD19 stimulation. The ERK response in PB is stronger in co-stimulated cells compared to CXCL12 stimulation alone. Together this may indicate a preference of CXCR4 mediated ERK signalling in PBs. Expression of CXCR4^{WHIM} will allow for further understanding of the signalling dynamics in these cell populations through CXCR4 and the relationship between overexpressed CXCR4 and CD19.

As previously, PBs were stimulated with CXCL12 and αCD19 bound to beads. Stronger ERK signal in co-stimulated transduced cells seems linked to level of CD2 expression and therefore CXCR4^{WHIM} expression, providing reasonable evidence that in PBs, the WHIM mutation may induce a stronger ERK phosphorylation compared to CXCR4^{WT}. Additionally there is evidence indicating an enhanced ERK signal in WHIM transduced cells. However, additional repeats are required to confirm these results. Comparing WT and WHIM CXCR4 cells treated with either CXCL12 or CXCL12 with αCD19 indicates, firstly that stimulation by either induces a similar response in WT cells and secondly that co-stimulated WHIM mutated cells generated the strongest ERK and AKT (S473) phosphorylation response. Together these results suggest that WHIM mutated PBs are especially responsive to CD19 activation, possess a larger CD19+ population at day 10 and utilise a unique and enhanced signalling pattern. Despite this there were no detectable functional effects determined through the analysis performed here. Additionally, effects on viability were likely clouded by the stresses induced by the transduction itself. Furthermore, assessment of this mutation outside of the WM context is unlikely to mirror what happens without the presence of the associated MYD88 mutations or BM niche conditions.

Further assessment would require repeats of the conditions and simulations performed here, followed by inclusion of BM factors. As WM differentiation occurs primarily within the BM, the cells are exposed to a specific set of stimulating factors secreted from a variety of support cells (Chu and Berek 2013). Therefore, it is crucial for the impact of CXCR4 signalling in the context of the WHIM mutation to be investigated in a BM niche setting. Factors to assess alone or in combination include CXCL12, TGFβ, macrophage inhibitory factor (MIF), anti-CD44 and the reintroduction of CD40L.

Data from our group has indicated that stimulation of PBs with CXCL12 and TGFβ can modulate ERK signalling and enhance survival (Stephenson *et al.* 2019). Here we show that CXCL12 and CD19

stimulation also enhances ERK signalling, however there were no detectable improvements to survival. Therefore, inclusion of TGFβ may introduce measurable improvement in cell viability. It is expected that this effect would likely be repeated in PCs.

CXCR4 can interact with the membrane receptor CD44, which can mediate improved myeloma PC growth/survival through adhesion interactions. CD44 forms a membrane receptor complex with CD74 which can promote PC survival. Additionally, this complex is a receptor for MIF, produced from perivascular dendritic cells in the bone marrow has been shown to play a role in mature B-cell survival. Indeed, CD74 forms functional complexes with CXCR4 to mediate MIF signalling. It is thought that long-lived PCs may also respond to MIF (Cassese *et al.* 2003; Van Driel *et al.* 2002; Sapoznikov *et al.* 2008)

Finally, assessment of signalling in confirmed CXCR4[WHIM] mutated WM patient samples in response to CXCL12 and αCD19 will be necessary to understand how these pathways interact in a disease setting. Functional assays would then be completed to fully assess survival capabilities and migration. Eventually, functional analysis of CXCR4 signalling with the inclusion of inhibitors could be utilised. Inhibitors for AKT/PI3K and ERK would enable clear understanding of how loss of these pathways affect both healthy and WM PB/PCs.

Ibrutinib and idelalisib have shown promise as treatment of WM, however there are some patients or do not respond to either effectively and additionally, may relapse after treatment (Treon *et al.* 2015; Dimopoulos *et al.* 2017). New therapeutic strategies will require the ability to overcome resistance and restore sensitivity to other drugs. To do this understanding how signalling pathways in WM are interconnected. In addition, these strategies must take into account the signalling rewiring that occurs as the WM B-cells mature towards the PC like phenotype. Next steps for assessment of vulnerabilities would involve the evaluation of inhibitors targeting the key signalling pathways. Inhibitors to assess include PI3K inhibitors, Ibrutinib and MEK inhibitors. These experiments would evaluate how these inhibitors affect signal transduction dynamics, cell death, differentiation, and secretory capability of ASCs (Immunoglobulin production). Combinations of various different inhibitors and modulation as the cells differentiate may be the key to overcoming the development of a CXCR4[WHIM] mutation and the associated changes to survival signalling. From this, treatments could be developed that are tailored for targeting the different populations of WM B-cells and PCs, based on the different signalling mechanisms and used in combination with therapeutics already used to treat WM e.g. rituximab or BTK inhibitors. Further treatment could be developed targeting CD19 to disrupt ERK survival signalling. By targeting several different pathways , the WM cells may be unable to rely on any survival signals and therefore may be more susceptible to traditional cancer therapeutics, e.g. chemotherapy.

6.0 - Final Discussion

6.1 Overview

Antibody mediated immunity relies on the development of B-cells and their subsequent differentiation into memory B-cells and PCs to secrete antibody against antigens and provide long-term immunological memory. To improve this response, B-cells must undergo a processes of affinity maturation, including formation of a GC, antibody class switching and somatic hypermutation, thereby increasing specificity for a unique antigen (Mesin, Ersching and Victora 2016).

Following a GC reaction, the fate of a B-cell may be to become a memory B-cell, which is able to recall the encounter with a familiar antigen and mount a rapid response upon secondary recognition. Alternatively, a B-cell is driven towards the PC programme, whereby they may migrate towards a survival niche as short-lived antibody secreting PBs, and once they arrive at their destination, mature into a PC and secrete a continuous high level of antibody, providing constant protection without the need for antigen re-stimulation. (Akkaya, Kwak and Pierce 2020; Suan, Sundling and Brink 2017)

The migration of B-cells and PBs requires the use of chemokine signals. Movement of B-cells within the GC, from the DZ towards to LZ and back, requires the finely tuned secretion of CXCL12 and CXCL13 from resident reticular cells and follicular dendritic cells (De Silva and Klein 2015; Allen *et al.* 2004). Immature PBs localise, most often, within the BM following the CXCR4/CXCL12 axis secreted by BM stromal cells (Cheng *et al.* 2018). It is crucial for PBs to reach the BM where they are supported by the niche environment and develop into LLPCs (Tokoyoda *et al.* 2004).

CXCR4 signalling provides more than migratory signals, however, and there is evidence that the linked transduction pathways are variable depending on the differentiation stage of the cells. In both pre-B-cells and mature B-cells, CXCL12 activates MAP kinase signalling leading to ERK1/2 activation. However, the pan-PI3K inhibitor Wortmanin more profoundly blocked ERK activation in mature B-cells, indicating that CXCR4 is capable of differentially coupling to downstream signalling pathways depending on stage of maturation (Palmesino *et al.* 2006)

Additionally, CXCR4 may associate with other B-cell surface receptors to alter the signalling response and therefore the downstream events. Recent publications have suggested that CXCR4 interacts with CD19 to generate signalling associated with survival and chemotaxis. Indeed, the disruption of CD19 motility and prevention of association with the BCR, CXCR4 and other surface receptors, reduced CD19 phosphorylation after stimulation of these receptors, placing CD19 as a crucial signalling hub for PI3K signalling (Keppler *et al.* 2015; Becker *et al.* 2017)

PI3K activity is essential for B-cell survival, migration and activation. In particular, class I PI3Ks play an important role in B-cells. These are comprised of a regulatory subunit and a catalytic subunit. There are four isoforms of class I PI3K catalytic subunits that have non-redundant functions. Both p110δ and p110α are used to relay signals from the antigen receptor (Okkenhaug *et al.* 2002; Ramadani *et al.* 2010), whereas P110γ is generally employed by GPCRs (Andrews, Stephens and Hawkins 2007). However, in B-cells p110δ can also be activated downstream of chemokine receptors (Reif *et al.* 2004).

Within the *in vitro* differentiation model, the *PIK3CD* isoform is expressed in resting and activated B-cells, but the mRNA is repressed at the later stages of differentiation. Conversely, *PIK3CA* mRNA is maintained at all stages of the differentiation and *PIK3CG* mRNA is induced at the PB stage and maintained at high levels in PCs. Inhibition of PIK3CG during *in vitro* culture severely affects PC survival, suggesting a major role of this isoform in signalling events relating to survival in PBs and PCs (unpublished data, Sophie Stephenson). Together, this indicates a dynamic and unique role of CXCR4 signalling and CD19 association to enhance PI3K signalling in PB/PCs. Understanding the signalling patterns in response to these stimuli is crucial to fully describe their role in LLPCs.

Juxtaposed with healthy B-cell differentiation is the aberrant signal transduction events associated with B-cell and PC malignancies. The development of the *in vitro* differentiation model allows for robust analysis of B-cell differentiation and understanding of what factors drive PC maturation and maintain this long-lived effector population. Indeed mutations in CXCR4 are present in WHIM syndrome, a rare immunodeficiency, characterised by warts, hypogammaglobulinemia, repeat infections and myelokathexis. The mutation results in the loss of the intracellular carboxyl tail of the protein and therefore prevention of CXCL12 induced receptor internalisation, leading to a maintenance of an activated state. A similar mutation is present in about 30% of WM patients, in addition to MYD88 mutations. These patients exhibit enhanced chemotaxis in response to CXCL12, increased ERK and AKT activation and relative resistance to therapeutics e.g. BTK inhibitors such as Ibrutinib (Cao *et al.* 2015). WM B-cells possess the unique ability to undergo the complete B-cell differentiation to the PC stage and unusually, undergo the entire maturation process within the BM (Treon *et al.* 2014). This perturbed localisation indicates there are defects in the migratory potential WM cells, and this is likely enhanced by the presence of the CXCR4[WHIM] mutation. Indeed, CXCR4[WHIM] mice show perturbed B-cell trafficking and a failure of retention of LLPC within the BM. Instead proliferating PB rapidly accumulate in the niches. This would suggest a unique signalling profile found in CXCR4[WHIM] PBs and PCs (Biajoux *et al.* 2016). The majority of studies investigating mutant CXCR4 signalling in WM has focused on the B-cells. Successful treatment of WM requires the targeting of both the B-cell and PC components. Further understanding of the signalling pathways controlling PB and PC survival is therefore key.

The initial aims of this study were to understand how the CXCR4 signal transduction events are different amongst the cell populations that arise during the differentiation process, how CD19 can modulate signalling in these populations and finally, how the CXCR4WHIM mutation can affect these pathways. To investigate these aims, the B-cell differentiation model was used to generate a reliable population of B-cells, PBs and PCs, and a range of techniques were utilised, but focused on flow cytometry analysis of surface protein expression to establish the effects of CD19 depletion/stimulation and CXCR4WHIM on B-cell/PC phenotype and CXCR4 expression. Additionally, signalling experiments were performed to define the signalling pathways in response to the aforementioned stimuli. The role of CD19 was assessed through investigation of direct CD19 stimulation and CD19 depleted B-cell patient samples. Finally, the effect of CXCR4WHIM mutation was assessed through retroviral transduction of the S338 WHIM mutation.

6.2 Establishment of pattern of CXCR4 expression in differentiating B-cells

The understanding how CXCR4 signal transduction in early B-cell lymphopoiesis and mature B-cells has been documented, however the signal dynamics in PBs and PCs are unknown. Therefore initially, it was prudent to understand how CXCR4 expression is modulated through the differentiation model for subsequent interpretation of signalling responses, as lower level of signal pathway activation may reflect either lower receptor engagement or change in signalling capacity. CXCR4 expression is low prior to B-cell activation, however by day 6 post activation, CXCR4 expression peaks, before decreasing to very low levels as the cells reach the PC stage. About 60-90% of the cells reach the PC stage at day 13 showing this model is sufficient for studying PCs, however attainment of a larger proportion of PC could have been achieved through memory B-cell selection following the initial B-cell isolation step. It is unlikely assessment of CXCR4 expression would vary substantially as memory B-cells are, once differentiated into PCs, phenotypically similar to PC generated from the naïve B-cell population. However, selection of the memory B-cell component would have enabled, firstly a purer PC population after day 13 and secondly, assessment of any potential differences in CXCR4 signalling characteristics for comparison to PB/PCs from naïve B-cells. Regardless, PB and PC phenotype attainment is significant in the differentiations performed here, and therefore there is reasonable assurance that these cell types of the main drivers of the expression and signalling results obtained. Peak CXCR4 expression at day 6 likely reflects the role of CXCR4 in driving PB chemotaxis towards the BM, as travelling this considerable distance requires a high sensitivity to CXCL12. Confirmation of a lower CXCR4 expression in PCs allowed for reasonable assumption that the enhanced signalling seen in PCs was due to a change in signalling capacity. It is interesting that, despite the importance of CXCR4 in PC retention in the BM, CXCR4 expression is so low. This likely reflects the fact that the cells no longer need to sense CXCL12 remotely to migrate and instead there may be rewiring of signal pathways to

prioritise localisation within the BM or activation of survival signalling. On the other hand, the culture conditions may modulate CXCR4 expression similar to what might be experienced in the context of the BM microenvironment. Therefore, an assessment of different culture conditions was completed. APRIL and TGFβ are molecules that a PC may encounter under normal conditions, whereas IFNα is secreted during an inflammatory response. Previous work has demonstrated that PBs will react according to their culture conditions, and this may alter CXCR4 expression (Stephenson *et al.* 2019). However, gene expression analysis indicated no differences in *CXCR4* and surface protein levels were largely comparable at day 9, despite some differences in loss of CXCR4. As previous experiments found that the change in CXCR4 was acute, additional investigation should assess this. Furthermore, combinations of different BM trophic factors may show more pronounced or sustained changes in CXCR4.

As WM B-cell differentiation occurs mainly within the BM, this highlights the importance of assessing the impact of BM niche factors on CXCR4 expression. As evidence suggests that CXCR4 aids in the survival of LLPC within the BM (Tokoyoda *et al.* 2004; Cassese *et al.* 2003) , this effect may be amplified in WM cells. Additionally, the presence if the CXCR4[WHIM] mutation may further build on this.

6.3 CXCR4 signal integration in ASCs

Evaluation the signal transduction events downstream of CXCR4 are crucial for understanding the nature of CXCL12-induced survival mechanisms in long-lived PCs and their malignant counterparts. Investigation of healthy PBs and PCs was done initially. As these two cell types vary in their proliferative capability, longevity, and tissue specificity, it can be assumed there is a rewiring in signal transduction associated with these aspects. It is thought that CXCR4 signalling is programmed for migration in PBs and survival in PCs (Benet, Jing and Fooksman 2021; Tokoyoda *et al.* 2004).

PBs and PCs were stimulated with CXCR4 show additional variation in their ERK response. PCs seem to maintain ERK phosphorylation to a higher level for an extended period. Changes to intensity or duration of a signalling pathway can be due to differences in stimulation strength by feedback loops (Mendoza, Er and Blenis 2011).

One potential effect of the difference seen between PBs and PCs is that the prolonged ERK signalling in PCs may affect immediate early gene (IEG) product expression, thereby affecting outcomes of signalling related to survival mechanisms. Prolonged ERK activation can induce stabilisation of c-FOS, whereas more transient ERK activation means less ERK activity, preventing accumulation of c-FOS, leading to instability. c-FOS is a driver of various cellular functions, including proliferation, survival, and differentiation (Murphy *et al.* 2002).

Counterintuitively, enhanced ERK activation is normally associated with increased activity of positive cell cycle regulators and downregulation of anti-proliferative genes. One notable characteristic of PCs is the inability to proliferate and a shift to a state of quiescence. Unusually, here we see a heightened ERK phosphorylation pattern in PCs, whereas PBs, which retain some proliferative capability, show a lower ERK activity (Khodadadi *et al.* 2019). This is clear evidence of a rewiring of CXCR4 signals.

Furthermore, hyper-activation of RAS-ERK signalling can induce expression of CDK inhibitors, leading to cell cycle arrest. Specifically, moderate ERK signalling generates a transient production of p21 and accumulation of cyclin D1 leading the G1 phase cell proliferation, however prolonged signalling induces long-term p21 induction, activating CDK inhibitors p16Ink4a and p15Ink4b. Therefore, the enhanced ERK signalling in PCs in response to CXCL12 stimulation may have been rewired to contribute to an anti-proliferative phenotype, which may pair with increased AKT signalling, often associated with survival signalling. The trigger for this switch of a migratory to a survival signal from CXCL12 likely is due to environmental cues specific to survival niches (Pumiglia and Decker 1997; Sewing *et al.* 1997; Malumbres *et al.* 2000).

AKT integrates signals originating from cell surface receptors that are associated with PI3K, such as CXCR4, leading to gene expression relating to cell cycle control and survival. The AKT signalling through CXCR4/CXCL12 interaction demonstrates an enhanced activation in PCs compared to PBs. Additionally, in PCs, AKT phosphorylation at the S473 residue showed activity that spanned from 1 minute to 10 minutes and maintained to a much higher degree than ERK signalling. Phosphorylation at the T308 residue was similarly prolonged, however signal intensity was weaker than at the S473 residue. AKT phosphorylation can be detected up to 120 minutes after stimulation with insulin. Compared with CXCR4 stimulation, detection of phosphorylation at both residues was variably detected for up to 10 minutes in PC but phosphorylation begins to decrease after one minute in PBs (Kubota *et al.* 2012). It may be necessary to extend the signalling studies, to fully confirm any differences in duration of signal transduction.

AKT dephosphorylation is rate limited by its disassociation with PIP3 at the plasma membrane. Investigation into the activity of PIP3 may aid in understanding AKT signalling dynamics in B-cells vs ASCs and potentially in WM cells (Ebner *et al.* 2017). Fine tuning of AKT signalling duration can modulate its downstream effects. Indeed, feedforward loops can regulate the duration of AKT signalling, for example, GAB1 recruitment if PI3K can generate PIP3. PIP3 may then recruit additional GAB1, repeating the cycle and leads to additional PI3K signalling (Mendoza, Er and Blenis 2011). In this context, CXCL12 may induce stronger AKT phosphorylation, promoting these feedforward loops, thereby maintaining enhanced survival signalling even after CXCR4 desensitisation has occurred.

Additionally, activation of AKT via phosphorylation at the S473 residue stabilises phosphorylation at the T308 residue, thereby enabling maximal AKT activation. AKT deficient for S473 is capable of some activity, but it is severely diminished (Alessi *et al.* 1996; Manning and Toker 2017).

6.4 Role of CD19 signalling hub in CXCR4 signalling

During B-cell differentiation, the fate of the cells is dependent on the strength and fine tuning of the initiating signal. Furthermore, B-cells utilise a collaboration of different surface receptors to modulate the signal strength and optimise activation. Co-ligation of the BCR and CD19 can occur through C3d bound antigen, via association of CD19 and complement receptor type 2 (CR2/CD21) which can bind to fragments of C3, thereby reducing the quantity of BCR ligation necessary to initiate B-cell activation (Fearon and Carter 1995).

There is variation in the signalling events downstream of the BCR when CD19 itself is co-ligated compared to BCR stimulation alone. Indeed, the choice of the stimulation can affect the isoform of the catalytic subunit of PI3K utilised. Stimulation through the BCR alone can promote recruitment of p110α, whereas BCR and CD19 co-ligation largely requires the p85α and p110δ subunits of PI3K (Vigorito *et al.* 2004). Additionally, constitutive BCR signalling in the absence of any exogenous antigen interaction, or 'tonic signalling' principally acts through p110α (Ramadani *et al.* 2010).

Together, this evidence suggests that the manner of B-cell stimulation can qualitatively change the signalling output. In line with this, CXCR4 receptor may also interact with additional surface receptors to generate a varied signal output. CXCR4, and other B-cell surface receptors, have been shown to associate with CD19 to recruit PI3K via CD19 phosphorylation, implicating CD19 as a signalling hub for B-cells (Keppler *et al.* 2015). Due to the presence of CD19+ and CD19-ve PC subsets, it is uncertain what role CD19 plays in these cells, especially now that they have switched to an antibody secreting phenotype. Therefore, CXCR4 signalling was assessed in association with CD19 ligation.

Initially, we looked to see if intrinsic CD19 stimulation may modulate downstream signalling events in ASCs. CD19 stimulation of ASCs failed to activate ERK phosphorylation, indicating that CD19 stimulation does not feed into the MAPK signalling pathway. The same experiments were conducted to assess if CD19 stimulation is linked to the PI3K pathway. PBs do not seem to respond to CD19 ligation however, in PCs at AKT S473, there is detectable phosphorylation but no clear activity at the T308 residue. This indicates that CD19 may contribute to PI3K signalling in terminally differentiated cells.

As there is minimal activity after both long-term and short-term direct CD19 ligation, it was necessary to understand how activation of CD19 in the context of its association with surface receptors impacts

signalling. Therefore, we next sought to understand how CXCR4 and CD19 interaction may modulate downstream signalling events in ASCs, as it has been shown to in murine B-cells (Becker et al., 2017). Despite initially seeing no association of the MAPK signalling pathway and CD19 ligation, co-stimulation however seems to amplify ERK phosphorylation in PBs. In PCs, CXCL12 stimulation alone generated a stronger signal than co-stimulation. Together this clearly shows a rewiring of signalling in response to CXCL12 and CD19 between PBs and PCs. Specifically, it may imply a negative regulatory role of CD19 for CXCR4 in PCs. CD19 has not been shown to have an effect like this, however multiple myeloma cells are consistently negative for CD19. It could be that a loss of CD19, evidence of which is detectable in healthy PCs populations, is compatible with altered signalling seen in malignant cells. Additionally, this negative control of ERK may be related to the transition from a proliferative phenotype to quiescent phenotype, focussing instead on AKT-driven survival signalling, and CD19 may be one mechanism controlling this shift.

AKT signalling at both residues is similar between stimulations, but again AKT phosphorylation was stronger in PCs. This suggests that CD19 ligation has limited effect on AKT signalling. CD19 ligation through this method may not have been sufficient to enhance survival in ASCs through enhanced AKT signal activation. Repeats of this experiment could be conducted firstly, with an increased number of αCD19 bound beads. Alternatively, as mentioned previously, CD19 associates with CD21 which can bind the complement C3d fragment of activated C3 that is attached to antigen. CD19, in complex with CD21 can co-stimulate signalling through the BCR. Therefore, multimerised C3d could be used to bind to CD21, therefore activating CD19 in a method more likely to induce CD19 ligation seen *in vivo*. Additionally, because the BCR ligation is required for B-cell activation, there may occasions when BCR ligation may be limited due to e.g., monovalent antigen or tonic signalling (Keppler *et al.* 2015).

CD19 can compensate for this through reducing the threshold required for BCR activation. Similarly, this balance could be applied to CXCR4 and CD19. CD19 signal amplification may be important when CXCL12 is limiting. An experiment could be designed whereby the amount if CXCL12 is reduced and then assess if CD19 stimulation can compensate for this via analysis of phosphorylated AKT/ERK.

The effects of CD19 deficiency are apparent in the signalling experiments. Loss of CD19 weakens the ability of PCs to generate a strong ERK or AKT signal. Despite this apparent defect in signalling there were no detectable flaws in cell viability, differentiation capability, CXCR4 expression or expression of B-cell and PC makers. Within this experiment, it may be that sufficient BCR stimulation is provided by ideal culture conditions and thus CD19's role of threshold reduction is not required by these cells to become activated. Utilising lower levels of F(Ab')$_2$ anti-Ig and CD40L cells in both healthy and CD19-ve cells would likely show the defects of CD19 deficiency.

CD19-ve PBs are capable of weak AKT and ERK phosphorylation, however by day 13, the PCs are almost completely unable to generate an ERK signal in response to CXCL12 and AKT signalling is dramatically depleted. This confirms the involvement of CD19 as a signalling element in ASCs. ERK signalling in plasma cells induced by co-stimulation appears reduced compared to CXCL12 alone, yet depletion of CD19 prevents strong ERK signalling. This could indicate that the effects of direct ligation of CD19 in B-cells becomes uncoupled once the cells mature to the PC stage. Indeed, the presence of surface BCR may be crucial for integration of signals induced from CD19 ligation. As PCs no longer express a BCR, the main role of CD19 mainly becomes the integration of signals, rather than a driver of signals. CD19-ve PBs may retain some capability to activate ERK/AKT signals as they are in a transitional state.

AKT signalling in co-stimulated PCs is comparable to that seen in CXCL12 stimulated PCs and AKT signalling is reduced in CD19-ve PCs. Again, this supports the notion that CD19 ligation, through this method at least, is ineffective for activation of AKT signalling in PCs, yet CD19 is necessary to drive AKT signalling in response to CXCL12. This further supports the use of complement activation of CD19 to confirm if CD19 stimulation has minimal effects for AKT signalling in this context.

The RNA sequencing analysis of CD19-ve cells reveals a normal expression of *CD19* mRNA confirming the defects are at a protein level. Furthermore, it confirms the maintenance of differentiation and lack of defects seen in the phenotypic data, as differentiation related mRNA expression is unaffected by CD19 depletion. Observation of the signalling-related mRNA expression reveals that the CD19-ve cells possess some variation in PI3K gene expression. There is a higher expression of *PIK3CB* and *PIK3R2* mRNA, potentially indicating the cells are attempting to mitigate the loss of ERK signalling by increasing PI3K signalling. Whilst AKT signalling is dampened by the loss of CD19, there is some signalling remaining, which would support this.

Finally, the defects in CXCR4 signalling would suggest changes to cell behaviour. Therefore, a long-term response to CXCL12 may reveal flaws in viability and phenotype. CD19-ve cells exposed to CXCL12 in culture revealed no major defects in cell survival and were comparable to APRIL conditions alone. CD20 downregulation is slightly slower in CXCL12 treated CD19-ve cells, however this effect is minimal. CD20 has been shown to become upregulated within the cell membrane through interactions of CXCL12 and CXCR4 (Pavlasova *et al.* 2016). The inclusion of CXCL12 did not induce upregulation of CD20 in HC, and whilst the difference is small, the CD19-ve cells show a higher retention of CD20 at day 13. CD19 may play a role in regulating CD20 expression, which could be affected by CD19 deficiency. However additional experiments would be required to confirm this. Additionally, repeats of this experiment could be improved through removal of APRIL conditions and forcing the cells to become reliant on CXCL12 to enhance survival signalling

Whilst this study has not identified the significance of CD19 ligation in ASCs, initial steps have confirmed the participation of CD19 in PB and PC CXCR4 signalling. The work completed here provide a strong basis for further investigation and additional experiments have been suggested to pursue.

6.5 Dysregulation of CXCR4 signalling

Having established the CXCR4 signalling pattern in key downstream kinase pathways and identifying CD19 as a key player in these pathways, the next step was to assess the role of dysregulated CXCR4 signalling. This was accomplished through the development of retroviral expression vectors and subsequent transduction of HEK293 cells before treatment of differentiating B-cells at day two with viral supernatant.

Firstly, successful transfer of CXCR4 encoding fragments from mammalian expression vectors to retroviral vectors through restriction digest and ligation was accomplished. The transduction protocol shows variable but efficient uptake of CXCR4 constructs into differentiating B-cells. Additional optimisation would have allowed for improved transduction efficiency.

Additionally, no selection via antibiotic kill curve was completed due to time constraints, selection of CD2+ cells would have provided a much clearer analysis of the effects of the WHIM mutation in ASCs. Antibiotic selection in a differentiating B-cell population would have likely been complex as clearly the cells were sensitive to the transduction process, indicated by the high levels of cell death compared to the un-transduced samples. As the cells transition between B-cell, PB and PC phenotype within a few days of each other, it may not provide enough time for total elimination of un-transduced cells. The cells are transduced at day 2 and once reaching day 3, the media is changed again to push the cells towards a PB phenotype. Antibiotic could have been included at each media change to provide the best opportunity for selection.

Phenotypic assessment shows an earlier acquisition of CD138 expression at day 6 in one population of WT and WHIM transduced cells. PB attainment of CD138 may confer some enhanced survival characteristics, such as greater AKT and ERK signalling, however this was not detected in the viability assessment, perhaps due to the effects of transfection. One of the roles of CD138 is to mediate cell-cell and cell-ECM interactions and is therefore crucial for cell adhesion (McCarron, Park and Fooksman 2017). In myeloma cells, it has also been shown to interact with APRIL to enhance cell survival (Moreaux *et al.* 2009). Furthermore, CD138 acts as a co-receptor for growth factors such as hepatocyte growth factor and epidermal growth factor, both heavily involved in MM survival within the BM (Derksen *et al.* 2003; Mahtouk *et al.* 2006). Perhaps the enhanced CXCR4 contributes to the attainment of CD138 expression, by some as yet unknown means, leading to improved survival of WM PBs within the BM by enabling improved adhesion and survival signalling.

In addition to this, CD20 expression is slightly altered in transduced samples. At day 10, some samples retain a higher CD20 level by day 10. Perhaps CXCR4 upregulation enhances CD20 expression due to the increased ability of these cells to maintain CXCR4 expression and therefore CXCL12 interaction, leading to enhanced signalling events, similar to its role of interacting with the BCR in B-cells and supporting BCR signal transduction. This may indicate that CXCR4 high PBs and PCs could be particularly sensitive to therapeutics that target CD20, e.g., rituximab (Pavlasova *et al.* 2016; Petrie and Deans 2002; Polyak *et al.* 2008; Pavlasova *et al.* 2018)

Despite the variable transduction efficiency, the data indicate that AKT and ERK signalling in response to CXCL12 is maintained to a higher signal intensity, relative to the peak phosphorylation, compared to the controls. This may be indicative of successful CXCR4[WHIM] expression as prolonged receptor residence on the cell surface contributes to both amplification and extended duration of signalling (Milanesi, Locati and Borroni 2020). Indeed, this likely matches evidence from the literature, which details prolongation of both calcium flux and motility in WHIM mutated cells stimulated with CXCL12 (Hernandez *et al.* 2003; Liu *et al.* 2012)

CD2 expression was included in the same flow panel as B-cell/PC markers but not the CXCR4 panel. Compensation issues prevented a clear analysis of CXCR4 and CD2 together, both within the normal CXCR4 panel and when looking assessing only these two stains. It is unclear why this issue was persisting and time constraints and cell viability at the later stages prevented further investigation.

Assessment of the role of CD19 in CXCR4[WHIM] expressing ASCs revealed that co-stimulated PBs generated a stronger ERK and AKT signalling compared to PBs stimulated with CXCL12 alone, indicating that CXCR4[WHIM] expressing PBs are more responsive to CD19 stimulation. They also retain a larger CD19+ population. Whilst the changes to signalling provided no detectable functional changes, it provides strong evidence to further investigate this stimulation in these cells, perhaps through complement activation of CD19 and specific selection of CD2+ cells, a stronger signal may be detected that may provide a functional effect. Migration assays should also be conducted to assess how these varying stimulations modulate this key CXCR4-mediated activity.

CD19-ve cells showed no defects in survival, which may be due to an intact APRIL/BCL-XL or BTK signalling priority that drives survival signals in B-cells and ASCs (Belnoue *et al.* 2008; de Weers *et al.* 1994). Potentially assessment of signal transduction events could be completed in conjunction with ibrutinib, a BTK inhibitor. A study could be designed to assess how selective inhibition of BTK may cause ASCs to become more reliant on CXCR4 signals induced by wither CXCL12 alone or CXCL12 with CD19. It would be expected that co-stimulated cells would generate a much stronger AKT and ERK phosphorylation pattern. CD19-ve cells treated with BTK inhibitors may have a flawed signalling

pattern and long-term treatment in culture could cause a collapse of viable cells. Additional inclusion of AKT/ERK inhibitors with BTK inhibitors in transduced cells would be expected to induce catastrophic cell death.

Ideally, acquisition of WM patient samples would have been the next step to assess these signalling mechanisms. These experiments conducted here have started the initial investigations into CXCR4 signalling and have enabled some understanding of the effects of CXCR4[WHIM] in isolation of other mutations, such as the MYD88 L265P mutation. The next step would be to assess CXCR4 signalling events within the context of WM, by running the differentiations on patient samples. The MYD88 L265P mutation is considered the activating mutation for WM, therefore, samples are described as WM because of this mutation, however as only 30% of WM patients present with a CXCR4 mutation, and even then, there are several different potential mutations of CXCR4 recorded in WM aetiology, it would be difficult to confirm the presence of a CXCR4 mutation unless current identifications for patient samples are assessed for CXCR4 mutations. Hence transductions were chosen as a viable alternative to patient samples.

Further investigation of CXCR4[WHIM] signalling dynamics will aid in the understanding of CXCR4 signal integration in ASCs. Truncation of the C-terminal tail of CXCR4 in patients expressing CXCR4[WHIM] prevents β-arrestin binding, however there is evidence that in addition to the enhanced signalling caused by the lack of receptor internalisation, there is also a augmentation of ERK signalling dependant on β-arrestin downstream of the truncated receptor. A study by Lagane at colleagues (Lagane *et al.* 2008) show an augmented responsiveness of WHIM mutated T-cells and CXCR4 transduced HEK cells to CXCL12 is partially mediated by enhanced β-arrestin2 dependant signalling downstream of the truncated CXCR4. Despite the loss of the regions required for β-arrestin to instigate receptor desensitisation, β-arrestin still maintains association with CXCR4[WHIM] and generates β-arrestin dependant ERK signalling. It would be interesting to see how β-arrestin interactions vary in WHIM mutated B-cells, PBs and PCs and also if CD19 interaction plays a role in this mechanism. It would be expected that the enhanced ERK activation due to β-arrestin would likely be detectable in B-cell/PBc and PCs, however the differences in the level of importance of β-arrestin at each stage is unknown. CXCR4[WHIM] may also form heterodimers with CXCR4[WT]. It would be interesting to investigate to what degree these heterodimers exist in B-cells, PBs and PCs and how much they contribute towards an enhanced signalling pattern.

6.6 Concluding remarks

In summary, the data presented here partially confirms the hypotheses set out. PBs follow the CXCR4/CXCL12 axis to migrate to survival niches (Cheng *et al.* 2018; Hargreaves *et al.* 2001) and PCs

likely utilise CXCR4, in coordination with other factors, mainly for survival signalling through retention within the BM (Cheng *et al.* 2018; Benet, Jing and Fooksman 2021; Tokoyoda *et al.* 2004). Here the data indicate a downregulation of CXCR4 expression as the cells reach the PC stage. This change in expression provides some indication of a rewiring of the role of CXCR4 as the cells transition.

Further evidence of a re-wiring of CXCR4 function in these two cell populations is shown by the changes to ERK activity in response to CXCL12 (Becker *et al.* 2017). PCs show a prolonged and stronger ERK phosphorylation pattern compared to PBs. This prolonged ERK activity may be associated with immediate early gene (IEG) product expression, thereby affecting outcomes of signalling related to survival mechanisms (Murphy *et al.* 2002). The enhanced AKT phosphorylation in PC may be associated with survival signalling required by PCs (van Spriel *et al.* 2012).

This study also assessed the role of CD19 in the modulation of CXCR4 signals (Becker *et al.* 2017). The literature suggests a role of CD19 as a signalling hub to bring together the activity of B-cell surface receptors to promote CXCR4 signalling (Keppler *et al.* 2015) however the role of CD19 in ASCs is less clear, especially due to the development of both CD19+ and CD19-ve fractions (Halliley *et al.* 2015; Mei *et al.* 2015; Groves *et al.* 2018). We show that CD19 stimulation alone can induce a weak AKT activity, but not ERK signalling. Whilst a superior method of CD19 stimulation would possibly yield some ERK stimulation (Mei *et al.* 2015), we have shown that some property of PCs enables sensitivity to CD19 that is not apparent in PBs. We see that co-stimulation with CXCL12 amplifies ERK phosphorylation in PBs. In PCs, CXCL12 stimulation alone generated a stronger signal than co-stimulation. Together this clearly shows a rewiring of signalling in response to CXCL12 and CD19 between PBs and PCs.

Most profoundly, we show significant defects in ERK and AKT signalling in CD19-ve PBs and a near total failure to activate these pathways in CD19-ve PCs, indicating a requirement of CD19 on the surface of these cell populations.

It is difficult to draw clear conclusions from the transduction experiments due to the variability of transduction efficiency and absence of any selection of transduced cells. However, we can infer some ideas about the effects of the CXCR4[WHIM] mutation. Firstly, there is an indication that the presence of enhanced CXCR4 expression induces an earlier acquisition of CD138. This may mediate enhanced survival in PBs by taking advantage of the supportive BM niche and improving their association with BM resident cells/matrix (McCarron, Park and Fooksman 2017; Moreaux *et al.* 2009) and could be a contributing factor to the ability of proliferative WM PBs to colonise the BM niche successfully (Biajoux *et al.* 2016). Assessment of signalling in these transduced cells failed to show clear evidence of enhanced signalling compared to HCs, likely due to the heterogeneous population of cells utilised. We

do show however that PCs transduced with CXCR4^{WHIM} appear to generate a stronger AKT/ERK signal compared to PBs.

Together this data provides evidence of CXCR4 signal rewiring in PBs and PCs, which is further modulated by CD19 and the presence of the CXCR4^{WHIM} mutation. Elucidating the nature of the signalling mechanisms that enable this rewiring to occur and the functional output of these signals will provide new and important insights into the biology of ASCs and their malignant counterparts.

7.0 References

AKKAYA, M., K. KWAK and S. K. PIERCE. 2020. B cell memory: building two walls of protection against pathogens. *Nat Rev Immunol,* **20**(4), pp.229-238.

ALDOSS, I. and S. J. FORMAN. 2020. How I treat adults with advanced acute lymphoblastic leukemia eligible for CD19-targeted immunotherapy. *Blood,* **135**(11), pp.804-813.

ALESSI, D. R., M. ANDJELKOVIC, B. CAUDWELL, P. CRON, N. MORRICE, P. COHEN and B. A. HEMMINGS. 1996. Mechanism of activation of protein kinase B by insulin and IGF-1. *Embo j,* **15**(23), pp.6541-51.

ALLEN, C. D., K. M. ANSEL, C. LOW, R. LESLEY, H. TAMAMURA, N. FUJII and J. G. CYSTER. 2004. Germinal center dark and light zone organization is mediated by CXCR4 and CXCR5. *Nat Immunol,* **5**(9), pp.943-52.

ALLMAN, D., J. R. WILMORE and B. T. GAUDETTE. 2019. The continuing story of T-cell independent antibodies. *Immunol Rev,* **288**(1), pp.128-135.

ANDREWS, S., L. R. STEPHENS and P. T. HAWKINS. 2007. PI3K class IB pathway. *Sci STKE,* **2007**(407), pcm2.

ANSEL, K. M., L. J. MCHEYZER-WILLIAMS, V. N. NGO, M. G. MCHEYZER-WILLIAMS and J. G. CYSTER. 1999. In vivo-activated CD4 T cells upregulate CXC chemokine receptor 5 and reprogram their response to lymphoid chemokines. *J Exp Med,* **190**(8), pp.1123-34.

ANSELL, S. M., R. A. KYLE, C. B. REEDER, R. FONSECA, J. R. MIKHAEL, W. G. MORICE, P. L. BERGSAGEL, F. K. BUADI, J. P. COLGAN, D. DINGLI, A. DISPENZIERI, P. R. GREIPP, T. M. HABERMANN, S. R. HAYMAN, D. J. INWARDS, P. B. JOHNSTON, S. K. KUMAR, M. Q. LACY, J. A. LUST, S. N. MARKOVIC, I. N. MICALLEF, G. S. NOWAKOWSKI, L. F. PORRATA, V. ROY, S. J. RUSSELL, K. E. SHORT, A. K. STEWART, C. A. THOMPSON, T. E. WITZIG, S. R. ZELDENRUST, R. J. DALTON, S. V. RAJKUMAR and M. A. GERTZ. 2010. Diagnosis and management of Waldenstrom macroglobulinemia: Mayo stratification of macroglobulinemia and risk-adapted therapy (mSMART) guidelines. *Mayo Clin Proc,* **85**(9), pp.824-33.

ARANBURU, A., S. CECCARELLI, E. GIORDA, R. LASORELLA, G. BALLATORE and R. CARSETTI. 2010. TLR ligation triggers somatic hypermutation in transitional B cells inducing the generation of IgM memory B cells. *J Immunol,* **185**(12), pp.7293-301.

ARUMUGAKANI, G., S. J. STEPHENSON, D. J. NEWTON, A. RAWSTRON, P. EMERY, G. M. DOODY, D. MCGONAGLE and R. M. TOOZE. 2017. Early Emergence of CD19-Negative Human Antibody-Secreting Cells at the Plasmablast to Plasma Cell Transition. *J Immunol,* **198**(12), pp.4618-4628.

BADR, G., G. BORHIS, D. TRETON and Y. RICHARD. 2005. IFN{alpha} enhances human B-cell chemotaxis by modulating ligand-induced chemokine receptor signaling and internalization. *Int Immunol,* **17**(4), pp.459-67.

BASSO, K. and R. DALLA-FAVERA. 2012. Roles of BCL6 in normal and transformed germinal center B cells. *Immunol Rev,* **247**(1), pp.172-83.

BECKER, M., E. HOBEIKA, H. JUMAA, M. RETH and P. C. MAITY. 2017. CXCR4 signaling and function require the expression of the IgD-class B-cell antigen receptor. *Proc Natl Acad Sci U S A,* **114**(20), pp.5231-5236.

BELNOUE, E., M. PIHLGREN, T. L. MCGAHA, C. TOUGNE, A. F. ROCHAT, C. BOSSEN, P. SCHNEIDER, B. HUARD, P. H. LAMBERT and C. A. SIEGRIST. 2008. APRIL is critical for plasmablast survival in the bone marrow and poorly expressed by early-life bone marrow stromal cells. *Blood,* **111**(5), pp.2755-64.

BENCE, K., W. MA, T. KOZASA and X. Y. HUANG. 1997. Direct stimulation of Bruton's tyrosine kinase by G(q)-protein alpha-subunit. *Nature,* **389**(6648), pp.296-9.

BENET, Z., Z. JING and D. R. FOOKSMAN. 2021. Plasma cell dynamics in the bone marrow niche. *Cell Rep,* **34**(6), p108733.

BENSON, M. J., S. R. DILLON, E. CASTIGLI, R. S. GEHA, S. XU, K. P. LAM and R. J. NOELLE. 2008. Cutting edge: the dependence of plasma cells and independence of memory B cells on BAFF and APRIL. *J Immunol,* **180**(6), pp.3655-9.

BERNARDINI, G., G. SCIUMÈ, D. BOSISIO, S. MORRONE, S. SOZZANI and A. SANTONI. 2008. CCL3 and CXCL12 regulate trafficking of mouse bone marrow NK cell subsets. *Blood,* **111**(7), pp.3626-34.

BIAJOUX, V., J. NATT, C. FREITAS, N. ALOUCHE, A. SACQUIN, P. HEMON, F. GAUDIN, N. FAZILLEAU, M. ESPÉLI and K. BALABANIAN. 2016. Efficient Plasma Cell Differentiation and Trafficking Require Cxcr4 Desensitization. *Cell Rep,* **17**(1), pp.193-205.

BIANCHI, M. E. and R. MEZZAPELLE. 2020. The Chemokine Receptor CXCR4 in Cell Proliferation and Tissue Regeneration. *Front Immunol,* **11**, p2109.

BIDKHORI, H. R., A. R. BAHRAMI, M. FARSHCHIAN, A. HEIRANI-TABASI, M. MIRAHMADI, H. HASANZADEH, N. AHMADIANKIA, R. FARIDHOSSEINI, M. DASTPAK, A. G. SHABGAH and M. M. MATIN. 2021. Mesenchymal Stem/Stromal Cells Overexpressing CXCR4(R334X) Revealed Enhanced Migration: A Lesson Learned from the Pathogenesis of WHIM Syndrome. *Cell Transplant,* **30**, p9636897211054498.

BIRAGYN, A., P. A. RUFFINI, C. A. LEIFER, E. KLYUSHNENKOVA, A. SHAKHOV, O. CHERTOV, A. K. SHIRAKAWA, J. M. FARBER, D. M. SEGAL, J. J. OPPENHEIM and L. W. KWAK. 2002. Toll-like receptor 4-dependent activation of dendritic cells by beta-defensin 2. *Science,* **298**(5595), pp.1025-9.

BOOTHBY, M. R., E. HODGES and J. W. THOMAS. 2019. Molecular regulation of peripheral B cells and their progeny in immunity. *Genes Dev,* **33**(1-2), pp.26-48.

BRADBURY, L. E., V. S. GOLDMACHER and T. F. TEDDER. 1993. The CD19 signal transduction complex of B lymphocytes. Deletion of the CD19 cytoplasmic domain alters signal transduction but not complex formation with TAPA-1 and Leu 13. *J Immunol,* **151**(6), pp.2915-27.

BRADDOCK, M. 2007. 11th annual Inflammatory and Immune Diseases Drug Discovery and Development Summit 12-13 March 2007, San Francisco, USA. *Expert Opin Investig Drugs,* **16**(6), pp.909-17.

BROMLEY, S. K., T. R. MEMPEL and A. D. LUSTER. 2008. Orchestrating the orchestrators: chemokines in control of T cell traffic. *Nat Immunol,* **9**(9), pp.970-80.

BRYNJOLFSSON, S. F., M. MOHADDES, J. KÄRRHOLM and M. J. WICK. 2017. Long-lived plasma cells in human bone marrow can be either CD19(+) or CD19(). *Blood Adv,* **1**(13), pp.835-838.

BUSILLO, J. M., S. ARMANDO, R. SENGUPTA, O. MEUCCI, M. BOUVIER and J. L. BENOVIC. 2010. Site-specific phosphorylation of CXCR4 is dynamically regulated by multiple kinases and results in differential modulation of CXCR4 signaling. *J Biol Chem,* **285**(10), pp.7805-17.

BUSILLO, J. M. and J. L. BENOVIC. 2007. Regulation of CXCR4 signaling. *Biochim Biophys Acta,* **1768**(4), pp.952-63.

CAESER, R., M. DI RE, J. A. KRUPKA, J. GAO, M. LARA-CHICA, J. M. L. DIAS, S. L. COOKE, R. FENNER, Z. USHEVA, H. F. P. RUNGE, P. A. BEER, H. ELDALY, H. K. PAK, C. S. PARK, G. S. VASSILIOU, B. J. P. HUNTLY, A. MUPO, R. J. M. BASHFORD-ROGERS and D. J. HODSON. 2019. Genetic modification of primary human B cells to model high-grade lymphoma. *Nat Commun,* **10**(1), p4543.

CAO, Y., Z. R. HUNTER, X. LIU, L. XU, G. YANG, J. CHEN, C. J. PATTERSON, N. TSAKMAKLIS, S. KANAN, S. RODIG, J. J. CASTILLO and S. P. TREON. 2015. The WHIM-like CXCR4(S338X) somatic mutation activates AKT and ERK, and promotes resistance to ibrutinib and other agents used in the treatment of Waldenstrom's Macroglobulinemia. *Leukemia,* **29**(1), pp.169-76.

CAPOLUNGHI, F., M. M. ROSADO, M. SINIBALDI, A. ARANBURU and R. CARSETTI. 2013. Why do we need IgM memory B cells? *Immunol Lett,* **152**(2), pp.114-20.

CARA, D. C., J. KAUR, M. FORSTER, D. M. MCCAFFERTY and P. KUBES. 2001. Role of p38 mitogen-activated protein kinase in chemokine-induced emigration and chemotaxis in vivo. *J Immunol,* **167**(11), pp.6552-8.

CASSESE, G., S. ARCE, A. E. HAUSER, K. LEHNERT, B. MOEWES, M. MOSTARAC, G. MUEHLINGHAUS, M. SZYSKA, A. RADBRUCH and R. A. MANZ. 2003. Plasma cell survival is mediated by synergistic effects of cytokines and adhesion-dependent signals. *J Immunol,* **171**(4), pp.1684-90.

CASTELLINO, F., A. Y. HUANG, G. ALTAN-BONNET, S. STOLL, C. SCHEINECKER and R. N. GERMAIN. 2006. Chemokines enhance immunity by guiding naive CD8+ T cells to sites of CD4+ T cell-dendritic cell interaction. *Nature,* **440**(7086), pp.890-5.

CASTILLO, J. J. and S. P. TREON. 2017. Toward personalized treatment in Waldenstrom macroglobulinemia. *Hematology Am Soc Hematol Educ Program,* **2017**(1), pp.365-370.

CHEN, S. S., B. Y. CHANG, S. CHANG, T. TONG, S. HAM, B. SHERRY, J. A. BURGER, K. R. RAI and N. CHIORAZZI. 2016. BTK inhibition results in impaired CXCR4 chemokine receptor surface expression, signaling and function in chronic lymphocytic leukemia. *Leukemia,* **30**(4), pp.833-43.

CHENG, Q., L. KHODADADI, A. TADDEO, J. KLOTSCHE, F. H. B, A. RADBRUCH and F. HIEPE. 2018. CXCR4-CXCL12 interaction is important for plasma cell homing and survival in NZB/W mice. *Eur J Immunol,* **48**(6), pp.1020-1029.

CHEVRIER, S., T. KRATINA, D. EMSLIE, D. M. TARLINTON and L. M. CORCORAN. 2017. IL4 and IL21 cooperate to induce the high Bcl6 protein level required for germinal center formation. *Immunol Cell Biol,* **95**(10), pp.925-932.

CHOU, W. C., D. E. LEVY and C. K. LEE. 2006. STAT3 positively regulates an early step in B-cell development. *Blood,* **108**(9), pp.3005-11.

CHU, V. T. and C. BEREK. 2013. The establishment of the plasma cell survival niche in the bone marrow. *Immunol Rev,* **251**(1), pp.177-88.

CHU, V. T., A. FROHLICH, G. STEINHAUSER, T. SCHEEL, T. ROCH, S. FILLATREAU, J. J. LEE, M. LOHNING and C. BEREK. 2011. Eosinophils are required for the maintenance of plasma cells in the bone marrow. *Nat Immunol,* **12**(2), pp.151-9.

COCCO, M., S. STEPHENSON, M. A. CARE, D. NEWTON, N. A. BARNES, A. DAVISON, A. RAWSTRON, D. R. WESTHEAD, G. M. DOODY and R. M. TOOZE. 2012. In vitro generation of long-lived human plasma cells. *J Immunol,* **189**(12), pp.5773-85.

COOPER, L. J., Z. AL-KADHIMI, D. DIGIUSTO, M. KALOS, D. COLCHER, A. RAUBITSCHEK, S. J. FORMAN and M. C. JENSEN. 2004. Development and application of CD19-specific T cells for adoptive immunotherapy of B cell malignancies. *Blood Cells Mol Dis,* **33**(1), pp.83-9.

DASU, T., V. SINDHAVA, S. H. CLARKE and S. BONDADA. 2009. CD19 signaling is impaired in murine peritoneal and splenic B-1 B lymphocytes. *Mol Immunol,* **46**(13), pp.2655-65.

DE FILIPPO, K., A. DUDECK, M. HASENBERG, E. NYE, N. VAN ROOIJEN, K. HARTMANN, M. GUNZER, A. ROERS and N. HOGG. 2013. Mast cell and macrophage chemokines CXCL1/CXCL2 control the early stage of neutrophil recruitment during tissue inflammation. *Blood,* **121**(24), pp.4930-7.

DE SILVA, N. S. and U. KLEIN. 2015. Dynamics of B cells in germinal centres. *Nat Rev Immunol,* **15**(3), pp.137-48.

DE WEERS, M., G. S. BROUNS, S. HINSHELWOOD, C. KINNON, R. K. SCHUURMAN, R. W. HENDRIKS and J. BORST. 1994. B-cell antigen receptor stimulation activates the human Bruton's tyrosine kinase, which is deficient in X-linked agammaglobulinemia. *J Biol Chem,* **269**(39), pp.23857-60.

DELPHIN, S. and J. STAVNEZER. 1995. Characterization of an interleukin 4 (IL-4) responsive region in the immunoglobulin heavy chain germline epsilon promoter: regulation by NF-IL-4, a C/EBP family member and NF-kappa B/p50. *J Exp Med,* **181**(1), pp.181-92.

DENT, A. L., A. L. SHAFFER, X. YU, D. ALLMAN and L. M. STAUDT. 1997. Control of inflammation, cytokine expression, and germinal center formation by BCL-6. *Science,* **276**(5312), pp.589-92.

DEPOIL, D., S. FLEIRE, B. L. TREANOR, M. WEBER, N. E. HARWOOD, K. L. MARCHBANK, V. L. TYBULEWICZ and F. D. BATISTA. 2008. CD19 is essential for B cell activation by promoting B

cell receptor-antigen microcluster formation in response to membrane-bound ligand. *Nat Immunol,* **9**(1), pp.63-72.

DERKSEN, P. W., D. J. DE GORTER, H. P. MEIJER, R. J. BENDE, M. VAN DIJK, H. M. LOKHORST, A. C. BLOEM, M. SPAARGAREN and S. T. PALS. 2003. The hepatocyte growth factor/Met pathway controls proliferation and apoptosis in multiple myeloma. *Leukemia,* **17**(4), pp.764-74.

DIEHL, S. A., H. SCHMIDLIN, M. NAGASAWA, S. D. VAN HAREN, M. J. KWAKKENBOS, E. YASUDA, T. BEAUMONT, F. A. SCHEEREN and H. SPITS. 2008. STAT3-mediated up-regulation of BLIMP1 Is coordinated with BCL6 down-regulation to control human plasma cell differentiation. *J Immunol,* **180**(7), pp.4805-15.

DIMOPOULOS, M. A., A. TEDESCHI, J. TROTMAN, R. GARCIA-SANZ, D. MACDONALD, V. LEBLOND, B. MAHE, C. HERBAUX, C. TAM, L. ORSUCCI, M. L. PALOMBA, J. V. MATOUS, C. SHUSTIK, E. KASTRITIS, S. P. TREON, J. LI, Z. SALMAN, T. GRAEF, C. BUSKE, N. S. G. I and M. THE EUROPEAN CONSORTIUM FOR WALDENSTROM'S. 2018. Phase 3 Trial of Ibrutinib plus Rituximab in Waldenstrom's Macroglobulinemia. *N Engl J Med,* **378**(25), pp.2399-2410.

DIMOPOULOS, M. A., J. TROTMAN, A. TEDESCHI, J. V. MATOUS, D. MACDONALD, C. TAM, O. TOURNILHAC, S. MA, A. ORIOL, L. T. HEFFNER, C. SHUSTIK, R. GARCÍA-SANZ, R. F. CORNELL, C. F. DE LARREA, J. J. CASTILLO, M. GRANELL, M. C. KYRTSONIS, V. LEBLOND, A. SYMEONIDIS, E. KASTRITIS, P. SINGH, J. LI, T. GRAEF, E. BILOTTI, S. TREON and C. BUSKE. 2017. Ibrutinib for patients with rituximab-refractory Waldenström's macroglobulinaemia (iNNOVATE): an open-label substudy of an international, multicentre, phase 3 trial. *Lancet Oncol,* **18**(2), pp.241-250.

DING, C., X. CHEN, P. DASCANI, X. HU, R. BOLLI, H. G. ZHANG, K. R. MCLEISH and J. YAN. 2016. STAT3 Signaling in B Cells Is Critical for Germinal Center Maintenance and Contributes to the Pathogenesis of Murine Models of Lupus. *J Immunol,* **196**(11), pp.4477-86.

DOGAN, I., B. BERTOCCI, V. VILMONT, F. DELBOS, J. MÉGRET, S. STORCK, C. A. REYNAUD and J. C. WEILL. 2009. Multiple layers of B cell memory with different effector functions. *Nat Immunol,* **10**(12), pp.1292-9.

DOWNWARD, J. 1998. Mechanisms and consequences of activation of protein kinase B/Akt. *Curr Opin Cell Biol,* **10**(2), pp.262-7.

DUY, C., J. J. YU, R. NAHAR, S. SWAMINATHAN, S. M. KWEON, J. M. POLO, E. VALLS, L. KLEMM, S. SHOJAEE, L. CERCHIETTI, W. SCHUH, H. M. JACK, C. HURTZ, P. RAMEZANI-RAD, S. HERZOG, H. JUMAA, H. P. KOEFFLER, I. M. DE ALBORAN, A. M. MELNICK, B. H. YE and M. MUSCHEN. 2010. BCL6 is critical for the development of a diverse primary B cell repertoire. *J Exp Med,* **207**(6), pp.1209-21.

EBNER, M., I. LUČIĆ, T. A. LEONARD and I. YUDUSHKIN. 2017. PI(3,4,5)P(3) Engagement Restricts Akt Activity to Cellular Membranes. *Mol Cell,* **65**(3), pp.416-431.e6.

EDEN, A., G. W. MILLER and V. NUSSENZWEIG. 1973. Human lymphocytes bear membrane receptors for C3b and C3d. *J Clin Invest,* **52**(12), pp.3239-42.

EGAWA, T., K. KAWABATA, H. KAWAMOTO, K. AMADA, R. OKAMOTO, N. FUJII, T. KISHIMOTO, Y. KATSURA and T. NAGASAWA. 2001. The earliest stages of B cell development require a chemokine stromal cell-derived factor/pre-B cell growth-stimulating factor. *Immunity,* **15**(2), pp.323-34.

ENGEL, P., L. J. ZHOU, D. C. ORD, S. SATO, B. KOLLER and T. F. TEDDER. 1995. Abnormal B lymphocyte development, activation, and differentiation in mice that lack or overexpress the CD19 signal transduction molecule. *Immunity,* **3**(1), pp.39-50.

ENGELS, N., L. M. KÖNIG, C. HEEMANN, J. LUTZ, T. TSUBATA, S. GRIEP, V. SCHRADER and J. WIENANDS. 2009. Recruitment of the cytoplasmic adaptor Grb2 to surface IgG and IgE provides antigen receptor-intrinsic costimulation to class-switched B cells. *Nat Immunol,* **10**(9), pp.1018-25.

FEARON, D. T. and M. C. CARROLL. 2000. Regulation of B lymphocyte responses to foreign and self-antigens by the CD19/CD21 complex. *Annu Rev Immunol,* **18**, pp.393-422.

FEARON, D. T. and R. H. CARTER. 1995. The CD19/CR2/TAPA-1 complex of B lymphocytes: linking natural to acquired immunity. *Annu Rev Immunol,* **13**, pp.127-49.

FEDYK, E. R., D. H. RYYAN, I. RITTERMAN and T. A. SPRINGER. 1999. Maturation decreases responsiveness of human bone marrow B lineage cells to stromal-derived factor 1 (SDF-1). *J Leukoc Biol,* **66**(4), pp.667-73.

FERLIN-BEZOMBES, M., M. JOURDAN, J. LIAUTARD, J. BROCHIER, J. F. ROSSI and B. KLEIN. 1998. IFN-alpha is a survival factor for human myeloma cells and reduces dexamethasone-induced apoptosis. *J Immunol,* **161**(6), pp.2692-9.

FERRETTI, E., M. PONZONI, C. DOGLIONI and V. PISTOIA. 2016. IL-17 superfamily cytokines modulate normal germinal center B cell migration. *J Leukoc Biol,* **100**(5), pp.913-918.

FÖRSTER, R., A. SCHUBEL, D. BREITFELD, E. KREMMER, I. RENNER-MÜLLER, E. WOLF and M. LIPP. 1999. CCR7 coordinates the primary immune response by establishing functional microenvironments in secondary lymphoid organs. *Cell,* **99**(1), pp.23-33.

FU, L., Y. C. LIN-LEE, L. V. PHAM, A. TAMAYO, L. YOSHIMURA and R. J. FORD. 2006. Constitutive NF-kappaB and NFAT activation leads to stimulation of the BLyS survival pathway in aggressive B-cell lymphomas. *Blood,* **107**(11), pp.4540-8.

FUJIMOTO, M., Y. FUJIMOTO, J. C. POE, P. J. JANSEN, C. A. LOWELL, A. L. DEFRANCO and T. F. TEDDER. 2000. CD19 regulates Src family protein tyrosine kinase activation in B lymphocytes through processive amplification. *Immunity,* **13**(1), pp.47-57.

FUJIMOTO, M., J. C. POE, A. B. SATTERTHWAITE, M. I. WAHL, O. N. WITTE and T. F. TEDDER. 2002. Complementary roles for CD19 and Bruton's tyrosine kinase in B lymphocyte signal transduction. *J Immunol,* **168**(11), pp.5465-76.

GABAY, C., V. KRENN, C. BOSSHARD, C. A. SEEMAYER, C. CHIZZOLINI and B. HUARD. 2009. Synovial tissues concentrate secreted APRIL. *Arthritis Res Ther,* **11**(5), pR144.

GARCIA-ZEPEDA, E. A., C. COMBADIERE, M. E. ROTHENBERG, M. N. SARAFI, F. LAVIGNE, Q. HAMID, P. M. MURPHY and A. D. LUSTER. 1996. Human monocyte chemoattractant protein (MCP)-4 is a novel CC chemokine with activities on monocytes, eosinophils, and basophils induced in allergic and nonallergic inflammation that signals through the CC chemokine receptors (CCR)-2 and -3. *J Immunol,* **157**(12), pp.5613-26.

GAYET, M., V. LEYMARIE, P. DEROUAULT, E. GUÉRIN, J. VAIDIÉ, V. PASCAL, M. BOULIN, N. DMYTRUK, J. CHAUZEIX, F. TRIMOREAU, N. GACHARD, J. FEUILLARD and D. RIZZO. 2022. Flow cytometry detection of CD138 expression continuum between monotypic B and plasma cells is associated with both high IgM peak levels and MYD88 mutation and contributes to diagnosis of Waldenström macroglobulinemia. *Cytometry B Clin Cytom,* **102**(1), pp.62-69.

GE, Z., B. L. QUEK, K. L. BEEMON and J. R. HOGG. 2016. Polypyrimidine tract binding protein 1 protects mRNAs from recognition by the nonsense-mediated mRNA decay pathway. *Elife,* **5**.

GEISBERGER, R., M. LAMERS and G. ACHATZ. 2006. The riddle of the dual expression of IgM and IgD. *Immunology,* **118**(4), pp.429-37.

GLADUE, R. P., L. A. TYLASKA, W. H. BRISSETTE, P. D. LIRA, J. C. KATH, C. S. POSS, M. F. BROWN, T. J. PARADIS, M. J. CONKLYN, K. T. OGBORNE, M. A. MCGLYNN, B. M. LILLIE, A. P. DIRICO, E. N. MAIRS, E. B. MCELROY, W. H. MARTIN, I. A. STOCK, R. M. SHEPARD, H. J. SHOWELL and K. NEOTE. 2003. CP-481,715, a potent and selective CCR1 antagonist with potential therapeutic implications for inflammatory diseases. *J Biol Chem,* **278**(42), pp.40473-80.

GOZANSKY, E. K., J. M. LOUIS, M. CAFFREY and G. M. CLORE. 2005. Mapping the binding of the N-terminal extracellular tail of the CXCR4 receptor to stromal cell-derived factor-1alpha. *J Mol Biol,* **345**(4), pp.651-8.

GRANDE, F., M. A. OCCHIUZZI, B. RIZZUTI, G. IOELE, M. DE LUCA, P. TUCCI, V. SVICHER, S. AQUARO and A. GAROFALO. 2019. CCR5/CXCR4 Dual Antagonism for the Improvement of HIV Infection Therapy. *Molecules,* **24**(3).

GRANT, S. M., M. LOU, L. YAO, R. N. GERMAIN and A. J. RADTKE. 2020. The lymph node at a glance - how spatial organization optimizes the immune response. *J Cell Sci,* **133**(5).

GRIFFITH, J. W., C. L. SOKOL and A. D. LUSTER. 2014. Chemokines and chemokine receptors: positioning cells for host defense and immunity. *Annu Rev Immunol,* **32**, pp.659-702.

GROOM, J. R., J. RICHMOND, T. T. MUROOKA, E. W. SORENSEN, J. H. SUNG, K. BANKERT, U. H. VON ANDRIAN, J. J. MOON, T. R. MEMPEL and A. D. LUSTER. 2012. CXCR3 chemokine receptor-ligand interactions in the lymph node optimize CD4+ T helper 1 cell differentiation. *Immunity,* **37**(6), pp.1091-103.

GROVES, C. J., J. CARRELL, R. GRADY, B. RAJAN, C. A. MOREHOUSE, R. HALPIN, J. WANG, J. WU, Y. SHRESTHA, R. RAYANKI, R. KOLBECK, Y. WANG and R. HERBST. 2018. CD19-positive antibody-secreting cells provide immune memory. *Blood Adv,* **2**(22), pp.3163-3176.

GUNN, M. D., K. TANGEMANN, C. TAM, J. G. CYSTER, S. D. ROSEN and L. T. WILLIAMS. 1998. A chemokine expressed in lymphoid high endothelial venules promotes the adhesion and chemotaxis of naive T lymphocytes. *Proc Natl Acad Sci U S A,* **95**(1), pp.258-63.

GUSTAVSSON, M. 2020. New insights into the structure and function of chemokine receptor:chemokine complexes from an experimental perspective. *J Leukoc Biol,* **107**(6), pp.1115-1122.

HABERLAND, K., J. A. ACKERMANN, N. IPSEIZ, S. CULEMANN, K. PRACHT, M. ENGLBRECHT, H. M. JACK, G. SCHETT, W. SCHUH and G. KRONKE. 2018. Eosinophils are not essential for maintenance of murine plasma cells in the bone marrow. *Eur J Immunol,* **48**(5), pp.822-828.

HALLILEY, J. L., C. M. TIPTON, J. LIESVELD, A. F. ROSENBERG, J. DARCE, I. V. GREGORETTI, L. POPOVA, D. KAMINISKI, C. F. FUCILE, I. ALBIZUA, S. KYU, K. Y. CHIANG, K. T. BRADLEY, R. BURACK, M. SLIFKA, E. HAMMARLUND, H. WU, L. ZHAO, E. E. WALSH, A. R. FALSEY, T. D. RANDALL, W. C. CHEUNG, I. SANZ and F. E. LEE. 2015. Long-Lived Plasma Cells Are Contained within the CD19(-)CD38(hi)CD138(+) Subset in Human Bone Marrow. *Immunity,* **43**(1), pp.132-45.

HARGREAVES, D. C., P. L. HYMAN, T. T. LU, V. N. NGO, A. BIDGOL, G. SUZUKI, Y. R. ZOU, D. R. LITTMAN and J. G. CYSTER. 2001. A coordinated change in chemokine responsiveness guides plasma cell movements. *J Exp Med,* **194**(1), pp.45-56.

HATZOGLOU, A., J. ROUSSEL, M. F. BOURGEADE, E. ROGIER, C. MADRY, J. INOUE, O. DEVERGNE and A. TSAPIS. 2000. TNF receptor family member BCMA (B cell maturation) associates with TNF receptor-associated factor (TRAF) 1, TRAF2, and TRAF3 and activates NF-kappa B, elk-1, c-Jun N-terminal kinase, and p38 mitogen-activated protein kinase. *J Immunol,* **165**(3), pp.1322-30.

HERNANDEZ, P. A., R. J. GORLIN, J. N. LUKENS, S. TANIUCHI, J. BOHINJEC, F. FRANCOIS, M. E. KLOTMAN and G. A. DIAZ. 2003. Mutations in the chemokine receptor gene CXCR4 are associated with WHIM syndrome, a combined immunodeficiency disease. *Nat Genet,* **34**(1), pp.70-4.

HESSELGESSER, J., H. P. NG, M. LIANG, W. ZHENG, K. MAY, J. G. BAUMAN, S. MONAHAN, I. ISLAM, G. P. WEI, A. GHANNAM, D. D. TAUB, M. ROSSER, R. M. SNIDER, M. M. MORRISSEY, H. D. PEREZ and R. HORUK. 1998. Identification and characterization of small molecule functional antagonists of the CCR1 chemokine receptor. *J Biol Chem,* **273**(25), pp.15687-92.

HICKMAN, H. D., L. LI, G. V. REYNOSO, E. J. RUBIN, C. N. SKON, J. W. MAYS, J. GIBBS, O. SCHWARTZ, J. R. BENNINK and J. W. YEWDELL. 2011. Chemokines control naive CD8+ T cell selection of optimal lymph node antigen presenting cells. *J Exp Med,* **208**(12), pp.2511-24.

HONCZARENKO, M., R. S. DOUGLAS, C. MATHIAS, B. LEE, M. Z. RATAJCZAK and L. E. SILBERSTEIN. 1999. SDF-1 responsiveness does not correlate with CXCR4 expression levels of developing human bone marrow B cells. *Blood,* **94**(9), pp.2990-8.

HORUK, R. 2009. Chemokine receptor antagonists: overcoming developmental hurdles. *Nat Rev Drug Discov,* **8**(1), pp.23-33.

HU, C. C., S. K. DOUGAN, A. M. MCGEHEE, J. C. LOVE and H. L. PLOEGH. 2009. XBP-1 regulates signal transduction, transcription factors and bone marrow colonization in B cells. *EMBO J,* **28**(11), pp.1624-36.

HUANG, C., H. GENG, I. BOSS, L. WANG and A. MELNICK. 2014. Cooperative transcriptional repression by BCL6 and BACH2 in germinal center B-cell differentiation. *Blood,* **123**(7), pp.1012-20.

HUNTER, Z. R., L. XU, G. YANG, Y. ZHOU, X. LIU, Y. CAO, R. J. MANNING, C. TRIPSAS, C. J. PATTERSON, P. SHEEHY and S. P. TREON. 2014. The genomic landscape of Waldenstrom macroglobulinemia is characterized by highly recurring MYD88 and WHIM-like CXCR4 mutations, and small somatic deletions associated with B-cell lymphomagenesis. *Blood,* **123**(11), pp.1637-46.

HUNTER, Z. R., G. YANG, L. XU, X. LIU, J. J. CASTILLO and S. P. TREON. 2017. Genomics, Signaling, and Treatment of Waldenstrom Macroglobulinemia. *J Clin Oncol,* **35**(9), pp.994-1001.

ISE, W. and T. KUROSAKI. 2019. Plasma cell differentiation during the germinal center reaction. *Immunol Rev,* **288**(1), pp.64-74.

JAHANI-ASL, A., A. BASAK and B. K. TSANG. 2007. Caspase-3-mediated cleavage of Akt: involvement of non-consensus sites and influence of phosphorylation. *FEBS Lett,* **581**(16), pp.2883-8.

JIMI, E., R. J. PHILLIPS, M. RINCON, R. VOLL, H. KARASUYAMA, R. FLAVELL and S. GHOSH. 2005. Activation of NF-kappaB promotes the transition of large, CD43+ pre-B cells to small, CD43- pre-B cells. *Int Immunol,* **17**(6), pp.815-25.

KALAYCIO, M. 2009. Bendamustine: a new look at an old drug. *Cancer,* **115**(3), pp.473-9.

KANEGANE, H., K. AGEMATSU, T. FUTATANI, M. M. SIRA, K. SUGA, T. SEKIGUCHI, M. C. VAN ZELM and T. MIYAWAKI. 2007. Novel mutations in a Japanese patient with CD19 deficiency. *Genes Immun,* **8**(8), pp.663-70.

KEPPLER, S. J., F. GASPARRINI, M. BURBAGE, S. AGGARWAL, B. FREDERICO, R. S. GEHA, M. WAY, A. BRUCKBAUER and F. D. BATISTA. 2015. Wiskott-Aldrich Syndrome Interacting Protein Deficiency Uncovers the Role of the Co-receptor CD19 as a Generic Hub for PI3 Kinase Signaling in B Cells. *Immunity,* **43**(4), pp.660-73.

KHODADADI, L., Q. CHENG, A. RADBRUCH and F. HIEPE. 2019. The Maintenance of Memory Plasma Cells. *Front Immunol,* **10**, p721.

KIRSTETTER, P., M. THOMAS, A. DIERICH, P. KASTNER and S. CHAN. 2002. Ikaros is critical for B cell differentiation and function. *Eur J Immunol,* **32**(3), pp.720-30.

KLEIN, U. and R. DALLA-FAVERA. 2008. Germinal centres: role in B-cell physiology and malignancy. *Nat Rev Immunol,* **8**(1), pp.22-33.

KRIANGKUM, J., B. J. TAYLOR, S. P. TREON, M. J. MANT, A. R. BELCH and L. M. PILARSKI. 2004. Clonotypic IgM V/D/J sequence analysis in Waldenstrom macroglobulinemia suggests an unusual B-cell origin and an expansion of polyclonal B cells in peripheral blood. *Blood,* **104**(7), pp.2134-42.

KUBOTA, H., R. NOGUCHI, Y. TOYOSHIMA, Y. OZAKI, S. UDA, K. WATANABE, W. OGAWA and S. KURODA. 2012. Temporal coding of insulin action through multiplexing of the AKT pathway. *Mol Cell,* **46**(6), pp.820-32.

KUFAREVA, I., C. L. SALANGA and T. M. HANDEL. 2015. Chemokine and chemokine receptor structure and interactions: implications for therapeutic strategies. *Immunol Cell Biol,* **93**(4), pp.372-83.

KYLE, R. A., J. BENSON, D. LARSON, T. THERNEAU, A. DISPENZIERI, L. J. MELTON III and S. V. RAJKUMAR. 2009. IgM monoclonal gammopathy of undetermined significance and smoldering Waldenstrom's macroglobulinemia. *Clin Lymphoma Myeloma,* **9**(1), pp.17-8.

KYLE, R. A., S. V. RAJKUMAR, T. M. THERNEAU, D. R. LARSON, M. F. PLEVAK and L. J. MELTON, 3RD. 2005. Prognostic factors and predictors of outcome of immunoglobulin M monoclonal gammopathy of undetermined significance. *Clin Lymphoma,* **5**(4), pp.257-60.

KYRTSONIS, M. C., G. LEVIDOU, P. KORKOLOPOULOU, E. KOULIERIS, V. BARTZI, D. MALTEZAS, G. A. PANGALIS, C. KALPADAKIS, M. DIMOU, G. GEORGIOU, T. P. VASSILAKOPOULOS, M. K. ANGELOPOULOU, V. SALPEAS, P. TSAFTARIDIS, E. PATSOURIS, P. PANAYIOTIDIS and T. K. TZENOU. 2011. CD138 expression helps distinguishing Waldenström's macroglobulinemia

(WM) from splenic marginal zone lymphoma (SMZL). *Clin Lymphoma Myeloma Leuk,* **11**(1), pp.99-102.

LAGANE, B., K. Y. CHOW, K. BALABANIAN, A. LEVOYE, J. HARRIAGUE, T. PLANCHENAULT, F. BALEUX, N. GUNERA-SAAD, F. ARENZANA-SEISDEDOS and F. BACHELERIE. 2008. CXCR4 dimerization and beta-arrestin-mediated signaling account for the enhanced chemotaxis to CXCL12 in WHIM syndrome. *Blood,* **112**(1), pp.34-44.

LAURENT, S. A., F. S. HOFFMANN, P. H. KUHN, Q. CHENG, Y. CHU, M. SCHMIDT-SUPPRIAN, S. M. HAUCK, E. SCHUH, M. KRUMBHOLZ, H. RÜBSAMEN, J. WANNGREN, M. KHADEMI, T. OLSSON, T. ALEXANDER, F. HIEPE, H. W. PFISTER, F. WEBER, D. JENNE, H. WEKERLE, R. HOHLFELD, S. F. LICHTENTHALER and E. MEINL. 2015. γ-Secretase directly sheds the survival receptor BCMA from plasma cells. *Nat Commun,* **6**, p7333.

LEBIEN, T. W. and T. F. TEDDER. 2008. B lymphocytes: how they develop and function. *Blood,* **112**(5), pp.1570-80.

LEE, H. H., H. DADGOSTAR, Q. CHENG, J. SHU and G. CHENG. 1999. NF-kappaB-mediated up-regulation of Bcl-x and Bfl-1/A1 is required for CD40 survival signaling in B lymphocytes. *Proc Natl Acad Sci U S A,* **96**(16), pp.9136-41.

LELEU, X., X. JIA, J. RUNNELS, H. T. NGO, A. S. MOREAU, M. FARAG, J. A. SPENCER, C. M. PITSILLIDES, E. HATJIHARISSI, A. ROCCARO, G. O'SULLIVAN, D. W. MCMILLIN, D. MORENO, T. KIZILTEPE, R. CARRASCO, S. P. TREON, T. HIDESHIMA, K. C. ANDERSON, C. P. LIN and I. M. GHOBRIAL. 2007. The Akt pathway regulates survival and homing in Waldenstrom macroglobulinemia. *Blood,* **110**(13), pp.4417-26.

LEONI, L. M., B. BAILEY, J. REIFERT, H. H. BENDALL, R. W. ZELLER, J. CORBEIL, G. ELLIOTT and C. C. NIEMEYER. 2008. Bendamustine (Treanda) displays a distinct pattern of cytotoxicity and unique mechanistic features compared with other alkylating agents. *Clin Cancer Res,* **14**(1), pp.309-17.

LEY, R., K. BALMANNO, K. HADFIELD, C. WESTON and S. J. COOK. 2003. Activation of the ERK1/2 signaling pathway promotes phosphorylation and proteasome-dependent degradation of the BH3-only protein, Bim. *J Biol Chem,* **278**(21), pp.18811-6.

LI, X. and R. H. CARTER. 1998. Convergence of CD19 and B cell antigen receptor signals at MEK1 in the ERK2 activation cascade. *J Immunol,* **161**(11), pp.5901-8.

LI, X. and R. H. CARTER. 2000. CD19 signal transduction in normal human B cells: linkage to downstream pathways requires phosphatidylinositol 3-kinase, protein kinase C and Ca2+. *Eur J Immunol,* **30**(6), pp.1576-86.

LIAN, J. and A. D. LUSTER. 2015. Chemokine-guided cell positioning in the lymph node orchestrates the generation of adaptive immune responses. *Curr Opin Cell Biol,* **36**, pp.1-6.

LIGHTMAN, S. M., A. UTLEY and K. P. LEE. 2019. Survival of Long-Lived Plasma Cells (LLPC): Piecing Together the Puzzle. *Front Immunol,* **10**, p965.

LIN, K. I., C. ANGELIN-DUCLOS, T. C. KUO and K. CALAME. 2002. Blimp-1-dependent repression of Pax-5 is required for differentiation of B cells to immunoglobulin M-secreting plasma cells. *Mol Cell Biol,* **22**(13), pp.4771-80.

LIN, K. I., Y. LIN and K. CALAME. 2000. Repression of c-myc is necessary but not sufficient for terminal differentiation of B lymphocytes in vitro. *Mol Cell Biol,* **20**(23), pp.8684-95.

LIN, L., A. J. GERTH and S. L. PENG. 2004. Active inhibition of plasma cell development in resting B cells by microphthalmia-associated transcription factor. *J Exp Med,* **200**(1), pp.115-22.

LIU, Q., H. CHEN, T. OJODE, X. GAO, S. ANAYA-O'BRIEN, N. A. TURNER, J. ULRICK, R. DECASTRO, C. KELLY, A. R. CARDONES, S. H. GOLD, E. I. HWANG, D. S. WECHSLER, H. L. MALECH, P. M. MURPHY and D. H. MCDERMOTT. 2012. WHIM syndrome caused by a single amino acid substitution in the carboxy-tail of chemokine receptor CXCR4. *Blood,* **120**(1), pp.181-9.

LIU, T., X. LI, S. YOU, S. S. BHUYAN and L. DONG. 2015. Effectiveness of AMD3100 in treatment of leukemia and solid tumors: from original discovery to use in current clinical practice. *Exp Hematol Oncol,* **5**, p19.

LIU, Y. J., C. BARTHÉLÉMY, O. DE BOUTEILLER, C. ARPIN, I. DURAND and J. BANCHEREAU. 1995. Memory B cells from human tonsils colonize mucosal epithelium and directly present antigen to T cells by rapid up-regulation of B7-1 and B7-2. *Immunity,* **2**(3), pp.239-48.

LÓPEZ-OREJA, I., H. PLAYA-ALBINYANA, F. ARENAS, M. LÓPEZ-GUERRA and D. COLOMER. 2021. Challenges with Approved Targeted Therapies against Recurrent Mutations in CLL: A Place for New Actionable Targets. *Cancers (Basel),* **13**(13).

LUO, J., J. M. BUSILLO, R. STUMM and J. L. BENOVIC. 2017. G Protein-Coupled Receptor Kinase 3 and Protein Kinase C Phosphorylate the Distal C-Terminal Tail of the Chemokine Receptor CXCR4 and Mediate Recruitment of β-Arrestin. *Mol Pharmacol,* **91**(6), pp.554-566.

LUO, W., W. HAWSE, L. CONTER, N. TRIVEDI, F. WEISEL, D. WIKENHEISER, R. T. CATTLEY and M. J. SHLOMCHIK. 2019. The AKT kinase signaling network is rewired by PTEN to control proximal BCR signaling in germinal center B cells. *Nat Immunol,* **20**(6), pp.736-746.

LUSTER, A. D. 1998. Chemokines--chemotactic cytokines that mediate inflammation. *N Engl J Med,* **338**(7), pp.436-45.

MACKAY, F., P. SCHNEIDER, P. RENNERT and J. BROWNING. 2003. BAFF AND APRIL: a tutorial on B cell survival. *Annu Rev Immunol,* **21**, pp.231-64.

MAHTOUK, K., F. W. CREMER, T. RÈME, M. JOURDAN, M. BAUDARD, J. MOREAUX, G. REQUIRAND, G. FIOL, J. DE VOS, M. MOOS, P. QUITTET, H. GOLDSCHMIDT, J. F. ROSSI, D. HOSE and B. KLEIN. 2006. Heparan sulphate proteoglycans are essential for the myeloma cell growth activity of EGF-family ligands in multiple myeloma. *Oncogene,* **25**(54), pp.7180-91.

MAILANKODY, S. and O. LANDGREN. 2016. Monoclonal gammopathy of undetermined significance and Waldenstrom's macroglobulinemia. *Best Pract Res Clin Haematol,* **29**(2), pp.187-193.

MAITY, P. C., M. DATTA, A. NICOLÒ and H. JUMAA. 2018. Isotype Specific Assembly of B Cell Antigen Receptors and Synergism With Chemokine Receptor CXCR4. *Front Immunol,* **9**, p2988.

MALUMBRES, M., I. PÉREZ DE CASTRO, M. I. HERNÁNDEZ, M. JIMÉNEZ, T. CORRAL and A. PELLICER. 2000. Cellular response to oncogenic ras involves induction of the Cdk4 and Cdk6 inhibitor p15(INK4b). *Mol Cell Biol,* **20**(8), pp.2915-25.

MANNING, B. D. and A. TOKER. 2017. AKT/PKB Signaling: Navigating the Network. *Cell,* **169**(3), pp.381-405.

MARTIN-FONTECHA, A., S. SEBASTIANI, U. E. HÖPKEN, M. UGUCCIONI, M. LIPP, A. LANZAVECCHIA and F. SALLUSTO. 2003. Regulation of dendritic cell migration to the draining lymph node: impact on T lymphocyte traffic and priming. *J Exp Med,* **198**(4), pp.615-21.

MARTIN, F., A. M. OLIVER and J. F. KEARNEY. 2001. Marginal zone and B1 B cells unite in the early response against T-independent blood-borne particulate antigens. *Immunity,* **14**(5), pp.617-29.

MATHIAN, A., M. GALLEGOS, V. PASCUAL, J. BANCHEREAU and S. KOUTOUZOV. 2011. Interferon-α induces unabated production of short-lived plasma cells in pre-autoimmune lupus-prone (NZB×NZW)F1 mice but not in BALB/c mice. *Eur J Immunol,* **41**(3), pp.863-72.

MATTHEWS, T., M. SALGO, M. GREENBERG, J. CHUNG, R. DEMASI and D. BOLOGNESI. 2004. Enfuvirtide: the first therapy to inhibit the entry of HIV-1 into host CD4 lymphocytes. *Nat Rev Drug Discov,* **3**(3), pp.215-25.

MCCARRON, M. J., P. W. PARK and D. R. FOOKSMAN. 2017. CD138 mediates selection of mature plasma cells by regulating their survival. *Blood,* **129**(20), pp.2749-2759.

MCDERMOTT, D. H. and P. M. MURPHY. 2019. WHIM syndrome: Immunopathogenesis, treatment and cure strategies. *Immunol Rev,* **287**(1), pp.91-102.

MCHEIK, S., N. VAN EECKHOUT, C. DE POORTER, C. GALÉS, M. PARMENTIER and J. Y. SPRINGAEL. 2019. Coexpression of CCR7 and CXCR4 During B Cell Development Controls CXCR4 Responsiveness and Bone Marrow Homing. *Front Immunol,* **10**, p2970.

MEI, H. E., I. WIRRIES, D. FRÖLICH, M. BRISSLERT, C. GIESECKE, J. R. GRÜN, T. ALEXANDER, S. SCHMIDT, K. LUDA, A. A. KÜHL, R. ENGELMANN, M. DÜRR, T. SCHEEL, M. BOKAREWA, C.

PERKA, A. RADBRUCH and T. DÖRNER. 2015. A unique population of IgG-expressing plasma cells lacking CD19 is enriched in human bone marrow. *Blood,* **125**(11), pp.1739-48.

MENDOZA, M. C., E. E. ER and J. BLENIS. 2011. The Ras-ERK and PI3K-mTOR pathways: cross-talk and compensation. *Trends Biochem Sci,* **36**(6), pp.320-8.

MESIN, L., J. ERSCHING and G. D. VICTORA. 2016. Germinal Center B Cell Dynamics. *Immunity,* **45**(3), pp.471-482.

MIKULASOVA, A., C. P. WARDELL, A. MURISON, E. M. BOYLE, G. H. JACKSON, J. SMETANA, Z. KUFOVA, L. POUR, V. SANDECKA, M. ALMASI, P. VSIANSKA, E. GREGORA, P. KUGLIK, R. HAJEK, F. E. DAVIES, G. J. MORGAN and B. A. WALKER. 2017. The spectrum of somatic mutations in monoclonal gammopathy of undetermined significance indicates a less complex genomic landscape than that in multiple myeloma. *Haematologica,* **102**(9), pp.1617-1625.

MILANESI, S., M. LOCATI and E. M. BORRONI. 2020. Aberrant CXCR4 Signaling at Crossroad of WHIM Syndrome and Waldenstrom's Macroglobulinemia. *Int J Mol Sci,* **21**(16).

MINGES WOLS, H. A., G. H. UNDERHILL, G. S. KANSAS and P. L. WITTE. 2002. The role of bone marrow-derived stromal cells in the maintenance of plasma cell longevity. *J Immunol,* **169**(8), pp.4213-21.

MIRANDOLA, L., L. APICELLA, M. COLOMBO, Y. YU, D. G. BERTA, N. PLATONOVA, E. LAZZARI, M. LANCELLOTTI, G. BULFAMANTE, E. COBOS, M. CHIRIVA-INTERNATI and R. CHIARAMONTE. 2013. Anti-Notch treatment prevents multiple myeloma cells localization to the bone marrow via the chemokine system CXCR4/SDF-1. *Leukemia,* **27**(7), pp.1558-66.

MØLLER, A. S., R. OVSTEBØ, K. B. HAUG, G. B. JOØ, A. B. WESTVIK and P. KIERULF. 2005. Chemokine production and pattern recognition receptor (PRR) expression in whole blood stimulated with pathogen-associated molecular patterns (PAMPs). *Cytokine,* **32**(6), pp.304-15.

MORBACH, H., J. N. SCHICKEL, C. CUNNINGHAM-RUNDLES, M. E. CONLEY, I. REISLI, J. L. FRANCO and E. MEFFRE. 2016. CD19 controls Toll-like receptor 9 responses in human B cells. *J Allergy Clin Immunol,* **137**(3), pp.889-98.e6.

MOREAUX, J., A. C. SPRYNSKI, S. R. DILLON, K. MAHTOUK, M. JOURDAN, A. YTHIER, P. MOINE, N. ROBERT, E. JOURDAN, J. F. ROSSI and B. KLEIN. 2009. APRIL and TACI interact with syndecan-1 on the surface of multiple myeloma cells to form an essential survival loop. *Eur J Haematol,* **83**(2), pp.119-29.

MUEHLINGHAUS, G., L. CIGLIANO, S. HUEHN, A. PEDDINGHAUS, H. LEYENDECKERS, A. E. HAUSER, F. HIEPE, A. RADBRUCH, S. ARCE and R. A. MANZ. 2005. Regulation of CXCR3 and CXCR4 expression during terminal differentiation of memory B cells into plasma cells. *Blood,* **105**(10), pp.3965-71.

MURPHY, L. O., S. SMITH, R. H. CHEN, D. C. FINGAR and J. BLENIS. 2002. Molecular interpretation of ERK signal duration by immediate early gene products. *Nat Cell Biol,* **4**(8), pp.556-64.

MUTO, A., K. OCHIAI, Y. KIMURA, A. ITOH-NAKADAI, K. L. CALAME, D. IKEBE, S. TASHIRO and K. IGARASHI. 2010. Bach2 represses plasma cell gene regulatory network in B cells to promote antibody class switch. *Embo j,* **29**(23), pp.4048-61.

NEPTUNE, E. R. and H. R. BOURNE. 1997. Receptors induce chemotaxis by releasing the betagamma subunit of Gi, not by activating Gq or Gs. *Proc Natl Acad Sci U S A,* **94**(26), pp.14489-94.

NERA, K. P., P. KOHONEN, E. NARVI, A. PEIPPO, L. MUSTONEN, P. TERHO, K. KOSKELA, J. M. BUERSTEDDE and O. LASSILA. 2006. Loss of Pax5 promotes plasma cell differentiation. *Immunity,* **24**(3), pp.283-93.

NGO, H. T., X. LELEU, J. LEE, X. JIA, M. MELHEM, J. RUNNELS, A. S. MOREAU, N. BURWICK, A. K. AZAB, A. ROCCARO, F. AZAB, A. SACCO, M. FARAG, R. SACKSTEIN and I. M. GHOBRIAL. 2008. SDF-1/CXCR4 and VLA-4 interaction regulates homing in Waldenstrom macroglobulinemia. *Blood,* **112**(1), pp.150-8.

NIE, Y., J. WAITE, F. BREWER, M. J. SUNSHINE, D. R. LITTMAN and Y. R. ZOU. 2004. The role of CXCR4 in maintaining peripheral B cell compartments and humoral immunity. *J Exp Med,* **200**(9), pp.1145-56.

NIETO, M., J. M. FRADE, D. SANCHO, M. MELLADO, A. C. MARTINEZ and F. SÁNCHEZ-MADRID. 1997. Polarization of chemokine receptors to the leading edge during lymphocyte chemotaxis. *J Exp Med,* **186**(1), pp.153-8.

NUTT, S. L., N. TAUBENHEIM, J. HASBOLD, L. M. CORCORAN and P. D. HODGKIN. 2011. The genetic network controlling plasma cell differentiation. *Semin Immunol,* **23**(5), pp.341-9.

O'CONNOR, B. P., V. S. RAMAN, L. D. ERICKSON, W. J. COOK, L. K. WEAVER, C. AHONEN, L. L. LIN, G. T. MANTCHEV, R. J. BRAM and R. J. NOELLE. 2004. BCMA is essential for the survival of long-lived bone marrow plasma cells. *J Exp Med,* **199**(1), pp.91-8.

OCHIAI, K., Y. KATOH, T. IKURA, Y. HOSHIKAWA, T. NODA, H. KARASUYAMA, S. TASHIRO, A. MUTO and K. IGARASHI. 2006. Plasmacytic transcription factor Blimp-1 is repressed by Bach2 in B cells. *J Biol Chem,* **281**(50), pp.38226-34.

OCHIAI, K., M. MAIENSCHEIN-CLINE, G. SIMONETTI, J. CHEN, R. ROSENTHAL, R. BRINK, A. S. CHONG, U. KLEIN, A. R. DINNER, H. SINGH and R. SCIAMMAS. 2013. Transcriptional regulation of germinal center B and plasma cell fates by dynamical control of IRF4. *Immunity,* **38**(5), pp.918-29.

OKKENHAUG, K., A. BILANCIO, G. FARJOT, H. PRIDDLE, S. SANCHO, E. PESKETT, W. PEARCE, S. E. MEEK, A. SALPEKAR, M. D. WATERFIELD, A. J. SMITH and B. VANHAESEBROECK. 2002. Impaired B and T cell antigen receptor signaling in p110delta PI 3-kinase mutant mice. *Science,* **297**(5583), pp.1031-4.

ORLANDO, E. J., X. HAN, C. TRIBOULEY, P. A. WOOD, R. J. LEARY, M. RIESTER, J. E. LEVINE, M. QAYED, S. A. GRUPP, M. BOYER, B. DE MOERLOOSE, E. R. NEMECEK, H. BITTENCOURT, H. HIRAMATSU, J. BUECHNER, S. M. DAVIES, M. R. VERNERIS, K. NGUYEN, J. L. BROGDON, H. BITTER, M. MORRISSEY, P. PIEROG, S. PANTANO, J. A. ENGELMAN and W. WINCKLER. 2018. Genetic mechanisms of target antigen loss in CAR19 therapy of acute lymphoblastic leukemia. *Nat Med,* **24**(10), pp.1504-1506.

ORSINI, M. J., J. L. PARENT, S. J. MUNDELL, A. MARCHESE and J. L. BENOVIC. 1999. Trafficking of the HIV coreceptor CXCR4. Role of arrestins and identification of residues in the c-terminal tail that mediate receptor internalization. *J Biol Chem,* **274**(43), pp.31076-86.

OWEN, R. G., S. P. TREON, A. AL-KATIB, R. FONSECA, P. R. GREIPP, M. L. MCMASTER, E. MORRA, G. A. PANGALIS, J. F. SAN MIGUEL, A. R. BRANAGAN and M. A. DIMOPOULOS. 2003. Clinicopathological definition of Waldenstrom's macroglobulinemia: consensus panel recommendations from the Second International Workshop on Waldenstrom's Macroglobulinemia. *Semin Oncol,* **30**(2), pp.110-5.

OZGA, A. J., M. T. CHOW and A. D. LUSTER. 2021. Chemokines and the immune response to cancer. *Immunity,* **54**(5), pp.859-874.

PAL SINGH, S., F. DAMMEIJER and R. W. HENDRIKS. 2018. Role of Bruton's tyrosine kinase in B cells and malignancies. *Mol Cancer,* **17**(1), p57.

PAL SINGH, S., F. DAMMEIJER and R. W. HENDRIKS. 2019. Correction to: Role of Bruton's tyrosine kinase in B cells and malignancies. *Mol Cancer,* **18**(1), p79.

PALMESINO, E., B. MOEPPS, P. GIERSCHIK and M. THELEN. 2006. Differences in CXCR4-mediated signaling in B cells. *Immunobiology,* **211**(5), pp.377-89.

PALUDO, J., J. P. ABEYKOON, A. SHREDERS, S. M. ANSELL, S. KUMAR, S. AILAWADHI, R. L. KING, A. B. KOEHLER, C. B. REEDER, F. K. BUADI, A. DISPENZIERI, M. Q. LACY, D. DINGLI, T. E. WITZIG, R. S. GO, W. I. GONSALVES, T. KOURELIS, R. WARSAME, N. LEUNG, T. M. HABERMANN, S. HAYMAN, Y. LIN, R. A. KYLE, S. V. RAJKUMAR, M. A. GERTZ and P. KAPOOR. 2018. Bendamustine and rituximab (BR) versus dexamethasone, rituximab, and cyclophosphamide (DRC) in patients with Waldenstrom macroglobulinemia. *Ann Hematol,* **97**(8), pp.1417-1425.

PAVLASOVA, G., M. BORSKY, V. SEDA, K. CERNA, J. OSICKOVA, M. DOUBEK, J. MAYER, R. CALOGERO, M. TRBUSEK, S. POSPISILOVA, M. S. DAVIDS, T. J. KIPPS, J. R. BROWN and M. MRAZ. 2016. Ibrutinib inhibits CD20 upregulation on CLL B cells mediated by the CXCR4/SDF-1 axis. *Blood,* **128**(12), pp.1609-13.

PAVLASOVA, G., M. BORSKY, V. SVOBODOVA, J. OPPELT, K. CERNA, J. NOVOTNA, V. SEDA, M. FOJTOVA, J. FAJKUS, Y. BRYCHTOVA, M. DOUBEK, S. POSPISILOVA, J. MAYER and M. MRAZ. 2018. Rituximab primarily targets an intra-clonal BCR signaling proficient CLL subpopulation characterized by high CD20 levels. *Leukemia,* **32**(9), pp.2028-2031.

PENELA, P., J. INSERTE, P. RAMOS, A. RODRIGUEZ-SINOVAS, D. GARCIA-DORADO and F. MAYOR, JR. 2019. Degradation of GRK2 and AKT is an early and detrimental event in myocardial ischemia/reperfusion. *EBioMedicine,* **48**, pp.605-618.

PEPERZAK, V., I. VIKSTRÖM, J. WALKER, S. P. GLASER, M. LEPAGE, C. M. COQUERY, L. D. ERICKSON, K. FAIRFAX, F. MACKAY, A. STRASSER, S. L. NUTT and D. M. TARLINTON. 2013. Mcl-1 is essential for the survival of plasma cells. *Nat Immunol,* **14**(3), pp.290-7.

PETRIE, R. J. and J. P. DEANS. 2002. Colocalization of the B cell receptor and CD20 followed by activation-dependent dissociation in distinct lipid rafts. *J Immunol,* **169**(6), pp.2886-91.

POLYAK, M. J., H. LI, N. SHARIAT and J. P. DEANS. 2008. CD20 homo-oligomers physically associate with the B cell antigen receptor. Dissociation upon receptor engagement and recruitment of phosphoproteins and calmodulin-binding proteins. *J Biol Chem,* **283**(27), pp.18545-52.

PORSTNER, M., R. WINKELMANN, P. DAUM, J. SCHMID, K. PRACHT, J. CÔRTE-REAL, S. SCHREIBER, C. HAFTMANN, A. BRANDL, M. F. MASHREGHI, K. GELSE, M. HAUKE, I. WIRRIES, M. ZWICK, E. ROTH, A. RADBRUCH, J. WITTMANN and H. M. JÄCK. 2015. miR-148a promotes plasma cell differentiation and targets the germinal center transcription factors Mitf and Bach2. *Eur J Immunol,* **45**(4), pp.1206-15.

POULAIN, S., C. ROUMIER, A. DECAMBRON, A. RENNEVILLE, C. HERBAUX, E. BERTRAND, S. TRICOT, A. DAUDIGNON, S. GALIEGUE-ZOUITINA, V. SOENEN, O. THEISEN, N. GRARDEL, O. NIBOUREL, C. ROCHE-LESTIENNE, B. QUESNEL, P. DUTHILLEUL, C. PREUDHOMME and X. LELEU. 2013. MYD88 L265P mutation in Waldenstrom macroglobulinemia. *Blood,* **121**(22), pp.4504-11.

POULAIN, S., C. ROUMIER, A. VENET-CAILLAULT, M. FIGEAC, C. HERBAUX, G. MAROT, E. DOYE, E. BERTRAND, S. GEFFROY, F. LEPRETRE, O. NIBOUREL, A. DECAMBRON, E. M. BOYLE, A. RENNEVILLE, S. TRICOT, A. DAUDIGNON, B. QUESNEL, P. DUTHILLEUL, C. PREUDHOMME and X. LELEU. 2016. Genomic Landscape of CXCR4 Mutations in Waldenström Macroglobulinemia. *Clin Cancer Res,* **22**(6), pp.1480-8.

POZZOBON, T., G. GOLDONI, A. VIOLA and B. MOLON. 2016. CXCR4 signaling in health and disease. *Immunol Lett,* **177**, pp.6-15.

PUMIGLIA, K. M. and S. J. DECKER. 1997. Cell cycle arrest mediated by the MEK/mitogen-activated protein kinase pathway. *Proc Natl Acad Sci U S A,* **94**(2), pp.448-52.

RAMADANI, F., D. J. BOLLAND, F. GARCON, J. L. EMERY, B. VANHAESEBROECK, A. E. CORCORAN and K. OKKENHAUG. 2010. The PI3K isoforms p110alpha and p110delta are essential for pre-B cell receptor signaling and B cell development. *Sci Signal,* **3**(134), pra60.

REIF, K., K. OKKENHAUG, T. SASAKI, J. M. PENNINGER, B. VANHAESEBROECK and J. G. CYSTER. 2004. Cutting edge: differential roles for phosphoinositide 3-kinases, p110gamma and p110delta, in lymphocyte chemotaxis and homing. *J Immunol,* **173**(4), pp.2236-40.

REIMOLD, A. M., N. N. IWAKOSHI, J. MANIS, P. VALLABHAJOSYULA, E. SZOMOLANYI-TSUDA, E. M. GRAVALLESE, D. FRIEND, M. J. GRUSBY, F. ALT and L. H. GLIMCHER. 2001. Plasma cell differentiation requires the transcription factor XBP-1. *Nature,* **412**(6844), pp.300-7.

RICKERT, R. C., K. RAJEWSKY and J. ROES. 1995. Impairment of T-cell-dependent B-cell responses and B-1 cell development in CD19-deficient mice. *Nature,* **376**(6538), pp.352-5.

ROSS, G. D., M. J. POLLEY, E. M. RABELLINO and H. M. GREY. 1973. Two different complement receptors on human lymphocytes. One specific for C3b and one specific for C3b inactivator-cleaved C3b. *J Exp Med,* **138**(4), pp.798-811.

ROT, A. and U. H. VON ANDRIAN. 2004. Chemokines in innate and adaptive host defense: basic chemokinese grammar for immune cells. *Annu Rev Immunol,* **22**, pp.891-928.

SAHOTA, S. S., F. FORCONI, C. H. OTTENSMEIER, D. PROVAN, D. G. OSCIER, T. J. HAMBLIN and F. K. STEVENSON. 2002. Typical Waldenstrom macroglobulinemia is derived from a B-cell arrested after cessation of somatic mutation but prior to isotype switch events. *Blood,* **100**(4), pp.1505-7.

SAITO, M., J. GAO, K. BASSO, Y. KITAGAWA, P. M. SMITH, G. BHAGAT, A. PERNIS, L. PASQUALUCCI and R. DALLA-FAVERA. 2007. A signaling pathway mediating downregulation of BCL6 in germinal center B cells is blocked by BCL6 gene alterations in B cell lymphoma. *Cancer Cell,* **12**(3), pp.280-92.

SAPOZNIKOV, A., Y. PEWZNER-JUNG, V. KALCHENKO, R. KRAUTHGAMER, I. SHACHAR and S. JUNG. 2008. Perivascular clusters of dendritic cells provide critical survival signals to B cells in bone marrow niches. *Nat Immunol,* **9**(4), pp.388-95.

SATO, S., P. J. JANSEN and T. F. TEDDER. 1997. CD19 and CD22 expression reciprocally regulates tyrosine phosphorylation of Vav protein during B lymphocyte signaling. *Proc Natl Acad Sci U S A,* **94**(24), pp.13158-62.

SCHMITT, C., C. TONNELLE, A. DALLOUL, C. CHABANNON, P. DEBRÉ and A. REBOLLO. 2002. Aiolos and Ikaros: regulators of lymphocyte development, homeostasis and lymphoproliferation. *Apoptosis,* **7**(3), pp.277-84.

SCHOLS, D., S. STRUYF, J. VAN DAMME, J. A. ESTÉ, G. HENSON and E. DE CLERCQ. 1997. Inhibition of T-tropic HIV strains by selective antagonization of the chemokine receptor CXCR4. *J Exp Med,* **186**(8), pp.1383-8.

SCIAMMAS, R., A. L. SHAFFER, J. H. SCHATZ, H. ZHAO, L. M. STAUDT and H. SINGH. 2006. Graded expression of interferon regulatory factor-4 coordinates isotype switching with plasma cell differentiation. *Immunity,* **25**(2), pp.225-36.

SECCHIERO, P., R. VOLTAN, E. RIMONDI, E. MELLONI, E. ATHANASAKIS, V. TISATO, S. GALLO, G. M. RIGOLIN and G. ZAULI. 2017. The γ-secretase inhibitors enhance the anti-leukemic activity of ibrutinib in B-CLL cells. *Oncotarget,* **8**(35), pp.59235-59245.

SEWING, A., B. WISEMAN, A. C. LLOYD and H. LAND. 1997. High-intensity Raf signal causes cell cycle arrest mediated by p21Cip1. *Mol Cell Biol,* **17**(9), pp.5588-97.

SHAFFER, A. L., K. I. LIN, T. C. KUO, X. YU, E. M. HURT, A. ROSENWALD, J. M. GILTNANE, L. YANG, H. ZHAO, K. CALAME and L. M. STAUDT. 2002. Blimp-1 orchestrates plasma cell differentiation by extinguishing the mature B cell gene expression program. *Immunity,* **17**(1), pp.51-62.

SHAFFER, A. L., M. SHAPIRO-SHELEF, N. N. IWAKOSHI, A. H. LEE, S. B. QIAN, H. ZHAO, X. YU, L. YANG, B. K. TAN, A. ROSENWALD, E. M. HURT, E. PETROULAKIS, N. SONENBERG, J. W. YEWDELL, K. CALAME, L. H. GLIMCHER and L. M. STAUDT. 2004. XBP1, downstream of Blimp-1, expands the secretory apparatus and other organelles, and increases protein synthesis in plasma cell differentiation. *Immunity,* **21**(1), pp.81-93.

SHAFFER, A. L., X. YU, Y. HE, J. BOLDRICK, E. P. CHAN and L. M. STAUDT. 2000. BCL-6 represses genes that function in lymphocyte differentiation, inflammation, and cell cycle control. *Immunity,* **13**(2), pp.199-212.

SHAPIRO-SHELEF, M., K. I. LIN, L. J. MCHEYZER-WILLIAMS, J. LIAO, M. G. MCHEYZER-WILLIAMS and K. CALAME. 2003. Blimp-1 is required for the formation of immunoglobulin secreting plasma cells and pre-plasma memory B cells. *Immunity,* **19**(4), pp.607-20.

SHINNAKASU, R., T. INOUE, K. KOMETANI, S. MORIYAMA, Y. ADACHI, M. NAKAYAMA, Y. TAKAHASHI, H. FUKUYAMA, T. OKADA and T. KUROSAKI. 2016. Regulated selection of germinal-center cells into the memory B cell compartment. *Nat Immunol,* **17**(7), pp.861-9.

SHINNAKASU, R. and T. KUROSAKI. 2017. Regulation of memory B and plasma cell differentiation. *Curr Opin Immunol,* **45**, pp.126-131.

SHRIMPTON, J., M. A. CARE, J. CARMICHAEL, K. WALKER, P. EVANS, C. EVANS, R. DE TUTE, R. OWEN, R. M. TOOZE and G. M. DOODY. 2020. TLR-mediated activation of Waldenström

macroglobulinemia B cells reveals an uncoupling from plasma cell differentiation. *Blood Adv,* **4**(12), pp.2821-2836.

SIDWELL, T. and A. KALLIES. 2016. Bach2 is required for B cell and T cell memory differentiation. *Nat Immunol,* **17**(7), pp.744-5.

SIGNORET, N., M. M. ROSENKILDE, P. J. KLASSE, T. W. SCHWARTZ, M. H. MALIM, J. A. HOXIE and M. MARSH. 1998. Differential regulation of CXCR4 and CCR5 endocytosis. *J Cell Sci,* **111 (Pt 18)**, pp.2819-30.

STEBEGG, M., S. D. KUMAR, A. SILVA-CAYETANO, V. R. FONSECA, M. A. LINTERMAN and L. GRACA. 2018. Regulation of the Germinal Center Response. *Front Immunol,* **9**, p2469.

STEPHENSON, S., M. A. CARE, G. M. DOODY and R. M. TOOZE. 2021. APRIL drives a co-ordinated but diverse response as a foundation for plasma cell longevity. p2021.06.15.448496.

STEPHENSON, S., M. A. CARE, I. FAN, A. ZOUGMAN, D. R. WESTHEAD, G. M. DOODY and R. M. TOOZE. 2019. Growth Factor-like Gene Regulation Is Separable from Survival and Maturation in Antibody-Secreting Cells. *J Immunol,* **202**(4), pp.1287-1300.

SUAN, D., C. SUNDLING and R. BRINK. 2017. Plasma cell and memory B cell differentiation from the germinal center. *Curr Opin Immunol,* **45**, pp.97-102.

SUNG, J. H., H. ZHANG, E. A. MOSEMAN, D. ALVAREZ, M. IANNACONE, S. E. HENRICKSON, J. C. DE LA TORRE, J. R. GROOM, A. D. LUSTER and U. H. VON ANDRIAN. 2012. Chemokine guidance of central memory T cells is critical for antiviral recall responses in lymph nodes. *Cell,* **150**(6), pp.1249-63.

SUZUKI, Y., M. RAHMAN and H. MITSUYA. 2001. Diverse transcriptional response of CD4+ T cells to stromal cell-derived factor SDF-1: cell survival promotion and priming effects of SDF-1 on CD4+ T cells. *J Immunol,* **167**(6), pp.3064-73.

TAMAMIS, P. and C. A. FLOUDAS. 2014. Molecular recognition of CCR5 by an HIV-1 gp120 V3 loop. *PLoS One,* **9**(4), pe95767.

TANGYE, S. G., Y. J. LIU, G. AVERSA, J. H. PHILLIPS and J. E. DE VRIES. 1998. Identification of functional human splenic memory B cells by expression of CD148 and CD27. *J Exp Med,* **188**(9), pp.1691-703.

TANGYE, S. G. and D. M. TARLINTON. 2009. Memory B cells: effectors of long-lived immune responses. *Eur J Immunol,* **39**(8), pp.2065-75.

TARLINTON, D., A. RADBRUCH, F. HIEPE and T. DORNER. 2008. Plasma cell differentiation and survival. *Curr Opin Immunol,* **20**(2), pp.162-9.

TEDDER, T. F., M. INAOKI and S. SATO. 1997. The CD19-CD21 complex regulates signal transduction thresholds governing humoral immunity and autoimmunity. *Immunity,* **6**(2), pp.107-18.

TEICHER, B. A. and S. P. FRICKER. 2010. CXCL12 (SDF-1)/CXCR4 pathway in cancer. *Clin Cancer Res,* **16**(11), pp.2927-31.

TENG, Y. H., R. S. AQUINO and P. W. PARK. 2012. Molecular functions of syndecan-1 in disease. *Matrix Biol,* **31**(1), pp.3-16.

TODD, D. J., L. J. MCHEYZER-WILLIAMS, C. KOWAL, A. H. LEE, B. T. VOLPE, B. DIAMOND, M. G. MCHEYZER-WILLIAMS and L. H. GLIMCHER. 2009. XBP1 governs late events in plasma cell differentiation and is not required for antigen-specific memory B cell development. *J Exp Med,* **206**(10), pp.2151-9.

TOKOYODA, K., T. EGAWA, T. SUGIYAMA, B. I. CHOI and T. NAGASAWA. 2004. Cellular niches controlling B lymphocyte behavior within bone marrow during development. *Immunity,* **20**(6), pp.707-18.

TREON, S. P., Y. CAO, L. XU, G. YANG, X. LIU and Z. R. HUNTER. 2014. Somatic mutations in MYD88 and CXCR4 are determinants of clinical presentation and overall survival in Waldenstrom macroglobulinemia. *Blood,* **123**(18), pp.2791-6.

TREON, S. P., C. K. TRIPSAS, K. MEID, D. WARREN, G. VARMA, R. GREEN, K. V. ARGYROPOULOS, G. YANG, Y. CAO, L. XU, C. J. PATTERSON, S. RODIG, J. L. ZEHNDER, J. C. ASTER, N. L. HARRIS, S. KANAN, I. GHOBRIAL, J. J. CASTILLO, J. P. LAUBACH, Z. R. HUNTER, Z. SALMAN, J. LI, M.

CHENG, F. CLOW, T. GRAEF, M. L. PALOMBA and R. H. ADVANI. 2015. Ibrutinib in previously treated Waldenström's macroglobulinemia. *N Engl J Med,* **372**(15), pp.1430-40.

TREON, S. P., C. K. TRIPSAS, G. YANG, Y. CAO, L. XU, Z. HUNTER, S. J. CROPPER, P. MOSTYN, K. MEID, D. WARREN, C. PATTERSON, G. VARMA, J. P. LAUBACH, C. E. PABA-PRADA, J. KUNSMAN, I. M. GHOBRIAL, S. KANAN, R. H. ADVANI and M. L. PALOMBA. 2013. A Prospective Multicenter Study Of The Bruton's Tyrosine Kinase Inhibitor Ibrutinib In Patients With Relapsed Or Refractory Waldenstrom's Macroglobulinemia. *Blood,* **122**(21).

TREON, S. P., L. XU, G. YANG, Y. ZHOU, X. LIU, Y. CAO, P. SHEEHY, R. J. MANNING, C. J. PATTERSON, C. TRIPSAS, L. ARCAINI, G. S. PINKUS, S. J. RODIG, A. R. SOHANI, N. L. HARRIS, J. M. LARAMIE, D. A. SKIFTER, S. E. LINCOLN and Z. R. HUNTER. 2012. MYD88 L265P somatic mutation in Waldenström's macroglobulinemia. *N Engl J Med,* **367**(9), pp.826-33.

TURNER, M. D., B. NEDJAI, T. HURST and D. J. PENNINGTON. 2014. Cytokines and chemokines: At the crossroads of cell signalling and inflammatory disease. *Biochim Biophys Acta,* **1843**(11), pp.2563-2582.

VAN DRIEL, M., U. GÜNTHERT, A. C. VAN KESSEL, P. JOLING, R. STAUDER, H. M. LOKHORST and A. C. BLOEM. 2002. CD44 variant isoforms are involved in plasma cell adhesion to bone marrow stromal cells. *Leukemia,* **16**(1), pp.135-43.

VAN SPRIEL, A. B., S. DE KEIJZER, A. VAN DER SCHAAF, K. H. GARTLAN, M. SOFI, A. LIGHT, P. C. LINSSEN, J. B. BOEZEMAN, M. ZUIDSCHERWOUDE, I. REINIEREN-BEEREN, A. CAMBI, F. MACKAY, D. M. TARLINTON, C. G. FIGDOR and M. D. WRIGHT. 2012. The tetraspanin CD37 orchestrates the $\alpha(4)\beta(1)$ integrin-Akt signaling axis and supports long-lived plasma cell survival. *Sci Signal,* **5**(250), pra82.

VAN VLASSELAER, P., J. PUNNONEN and J. E. DE VRIES. 1992. Transforming growth factor-beta directs IgA switching in human B cells. *J Immunol,* **148**(7), pp.2062-7.

VAN ZELM, M. C., I. REISLI, M. VAN DER BURG, D. CASTAÑO, C. J. VAN NOESEL, M. J. VAN TOL, C. WOELLNER, B. GRIMBACHER, P. J. PATIÑO, J. J. VAN DONGEN and J. L. FRANCO. 2006. An antibody-deficiency syndrome due to mutations in the CD19 gene. *N Engl J Med,* **354**(18), pp.1901-12.

VARGHESE, A. M., A. C. RAWSTRON, A. J. ASHCROFT, P. MORETON and R. G. OWEN. 2009. Assessment of bone marrow response in Waldenstrom's macroglobulinemia. *Clin Lymphoma Myeloma,* **9**(1), pp.53-5.

VICTORA, G. D., T. A. SCHWICKERT, D. R. FOOKSMAN, A. O. KAMPHORST, M. MEYER-HERMANN, M. L. DUSTIN and M. C. NUSSENZWEIG. 2010. Germinal center dynamics revealed by multiphoton microscopy with a photoactivatable fluorescent reporter. *Cell,* **143**(4), pp.592-605.

VIGORITO, E., G. BARDI, J. GLASSFORD, E. W. LAM, E. CLAYTON and M. TURNER. 2004. Vav-dependent and vav-independent phosphatidylinositol 3-kinase activation in murine B cells determined by the nature of the stimulus. *J Immunol,* **173**(5), pp.3209-14.

VINCENT, F. B., D. SAULEP-EASTON, W. A. FIGGETT, K. A. FAIRFAX and F. MACKAY. 2013. The BAFF/APRIL system: emerging functions beyond B cell biology and autoimmunity. *Cytokine Growth Factor Rev,* **24**(3), pp.203-15.

WANG, J. H., N. AVITAHL, A. CARIAPPA, C. FRIEDRICH, T. IKEDA, A. RENOLD, K. ANDRIKOPOULOS, L. LIANG, S. PILLAI, B. A. MORGAN and K. GEORGOPOULOS. 1998. Aiolos regulates B cell activation and maturation to effector state. *Immunity,* **9**(4), pp.543-53.

WARNATZ, K., A. DENZ, R. DRÄGER, M. BRAUN, C. GROTH, G. WOLFF-VORBECK, H. EIBEL, M. SCHLESIER and H. H. PETER. 2002. Severe deficiency of switched memory B cells (CD27(+)IgM(-)IgD(-)) in subgroups of patients with common variable immunodeficiency: a new approach to classify a heterogeneous disease. *Blood,* **99**(5), pp.1544-51.

WELLER, S., M. BONNET, H. DELAGREVERIE, L. ISRAEL, M. CHRABIEH, L. MARÓDI, C. RODRIGUEZ-GALLEGO, B. Z. GARTY, C. ROIFMAN, A. C. ISSEKUTZ, S. E. ZITNIK, C. HOARAU, Y. CAMCIOGLU, J. VASCONCELOS, C. RODRIGO, P. D. ARKWRIGHT, A. CERUTTI, E. MEFFRE, S. Y. ZHANG, A.

ALCAIS, A. PUEL, J. L. CASANOVA, C. PICARD, J. C. WEILL and C. A. REYNAUD. 2012. IgM+IgD+CD27+ B cells are markedly reduced in IRAK-4-, MyD88-, and TIRAP- but not UNC-93B-deficient patients. *Blood,* **120**(25), pp.4992-5001.

WENTINK, M. W. J., M. C. VAN ZELM, J. J. M. VAN DONGEN, K. WARNATZ and M. VAN DER BURG. 2018. Deficiencies in the CD19 complex. *Clin Immunol,* **195**, pp.82-87.

WILKINSON, P. C. 1986. The locomotor capacity of human lymphocytes and its enhancement by cell growth. *Immunology,* **57**(2), pp.281-9.

WILLIS, S. N., K. L. GOOD-JACOBSON, J. CURTIS, A. LIGHT, J. TELLIER, W. SHI, G. K. SMYTH, D. M. TARLINTON, G. T. BELZ, L. M. CORCORAN, A. KALLIES and S. L. NUTT. 2014. Transcription factor IRF4 regulates germinal center cell formation through a B cell-intrinsic mechanism. *J Immunol,* **192**(7), pp.3200-6.

WOYACH, J. A., A. J. JOHNSON and J. C. BYRD. 2012. The B-cell receptor signaling pathway as a therapeutic target in CLL. *Blood,* **120**(6), pp.1175-84.

WU, Y. T., W. OUYANG, A. S. LAZORCHAK, D. LIU, H. M. SHEN and B. SU. 2011. mTOR complex 2 targets Akt for proteasomal degradation via phosphorylation at the hydrophobic motif. *J Biol Chem,* **286**(16), pp.14190-8.

XU, L., Z. R. HUNTER, N. TSAKMAKLIS, Y. CAO, G. YANG, J. CHEN, X. LIU, S. KANAN, J. J. CASTILLO, Y. T. TAI, J. L. ZEHNDER, J. R. BROWN, R. D. CARRASCO, R. ADVANI, J. M. SABILE, K. ARGYROPOULOS, M. LIA PALOMBA, E. MORRA, A. TROJANI, A. GRECO, A. TEDESCHI, M. VARETTONI, L. ARCAINI, N. M. MUNSHI, K. C. ANDERSON and S. P. TREON. 2016. Clonal architecture of CXCR4 WHIM-like mutations in Waldenström Macroglobulinaemia. *Br J Haematol,* **172**(5), pp.735-44.

XU, L., Z. R. HUNTER, G. YANG, Y. ZHOU, Y. CAO, X. LIU, E. MORRA, A. TROJANI, A. GRECO, L. ARCAINI, M. VARETTONI, J. R. BROWN, Y. T. TAI, K. C. ANDERSON, N. C. MUNSHI, C. J. PATTERSON, R. J. MANNING, C. K. TRIPSAS, N. I. LINDEMAN and S. P. TREON. 2013. MYD88 L265P in Waldenstrom macroglobulinemia, immunoglobulin M monoclonal gammopathy, and other B-cell lymphoproliferative disorders using conventional and quantitative allele-specific polymerase chain reaction. *Blood,* **121**(11), pp.2051-8.

YANG, G., Y. ZHOU, X. LIU, L. XU, Y. CAO, R. J. MANNING, C. J. PATTERSON, S. J. BUHRLAGE, N. GRAY, Y. T. TAI, K. C. ANDERSON, Z. R. HUNTER and S. P. TREON. 2013. A mutation in MYD88 (L265P) supports the survival of lymphoplasmacytic cells by activation of Bruton tyrosine kinase in Waldenstrom macroglobulinemia. *Blood,* **122**(7), pp.1222-32.

YANG, Z., B. M. SULLIVAN and C. D. ALLEN. 2012. Fluorescent in vivo detection reveals that IgE(+) B cells are restrained by an intrinsic cell fate predisposition. *Immunity,* **36**(5), pp.857-72.

YASUDA, S., J. SUN, Y. ZHOU, Y. WANG, Q. LU, M. YAMAMURA and J. Y. WANG. 2018. Opposing roles of IgM and IgD in BCR-induced B-cell survival. *Genes Cells,* **23**(10), pp.868-879.

YE, B. H., G. CATTORETTI, Q. SHEN, J. ZHANG, N. HAWE, R. DE WAARD, C. LEUNG, M. NOURI-SHIRAZI, A. ORAZI, R. S. CHAGANTI, P. ROTHMAN, A. M. STALL, P. P. PANDOLFI and R. DALLA-FAVERA. 1997. The BCL-6 proto-oncogene controls germinal-centre formation and Th2-type inflammation. *Nat Genet,* **16**(2), pp.161-70.

YELVINGTON, B. J. 2018. Subcutaneous Rituximab in Follicular Lymphoma, Chronic Lymphocytic Leukemia, and Diffuse Large B-Cell Lymphoma. *J Adv Pract Oncol,* **9**(5), pp.530-534.

ZHANG, Y., P. B. ALEXANDER and X. F. WANG. 2017. TGF-β Family Signaling in the Control of Cell Proliferation and Survival. *Cold Spring Harb Perspect Biol,* **9**(4).

ZHOU, L. J., D. C. ORD, S. A. OMORI and T. F. TEDDER. 1992. Structure of the genes encoding the CD19 antigen of human and mouse B lymphocytes. *Immunogenetics,* **35**(2), pp.102-11.

ZHU, Z., A. SHUKLA, P. RAMEZANI-RAD, J. R. APGAR and R. C. RICKERT. 2019. The AKT isoforms 1 and 2 drive B cell fate decisions during the germinal center response. *Life Sci Alliance,* **2**(6).

ZWANG, Y., A. SAS-CHEN, Y. DRIER, T. SHAY, R. AVRAHAM, M. LAURIOLA, E. SHEMA, E. LIDOR-NILI, J. JACOB-HIRSCH, N. AMARIGLIO, Y. LU, G. B. MILLS, G. RECHAVI, M. OREN, E. DOMANY and Y.

YARDEN. 2011. Two phases of mitogenic signaling unveil roles for p53 and EGR1 in elimination of inconsistent growth signals. *Mol Cell,* **42**(4), pp.524-35.
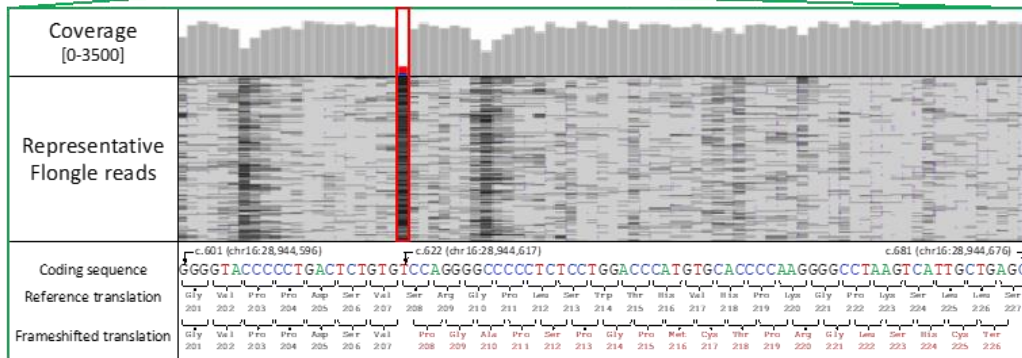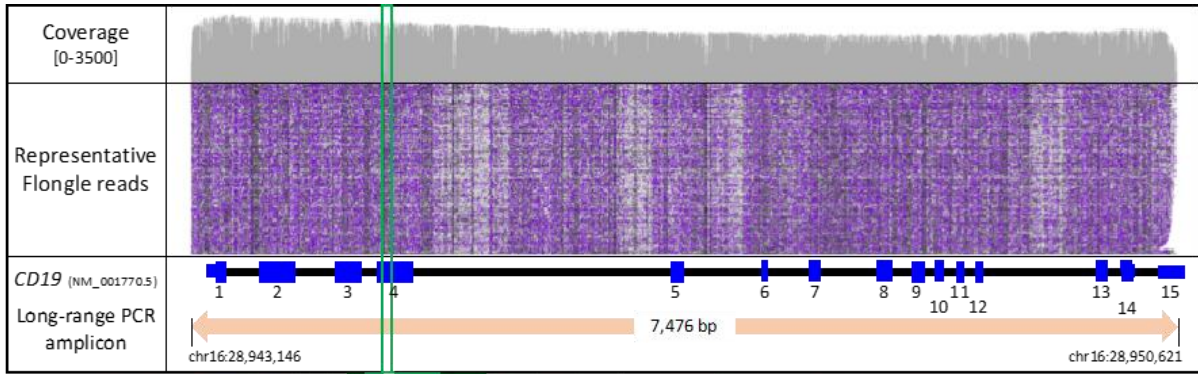
8.0 Appendix

|	
Sex / Age at diagnosis	F/30 years
Recurrent infections	++
Autoimmunity	-
Lymphoproliferation	-
Malignancy	-
IgM [g/l]	0.59 (0.4-2.5)
IgG [g/l]	3.50 (6-16)
IgA [g/l]	1.34 (0.8-3)
Functional antibodies post-vaccination **(Pneum/Haem/Tet)**	↓

Appendix 1 – Major clinical features of CD19-deficient patient.
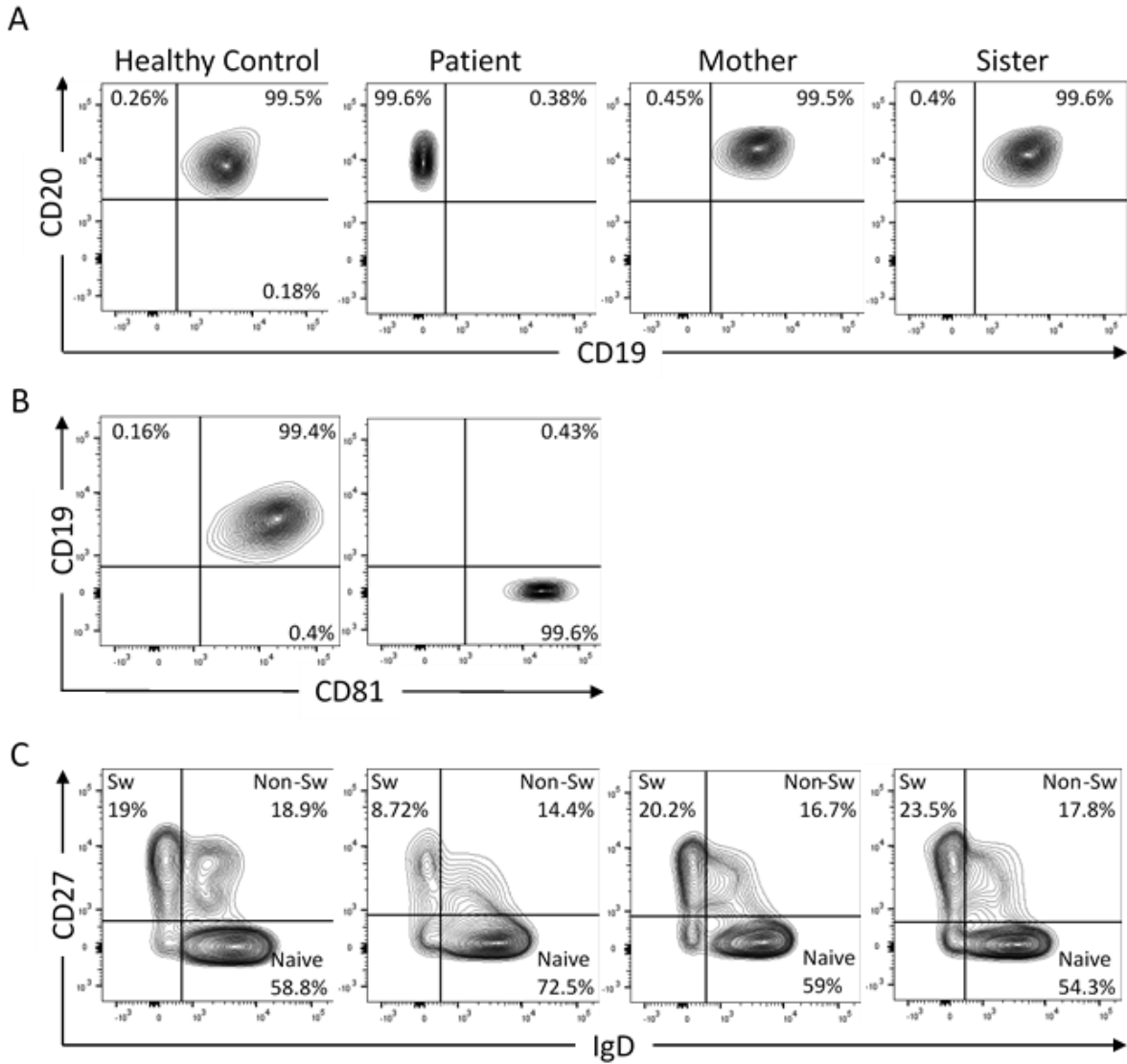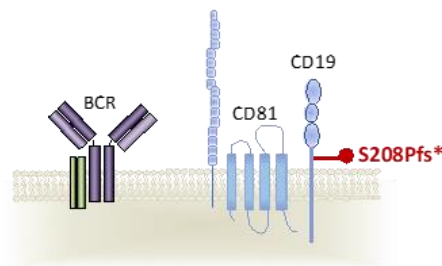
Appendix 2 – Flow Cytometry data showing Loss of CD19 surface expression and reduced memory B-cells. The peripheral blood B-cells from a healthy control, the patient, her mother and sister were evaluated by flow cytometry using antibodies against (A) CD20 and CD19 (B) CD19 and CD81 or (C) CD27 and IgD. Sw, switched memory B-cells and Non-Sw, non-switched memory B-cells.
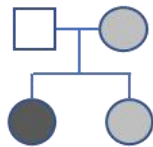
Appendix 3 - Long-read sequencing showing representative reads supporting the identification of the homozygous c.622del (NM_001770.5) (p.Ser208Profs*19) variant in CD19 exon 4. (A) Deletion-spanning gapped alignments are depicted by black lines in alignment track. The cumulative read count is displayed per nucleotide (y-axis scale is 0-3500). To aid visualization the IGV's "quick-consensus mode" was used. Transcript and genomic coordinates are provided according to NM_001770.5 and human genome build hg19 respectively. IGV: Integrative Genomics Viewer. (B) Pedigree of patient and unaffected family members. Affected patient with homozygous variant is indicated by filled black symbol, heterozygous family members are indicated by gray symbols. The CD19 variant status of the father was not tested. (C) Schematic diagram of CD19 structure in cell surface co-receptor complex with highlighted mutated residue.